



**Ciências  
ULisboa**

# **Northern Hemisphere blockings and their impacts over the European continent – historical overview and associated mechanisms**

Documento Provisório

**Doutoramento em Ciências Geofísicas e da Geoinformação  
Meteorologia**

**Pedro Miguel Ribeiro de Sousa**

Tese orientada por:  
Dr. Ricardo Machado Trigo  
Dr. David Barriopedro

Documento especialmente elaborado para a obtenção do grau de doutor







# Acknowledgments

First of all, I would like to thank my supervisors.

My most sincere thank you to Dr. Ricardo Machado Trigo and to Dr. David Barriopedro, for their close monitoring of my work, for the teaching through all this process, and of course for their patience! I also acknowledge their constructive criticism which has supported an important development of my investigation skills throughout these years. Thanks to all these facts this thesis has reached its end, and I hope in a satisfactory way for all.

Secondly, I would like to thank my family.

Special emphasis to my parents, which throughout all my life have encouraged my beliefs and my life goals. Amongst these, of course my passion for Meteorology is included. And undoubtedly they have motivated me to perform my academic education until this point of finishing a PhD.

I must also extend my gratitude to all the researchers who have participated in the investigation and peer-review processes throughout my PhD. Without their participation, ideas and effort, none of the published papers presented in this thesis would reach such a satisfactory level.

Finally, a special thank you to all my friends.

A warm salutation to all my dearest friends, ranging from work colleagues to long-time friends from my childhood who remain close to me. Friends are a really important part and balance in my life, balance without I am sure I would not be able to succeed in my professional and academic life!

This PhD was supported by the following FCT grant: *SFRH/BD/84395/2012*



# Abstract

Blocking high pressure systems are large-scale atmospheric circulation patterns with meteorological impacts that vary across regions and seasons, depending on the blocking location, spatial characteristics and temporal length. While blocking episodes are an important component of intra-seasonal and inter-annual variability at mid-latitudes, particularly in Europe, previous studies have mostly focused on characterizing European blocking impacts on either winter or summer seasons. In this thesis, a thorough characterization of Euro-Atlantic blocking occurrence within different longitudinal sectors (Atlantic, European and Russian) was performed, followed by a comprehensive analysis of their seasonal impacts in temperature and in the precipitation regimes of the European continent and specific sub-regions, with particular emphasis on Iberia, and on extreme events. In order to distinguish high-latitude blocking from other common high pressure systems affecting Europe, namely sub-tropical ridges, a novel ridge detection scheme was developed. Ridges do not require a wave-breaking occurrence as blockings do, although they are frequent precursors of wave-breaking, which may lead to blocking. Thus, as an additional novelty, this thesis also characterizes the distinctive seasonal impacts associated with sub-tropical ridges occurring at different longitudinal sectors of the Euro-Atlantic region. Finally, an assessment of the involved mechanisms behind the temperature and precipitation responses to blocking is also carried out. This included for precipitation the role of cyclonic activity (storm-tracks and cut-off lows), moisture transport, and large-scale atmospheric instability, while for temperature the focus was on the role played by horizontal advection, subsidence and imbalances in various radiation budgets.

This distinction clarifies that most extreme heat episodes in southern Europe and Mediterranean areas should not be attributed to blockings, but rather to ridges. In central and northern areas of the continent, both regimes are responsible for warm conditions in summer, due to enhanced radiative heating and increased subsidence. During winter, blocking and ridges lead to opposite temperature responses. Blocking reinforces cold northerly advection in its eastern flank, thus promoting European cold winter spells, especially those located in the eastern Atlantic and western Europe, while mild Atlantic flows associated to ridge patterns result in warmer conditions.

Regarding the impacts on precipitation, blocking and ridges are associated with a marked north-south dipole for the three considered longitudinal sectors of occurrence. While blocking patterns force a split of the storm-track, ridges are associated with a stronger zonal flow at higher latitudes. Thus, negative (positive) precipitation anomalies during blocks occur at higher (lower) latitudes. Enhanced atmospheric instability and cyclonic activity south of blocking centers relate very well with increased rainfall in southern Europe, including Iberia, where torrential regimes are more relevant in the precipitation totals. This dipole is reversed during ridges, which lead to dry conditions in southern Europe. The seasonal analysis further reveals that winters characterized by high frequencies of blocking (ridge) occurrence present above (below) average snow covered soils.

Blocking/ridge impacts on temperature and precipitation have also additional effects on meteorological and climate extreme events with large socio-economic impacts. Thus, the results show a blocking/ridge role at different time-scales in controlling a significant part of wildfire inter-

annual variability in Mediterranean areas. Meteorological pre-conditioning raises vegetation stress during dry winters, while increased ridge and blocking occurrence in summer fosters meteorological conditions which are prone to fire ignition and spread. Finally, outputs from state-of-the-art General Circulation Models raise the challenge to develop further these automated schemes for blocking/ridges detection, as their representation in climate models is crucial to understand impacts towards the later decades of the 21<sup>st</sup> century.

Summing up, the main novelties and achievements of this thesis are: 1) the clear disentanglement between blocks and ridges; 2) the seasonal analyses of specific regional impacts resulting from different locations of blocking/ridge structures; 3) the detailed analysis of dynamical/physical forcing mechanisms associated to each considered weather pattern.

**Keywords:** Atmospheric blocking, Sub-tropical ridges, Climate variability, Europe, Atlantic, Impacts, Precipitation, Temperature, Droughts, Wildfires.

## Resumo

Apesar de não existir uma definição unanimemente aceite para o conceito de bloqueio atmosférico, este pode ser descrito como uma supressão do fluxo zonal devido à presença de um sistema de alta pressão. Esta circulação anticiclónica, normalmente localizada nas latitudes onde se observa a corrente de jato polar, apresenta uma dimensão espacial de larga-escala, é geralmente quase-estacionária, e tem um tempo de vida útil entre vários dias a várias semanas. Os sectores orientais dos oceanos Atlântico e Pacífico são geralmente as regiões de ocorrência preferencial de bloqueios no Hemisfério Norte. A ocorrência de bloqueios atmosféricos está diretamente associada a condições prolongadas de tempo seco e estável nas regiões diretamente localizadas sob o sistema de altas pressões. O seu posicionamento geralmente origina uma divisão em dois ramos da corrente de jato. Esta perturbação do habitual padrão zonal resulta em alterações significativas das condições meteorológicas a outras latitudes (tanto meridional como setentrional) distintas da zona diretamente afetada pela posição central do bloqueio.

Torna-se necessária assim uma compreensão mais detalhada da climatologia associada aos bloqueios atmosféricos centrados no setor Euro-Atlântico, com especial ênfase aos impactos específicos associados às diferentes localizações que os seus centros de ação possam ter. Apesar de serem um fenómeno que ocorre à escala sinóptica, os bloqueios podem implicar impactos climáticos muito distintos à escala regional, ou mesmo local. Desta forma, um dos principais objetivos desta tese centra-se na elaboração de uma climatologia completa da sua ocorrência, e na respetiva caracterização dos impactos climáticos regionais resultantes da ocorrência de bloqueios em diferentes sectores longitudinais: Atlântico (ATL; 30W-0W), Europeu (EUR; 0E-30E) e Russo (RUS; 30E-60E).

Tendo-se verificado na literatura uma certa confusão entre bloqueio de alta latitude e outros sistemas comuns de alta pressão que afetam a Europa, nomeadamente as cristas sub-tropicais, foi considerado prioritário obter um novo catálogo de cristas de alta pressão para o setor Euro-Atlântico. Desta forma, um segundo objetivo central da tese foi o do desenvolvimento de um novo algoritmo automático de deteção de cristas sub-tropicais, que permita assim realizar uma clara distinção fenomenológica e dos impactos destes dois padrões atmosféricos (bloqueios *versus* cristas). Assim, a compreensão das condições sinópticas e dos mecanismos físicos envolvidos em cada um destes padrões é também tema central desta tese. No caso da precipitação, esta análise de mecanismos incluiu o papel da atividade ciclónica (*storm-tracks* e *cut-off lows*), do transporte de humidade e da instabilidade atmosférica em larga escala. Para avaliar os impactos na temperatura analisou-se a contribuição da advecção horizontal, da subsidência e das alterações nos vários balanços radiativos.

A desagregação bloqueios-cristas permite distinguir fenomenologias por vezes confundidas na literatura, nomeadamente aquando da análise de episódios de calor extremo no sul da Europa. Verifica-se dos resultados obtidos que, devido a uma clara distinção no posicionamento latitudinal dos centros de ação entre bloqueios e cristas, as respostas na temperatura associadas a cada padrão são também bem distintas, sendo estas diferenças particularmente notáveis no inverno. De uma forma geral, nesta estação, os bloqueios (essencialmente os centrados nos

sectores ATL e EUR) resultam em valores das temperaturas do ar bastante abaixo da média, provocadas pela advecção de ar frio de latitudes mais elevadas ao longo do flanco este dos anticiclones. Em oposição, as cristas originam anomalias positivas na temperatura na maior parte do continente europeu, essencialmente como resultado do transporte de massas de ar de origem Atlântica, e de uma redução do arrefecimento radiativo, associado ao aumento da nebulosidade. Durante o verão, ambos os padrões atmosféricos estão associados a temperaturas acima da média em vastas áreas da Europa central e do norte. Em contrapartida, nas regiões mais a sul, e em particular na área da bacia do Mediterrâneo, as cristas controlam a ocorrência de dias extremamente quentes (usualmente identificados como ondas de calor). No verão é também de salientar o papel dominante do aquecimento radiativo solar (sob condições de céu limpo) como principal impulsor destas anomalias positivas de temperatura em dias de ocorrência de bloqueio/crista, particularmente para os sistemas localizados sobre áreas continentais.

Relativamente aos impactos nos regimes de precipitação, existe um claro dipolo norte-sul ao analisar as anomalias associadas a dias de bloqueio/crista. A ocorrência de bloqueios leva a uma redução da precipitação na metade norte do continente Europeu (em algumas áreas superior a 50%) devido ao bloqueio dos sistemas de depressão de médias-latitudes (e do correspondente transporte de humidade) provenientes do Atlântico. No entanto, esta configuração sinótica leva a um aumento da precipitação (relativamente à média) nas zonas mais a sul, fundamentalmente relacionado com o desvio do *storm-track* nesta direção, e a um consequente aumento da instabilidade atmosférica e da convecção. Este padrão resulta numa clara mudança nas distribuições de regimes de precipitação nos países do sul da Europa, e demonstra também a ligação entre bloqueios atmosféricos e os regimes de precipitação torrencial na área do Mediterrâneo. Em padrões de fluxo zonal intenso as anomalias da precipitação são no geral opostas às encontradas durante bloqueios, originando um *deficit* de precipitação no sul da Europa. No contexto dos vários regimes possíveis de fluxo zonal forte, as cristas sub-tropicais estão associadas a condições particularmente secas nos países do sul da Europa. Isto naturalmente também se aplica à Península Ibérica, onde os totais anuais de precipitação dependem largamente da atividade frontal de origem Atlântica (em particular nos meses de inverno), sendo esta afastada da região durante a ocorrência de cristas nos sectores ATL e EUR. Neste contexto, mostra-se crucial o recurso a bases de dados de alta-resolução com uma densidade de estações muito mais elevada, permitindo uma análise regional mais detalhada para o domínio da Península Ibérica.

Os bloqueios centrados em latitudes elevadas, em particular os que ocorrem no sector ATL, são responsáveis por invernos com maior cobertura de neve no continente Europeu (até cerca de 50% mais dias com a superfície coberta de neve na Europa central), devido a uma maior frequência de dias frios sob os fluxos de norte associados à circulação anticiclónica. Por outro lado, a ocorrência de cristas nos sectores ATL e EUR (que estão associadas a dias de inverno bastante amenos) impõe uma frequência muito mais baixa de dias com neve no solo.

Foi também concluído que os padrões de bloqueio/crista exercem um efeito regulador importante na variabilidade inter-anual de incêndios florestais. Mostra-se que o *feedback*

existente entre a ocorrência destes padrões atmosféricos, a ocorrência de secas, e os incêndios florestais, acontece a diferentes escalas temporais. Nos meses antecedentes à época de incêndios, uma frequência superior ao normal de cristas (bloqueios) é responsável por valores de precipitação abaixo (acima) da média no sul da Europa, aumentando a vulnerabilidade da vegetação. Durante a própria época de incêndios, este padrão atmosférico está associado a condições anormalmente quentes e secas que promovem a ignição e fácil propagação do fogo.

Finalmente, no contexto das alterações climáticas, verificou-se que nas últimas décadas a frequência de cristas sub-tropicais aumentou bastante no sul da Europa. As projeções futuras dos Modelos de Circulação Geral sugerem uma expansão para norte das altas pressões sub-tropicais (associadas à expansão da célula de Hadley). Por outro lado, não existem sinais dinâmicos de alterações muito significativas na frequência e localização dos bloqueios de alta latitude no sector Euro-Atlântico, exceto uma ligeira tendência de deslocamento para nordeste na sua região preferencial de ocorrência. Pretende-se como trabalho futuro utilizar também uma abordagem dinâmica (não apenas baseada em campos de anomalia) para o algoritmo de deteção de cristas, que permitirá uma maior confiança na extrapolação para cenários futuros.

**Palavras-chave:** Bloqueios atmosféricos, Cristas sub-tropicais, Variabilidade climática, Europa, Atlântico, Impactos, Precipitação, Temperatura, Secas, Incêndios.



# Contents

<b>List of Acronyms and Abbreviations</b>	xi
<b>List of Figures</b>	xiii
<b>List of Tables</b>	xvii
<b>1. Introduction</b>	<b>1</b>
1.1. Large-scale variability and the European climate	3
1.1.1. <i>Inter-decadal and inter-annual temperature variability</i>	4
1.1.2. <i>European temperature extremes</i>	7
1.1.3. <i>European precipitation regimes</i>	10
1.1.4. <i>Drought conditions throughout the 20<sup>th</sup> century</i>	11
1.2. Atmospheric blocking: climatology and associated impacts	14
1.2.1. <i>Blocking definition</i>	14
1.2.2. <i>Euro-Atlantic blocking climatology</i>	17
1.2.3. <i>Blocking life cycle: onset, maintenance and decay</i>	21
1.2.4. <i>Sub-tropical ridges</i>	25
1.2.5. <i>Blocking and ridge impacts</i>	27
1.3. Goals and structure of the thesis	29
<b>2. European temperature responses to blocking</b>	<b>31</b>
<i>Summary</i>	32
2.1. Paper in <i>Climate Dynamics</i>	33
2.1.1. <i>Introduction</i>	33
2.1.2. <i>Data and Methods</i>	35
2.1.3. <i>Results</i>	38
2.1.3.1 <i>Blocking and ridge seasonal distribution</i>	38
2.1.3.2 <i>Seasonal temperature responses</i>	39
2.1.3.3 <i>Synoptic and forcing mechanisms</i>	43
2.1.3.4 <i>Changes in regional temperature distribution</i>	50
2.1.4. <i>Discussion and Conclusions</i>	55
2.1.5. <i>Supplementary Material</i>	58

<b>3.</b>	<b>Blocking impacts on European precipitation regimes</b>	<b>63</b>
Summary		64
3.1.	Paper in <i>Climate Dynamics</i>	65
3.1.1.	Introduction	66
3.1.2.	Data and Methods	68
3.1.3.	Changes in mean precipitation rates	71
3.1.4.	Synoptic and dynamics associated to different blocking locations	74
3.1.5.	Shifts in precipitation distributions	82
3.1.6.	Discussion and Conclusions	87
3.1.7.	Supplementary material	90
3.2.	Dry fingerprint of ridge patterns in southern Europe	95
3.3.	Impacts in European snow-cover	98
<b>4.</b>	<b>Blocking impacts on Iberian precipitation and temperature</b>	<b>101</b>
Summary		102
4.1.	Paper in <i>Climate Dynamics</i>	103
4.1.1.	Introduction	104
4.1.2.	Data	106
4.1.3.	Seasonal impacts of blocking in Iberian precipitation	109
4.1.4.	Synoptic forcing	114
4.1.5.	Extreme Value Analysis	119
4.1.6.	Discussion	125
4.1.7.	Supplementary material	127
4.2.	High-resolution Iberian rainfall deficits during ridge patterns	129
4.3.	High-resolution Iberian temperature responses at a finer scale	130
<b>5.</b>	<b>Conclusions and open threads for Future work</b>	<b>135</b>
Summary		136
5.1.	Conclusions	137
5.2.	Open threads for Future work	138
5.1.1.	The feedbacks between blocking, droughts and wildfires	139
5.1.2.	Future scenarios of blocking variability in the 21 <sup>st</sup> century	144
5.3.	Perspectives	149
	<b>References</b>	<b>151</b>
	<b>Annex – additional papers</b>	<b>171</b>

# List of Acronyms and Abbreviations

<i>AMO</i>	Atlantic Multidecadal Oscillation
<i>ATL</i>	Atlantic sector (30W-0W)
<i>CMIP3</i>	Coupled Model Intercomparison Project (phase 3)
<i>CMIP5</i>	Coupled Model Intercomparison Project (phase 5)
<i>COL</i>	Cut-Off Low
<i>DG</i>	Dole and Gordon blocking index
<i>EA</i>	East Atlantic pattern
<i>EA/WR</i>	East Atlantic / Western Russia pattern
<i>ECA&amp;D</i>	European Climate Assessment and Dataset
<i>EFD</i>	European Fire Database
<i>ENSO</i>	El Niño - Southern Oscillation
<i>EPNP</i>	East Pacific North Pacific pattern
<i>ESM</i>	Eddy Straining Mechanism
<i>EUR</i>	European sector (0E-30E)
<i>FUME</i>	Forest fires Under the Mediterranean Environment
<i>GCM</i>	General Circulation Model
<i>GP</i>	Generalized Pareto
<i>IP</i>	Iberian Peninsula
<i>IPO</i>	Inter-Decadal Pacific Oscillation
<i>IVT</i>	Integrated water Vapor Transport
<i>KStest</i>	Kolmogorov-Smirnov test
<i>LHF</i>	Latent Heat Flux
<i>LI</i>	Lifted Index
<i>LMM</i>	Late Maunder Minimum
<i>NAM</i>	Northern Annular Mode
<i>NAO</i>	North Atlantic Oscillation
<i>NCEP</i>	National Centers for Environmental Prediction

<i>NCAR</i>	National Center for Atmospheric Research
<i>NH</i>	Northern Hemisphere
<i>NOAA</i>	National Oceanic and Atmospheric Administration
<i>PDF</i>	Probability Density Function
<i>PDO</i>	Pacific Decadal Oscillation
<i>PMAX</i>	Maximum daiyly precipitation
<i>PNA</i>	Pacific North American pattern
<i>PT</i>	Potential Temperature
<i>PTOT</i>	Total event/episode precipitation
<i>PV</i>	Potential Vorticity
<i>RCP4.5</i>	Representative Concentration Pathway for greenhouse gases (4.5 W.m <sup>-2</sup> radiative forcing)
<i>RCP8.5</i>	Representative Concentration Pathway for greenhouse gases (8.5 W.m <sup>-2</sup> radiative forcing)
<i>RUS</i>	Russian sector (30E-60E)
<i>RUCL</i>	Rutgers Univeristy Climate Lab
<i>SCA</i>	Scandinavian pattern
<i>SPEI</i>	Standardized Precipitation Evapotranspiration Index
<i>SPRE</i>	Strong Persistent Ridge Events
<i>SST</i>	Sea Surface Temperature
<i>SSW</i>	Sudden Stratospheric Warming
<i>TM</i>	Tibaldi and Molteni blocking index
<i>TN</i>	Minimum temperature
<i>TN10</i>	Days with minimum temperature below the 10 <sup>th</sup> percentile of climatology
<i>TX</i>	Maximum temperature
<i>TX90</i>	Days with maximum temperature above the 90 <sup>th</sup> percentile of climatology
<i>UK</i>	United Kingdom
<i>WMO</i>	World Meteorological Organization
<i>WP</i>	West Pacific pattern
<i>WWII</i>	World War II
<i>Z500</i>	Geopotential height at the 500 hPa level

# List of Figures

<b>Fig. 1.1</b> – Map of updated Köppen-Geiger climate classification for Europe . . . . .	3
<b>Fig. 1.2</b> – Comparison between NH temperature anomaly trends and the NAO and AMO indices . . . . .	5
<b>Fig. 1.3</b> – Main large-scale circulation modes in the NH . . . . .	6
<b>Fig. 1.4</b> – Dominant large-scale circulation modes influencing temperature variability in Europe . . . . .	7
<b>Fig. 1.5</b> – Reconstruction of the warmest/coldest summers in Europe (1500-2010) . . . . .	9
<b>Fig. 1.6</b> – Dominant large-scale circulation modes influencing precipitation variability in Europe . . . . .	11
<b>Fig. 1.7</b> – Annual series of drought conditions in distinct European regions . . . . .	12
<b>Fig. 1.8</b> – Percentages of Mediterranean areas under wet/dry conditions during the 20 <sup>th</sup> century . . . . .	13
<b>Fig. 1.9</b> – Typical synoptic configurations for Omega blocks and Rex blocks . . . . .	14
<b>Fig. 1.10</b> – Schematic of the automated blocking detection method used throughout the thesis . . . . .	16
<b>Fig. 1.11</b> – Blocking center location frequencies in the NH . . . . .	18
<b>Fig. 1.12</b> – Histograms for blocking episodes duration in the NH . . . . .	19
<b>Fig. 1.13</b> – Preferred blocking genesis and decay locations in the NH . . . . .	20
<b>Fig. 1.14</b> – Schematics for different types of wave-breaking . . . . .	22
<b>Fig. 1.15</b> – Distribution of winter blocking genesis, tracks and lysis during different NAO phases . . . . .	23
<b>Fig. 1.16</b> – Schematics for the Eddy Straining Mechanism and the Selective Absorption Process . . . . .	24
<b>Fig. 1.17</b> – Idealized atmospheric circulation around a sub-tropical ridge in the NH . . . . .	26
<b>Fig. 1.18</b> – Synoptic configurations for ridge events with or without wave-breaking . . . . .	27
<b>Fig. 1.19</b> – Temperature and precipitation responses in Europe during winter blocks . . . . .	28
<b>Fig. 2.1</b> – Geographical representation of the considered sectors of blocking/ridges occurrence . . . . .	36
<b>Fig. 2.2</b> – Absolute and anomalous Z500 composites for blocking/ridge episodes in each sector . . . . .	39
<b>Fig. 2.3</b> – Composites for winter TN and TX during blocking and ridge days . . . . .	40
<b>Fig. 2.4</b> – Composites for summer TN and TX during blocking and ridge days . . . . .	42
<b>Fig. 2.5</b> – Dominant forcing mechanisms associated to European temperature anomalies . . . . .	44
<b>Fig. 2.6</b> – Winter surface radiative fluxes budgets during blocking and ridge days . . . . .	46
<b>Fig. 2.7</b> – Summer surface radiative fluxes budgets during blocking and ridge days . . . . .	48
<b>Fig. 2.8</b> – Total cloud cover anomalies during blocking and ridge days . . . . .	49

<b>Fig. 2.9</b> – Changes in European winter TN and TX distributions during blocking and ridge days . . . . .	51
<b>Fig. 2.10</b> – Changes in European summer TN and TX distributions during blocking and ridge days . . .	53
<b>Fig. 2.11</b> – Changes in European extreme temperature days during blocking and ridge days . . . . .	55
<b>Fig. 2.12</b> – Composites for winter TN and TX considering smaller sub-sectors of occurrence . . . . .	58
<b>Fig. 2.13</b> – Composites for summer TN and TX considering smaller sub-sectors of occurrence . . . . .	58
<b>Fig. 2.14</b> – Detailed contribution of different forcing terms for temperature changes during winter . . .	59
<b>Fig. 2.15</b> – Detailed contribution of different forcing terms for temperature changes during summer . .	60
<b>Fig. 2.16</b> – Anomalies in the winter mean lapse-rate during blocking and ridge days . . . . .	61
<b>Fig. 2.17</b> - Changes in TN and TX distributions for Turkey and Russia . . . . .	62
<b>Fig. 2.18</b> - Changes in extreme temperature days for Turkey and Russia . . . . .	62
<b>Fig. 3.1</b> – Sectors of Euro-Atlantic blocking occurrence . . . . .	69
<b>Fig. 3.2</b> – Seasonal daily anomalies and absolute values for Z500 during blocking days . . . . .	70
<b>Fig. 3.3</b> – Annual composites for daily precipitation anomalies during blocking and zonal days . . . . .	72
<b>Fig. 3.4</b> – Differences in seasonal precipitation anomalies between blocking and zonal days . . . . .	74
<b>Fig. 3.5</b> – Changes in the frequency of cyclone locations during blocking and zonal days . . . . .	75
<b>Fig. 3.6</b> – Changes in spatial patterns of the IVT and the LI during blocking and zonal days . . . . .	77
<b>Fig. 3.7</b> – Seasonal changes in the IVT and LI spatial patterns during blocking and zonal days . . . . .	79
<b>Fig. 3.8</b> – Changes in the mean LHF spatial patterns during blocking and zonal days . . . . .	81
<b>Fig. 3.9</b> – Shifts in precipitation distributions for each synoptic pattern in the UK . . . . .	83
<b>Fig. 3.10</b> – Shifts in precipitation distributions for each synoptic pattern in the Iberian Peninsula . . . .	85
<b>Fig. 3.11</b> – Shifts in summer precipitation distributions for each synoptic pattern in Russia . . . . .	86
<b>Fig. 3.12</b> – Shifts in precipitation distributions for each synoptic pattern in Turkey . . . . .	87
<b>Fig. 3.13</b> – Changes in the number of dry days during blocking and zonal patterns . . . . .	90
<b>Fig. 3.14</b> – Forward trajectories of air parcels during ATL blocking days . . . . .	91
<b>Fig. 3.15</b> – Shifts in winter precipitation distributions for each synoptic pattern in NW Iberia . . . . .	92
<b>Fig. 3.16</b> – Shifts in summer precipitation distributions for each synoptic pattern in NW Iberia . . . . .	93
<b>Fig. 3.17</b> – Shifts in precipitation distributions for each synoptic pattern in Central Europe . . . . .	93
<b>Fig. 3.18</b> – Shifts in precipitation distributions for each synoptic pattern in Italy . . . . .	94
<b>Fig. 3.19</b> – Shifts in winter precipitation distributions for each synoptic pattern in Turkey . . . . .	94
<b>Fig. 3.20</b> – Shifts in summer precipitation distributions for each synoptic pattern in Turkey . . . . .	95

<b>Fig. 3.21</b> – Seasonal composites for daily precipitation anomalies during ridge days . . . . .	96
<b>Fig. 3.22</b> – Seasonal composites for daily precipitation anomalies during zonal days . . . . .	97
<b>Fig. 3.23</b> – Mean percentage of days with snow covered soil during European winter . . . . .	98
<b>Fig. 3.24</b> – Changes in the number of snow covered soil days during blocking and ridge days . . . . .	99
<b>Fig. 4.1</b> – Climatology of blocking occurrence in the ATL and EUR sectors . . . . .	108
<b>Fig. 4.2</b> – Seasonal patterns of Z500 departures for ATL and EUR blocks . . . . .	109
<b>Fig. 4.3</b> – Iberian precipitation seasonal anomalies during blocking days using different datasets . . . . .	110
<b>Fig. 4.4</b> – High-resolution precipitation anomalies in Iberia for blocked and zonal patterns . . . . .	112
<b>Fig. 4.5</b> – Changes in the rainy days in Iberia during blocked and zonal patterns . . . . .	114
<b>Fig. 4.6</b> – Changes in the IVT and the LI for ATL and EUR blocked/zonal days . . . . .	115
<b>Fig. 4.7</b> – Changes in the frequency of cyclone locations for ATL and EUR blocked/zonal days . . . . .	117
<b>Fig. 4.8</b> – Changes in the frequency of COL locations for ATL and EUR blocked/zonal days . . . . .	118
<b>Fig. 4.9</b> – Extreme precipitation efficiency for blocking/zonal days in Iberia . . . . .	120
<b>Fig. 4.10</b> – Regional boxes chosen to perform the GP fit for Iberian precipitation . . . . .	121
<b>Fig. 4.11</b> – Choosing the best Extreme Value distribution fit – L-Moment Ratio diagrams . . . . .	123
<b>Fig. 4.12</b> – Seasonal patterns of Z500 departures for smaller sub-sectors of blocking occurrence . . . . .	127
<b>Fig. 4.13</b> – Precipitation anomalies in Iberia in the days prior to blocking occurrence . . . . .	127
<b>Fig. 4.14</b> – Probability-probability plots for the GP fit during blocking days . . . . .	128
<b>Fig. 4.15</b> – Probability-probability plots for the GP fit during zonal days . . . . .	128
<b>Fig. 4.16</b> – Winter and summer precipitation anomalies in Iberia during ridge days . . . . .	129
<b>Fig. 4.17</b> – Anomalies in winter TN and TX in Iberia during blocking and ridge days . . . . .	131
<b>Fig. 4.18</b> – Anomalies in summer TN and TX in Iberia during blocking and ridge days . . . . .	132
<b>Fig. 5.1</b> – Links between late spring SPEI and the previous month’s blocking/ridge frequencies . . . . .	140
<b>Fig. 5.2</b> – Summer blocking/ridge enhancement due to prolonged surface moisture deficits . . . . .	142
<b>Fig. 5.3</b> – Intra-annual evolution of drought conditions in severe wildfire years . . . . .	143
<b>Fig. 5.4</b> – Inter-annual variability in the frequency of winter blocking and ridges . . . . .	145
<b>Fig. 5.5</b> – Inter-annual variability in the frequency of summer blocking and ridges . . . . .	146
<b>Fig. 5.6</b> – Past and projected changes in winter Z500 at different latitudes . . . . .	147
<b>Fig. 5.7</b> – Past and projected changes in summer Z500 at different latitudes . . . . .	148



## List of Tables

<b>Table 1.1</b> – Ranked coldest top 10 months and winters in Central England (1659-2013) . . . . .	7
<b>Table 4.1</b> – Number of extreme rainy days in different areas of Iberia under each weather pattern . . . .	122
<b>Table 4.2</b> – Confidence levels of the GP fits for the maximum event precipitation . . . . .	124
<b>Table 4.3</b> – Confidence levels of the GP fits for the total event precipitation . . . . .	124
<b>Table 5.1</b> – Links between summer burnt areas and the previous month’s blocking/ridge frequencies . .	141
<b>Table 5.2</b> – Links between summer burnt areas and concurrent blocking/ridge frequencies . . . . .	141



# Chapter 1

## Introduction

### Contents

---

#### **1.1 Large-scale variability and the European climate**

*1.1.1 Inter-decadal and inter-annual temperature variability*

*1.1.2 European temperature extremes*

*1.1.3 European precipitation regimes*

*1.1.4 Drought conditions throughout the 20<sup>th</sup> century*

#### **1.2 Atmospheric blocking: climatology and associated impacts**

*1.2.1 Blocking definition*

*1.2.2 Euro-Atlantic blocking climatology*

*1.2.3 Blocking life cycle: onset, maintenance and decay*

*1.2.4 Sub-tropical ridges*

*1.2.5 Blocking and ridge impacts*

#### **1.3 Goals and structure of the thesis**

---



### 1.1 Large-scale variability and the European climate

Although Europe lies within the northern temperate climate zone, its relative large extension encloses a wide range of different climates (Barry and Chorley, 2010). Kotték et al (2006) have developed an updated version of the Köppen-Geiger climatic classification map that is shown here for the European continent (Fig 1.1). While oceanic climate classifications predominate in western sectors, temperate and cool continental climates are characteristic of eastern and northern countries. The Mediterranean basin is dominated by warm and temperate Mediterranean classes, which are characterized by wet winter and dry and hot summers (see Fig. 1.1). The prevailing westerly zonal flow and the associated Jetstream control a large fraction of the European climate, although disruptions of the Jetstream frequently alter significantly the usual precipitation and temperature distributions. A large part of the inter-annual variability in European weather is modulated by a few synoptic structures (e.g. the Azores high, Iceland low, Jetstream, storm-tracks). Amongst them, quasi-stationary high pressure systems referred to as blocking, are one of the main weather regimes disrupting the mean European conditions (Rex, 1950a,b).

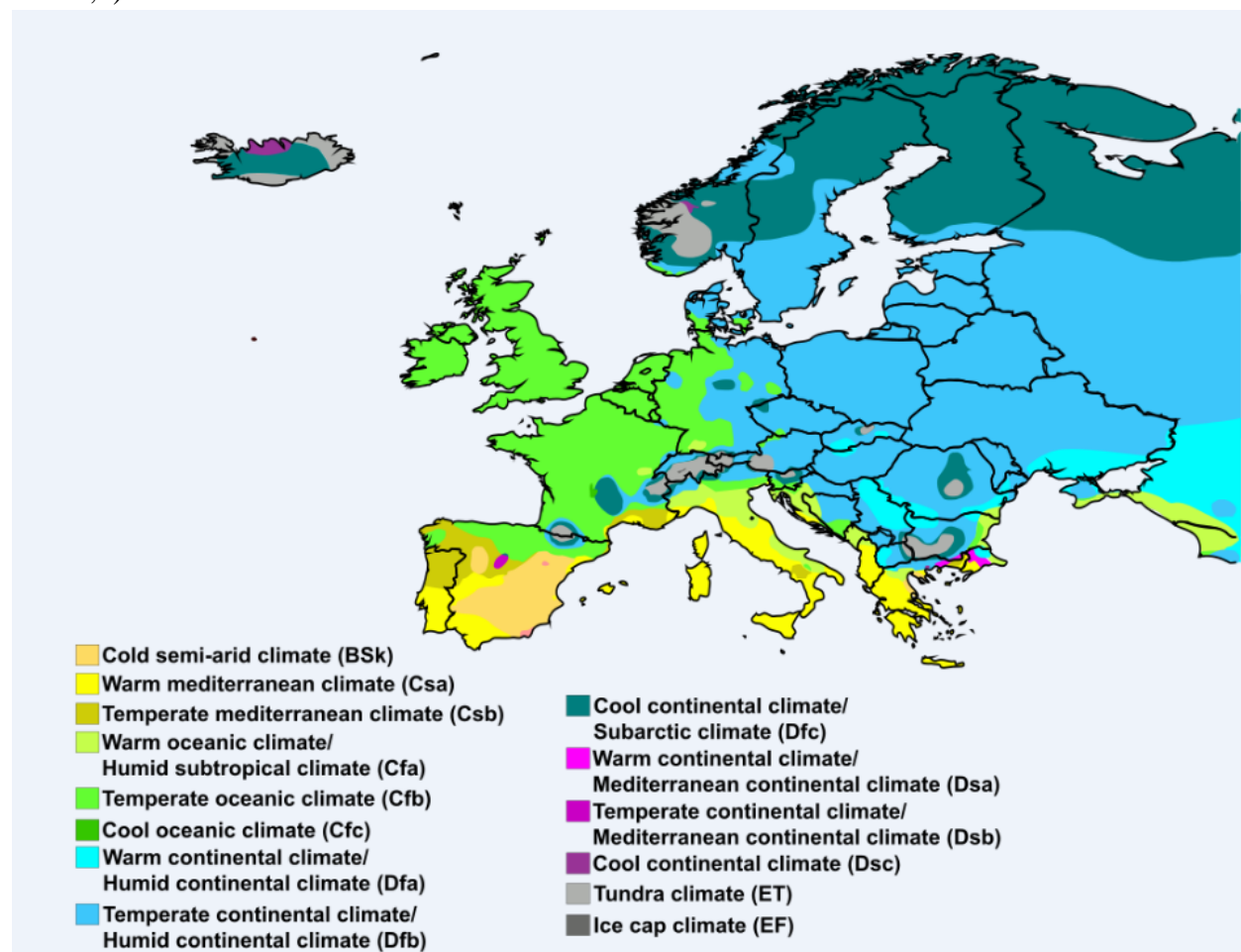


**Fig. 1.1** European map of updated Köppen-Geiger climate classification. *Adapted from Kotték et al., 2016.*

In order to frame a large-scale phenomenon such as blocking, in terms of climatology and impacts over the European continent, as intended throughout this thesis, it is firstly required to present the main large-scale atmospheric variability modes that affect the study area at different time scales. In the following sub-sections, the links between these circulation modes (as well as other remote atmospheric and oceanic phenomena) and the European climate variability at different time-scales (from a long-term perspective to inter-annual variations), are briefly described, taking also into account the Mediterranean environment.

### 1.1.1 Inter-decadal and inter-annual temperature variability

At long temporal scales, the rate of global warming in the post-industrial era is unprecedented (Luterbacher et al., 2004; Mann et al. 2009; Ljungqvist et al., 2012) and leads to a generalized consensus on an anthropogenic fingerprint (Cook et al., 2013; Fischer and Knutti, 2015). An apparent hiatus in this steep recent warming trend has been discussed in recent years (e.g. Seneviratne et al., 2014). However, the successive record temperature years at the global scale, including 2014, 2015 and 2016 have now undermined the concept of hiatus (e.g. Su et al., 2017).

Superimposed on this long-term trend, the mean temperature in the Northern Hemisphere (NH) during the 20th century has been characterized by a multi-decadal warming-cooling-warming pattern (Li et al., 2013), with the latter being particularly notable through the early stages of the 21st century. The work by Peña-Ortiz et al. (2015) corroborates a similar behavior in the European region, as the authors refer to a shortening of the summer season in Europe throughout the 1950-1978 period, and a notable lengthening in the post-1979 period. To understand the multi-decadal changes within the long-term temperature trend it is mandatory to take into account the effects of internal variability, including several oscillatory phenomena associated with Sea Surface Temperature (SST) anomalies, such as the Atlantic Multi-decadal Oscillation (AMO) or the Pacific Decadal Oscillation (PDO). A close relation between the AMO phase and the mean temperature of the NH and the European continent has been reported by several authors (Li et al., 2013; Mann et al., 2014; Peña-Ortiz et al., 2015; Zampieri et al., 2016), with the cooling phases of the AMO signal likely offsetting some of the anthropogenic warming (see Fig. 1.2). Gámiz-Fortis et al. (2011) have shown that the Sea Surface Temperature (SST) of the Atlantic Ocean is able to account for about 12% of the north-western European land surface temperature variance. These authors also stress that the AMO influence on European temperature is not only regional-dependent, but also non-stationary in time, as links change significantly throughout the decades.

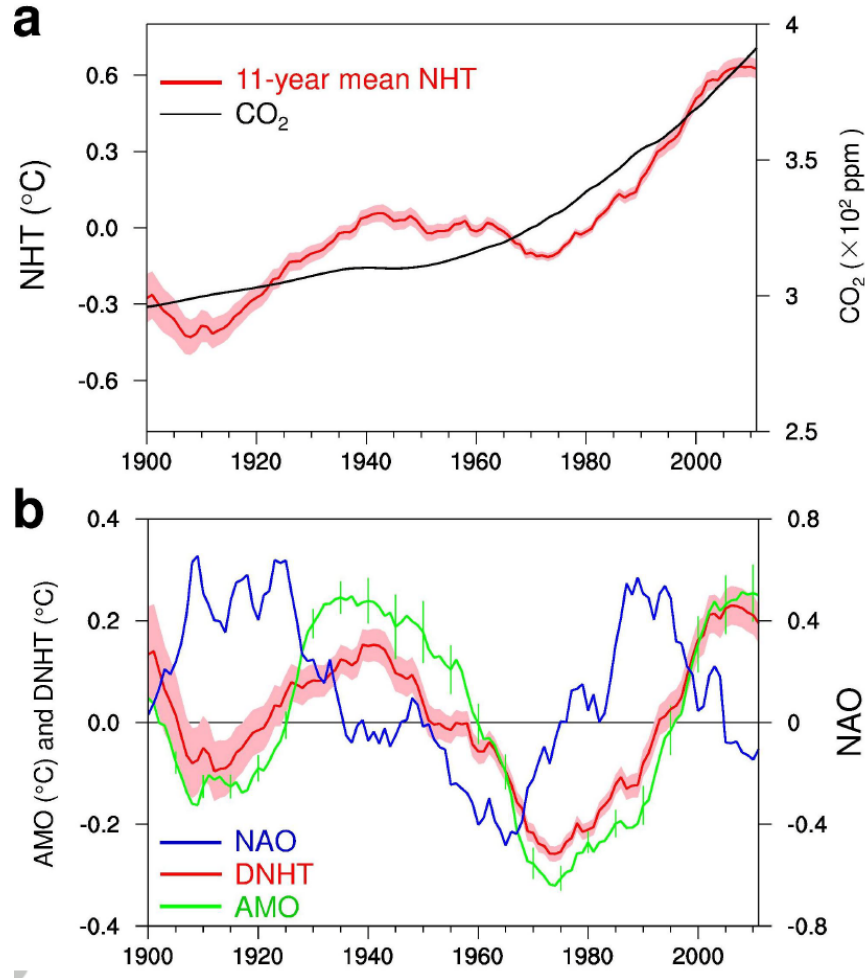


**Fig. 1.2** a) The 11-year running mean (red line) Northern Hemisphere temperature (NHT) anomalies from the HadCRUT4 dataset, relative to the base period 1961–1990. The black line shows the global atmospheric CO<sub>2</sub> concentrations. b) The 11-year running means of the de-trended Northern Hemisphere Temperature (DNHT), the North Atlantic Oscillation (NAO) and the Atlantic Multi-decadal Oscillation (AMO). The pink shaded areas in (a) and (b) show the 2-sigma uncertainty ranges. **From Li et al. (2013).**

At the inter- and intra-annual temporal scales, multi-decadal variability modes, such as the AMO and PDO are not critical due to the intrinsic mismatch of temporal scales. Instead, emphasis must be oriented toward large-scale teleconnection patterns which in turn modulate atmospheric circulation conditions at shorter spatio-temporal scales. With this aim, a number of different methodological approaches have been developed to derive the most important large-scale patterns of atmospheric circulation, particularly those affecting Europe and North America, as summarized in major review works (e.g. Wallace and Gutzler, 1981; Yarnal, 1993; Barry and Carleton 2001). Besides the methodology to extract the relevant atmospheric patterns, many authors have been particularly interested in evaluating the associated impacts on the surface climate at the continental and regional scales. In Europe, some of the most important circulation patterns are connected with anomalies of the North Atlantic eddy-driven Jetstream, particularly

## 1. Introduction

for winter. These most relevant circulation modes are depicted in Fig.1.3, namely: a) North Atlantic Oscillation (NAO); b) East Atlantic (EA); c) East Atlantic / Western Russia (EA/WR); d) Scandinavian (SCA) patterns. In other seasons, the climate of the region is also influenced by remote patterns from subtropical latitudes, as well as global phenomena, often involving atmosphere-ocean interactions (García-Herrera and Barriopedro, 2017).

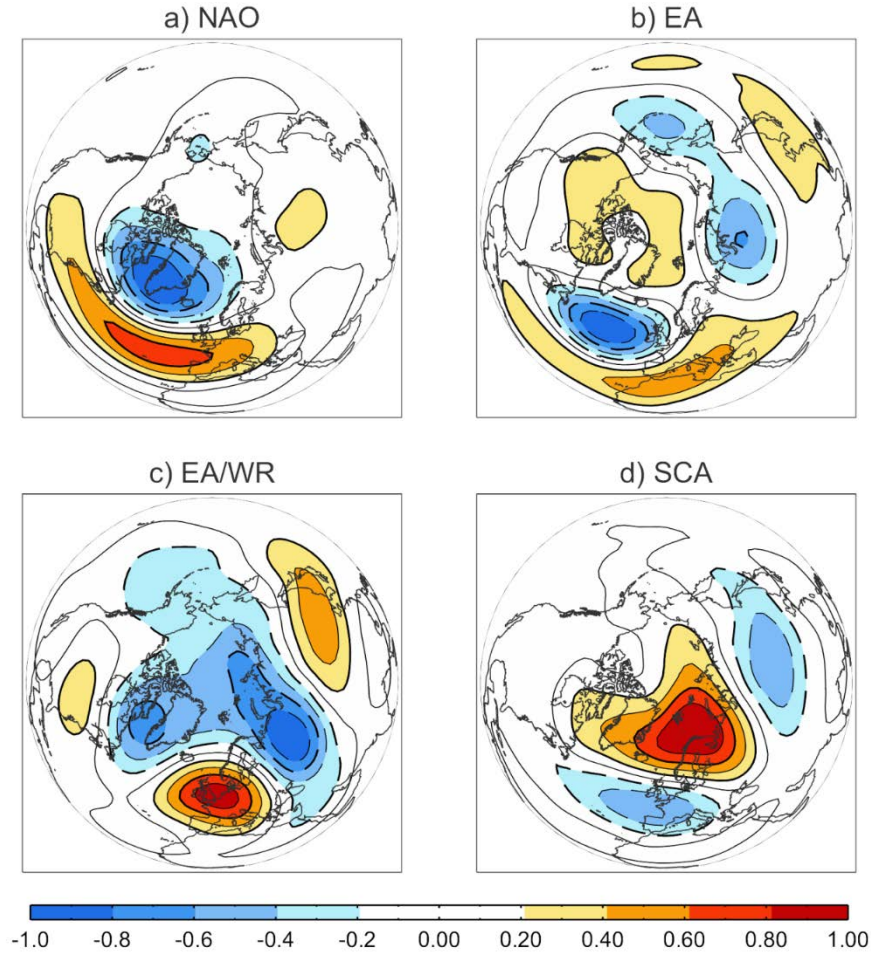


**Fig. 1.3** Spatial patterns of regression for the Principal Components Analysis of NH geopotential height fields at 500 hPa during winter.

The NAO (Fig. 1.3a) is the leading mode of atmospheric circulation variability over the Euro-Atlantic sector, and is characterized by a seesaw of atmospheric mass between the Iceland Low and the Azores High (e.g., Hurrell and Deser 2009). On intra-seasonal time-scales, the NAO is associated with variations in the latitude of the North Atlantic Jetstream and storm-tracks, while on the inter-annual time-scales it characterizes changes in their strength (Woollings et al., 2014). Regarding the European temperature responses to NAO, characterized by warmer conditions in central and northern Europe during its positive phase, it has been shown that besides its phase, the exact location of the NAO centers of action is more determinant in southern than in central and northern Europe (e.g. Castro-Díez et al., 2002). Also, the particularities of the summer NAO - characterized by a meridional dipole with low pressures over Greenland and high

## 1. Introduction

pressures over the UK - have also been explored. For example, its positive phase promotes cold and wet summers in central and eastern Mediterranean (Bladé et al. 2012; Mariotti and Dell'Aquila 2012). Other atmospheric circulation patterns (e.g., SCA, EA and EA/WR) become also quite relevant in terms of inter-annual variability of temperature at the European and regional scales (e.g. Trigo et al., 2008; García-Herrera and Barriopedro, 2017). Fig. 1.4 shows the most relevant modes of variability for this variable in European areas, including the Mediterranean basin.

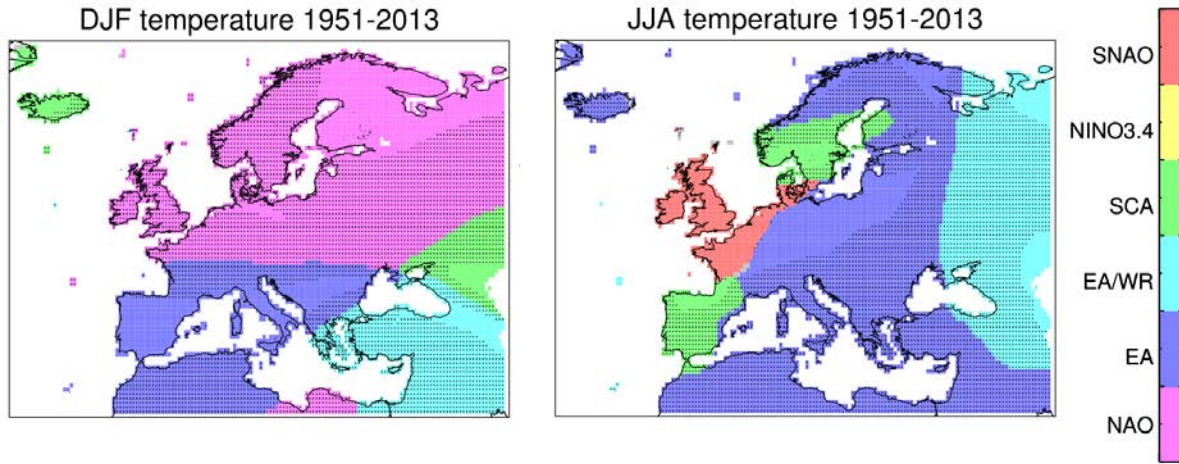


**Fig. 1.4** Spatial distribution of the dominant large-scale phenomenon influencing temperature inter-annual variations during winter (DJF, left panel) and summer (JJA, right panel) seasons of the 1951-2013 period. Colors identify the large-scale phenomenon with the largest Pearson correlation coefficient with seasonal-mean temperature data. Dots highlight areas displaying significant correlations with more than one teleconnection pattern. The following large-scale phenomena are considered in the analysis: North Atlantic Oscillation (NAO), East Atlantic pattern (EA), East Atlantic / Western Russian pattern (EA/WR), Scandinavian pattern (SCA), El Niño index (NINO3.4) and the high-summer NAO (SNAO). *Adapted from García-Herrera and Barriopedro (2017).*

As mentioned above, atmospheric teleconnections are closely related to the occurrence of specific weather regimes, such as atmospheric blocks, albeit often not explicitly. As better described in Section 1.2, atmospheric blocking is associated with disruptions of the usual westerly flow from a few days to weeks, thus causing significant changes in the synoptic environment (Trigo et al., 2004; Silmann and Croci-Maspolli, 2009), and consequently on the regional temperature in Europe. This topic will be discussed in detail in Chapter 2.

### 1.1.2 European temperature extremes

There is a vast literature focusing on European temperature extremes, including both cold and hot extremes, regional impacts, and the atmospheric circulation patterns which enhance them (e.g. Barriopedro et al., 2011, Horton et al., 2015). Several studies have pointed that anomalies in the North Atlantic atmospheric flow are crucial to modulate winter, spring and autumn

## 1. Introduction

---

occurrences of both cold nights and warm days in Europe (e.g. Andrade et al., 2012; Cattiaux et al., 2012). More specifically, atmospheric blocking is tightly linked with the occurrence of extreme temperature events (Trigo et al., 2004; Buehler et al., 2011; Pfahl, 2014), although the majority of the studies focus on cold extremes during the winter season only.

In recent years, some exceptional extreme cold winter episodes have occurred in Europe, such as the 2009-2010 winter (Cattiaux et al., 2010), driven by record persistent negative phases of the NAO and enhanced blocking conditions. The late stages of the 2011-2012 winter were also exceptionally cold over large parts of Europe, and took place after the occurrence of a Sudden Stratospheric Warming episode (WMO, 2012). Further back in time, a close link between anomalously cold winters in Europe and enhanced blocking occurrence had already been explored by Lejenäs (1989), presenting the winter of 1941-1942 as a vivid example. The blocking-driven frigid conditions were associated with some of the most poignant episodes of World War II, particularly the dramatic siege of Leningrad. Similarly, the historical cold winter of 1962-1963, one the bitterest seasons of the 20<sup>th</sup> century in the UK (see Table 1.1), was recently explored by Burt (2013), who reported prolonged cold temperatures that were only comparable to episodes occurring in one of the coldest periods of the last millennium, i.e. during the so-called Late Maunder Minimum (LMM, ca. 1685–1715 - Wanner et al. 1995; Luterbacher et al. 2001, 2004; Xoplaki et al. 2005). Several studies have suggested that the LMM exhibited recurrent winter anticyclonic conditions over eastern Europe (Luterbacher et al. 2001; Jacobeit et al. 2003; Pauling et al. 2006). More specifically, Wanner et al. (1995) indicated an enhanced blocking frequency in the 1690's decade, and Kington (1999) indicated that in the 1698 winter, the circulation over the British Isles was dominated by blocking conditions.

**Table 1.1** Ranked coldest top 10 months and winters in Central England, for the period 1659-2013. From Burt (2013).

Rank	December	January	February	Winter
1	-0.8 1890	-3.1 1795	-1.9 1947	-1.2 1684
2	-0.7 2010	-3.0 1684	-1.8 1895	-0.4 1740
3	-0.5 1676	-2.9 1814	-1.7 1855	<b>-0.3 1963</b>
4	-0.3 1788	-2.8 1740	-1.6 1740	0.4 1814
5	-0.3 1796	<b>-2.1 1963</b>	-1.1 1986	0.5 1795
6	-0.3 1878	-2.0 1716	-1.0 1684	0.7 1695
7	-0.2 1874	-1.6 1776	<b>-0.7 1963</b>	0.7 1879
8	0.3 1784	-1.5 1709	-0.2 1956	0.8 1716
9	0.3 1981	-1.5 1838	0.0 1692	1.0 1679
10	0.4 1844	-1.5 1881	0.1 1942	1.0 1681

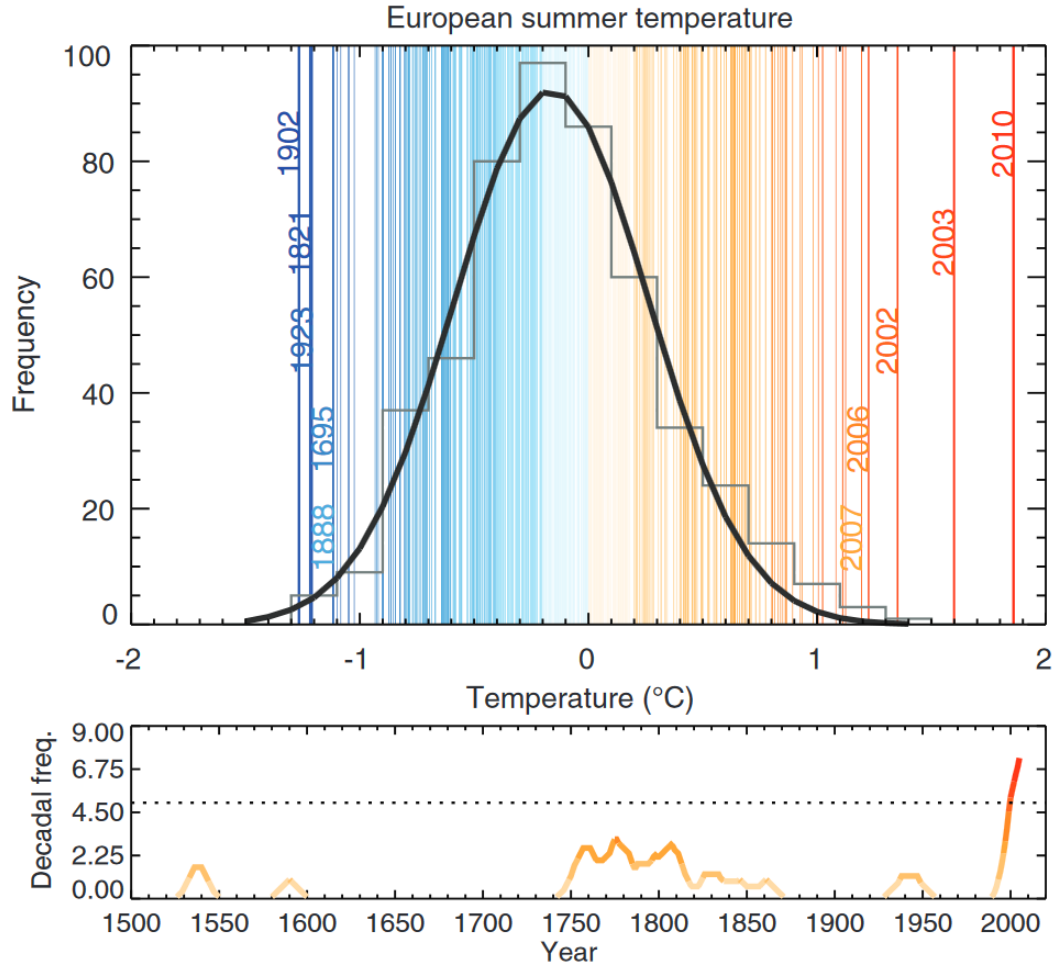


**Fig. 1.5** European summer temperatures for 1500-2010. Statistical frequency distribution of best-guess reconstructed and instrument-based European ( $[35^{\circ}\text{N}, 70^{\circ}\text{N}]$ ,  $[25^{\circ}\text{W}, 40^{\circ}\text{E}]$ ) summer land temperature anomalies (degrees Celsius, relative to the 1970-1999 period) for the 1500-2010 period (vertical lines). The five warmest and coldest summers are highlighted. Gray bars represent the distribution for the 1500-2002 period, with a Gaussian fit in black. (Bottom) The running decadal frequency of extreme summers, defined as those with temperature above the 95th percentile of the 1500-2002 distribution. A 10-year smoothing is applied. Dotted line shows the 95th percentile of the distribution of maximum decadal values that would be expected by random chance. **From Barriopedro et al. (2011).**

Some of the most remarkable extreme temperature episodes in Europe correspond to recent major summer heatwaves, sometimes coined mega-heatwaves (Barriopedro et al. 2011; Miralles et al., 2014). The striking heatwave of 2003 affected large parts of western and central Europe, and caused substantial socio-economic impacts, including excessive mortality, damages in agricultural crops (Poumadere et al., 2005; García-Herrera et al., 2010) or intensive wildfires (e.g. Trigo et al., 2006b). This persistent episode, culminating in the first two weeks of August, reached summer temperature anomalies as large as  $5^{\circ}\text{C}$  (Black et al., 2004). Another outstanding episode occurred in the summer of 2010 - the warmest summer at the European scale since at

least 1500 (Barriopedro et al. 2011). This prolonged episode caused unprecedented catastrophic wildfires, and increased mortality in Russia. These mega-heatwaves lasted for a period longer than usual and achieved record-breaking temperatures over extensive swathes of land, thus being also unusual from a full summer seasonal perspective (Fig. 1.5). While the exceptional 2010 Russian event was unambiguously associated with persistent blocking over the area (e.g., Barriopedro et al. 2011; Dole et al. 2011), the characterization of the weather conditions that occurred during the mega-heatwave of 2003 was not so clear, with some studies pointing to blocking systems (e.g., Trigo et al., 2005) and others suggesting an anomalous northward intrusion of sub-tropical ridges (e.g., García-Herrera et al. 2010). Given the outstanding effects of the 2003 event, it is of paramount importance to characterize these two weather systems and disentangle their associated impacts. This question will be further addressed in Section 1.2.

### 1.1.3 European precipitation regimes

A wide range of approaches to characterize atmospheric circulation and its links with European precipitation regimes is available in the literature, ranging from teleconnection patterns to weather type catalogues (e.g., Barry and Carleton 2001). The role of the NAO has been recurrently analyzed, with its positive phase being associated to a stronger Jetstream and wetter conditions in central and northern areas of Europe (e.g. Trigo et al., 2008), and drier than average conditions in southern areas of the European continent (Lavers and Villarini, 2013). This dipole of positive (negative) correlation between the NAO and precipitation in northern (southern) regions represents the leading canonical correlation mode between atmospheric circulation and European precipitation inter-annual variability (e.g., Trigo et al., 2008). This signature is particularly relevant in autumn, winter and spring, with weaker links obtained in summer, where the NAO effects are more restricted to northern areas of the continent and the Balkans (Folland et al., 2009; Bladé et al. 2012). Vicente-Serrano and López-Moreno (2008) have analyzed the nonstationary influence of the NAO in European precipitation, pointing to inter-decadal shifts in the location of the NAO pressure centers, and to a general trend towards a strengthening of the NAO-precipitation relationship over most of Europe during the 20<sup>th</sup> century.

Other teleconnection indices have been widely linked with anomalous European precipitation, such as the SCA (related to high-latitude blocking occurrence over Scandinavia), or the EA pattern (Trigo et al., 2008; García-Herrera and Barriopedro, 2017). Figure 1.6 shows the European areas affected by some of the most relevant modes of variability for precipitation inter-annual variability. The role of global phenomena such as ENSO should also not be disregarded (Pozo-Vázquez et al., 2005; Bulic et al., 2012). Taking into account the reasonable predictability of the ENSO, several authors have explored this link in order to improve the skill of seasonal forecast for Europe. However, this is not easy to achieve, as the influence of the ENSO signal on the European climate is seasonal- and regional-dependent, not linear with respect to the magnitude of the ENSO event, and depends on other inter-annual and even inter-decadal variability modes (e.g. Brönnimann, 2007).

At shorter time scales, several authors have linked Weather Types daily classifications with precipitation regimes. For example, Cortesi et al. (2014) used a Lamb classification to analyze the spatial variability of Iberian precipitation, following pioneering works in this topic, such as Trigo and DaCamara (2000). Circulation Weather Types have often been used to characterize regional responses, as they are usually defined and calibrated on relatively small domains, thus reflecting atmospheric configurations at synoptic. Differently, European precipitation responses to large-scale atmospheric systems, such as blocking, can be explored by describing blocking-related synoptic conditions (Trigo et al., 2004). Using this approach, European blocking has been found to exert a large influence on winter precipitation over large areas of Europe (Trigo et al., 2004). For seasons other than winter, the impacts of blocking remain unexplored. In addition, a regional classification of blocking is needed, since blocking occurrence within different longitudinal sectors can lead to very distinct synoptic configurations. These questions will be addressed in Chapter 3, paying special attention to the precipitation responses over the Iberian Peninsula in Chapter 4.

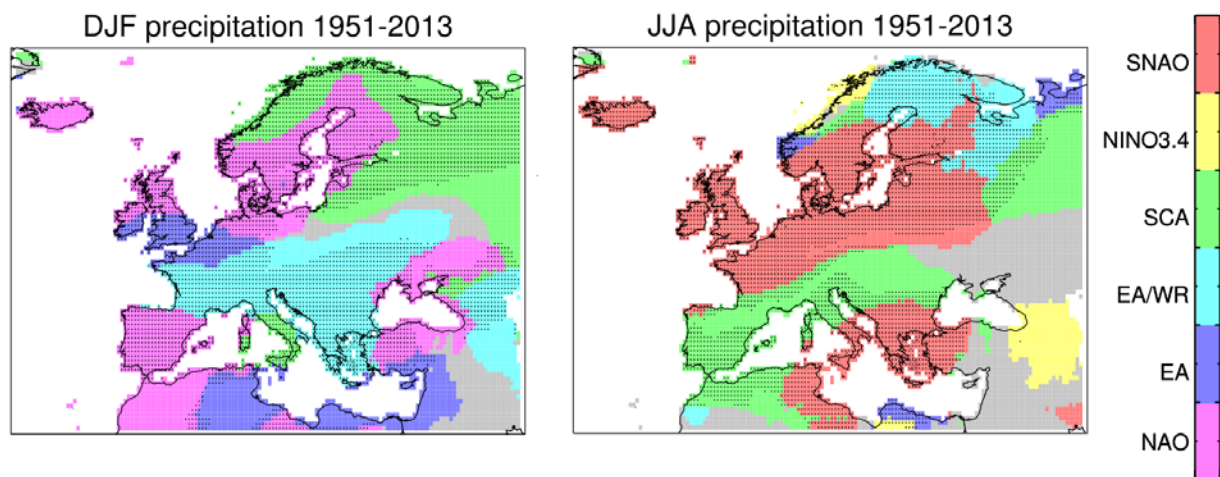


**Fig. 1.6** Spatial distribution of the dominant large-scale phenomenon influencing precipitation inter-annual variations during winter (DJF, left panel) and summer (JJA, right panel) seasons of the 1951-2013 period. Colors identify the large-scale phenomenon with the largest Spearman correlation coefficient with seasonal-mean precipitation data. Dots highlight areas displaying significant correlations with more than one teleconnection pattern. The following large-scale phenomena are considered in the analysis: North Atlantic Oscillation (NAO), East Atlantic pattern (EA), East Atlantic / Western Russian pattern (EA/WR), Scandinavian pattern (SCA), El Niño index (NINO3.4) and the high-summer NAO (SNAO). *Adapted from García-Herrera and Barriopedro (2017).*

### 1.1.4 Drought conditions throughout the 20th century

Droughts are complex events with severe environmental, economic and social impacts. From a meteorological and hydrological point of view, droughts can be defined as shortages in water availability throughout prolonged periods, which may be considered at different time-scales, depending on the specific water resource we are interested in (Vicente-Serrano et al., 2010).

## 1. Introduction

In Europe, droughts have recurrently affected wet areas, such as western and central Europe (Rebetez et al., 2006), eastern Europe (Spinoni et al., 2013) or Scandinavia (Hisdal et al., 2006). Spinoni et al. (2015) have shown that droughts have been more frequent in northern Europe and Russia in the 1950s and 1960s, whilst for central areas it was during the 1970s, and for southern European regions in the later decades of the 20<sup>th</sup> century (see Fig. 1.7). In agreement with such assessment, Lloyd-Hughes and Saunders (2002) stated that the secular trend in rainfall has been positive in the region from the Alps to northern Scandinavia, while a drying tendency is found for eastern Europe and Mediterranean regions.

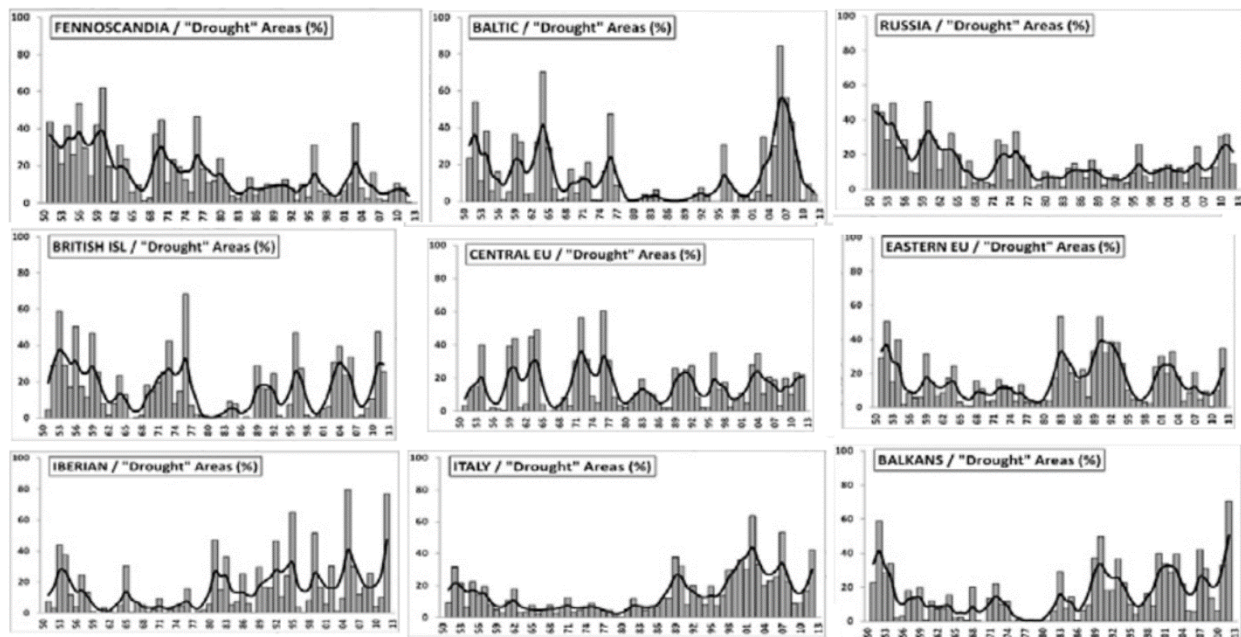


**Fig. 1.7** Annual series of areas in drought conditions (12-month scale) for different European regions. The bold lines represent the 5-year moving weighted averages. *Adapted from Spinoni et al. (2015).*

Overall, most concerns have been centered in semi-arid regions, such as southern Europe, and in particular, over the Mediterranean basin (Hoerling et al., 2012; Vicente-Serrano et al., 2014). The observed drying trends (particularly notable in the late 20th century) have persisted during the beginning of the 21<sup>st</sup> century. Major drought episodes have occurred in the western Mediterranean during 2005 (García-Herrera et al., 2007) and 2012 (Trigo et al., 2013a), with an almost continuous drought in the eastern Mediterranean and the contiguous unstable area of the Fertile Crescent (Trigo et al., 2010; Kelley et al., 2015). This has raised concerns on water availability in the region, especially taking into account the drying and warming projected scenarios for the Mediterranean area (e.g. Giorgi and Lionello, 2008), with the resulting increases in evapotranspiration demand and drought severity (Vicente-Serrano et al. 2010).

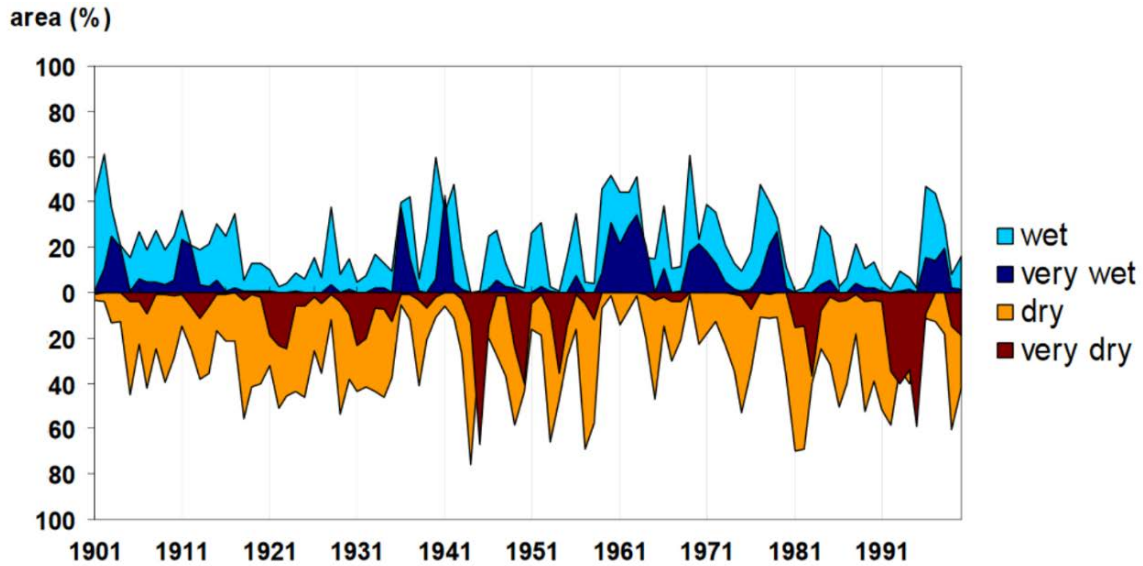


**Fig. 1.8** Percentages of area under wet (blue) and dry (orange) conditions in the Mediterranean basin during the 20<sup>th</sup> century. *From Sousa et al. (2011).*

Sousa et al. (2011) studied the trends and extremes in drought conditions in the Mediterranean and a few subareas during the 20th century (Fig. 1.8). They found that the positive phase of the NAO during winter is the main large-scale circulation pattern driving severe moisture scarcity in southwestern Europe, while the SCA pattern becomes more relevant for central Mediterranean areas (in agreement with the precipitation assessment provided in Fig. 1.6). The link between water balance and sustained anomalies in European, which are strongly connected to perturbations in the mean zonal flow, suggests that atmospheric blocking may play a role in the hydrological balance. This issue will be further discussed in Chapter 5.

## 1.2. Atmospheric blocking: climatology and associated impacts

### 1.2.1 Blocking definition

There is no universally accepted definition for atmospheric blocking, although it can be fundamentally described as a suppression of the normal westerly flow in mid-to-high latitudes due to the presence of a relatively stationary high-pressure system. In this sense, several features are generally accepted as specific characteristics of a standard blocking system, as summarized by Barriopedro et al. (2010a), namely:

- 1) a large-scale high pressure system with a quasi-stationary anticyclonic circulation located on the usual track of the prevailing westerlies;
- 2) spatio-temporal signatures typical of the large-scale, with lifetimes spanning from a few days to several weeks;

The traditional definition of blocks consists in a split-flow regime, with an associated low-pressure system located southwards of the blocking structure (Rex 1950b). However, such a dipole is not observed during the so-called Omega block, where the flow reversal is tightly connected to a high-latitudinal extension of the sub-tropical ridge belt, and negative anomalies in the geopotential height field are located southwest and southeast of the blocking center (Barriopedro et al., 2006). Two examples of these typical blocking patterns are depicted in Fig. 1.9.

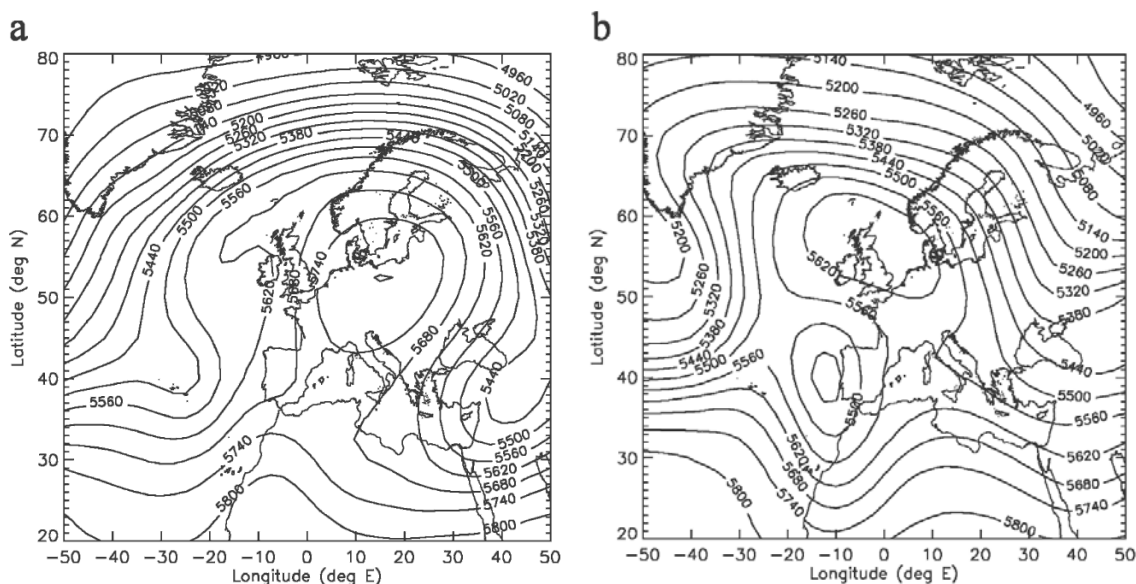


**Fig. 1.9** The 500-hPa height field showing typical blocking patterns: (a) Omega block (6 Mar 1948) and (b) Rex block (23 Dec 1948). **From Barriopedro et al. (2006).**

The exact definition of blocking has been a matter of wide discussion in the scientific community, and several indices and methodologies for detection have been developed. As expected, the use of different definitions may result in discrepancies in the blocking climatologies, namely in their frequency and location (Barriopedro et al., 2010a). Most of the approaches have been based on the 500 hPa geopotential height (Z500) or, on dynamical fields (vertically integrated Potential Vorticity, PV, or Potential Temperature on the dynamical tropopause, PT). Generally speaking, these algorithms impose certain criteria in terms of minimum spatial extension and temporal duration (some criteria are objective and other subjective). Still, there are profoundly different rationales in these methodologies, particularly in what concerns the use of absolute vs. anomaly (departure) fields. As such, blocking methodologies can be classified into two groups:

- 1) The flow reversal or wave-breaking approach, which identifies blocks as an easterly geostrophic flow around a reference Jetstream latitude, using absolute Z500 or PT fields (e.g., Tibaldi and Molteni, 1990; Trigo et al., 2004; Barriopedro et al., 2006);
- 2) Persistent departures from the climatological mean of the Z500 or PV fields (e.g. Dole and Gordon, 1983; Knox and Hay, 1985; Schwierz et al., 2004).

These methodologies, originally proposed by Tibaldi and Molteni (1990) and Dole and Gordon (1983) and, hereafter TM and DG, respectively, have been modified with further features and criteria in subsequent works (e.g. Barriopedro et al. 2006, 2010a; Masato et al., 2011).

All methods present specific caveats and shortcomings. Regarding the DG index, some of the main criticisms are based on the difficulty of defining proper thresholds for blocking detections, and the fact that a variety of synoptic situations which cannot be defined as blocking may be detected as so, such as northward shifts of the jet or amplifications of subtropical or subpolar anticyclones. Methodologies based on departure fields, such as DG have also the disadvantage of requiring longer time-series, in order to create robust climatological reference fields (Barriopedro et al., 2010a).

On the other hand, the 1-D nature of the TM methodology is a limiting factor, not allowing the 2-D description of the blocking structure. Another limitation of this method has been ascribed to the eventual identification of blockings due to the occurrence of cut-off lows. Also, early stages of block development and some Omega blocks can be missed using this approach, due to the too demanding extension and flow reversal criteria. Several modifications to the original algorithm have been introduced in order to minimize such problems, including a 2-D extension of the TM method (e.g., Barriopedro et al. 2006; Woollings et al. 2008; Davini et al. 2012a). Using this 2-D diagnosis of blocking, Davini et al. (2012a) explored the distinction between high-latitude and low-latitude blocking, noting that the latter structures are unable to divert or completely block the zonal flow. This example highlights the need to distinguish high- and low-latitude high pressure systems and to explore their dynamical characteristics, as detailed in the following subsections.

Throughout this thesis, the climatology of high-latitude blocking and the impacts on the European continent will be addressed relying on the catalogue developed by Barriopedro et al.

## 1. Introduction

(2006), which results from a 2-D adapted version of the Tibaldi and Molteni (1990) index. A schematic of this automated detection algorithm is presented in Fig. 1.10, using daily Z500 data on a  $2.5^\circ \times 2.5^\circ$  grid as input.

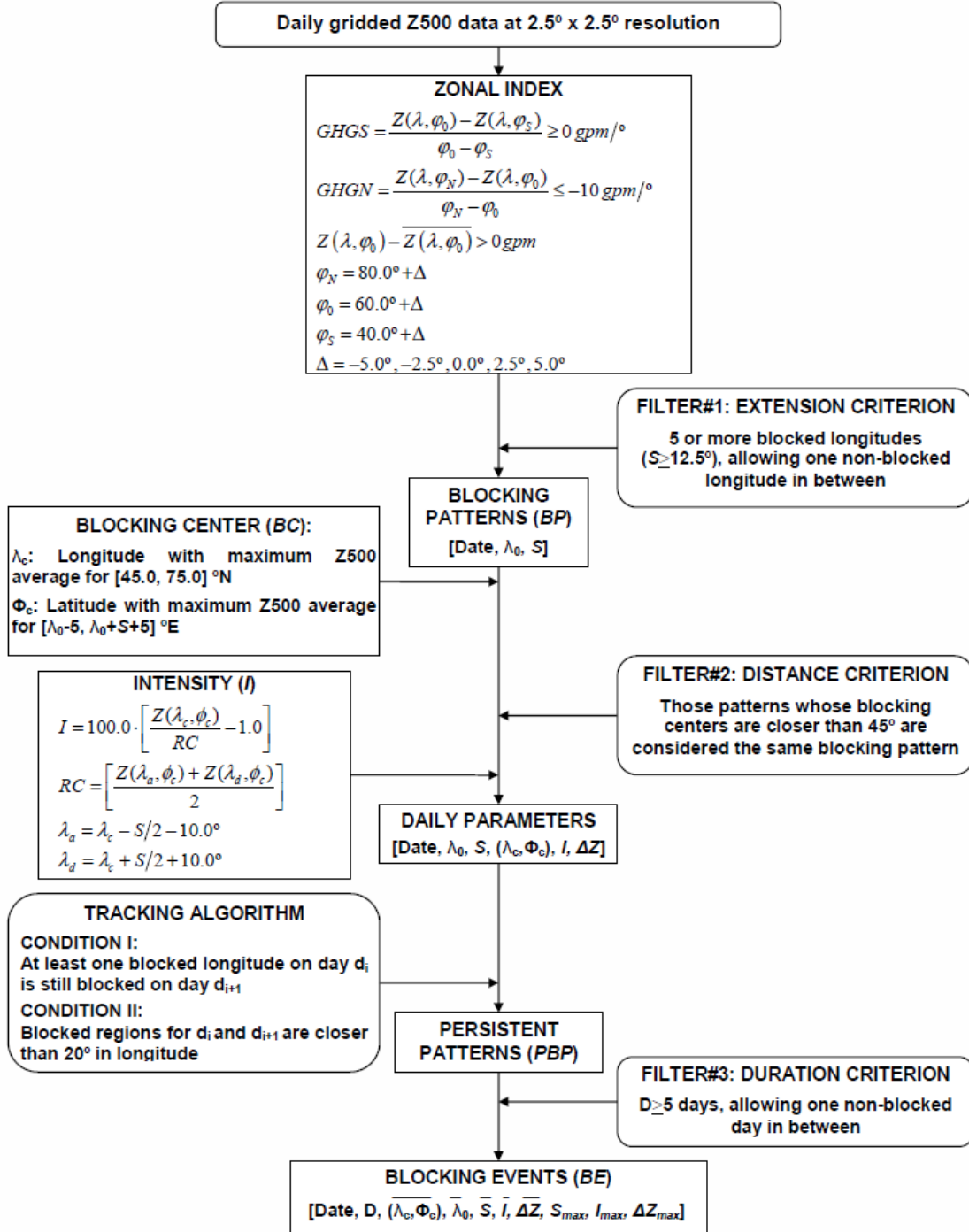


**Fig. 1.10** Schematic of the automatic blocking detection method used throughout the thesis. *From Barriopedro et al. (2006).*

According to the scheme from Fig. 1.10, two Z500 gradients ( $GHGN$  and  $GHGS$ ) have been simultaneously computed for each longitude on the NH and for each day of study, where  $Z(\lambda, \phi)$  is the Z500 at a given longitude  $\lambda$  and latitude  $\phi$ .  $GHGS$  is proportional to the zonal geostrophic wind component and provides a measure of the zonal flow intensity for each longitude, while  $GHGN$  is imposed in order to exclude non blocked flows. A given longitude is considered blocked when both  $GHGN < -10 \text{ gpm}^\circ$  and  $GHGS > 0 \text{ gpm}^\circ$  for at least one of the five  $\Delta$  values, evaluated around a reference latitude  $\Phi_0$ , and simultaneously the  $Z(\lambda, \Phi_0)$  anomaly is positive. A large-scale instantaneous blocking pattern is detected when there are at least five blocked longitudes. The method includes a tracking algorithm to follow the daily evolution of these blocking patterns by demanding a minimum overlapping between them, and a blocking event is said to occur when the blocking pattern persists for at least five days.

This detection scheme also incorporates a procedure to detect the 2-D center of each blocking pattern (defined as the gridpoint with the maximum Z500 within the anticyclonic flow), and the blocking intensity. The final catalogue includes individual blocking events, tracked on a daily basis, with daily information about their central location, longitudinal extension and intensity. In this thesis, this daily catalogue is used to identify blocking occurrence in different longitudinal sectors, according to their central location, as it will be described in detail further ahead in Section 2.1

Furthermore, taking advantage of the Z500 gradients ( $GHGN$  and  $GHGS$ ), a catalogue of strong zonal westerly flows is also computed, by simply identifying days with zonal flow as those characterized by  $GHGS < 22.5 \text{ gpm}^\circ$ , following the approach developed in Trigo et al. (2004). This distinction between zonal and blocked days will be exploited in the following Chapters.

### 1.2.2 Euro-Atlantic blocking climatology

Some fundamental characteristics of blocking climatology in the NH, and in the particular frame of the Euro-Atlantic sector, are discussed in this section. For this purpose, the blocking catalogue described in Section 1.2.1 has been used, and several diagnostics such as frequency of occurrence, mean duration, mean extension, and blocking life-cycles are herein presented. The comprehension of these blocking climatological features is an important first step to understand their associated impacts in different meteorological fields at local and regional scales, as it will be discussed throughout the remaining chapters of this thesis.

There are two preferential areas of blocking occurrence in the NH, which overlap with the climatological regions of wave amplification and the exit zones of the principal storm-tracks (i.e., the eastern sides of the Atlantic and Pacific oceans, e.g., Barriopedro et al. 2010a). This is clear in Fig. 1.11, which shows the annual and seasonal frequencies of the blocking centers. The largest frequencies are located in the longitudes surrounding the Greenwich Meridian (between the British Isles and Scandinavia), and near the international date line in the Pacific area. Even though they occur throughout the whole year, blocking is more frequent during winter and spring (e.g. Tibaldi et al., 1994, Barriopedro et al., 2006; Masato et al., 2011). In summer, there is a

## 1. Introduction

smoother distribution, with a larger tendency for blocking to occur in continental areas and at higher latitudes. In the Euro-Atlantic region, this northeastward migration of blocking locations leads to a third smaller maximum close to the Urals mountain range, a feature already known (Tibaldi and Molteni, 1990; D'Andrea et al., 1998). In autumn, Pacific blocking occurrence decreases, while it persists in the Euro-Atlantic region, although less frequently when compared to winter and spring. Overall, these preferred locations at the seasonal scale are in agreement with those found in other works that used either subjective identification of blocks or detection schemes based on the TM approach (Treidl et al. 1981; Wiedenmann et al. 2002).

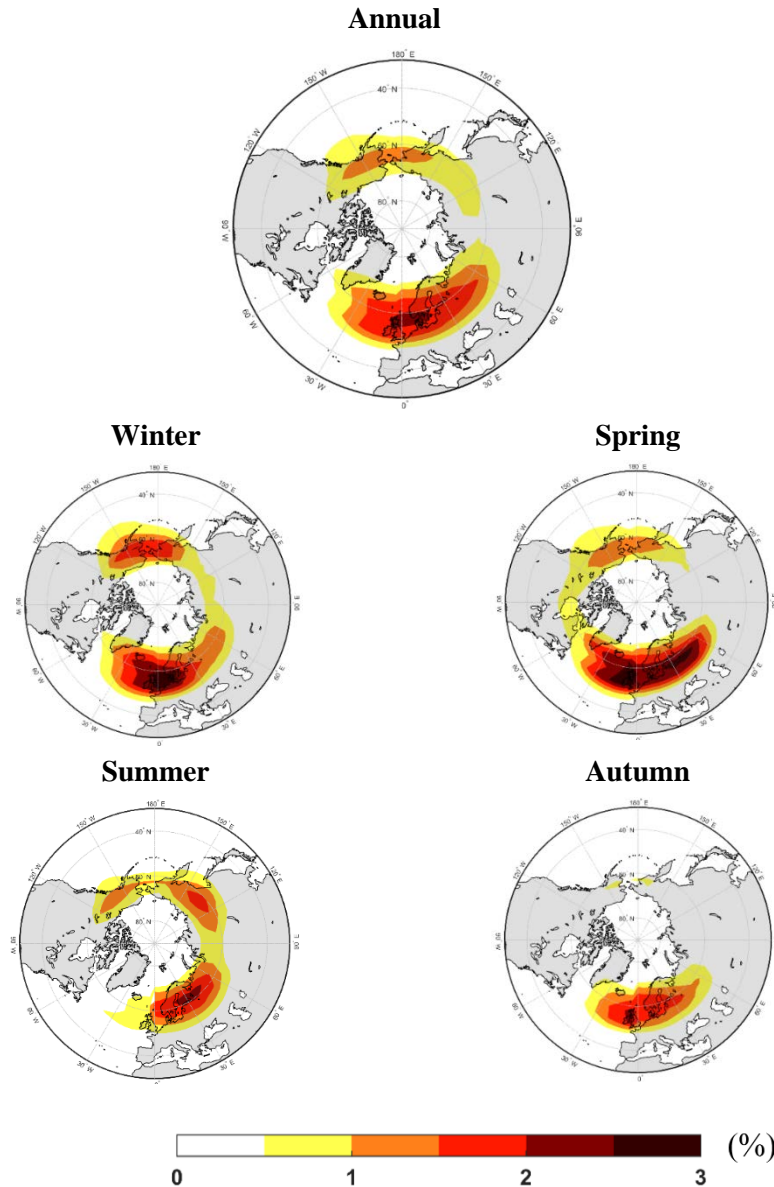


**Fig. 1.11** Climatological mean blocking center frequency (in percentage of days per year/season), computed in boxes of  $5^\circ \times 5^\circ$  for the period 1950-2012.

## 1. Introduction

---

The duration distribution of NH blocking episodes presents the well-known one side tailed distribution (Fig. 1.12). This is observed through the whole year, although long-lasting blocks (more than 20 days) are more frequent in winter and spring. A similar seasonal behavior is observed for the spatial extension of the blocking patterns (not shown), with blocking covering larger areas during the coldest seasons of the year.

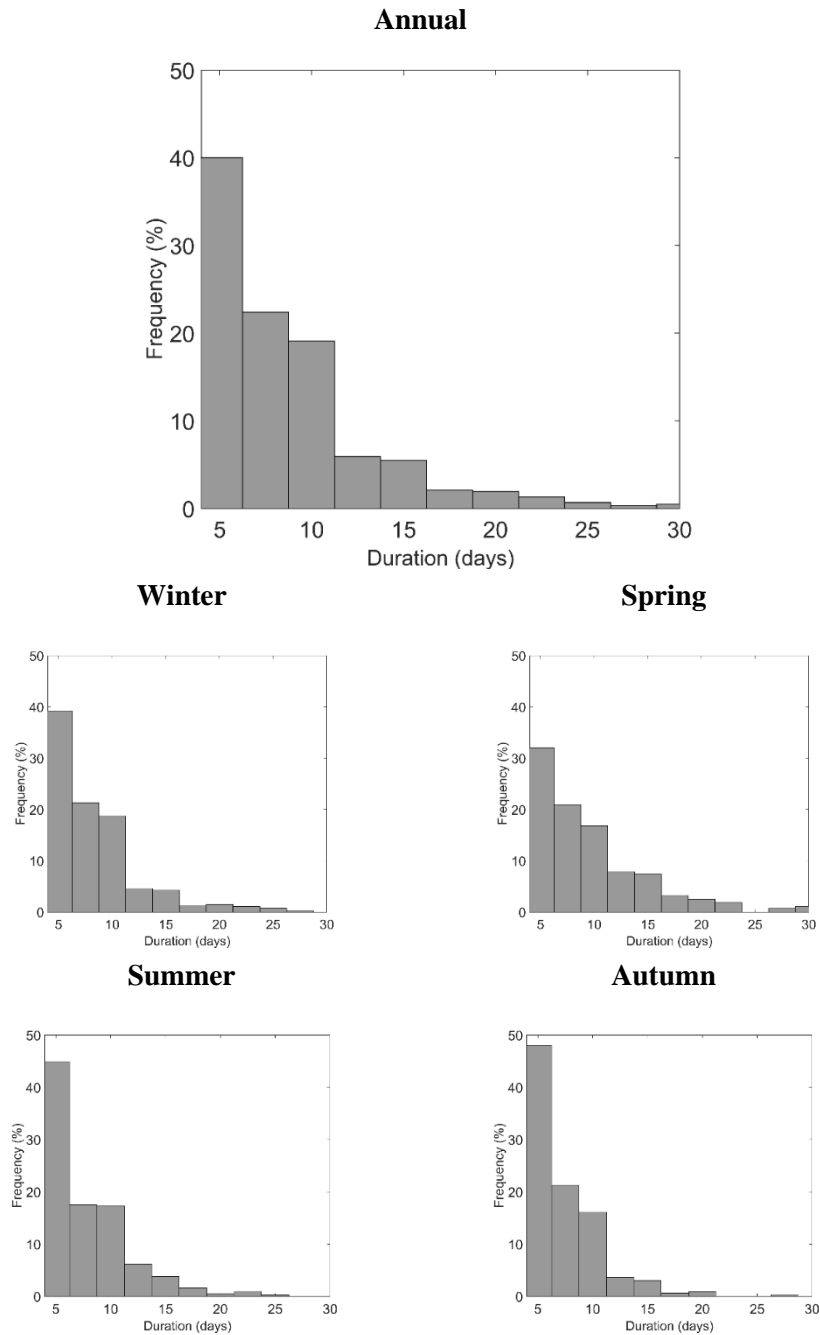


**Fig. 1.12** Climatological distributions of blocking episodes duration in the Northern Hemisphere for the period 1950-2012.

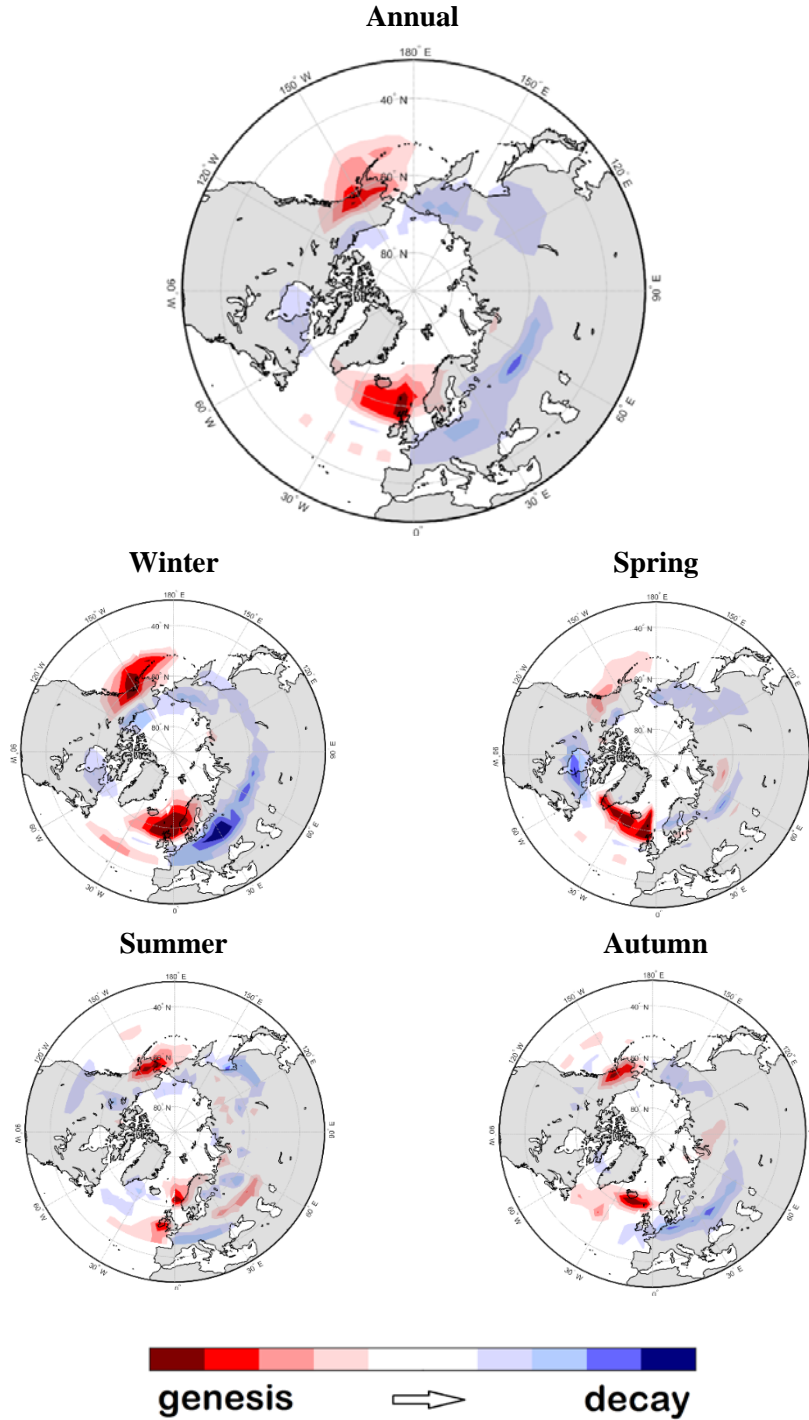


**Fig. 1.13** Climatologically preferred blocking genesis and decay locations for the period 1950-2012. Red (blue) areas represent locations where the difference between the percentage of days with blocking centers in the early and mature stages is positive (negative). The two first (last) days of detection within the life cycle of each blocking event were considered for early (mature) stages.

Understanding blocking genesis and decay processes throughout the whole blocking life-cycle is not a simple task. The existent literature on this topic will be discussed in Section 1.2.3. As a first approach on this subject, the preferred locations for blocking genesis and decay are shown herein in Fig. 1.13. To do so, the differences in the frequencies of blocking center locations during their onset (two first days of detection) and decay (last two days of detection) in each geographical location were computed. Taking into account the averaged blocking persistence (~8 days), Fig. 1.13 corroborates the quasi-stationary character of blocking, with a slight tendency for Euro-Atlantic blocks to slowly migrate eastwards during their lifecycle, and a more unclear displacement pattern for Pacific blocks.

### 1.2.3 Blocking life cycle: onset, maintenance and decay

The life-cycle of blocks is influenced by both large-scale waves and small-scale perturbations (Nakamura et al., 1997; Tsou and Smith, 1990). The blocking life-cycle has been a widely discussed topic in the literature, both from a dynamical point of view, and also to evaluate the ability of models to represent blocking phenomenology (e.g., D’Andrea et al., 1998; Scaife et al., 2010). A good model performance in simulating blocking becomes relevant in operational forecasts and climatological contexts, with the latter framing both to model the mid-latitude climate, as well to perform reliable climate projections (Barriopedro et al., 2010b; Davini and D’Andrea, 2016).

#### *Blocking precursors and onset*

The onset of blocks is closely related to the amplification of planetary waves and their underlying mechanisms, such as: a) planetary wave-wave interaction (Égger, 1978; Kung et al., 1990; DaCamara et al., 1991), including resonant amplification between free and topographic Rossby waves (Tung and Lindzen 1979), b) non-linear interactions between synoptic and planetary-scale waves (Shutts 1983; Tsou and Smith, 1990; Lupo and Smith, 1995). More specifically, transient eddy activity is considered to play a crucial role in the genesis and maintenance of block, primarily through feedbacks between synoptic eddies and the large-scale flow (e.g., Yamazaki and Itoh, 2009).

The precursor role of the synoptic-scale has been widely studied. Altenhoff et al. (2008) confirmed the existence of precursor signals several days (up to 10) prior to blocking onset, namely: 1) a coherent wave-train emanating approximately 110° upstream of Atlantic blocking; 2) a long-lived northerly wind signal preceding Pacific blocking. Masato et al. (2011) distinguished the influence of cyclonic and anticyclonic wave-breaking towards blocking onset, as well as the separation between warm/cold air extrusions (as depicted in Fig. 1.14). The authors found that anticyclonic breaking dominates over Europe, as previously discussed by Martius et al. (2007) or Gabriel and Peters (2008), while cyclonic breaking tend to occur mainly over oceanic areas.

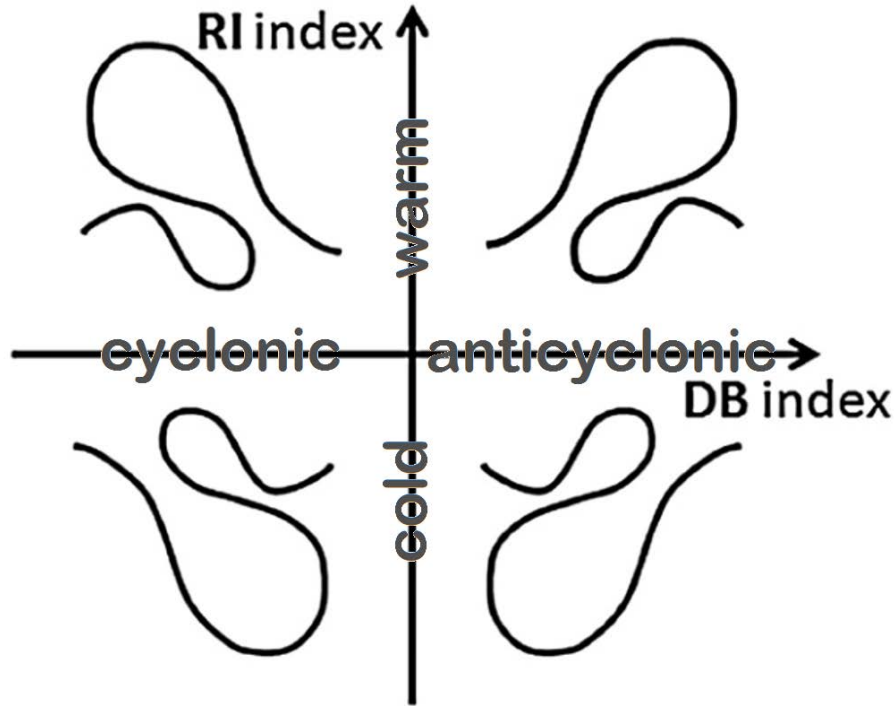


**Fig. 1.14** Schematic for the Direction of Breaking (DB) and Relative Intensity (RI) phase space plot. On the x-axis is DB, while on the y-axis is RI. Positive values of DB are for anticyclonic wave breaking and positive values of RI indicate warm air extrusion dominance. As sketched, a unique wave-breaking type is identified for each quadrant of this plot. *Adapted from Masato et al. (2011).*

Michel et al. (2012) have shown that during the onset of Scandinavian blocks, Atlantic cyclones display trajectories towards northern Scandinavia, associated with anticyclonic wave-breaking in the upper troposphere. With such atmospheric configurations, low PV air masses are advected northeastwards contributing to this type of wave-breaking over Europe and preventing the occurrence of cyclonic wave-breaking further west. As a consequence, the occurrence of blocks in the eastern Atlantic is not favored under such atmospheric patterns. On the other hand, blocks originating in the Atlantic and Greenland area are preceded by a rapid poleward deflection of low PV values towards the southeast of Greenland, which acts as a barrier for the downstream motion of cyclones, favoring a cyclonic wave-breaking in the Atlantic region.

Croci-Maspolli et al (2007) and Woollings et al. (2008) have explored the dynamical links between blocking and the NAO. Woollings et al. (2010a) further discussed how features such as the NAO and EA patterns (which are associated to the location of the eddy-driven jet over the Atlantic) are closely linked to blocking occurrence. These studies have shown that blocking reinforces the pre-existing negative NAO phases, and that long-lasting blocks may even instigate phase changes in the NAO (from positive to negative). Also, blocking genesis locations vary according to the NAO phase (Fig. 1.15). Such findings highlight that small-scales may force larger-scales.

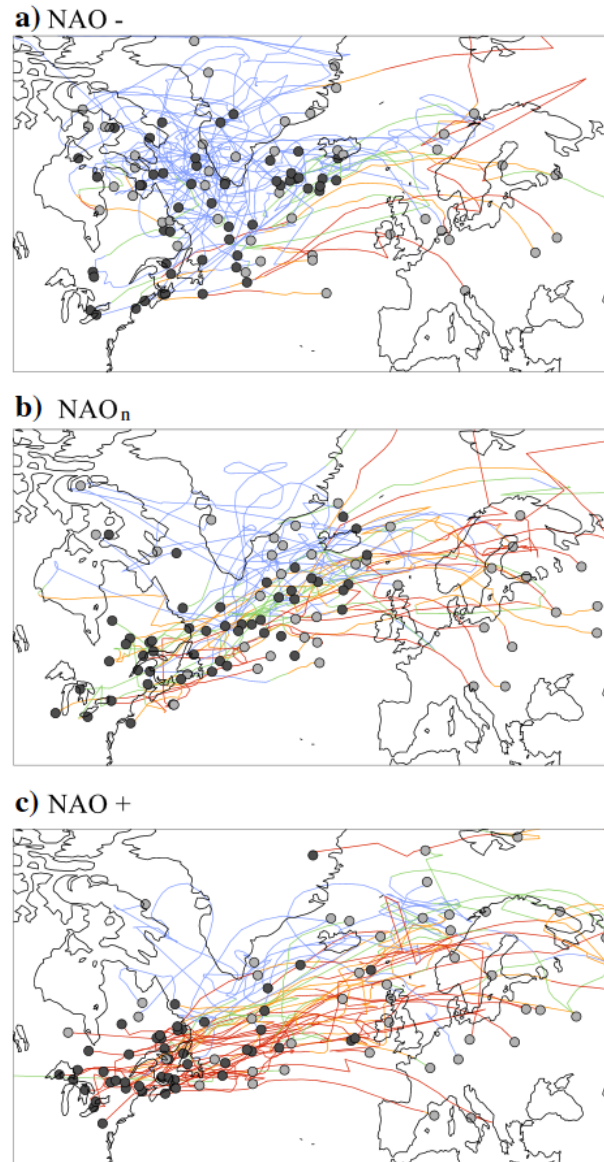


**Fig. 1.15** Distribution of winter blocking genesis (dark dots) and lysis (light dots) with the corresponding track lines during **a** negative, **b** neutral, **c** positive NAO phases in the Atlantic region. The color scaling indicates four partitions of the index values, namely; blue  $NAO < -0.34$ ; green  $NAO < 0$ ; orange  $NAO > 0$ ; red  $NAO > 0.52$ . **From Croci-Maspoli et al. (2007).**

More recently, a particular emphasis has also been devoted to the coupling between stratospheric dynamics and blocking occurrence, particularly during the incidence of major Sudden Stratospheric Warmings (SSWs). These SSW events are characterized by a significant weakening of the polar cyclonic vortex and an abrupt warming of the polar stratosphere during the extended winter. SSWs result in stratospheric anomalies that can propagate downwards towards the troposphere in the form of negative values of the Northern Annular Mode (NAM, e.g., Baldwin and Dunkerton 2001). The tropospheric NAM is associated to significant anomalies in the Jetstream and hence in blocking occurrence (e.g., Davini et al. 2014).

Interestingly, the SSW-blocking link is not purely one-directional, and the role of blocks on forcing SSWs has also been discussed by several authors (e.g. Martius et al., 2009; Nishii et al., 2011; Barriopedro and Calvo 2014). In addition to internal atmospheric dynamics, external forcings may also modulate blocking onset, such as: snow cover (García-Herrera and Barriopedro, 2006), solar activity (Barriopedro et al., 2008) or the AMO (Martinez, 2014).

### **Blocking maintenance**

The comprehension of processes responsible for blocking maintenance is a complex subject, which led several authors to make use of numerical models.

Works such as Green (1977) and Shutts (1983) detail the Eddy Straining Mechanism (ESM), where transient eddies act to maintain the blocking through the input of anticyclonic vorticity to the western flank of the block, thus indicating a contribution of the high frequency for the development and sustainment of blocks (see Fig. 1.16a). Synoptic eddies are strained by the block in the north-south direction, and provide negative (positive) vorticity to the blocking high (low), which maintains the blocking dipole against dissipation. The meridional stretching of Rossby waves in the blocked area can in turn result in additional synoptic disturbances (Tanaka 1998). The positive feedback can be lost by a subtle change in the synoptic forcing (Maeda et al. 2000, Arai and Mukougawa 2002). The ESM is not so clear for Omega-type blocks, as a split/meridional dipole is not present. In these blocks, a different mechanism, the Selective Absorption Mechanism (Yamazaki and Itoh 2009, see Fig. 1.16b) has been proposed. Accordingly, the blocking high selectively absorbs the anticyclonic vorticity of the transient anticyclones, reinforcing its low potential vorticity, while synoptic cyclones will either travel south and downstream of an Omega-type block, or be attracted to the blocking low in a dipole-type block, in both cases maintaining the whole blocking structure.

The important role played by transient eddies in blocking maintenance is well recognized (e.g. Green, 1977; Dole, 1986), although some authors consider that these feedbacks are secondary contributors, and that low-frequency dynamics should still be considered as the primary driver of blocking intensification and maintenance (e.g., Nakamura et al. 1997).

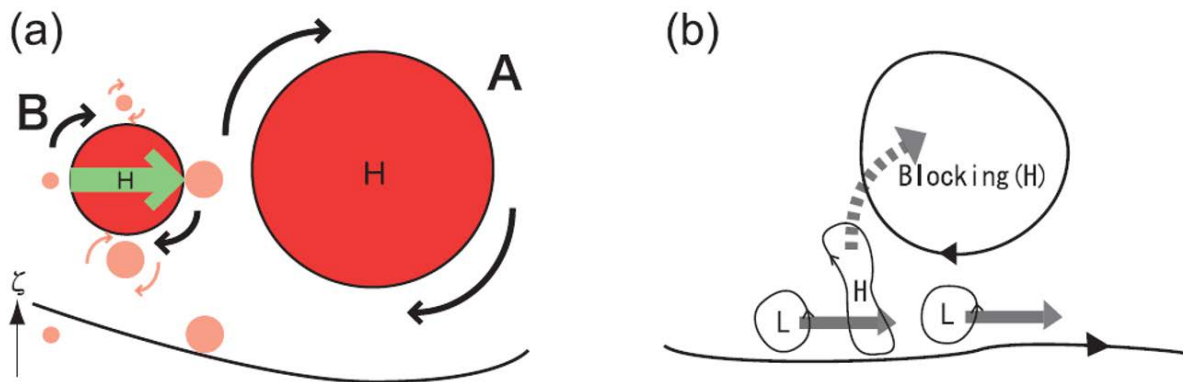


**Fig. 1.16** Schematic representation of: a) the Eddy Straining Mechanism; b) the Selective Absorption Process. From Yamazaki and Itoh (2009).

### ***Blocking decay***

As discussed above, the planetary scale is very influential in the blocking onset. This is also valid regarding the decay phase of blocking systems. Nakamura et al. (1997) attributed blocking decay to the low-frequency dynamics, more precisely, to the downstream emanation of a quasi-stationary Rossby wave train, as also pointed out by Dole (1986, 1989) and Black (1997). Haines and Holland (1998) suggested that blocking regimes may persist for, as long as, the large-scale flow remains balanced and does not become unstable or transition to a new state.

Michel et al. (2012) have shown that during the decay process of Scandinavian blocks, cyclonic wave-breaking is more frequent than the anticyclonic type. Blocks located in the referred area usually decay throughout a transition to a Greenland anticyclone, driven by a sustained advection of low PV under curved cyclone trajectories over the mid-Atlantic. This agrees with the previous work of Nakamura et al. (1997), whom already noted an eastward shift of the low-PV center concurrent with the slow retrograding high pressure center when blocking decay begins. Croci-Maspoli et al. (2007) noted that in its decaying phase, blocking is characterized by a strong decrease of the spatial scale irrespective of the block type and geographical location. This implies some difficulties for tracking algorithms to correctly characterize the final stages of the blocking life-cycle.

### **1.2.4 Sub-tropical ridges**

A sub-tropical ridge is often regarded as an extension of the sub-tropical high pressure belt northwards into mid-latitude areas. This atmospheric structure is usually characterized by a meridional stretch of anomalously high values in the Z500 field. The synoptic pattern acts as a “barrier” for the local westerly flow, thus disturbing the zonal circulation at sub-tropical latitudes, similar to the blocking action on the extratropical Jetstream. However, and unlike high-latitude blocks, the Jetstream does not split into two branches. Instead, it is reinforced and pushed northwards of the ridge structure, although often embedded in a much larger-scale meandering circulation with alternating ridges and troughs (Fig. 1.17). Furthermore, the full connection between the ridge structure and the sub-tropical high pressure area prevents a reversal of the zonal flow on the eastern and western flanks of the system, contrarily to canonical blocking systems.

From a more dynamical point of view, a sub-tropical ridge is not necessarily accompanied by a wave-breaking event as blocks do (see Section 1.2.3) and may (or may not) evolve into a blocking structure at a later stage. In the case of blocking, the early stages may be characterized by a sub-tropical or an extra-tropical ridge structure, which eventually breaks and becomes partially or fully isolated from the sub-tropical belt at higher latitudes (Woollings et al., 2011). As ridges and blocks may correspond to different stages of the same wave-breaking event, the distinction between a more traditional Rex-type block and an Omega-type block should be once again considered. Frequently, an Omega block structure represents the intermediate stage between a sub-tropical ridge, and a final isolated Rex block. In fact, in pioneering studies on this topic, blocking systems were often defined as “blocking ridges”, although authors were referring

specifically to blocks with wave-breaking (e.g. White and Clark, 1975). Recent works, such as Santos et al. (2009) or Woollings et al. (2011) have addressed in more detail sub-tropical ridges (defined as strong persistent ridge events – SPREs) in the eastern Atlantic area. The latter work highlights the differences between ridges occurring with and without posterior Rossby wave-breaking, as presented in Fig. 1.18. Ridges with Rossby wave-breaking display similar signatures to the so-called low-latitude blocking events (Davini et al. 2012a), including a strengthened and northward shifted Jetstream.

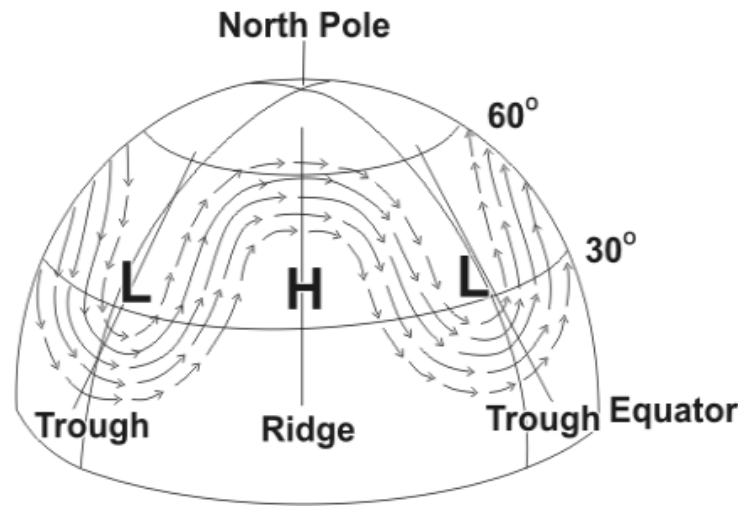


**Fig. 1.17** Idealized atmospheric circulation around a sub-tropical ridge in the Northern Hemisphere. From [http://www.cmosarchives.ca/ProjectAtmosphere/module9 westerlies and the jet stream e.html](http://www.cmosarchives.ca/ProjectAtmosphere/module9%20westerlies%20and%20the%20jet%20stream%20e.html).

Low-latitude blocks are very different from high-latitude blocks, which instead, are associated to a weakening and reversal of the extra-tropical Jetstream. In this sense, attending to the characteristic perturbations that these weather systems impinge on the Jetstream, it can be concluded that the low-latitude and high-latitude blocks display larger differences than sub-tropical ridges with and without Rossby wave-breaking. In order to address the distinct impacts of these weather systems, it is mandatory to separate high-latitude blocks and subtropical ridges, the latter group including both, those with Rossby wave-breaking (i.e., low-latitude blocks) and those without it. These low-latitude structures will be named as sub-tropical ridges (or simply ridges) throughout the remaining of the thesis. In order to perform this disentanglement, an automated ridge detection algorithm was developed, as published in Sousa et al. (2017b). The complete description of the methodology will be addressed further ahead, in Section 2.1.

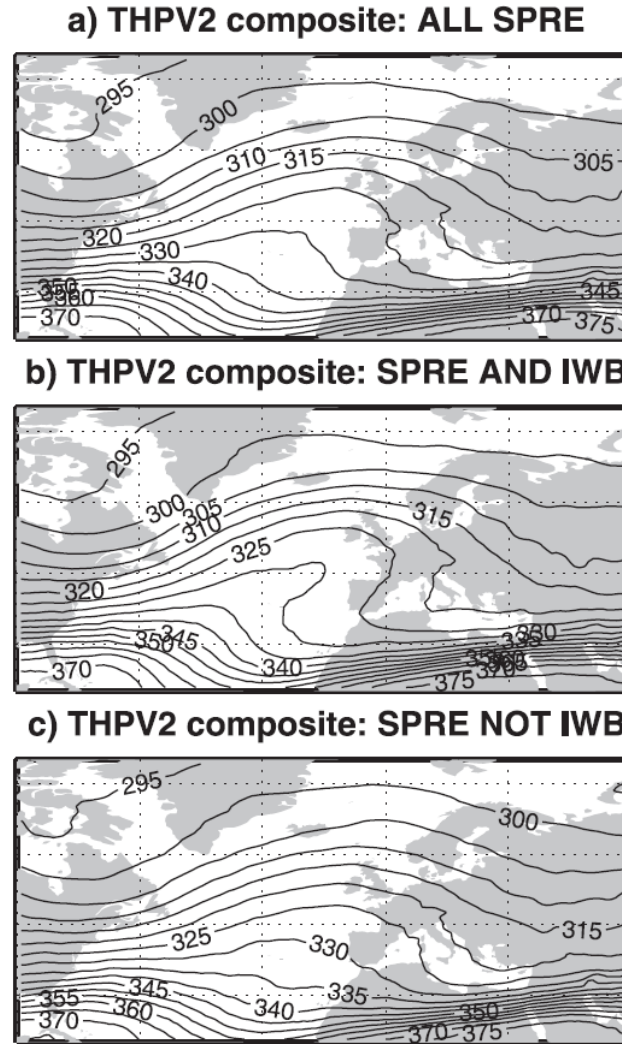


**Fig. 1.18** Composites of potential temperature (K) on the 2-PVU (Potential Vorticity Units) surface for the sets of days with a) Strong Persistent Ridge Events; b) Strong Persistent Ridge Events with wave-breaking in the vicinity of Iberia; c) Strong Persistent Ridge Events without wave-breaking. From Woollings et al. (2011).

### 1.2.5 Blocking and ridges impacts

Blocking occurrence is related to anomalous weather conditions over wide areas of the mid and high latitudes. Trigo et al. (2004) firstly explored in a long-term context the European precipitation and temperature responses to winter blocking occurrence over the whole Euro-Atlantic sector (Fig. 1.19). As shown in that study, blocking is associated with prolonged cloudless and dry periods in the areas under the blocking high. Euro-Atlantic winter blocks also tend to deflect storm-tracks to northern or southern areas of the continent, often increasing precipitation in the Mediterranean (Trigo et al., 2004). On the other hand, the meridional circulation associated with blocks favors the advection of cold air from higher latitudes, thus

promoting cold winter spells over the European continent (Buehler et al., 2011; Sillmann et al., 2011). However, the regional responses and the involved processes can be highly dependent on the specific location of the blocking system (e.g., García-Herrera et al. 2007), and on the specific season in which they occur.

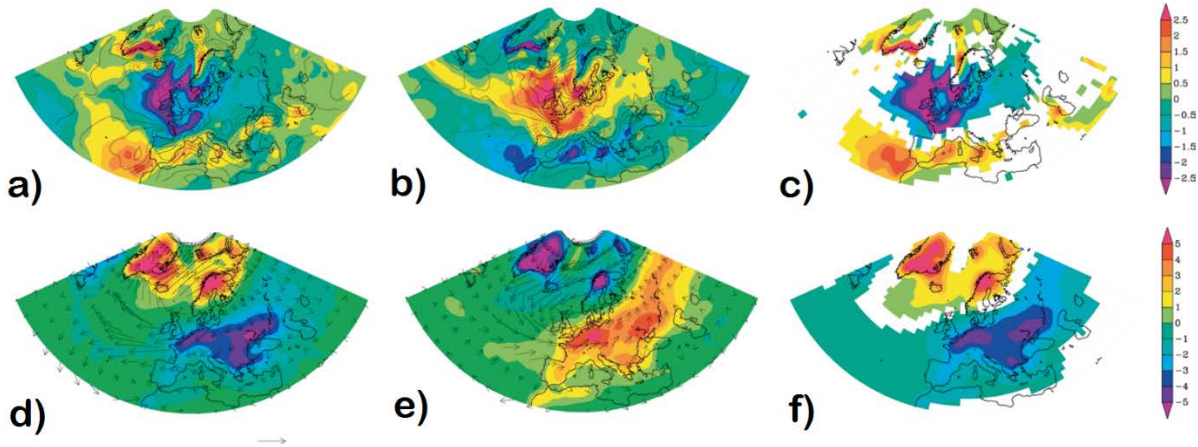


**Fig. 1.19** Upper panels - anomalies of the precipitation rate (shading,  $\text{mm}\cdot\text{day}^{-1}$ ) for winter composites of: a) blocking episodes, b) non-blocking episodes, and c) their difference (represented only if significant at the 5% level). Solid (dashed) contours in a) and b) show positive (negative) values of the 10 m vorticity anomaly field, with intervals in  $0.2 \cdot 10^{-6} \text{ s}^{-1}$ . Lower panels: anomalies of the daily maximum temperature field ( $^{\circ}\text{C}$ ) for winter composites of: d) blocking episodes, e) non-blocking episodes, and f) their difference (represented only if significant at the 1% level). The arrows in a) and b) show the respective anomaly of the 10 m wind field ( $\text{m}\cdot\text{s}^{-1}$ ). **From Trigo et al. (2004).**

Therefore, a good characterization of the synoptic environment associated to blocking patterns is crucial in the assessment of their impacts. In addition, a regional classification of blocking is mandatory, since blocking occurrence within different sectors of the Euro-Atlantic-Russian area can lead to very distinct atmospheric configurations. Taking these facts into account, it was considered a priority in this thesis to: 1) update results from previous works using higher resolution datasets to better characterize the regional/local responses; 2) characterize the associated impacts as a function of the specific blocking location (thus defining distinct longitudinal sectors of blocking occurrence); 3) extend previous analyses to other seasons and to extreme episodes; 4) better characterize the associated synoptic environment and underlying processes; 5) distinguish the blocking impacts from those associated to ridges, whose effects have not been described so far over the European continent.

### 1.3 Goals and structure of the thesis

In this thesis, a thorough description of blocking occurrence and the associated impacts on the European climate is provided, by distinguishing regional blocking patterns in three sectors within the Euro-Atlantic region: a western (Atlantic), a central (European) and an eastern (Russian) sector. Furthermore, a clear separation between opposite regimes of the Jetstream is explored, by distinguishing periods of: 1) strong zonal flow, and 2) high-latitude blocking. Sub-tropical ridges are herein considered among the synoptic systems that are associated with strong Jetstream episodes. The consideration of sub-tropical ridges is further motivated by the need to distinguish the impacts of blocking from those associated to high-pressure systems occurring at sub-tropical latitudes. This separation is necessary in order to clarify a relatively widespread misuse of blocking patterns when attributing extreme temperatures events (both hot and cold), a misconception that still abounds in the literature.

Thus, the main objectives of this thesis are:

- 1) Characterize the blocking impacts in the European climate (temperature and precipitation), according to their location;
- 2) Develop a novel detection scheme for sub-tropical ridges;
- 3) Distinguish the impacts of high-latitude blocking from the ones associated to other large-scale patterns (zonal flows and ridges), and the underlying processes;
- 4) Perform a finer description of the aforementioned impacts at the regional scale, with special emphasis on the Iberian Peninsula;
- 5) Explore impacts in extreme temperature and precipitation events, as well as in derived fields with socio-economic relevance (e.g. droughts, wildfires).

The thesis is structured around three core chapters that correspond to the three published papers comprising the main outcome of the work performed during the PhD (Sousa et al., 2016, Sousa et al., 2017a and Sousa et al., 2017b). Given that the three papers are integrally presented as they were published, there are some unavoidable repetitions in the chapter sections addressing datasets, methodology and climatologies. It must also be noted that the order of the chapters does not follow the chronological order of the publications (taking into consideration the need to present the disentanglement between blocking and ridges at an early stage of the thesis). However, some additional unpublished material has been included in the required Chapters to provide coherence to the thesis. This extra material corresponds to additional sections in Chapters 3 and 4 and to the outlook of Chapter 5.

The thesis is structured as follows:

- **Chapter 1** introduced overviews on: 1) the large-scale variability and its influence on the European climate; 2) blocking definitions, climatology and the dynamics behind its life-cycle, as well as the distinction between blocking and ridges.

- **Chapter 2** introduces the methodology used to detect sub-tropical ridges in order to distinguish them from high-latitude blocks (Sousa et al., 2017b). A comprehensive characterization of the impacts on European temperature and extreme events associated to both patterns is then performed, outlining the relative roles of the involved mechanisms.

- **Chapter 3** describes the specific impacts of regional blocks on European precipitation, precipitation extremes, and the associated synoptic environment (Sousa et al., 2017a). The distinct impacts of blocking and strong zonal flow (herein including ridges) regimes on regional precipitation distributions are addressed in this chapter. Furthermore, the responses in solid precipitation (i.e., snow cover) to regional blocking occurrence are also presented.

- **Chapter 4** presents the detailed impacts of blocks in the Iberian Peninsula, relying on precipitation (Sousa et al., 2016) and temperature datasets at higher spatial resolutions than those used in previous chapters. Similar to the larger-scale analyses, changes in the regional precipitation distributions, extreme events and the driving mechanisms are explored.

- **Chapter 5** summarizes the Conclusions, and the main achievements of this thesis. It also highlights the topics of research that remain open after the work performed during the PhD. In particular, it provides preliminary insights on the impacts of blocks/ridges in other relevant variables at the European scale (such as drought variability and wildfire occurrence). A brief outlook at future changes in blocking/ridge occurrence is also presented in this section.

In **Annex**, two additional studies which were published during the course of this PhD are presented (Sousa et al., 2015; Trigo et al., 2013b). Although these works are not directly connected with the main motivation of this PhD, their datasets and part of the addressed topics are discussed throughout this thesis.

## Chapter 2

# European temperature responses to blocking

### Contents

---

#### **2.1 Paper in *Climate Dynamics***

*2.1.1 Introduction*

*2.1.2 Data and Methods*

*2.1.3 Results*

*2.1.3.1 Blocking and ridge seasonal distribution*

*2.1.3.2 Seasonal temperature responses*

*2.1.3.3 Synoptic and forcing mechanisms*

*2.1.3.4 Changes in regional temperature distribution*

*2.1.4 Discussion and Conclusions*

*2.1.5 Supplementary Material*

---

### Summary

#### **Context and objectives**

This chapter is devoted to the characterization of the seasonal impacts of blocks and ridges on European temperature at continental and regional scales by using the E-OBS dataset, as described in Sousa et al. (2017b). Section 2.1.2 provides a novel approach to disentangle high-latitude blocks from sub-tropical ridges. Geopotential height (Z500) from the NCEP/NCAR dataset is used to develop a catalogue of sub-tropical ridges, which will be employed throughout the remaining of this thesis. As an important novelty, the temperature impacts of blocking and ridges are disentangled by considering three different sectors of occurrence (ATL, EUR and RUS) within the Euro-Atlantic region. Special attention is paid to explore extreme temperature events and the driving mechanisms of the temperature responses associated to each considered atmospheric pattern.

#### **Methods**

An algorithm based on exceedances of Z500 thresholds (against the daily climatology) in three longitudinal consecutive sectors (ATL, EUR and RUS) was developed to detect ridges, avoiding their overlap with blocking occurrence. These two catalogues are used to compute composites of minimum and maximum temperatures for each regime and sector. An analysis of the tendency equation was performed, detecting the main contributing term to the regional temperature anomalies induced by each weather regime. This was supported by a surface radiative budget decomposition. Finally, changes in regional extreme temperature occurrences were examined.

#### **Results**

There are substantial differences in the European 2 m temperature responses to blocking and ridge regimes, particularly during winter. While winter blocking (essentially in the ATL and EUR sectors) leads to generalized below average temperatures and cold spells, prompted by cold advection from northerly flows, mild winter days occur during ridge regimes, with increases up to 7°C in parts of central Europe, through enhanced transport from Atlantic air masses and reduced long-wave cooling.

During summer, both atmospheric patterns are associated with warmer temperatures in central and northern Europe. However, in southernmost countries, and in particular in the Mediterranean area, only ridges (mainly those occurring in the EUR sector) exert a large influence on the occurrence of hot summer days. During this season, and for both weather regimes, the anomalous radiative heating due to enhanced clear sky conditions plays a leading role in explaining the positive temperature anomalies over continental areas.

### 2.1 Paper in *Climate Dynamics*

*Pedro M. Sousa, Ricardo M. Trigo, David Barriopedro, Pedro M. M. Soares, João A. Santos*

*Paper published in Climate Dynamics (2017b)*

Blocking occurrence and its impacts on European temperature have been studied in the last decade. However, most previous studies on blocking impacts have focused on winter only, disregarding its fingerprint in summer and differences with other synoptic patterns that also trigger temperature extremes. In this work, we provide a clear distinction between high-latitude blocking and sub-tropical ridges occurring in three sectors of the Euro-Atlantic region, describing their climatology and consequent impacts on European temperature during both winter and summer.

Winter blocks (ridges) are generally associated to colder (warmer) than average conditions over large regions of Europe, in some areas with anomalies larger than 5°C, particularly for the patterns occurring in the Atlantic and Central European sectors. During summer, there is a more regional response characterized by above average temperature for both blocking and ridge patterns, especially those occurring in continental areas, although negative temperature anomalies persist in southernmost areas during blocking.

An objective analysis of the different forcing mechanisms associated to each considered weather regime has been performed, quantifying the importance of the following processes in causing the temperature anomalies: horizontal advection, vertical advection and diabatic heating. While during winter advection processes tend to be more relevant to explain temperature responses, in summer radiative heating under enhanced insolation plays a crucial role for both blocking and ridges.

Finally, the changes in the distributions of seasonal temperature and in the frequencies of extreme temperature indices were also examined for specific areas of Europe. Winter blocking and ridge patterns are key drivers in the occurrence of regional cold and warm extreme temperature, respectively. In summer, they are associated with substantial changes in the frequency of extremely warm days, but with different signatures in southern Europe. We conclude that there has been some misuse of the traditional blocking definition in the attribution of extreme events.

#### 2.1.1 Introduction

Anomalous temperature episodes are one of the most widely addressed topics in climatological studies, and numerous works have been published in the last decades concerning this subject in Europe, at both continental and regional scales. They cover a wide range of sub-topics, ranging from winter cold spells to summer heatwaves (e.g. Santos et al., 2006; Cattiaux et al., 2010; Andrade et al., 2012; Simolo et al., 2012; Monteiro et al., 2013; Lowe et al., 2015), heatwave-related mortality (García-Herrera et al., 2005b; Trigo et al., 2009; Muthers et al., 2010; Green et al., 2016), forest fires (Pereira et al., 2005; Marcos et al., 2015; Sousa et al., 2015), drought occurrence and agricultural management (Bastos et al., 2014; Gouveia et al., 2016), amongst other topics. The physical and dynamical mechanisms that trigger such extreme episodes are interpreted

## 2. *European temperature responses to blocking*

---

with very distinct methodologies. In this sense, an increasing number of studies are focusing on the contribution from large-scale dynamics and mid-latitude synoptic circulation patterns to the occurrence of these anomalously cold/warm temperature episodes (e.g. Andrade et al., 2012; Cattiaux et al., 2012; Li et al., 2013; Pfahl, 2014).

In the context of climatic change, trends in global mean temperature have been accompanied by an increase of warm extreme temperature events (Fischer and Knutti 2015), which has not been offset by the hiatus or slowdown in global mean temperature rise of the last 15 years (Seneviratne et al. 2014). These recent trends do not only indicate a thermodynamic forcing, but also changes in the frequency of occurrence of mid-latitude circulation patterns (Horton et al., 2015), thus stressing the need of characterizing their associated impacts.

Regarding European winter cold spells, there is a wide consensus on the critical role played by atmospheric blocking episodes over large sectors of the European continent. In works such as Trigo et al. (2004), Cattiaux et al. (2010), Sillmann et al. (2011), de Vries et al. (2012) or Pfahl (2014), the role of blocking structures in transporting cold air from higher latitudes or from cold landmasses becomes quite clear. Other studies have undertaken a deeper analysis of some specific European winter cold spells, as well as of their associated synoptic context, and have also addressed feedback processes that may amplify the resulting anomalies, such as Eurasian autumn snow-cover anomalies (García-Herrera and Barriopedro, 2006; Cohen and Jones, 2011). The interplay between Rossby wave-breaking and jet stream regimes (Woollings et al., 2011), or the occurrence of Sudden Stratospheric Warmings (Barriopedro and Calvo, 2014; Liu et al., 2014), are potential mediators of blocking activity, and hence, important precursors of cold events. Episodes like the extensive cold spell which occurred on the later stages of the previously mild winter of 2012 (WMO, 2012) are pertinent examples of the relevance of complex feedback processes in triggering significant European cold blasts.

Blocking has also been associated with extremely warm episodes in summer (Buehler et al., 2011; Andrade et al., 2012; Pfahl, 2014). However, using the well-known 2003 heatwave in Europe as an example, García-Herrera et al. (2010) stressed that there is some overstatement when attributing these episodes to standard definitions of atmospheric blocking – high-latitude quasi-stationary anticyclones associated with a reversal of the prevailing westerly flow (e.g., Rex, 1950a,b; Treidl et al., 1981; Barriopedro et al., 2006, 2010a). These weather systems are indeed in clear association with summer heat episodes over European mid/high-latitudes (e.g. Barriopedro et al., 2011; Pfahl, 2014). However, this is not the case for southern European sectors, where high-latitude blocks are frequently associated with colder than average temperatures throughout the year. Therefore, there is a clear need to distinguish high-latitude blocking structures from low-latitude systems, including the extensions of sub-tropical high pressure systems, commonly denominated as sub-tropical ridges. Unlike canonical blocking systems, sub-tropical ridges do not have the necessary condition of a wave-breaking occurrence (Woollings et al., 2011; Masato et al., 2011; Santos et al., 2013). They manifest as relatively narrow bands of positive anomalies of geopotential height extending from sub-tropical latitudes towards southern Europe and often reaching higher latitudes. Although sub-tropical ridges can be precursors of wave-breaking and

subsequent blocking (Altenhoff et al., 2008; Masato et al., 2011; Davini et al., 2012a), their impacts on European surface temperatures are rather different from those of high-latitude blocks.

García-Herrera et al. (2005b) briefly introduced the importance of sub-tropical ridging patterns on extreme summer temperatures over Iberia. Other studies have analyzed ridge patterns over Europe and their influence on rainfall regimes and droughts in southwestern Europe (Santos et al., 2009; Santos et al., 2013). However, there are no systematic studies aiming to characterize and distinguish the impacts on European temperature due to blocking and ridge patterns, at both regional and seasonal scales. In this paper, we characterize the local and regional European temperature responses associated with blocking and ridging patterns occurring over different locations of the Euro-Atlantic sector and on different seasons. We also clarify some of the referred ambiguity on the impacts' attribution to these weather systems. More specifically, the main objectives are to: 1) distinguish blocking and ridge structures with objective detection schemes; 2) characterize the seasonal impacts of these patterns, considering their specific location, on European surface temperature (including extremes); 3) objectively quantify the contribution and seasonality of the main physical mechanisms involved in the regional temperature anomalies associated to blocking and ridging regimes.

### **2.1.2 Data and Methods**

#### ***Meteorological Data***

Maximum and minimum near-surface temperatures (at 2 m above the ground, T2m hereafter) are considered for the period spanning between 1950 and 2012 from the E-OBS dataset (Haylock et al., 2008). This high-resolution gridded dataset is provided by the European Climate Assessment and Dataset (ECA&D) project, and is available on a daily basis and on a horizontal resolution of  $0.25^\circ$  latitude  $\times$   $0.25^\circ$  longitude. This regular grid is obtained by interpolating observations from local meteorological stations. Despite the overall good quality of this dataset, it must be acknowledged that it has some caveats in areas where the spatial distribution of stations is sparser (e.g., Kysely and Plavcová 2010). Moreover, the E-OBS temperature dataset suffers from other limitations such as inhomogeneities in input records, statistical interpolation errors and “heat island” effects (Hofstra et al. 2009; van der Schrier et al. 2013).

The NCEP/NCAR reanalysis daily dataset is also used (Kalnay et al., 1996), at a  $2.5^\circ$  latitude  $\times$   $2.5^\circ$  longitude horizontal resolution for the same period. The following mean daily fields are selected: 500 hPa geopotential height (Z500); 850 hPa temperature, omega-vertical velocity and horizontal wind components; upward, downward and net long-wave and short-wave surface fluxes; and total cloud cover. The Z500 field was used to compute the blocking (Barriopedro et al., 2006) and ridge days catalogues separately, as described below. These two different dynamical indicators will be used to distinguish the impacts of anomalous geopotential fields at different European sectors (see next section).

### *Blocking and Ridge Catalogues*

The catalogue of days adopted in this work for high-latitude blocking (hereafter only referred as blocking) was developed by Barriopedro et al. (2006). The algorithm is an adapted version of the Tibaldi and Molteni (1990) index based on the reversal of the meridional Z500 gradient around the typical latitudes of the extra-tropical jet stream. It further imposes spatial (minimum longitudinal extension of  $12.5^\circ$ ) and temporal (minimum duration of 5 days) criteria to account for the characteristic spatio-temporal scales of blocking. The algorithm also enables the characterization of useful daily parameters, such as the location of the blocking center, the intensity or the spatial extension. Following previous studies (Sousa et al., 2016, 2017), where the same catalogue was used to assess the impacts of blocking patterns on precipitation regimes over Europe, three non-overlapping blocking sectors covering the Europe and the eastern Atlantic are defined. More specifically, daily blocking occurrences are assigned to one of the following spatial sectors according to the location of their blocking centers (Fig. 2.1): ATL ( $30^\circ\text{W}$ – $0^\circ$ ), EUR ( $0^\circ$ – $30^\circ\text{E}$ ) and RUS ( $30^\circ\text{E}$ – $60^\circ\text{E}$ ).

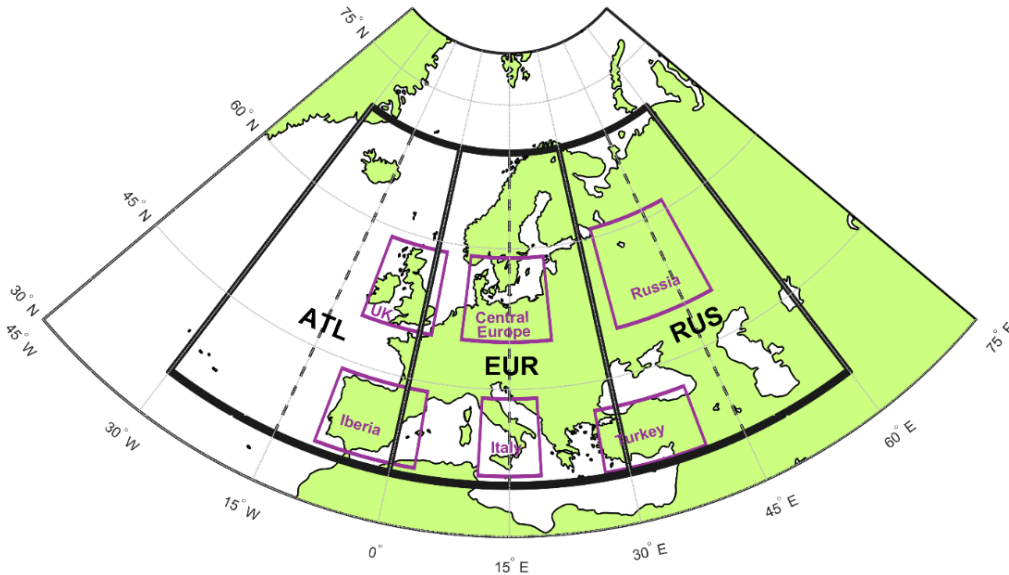


**Fig. 2.1** Geographical representation of the considered sectors for blocking location (thick black frames): Atlantic (ATL) – from  $30^\circ\text{W}$  to  $0^\circ$ ; European (EUR) – from  $0^\circ$  to  $30^\circ\text{E}$ ; Russian (RUS) – from  $30^\circ\text{E}$  to  $60^\circ\text{E}$ . Each of these sectors was also sub-divided into two smaller  $15^\circ$  longitude-wide sub-sectors (west and east, dashed black lines). Magenta boxes identify areas for regional-scale assessments (cf. Section 2.1.3).

To compute the catalogue of sub-tropical ridge days (hereafter only referred to as ridges), we follow a similar methodology as in Santos et al. (2009), which is based on daily anomalies of the Z500 field. In order to compare it with the blocking catalogue, we also classified ridge occurrence into the same three sectors (ATL, EUR and RUS). Furthermore, each sector is split into two halves: south ( $30^\circ\text{N}$ – $50^\circ\text{N}$ ) and north ( $50^\circ\text{N}$ – $70^\circ\text{N}$ ). These latitudinal bands are used for winter and, to accommodate the annual cycle, they are shifted  $5^\circ$  northward for summer. This partition enables classifying ridges as strong Z500 positive departures in sub-tropical and mid-latitudes that do not

## 2. European temperature responses to blocking

---

extend significantly northwards, thus avoiding overlapping days between blocking and ridge patterns. For each grid point, we computed Z500 departures for each specific day, and a 30-day running threshold based on the 80th percentile of the daily Z500 series. We then obtained, on a daily basis and for each longitudinal sector, the percentage of area above that threshold in its northern and southern halves. To classify a ridge day in one of the three considered longitudinal sectors the following criteria are employed: 1) at least 75% of the area in the southern half is above the threshold; 2) less than 50% of the area in the northern half is above the same threshold. These percentages and thresholds were tested and calibrated in order to avoid overlaps between blocking and ridge dates, and furthermore to obtain climatological ridge frequencies comparable to previous studies (e.g. Santos et al. 2009).

We also evaluate for each blocking and ridge day the contribution to grid point temperature anomalies of three major physical forcings: horizontal advection, vertical advection and diabatic processes. This is carried out by separating and identifying the process associated with the largest daily temperature change at each grid point (considering only those cells where the absolute temperature anomalies exceed 1°C under the given weather regime). Daily mean horizontal and vertical temperature advections are explicitly calculated as in Equations (1) and (2), respectively:

$$\left(\frac{\Delta T}{\Delta t}\right)_h(\lambda, \phi, t) = -\vec{v} \cdot \nabla_p T \quad (1)$$

$$\left(\frac{\Delta T}{\Delta t}\right)_v(\lambda, \phi, t) = -\omega \frac{T}{\theta} \frac{\partial \theta}{\partial p} \quad (2)$$

where the term  $\left(\frac{\Delta T}{\Delta t}\right)_h$  is the temperature advection by the horizontal wind, and  $\left(\frac{\Delta T}{\Delta t}\right)_v$  the temperature advection by vertical motion. Equations (1) and (2) are computed from daily mean fields in constant pressure coordinates, according to the pressure levels available in the NCEP/NCAR dataset, with  $(\lambda, \phi, t)$  representing latitude, longitude and time, respectively, and  $\vec{v}$  being the horizontal wind,  $T$  the temperature,  $\omega$  the vertical velocity and  $\theta$  the potential temperature. The daily mean temperature rate due to diabatic processes,  $\left(\frac{\Delta T}{\Delta t}\right)_d$ , is estimated as a residual from the previous two terms based on the temperature tendency equation:

$$\left(\frac{\Delta T}{\Delta t}\right)_d(\lambda, \phi, t) = \frac{\Delta T}{\Delta t} - \left(\frac{\Delta T}{\Delta t}\right)_h - \left(\frac{\Delta T}{\Delta t}\right)_v \quad (3)$$

where  $\frac{\Delta T}{\Delta t}$  is the daily mean temperature tendency (in K day<sup>-1</sup>). The residual approximation for the diabatic term has been previously applied to reanalyses datasets in Chan and Nigam (2009) or Wright and Fueglistaler (2013). It must be kept in mind that different factors such as sub-grid turbulent mixing, analysis increments and other numerical errors may contribute to the residual term. Further, this approach does not consider sub-daily fluctuations of the contributing terms, potential interactions among the underlying processes and feedbacks between the dynamics and thermodynamics. For example, in addition to horizontal warm advection, diabatic and adiabatic

## 2. European temperature responses to blocking

---

heating experienced during the re-circulation of air masses around high pressure systems can contribute to the warm anomalies. Similarly, warm temperatures induced by a given weather system can in turn modulate the contributing terms by reinforcing the Z500 anomaly. Thus, the attribution of the temperature responses should be taken with caution, as some one-directional causal relationships cannot be fully inferred from a composite analysis.

This bulk analysis is performed for the 1000-850 hPa layer. Then, we compute the daily anomalies of all terms in Equation (3) and the relative contribution of each term  $\left(\frac{\Delta T}{\Delta t}\right)_i'$  (in %) to the total change  $\left(\frac{\Delta T}{\Delta t}\right)'$ , where primes denote daily anomalies. Finally, we derive the composited values of  $\left(\frac{\Delta T}{\Delta t}\right)_i'$  for blocking and ridge days, and the leading process  $i$  with the largest contribution to the temperature tendency anomaly.

In this work, the analyses are performed for winter and summer separately, using the meteorological seasons: December to February and June to August, respectively. The statistical significance of the anomalies presented in the Results section was assessed with a two-sample Kolmogorov-Smirnov test (the 5% significance level was considered).

### 2.1.3 Results

#### 2.1.3.1 Blocking and ridge seasonal distribution

The classification of events according to their position enables a simple and objective way of grouping blocking and ridge days in each sector and season. It also allows the computation of composites for the aforementioned meteorological variables under each specific synoptic pattern. The winter and summer composites of Z500 anomalies for blocking and ridge days of each sector are shown in Fig. 2.2. Overall, blocking and ridges display a clear difference in the latitude of their maximum Z500 anomalies. The composites for blocking days show an omega-like structure, which is distinguishable from the non-wave-breaking pattern that is evident in the composites corresponding to days of ridge. Furthermore, the absolute anomalies are larger in winter, and for blocking regimes (Fig. 2.2a-c). During winter, around one third of the days comprises blocking occurrence in at least one sector of the Euro-Atlantic region, while summer frequencies are smaller, particularly over the ATL sector (Fig. 2.2g). The composites accurately capture the signatures associated with blocking over preferred sectors of occurrence in the Eurasian sector (Barriopedro et al. 2006). It is still worth noting that some events contribute to the composites of more than one sector during their lifecycle (Sousa et al., 2017a). Ridge frequencies are more equally distributed throughout the three sectors and seasons, with closer values to those of blocking during summer. The largest Z500 anomalies under ridging patterns are found for ATL and EUR ridges in winter (Fig. 2.2d-e). The positive anomalies of Z500 during blocking and ridge regimes are often accompanied by negative anomalies, but much less pronounced. The most relevant negative Z500 anomalies occur southwards (northwards) of the blocking (ridges) centers, mainly for ATL structures in winter (Fig. 2.2a and 2.2d).

## 2. European temperature responses to blocking

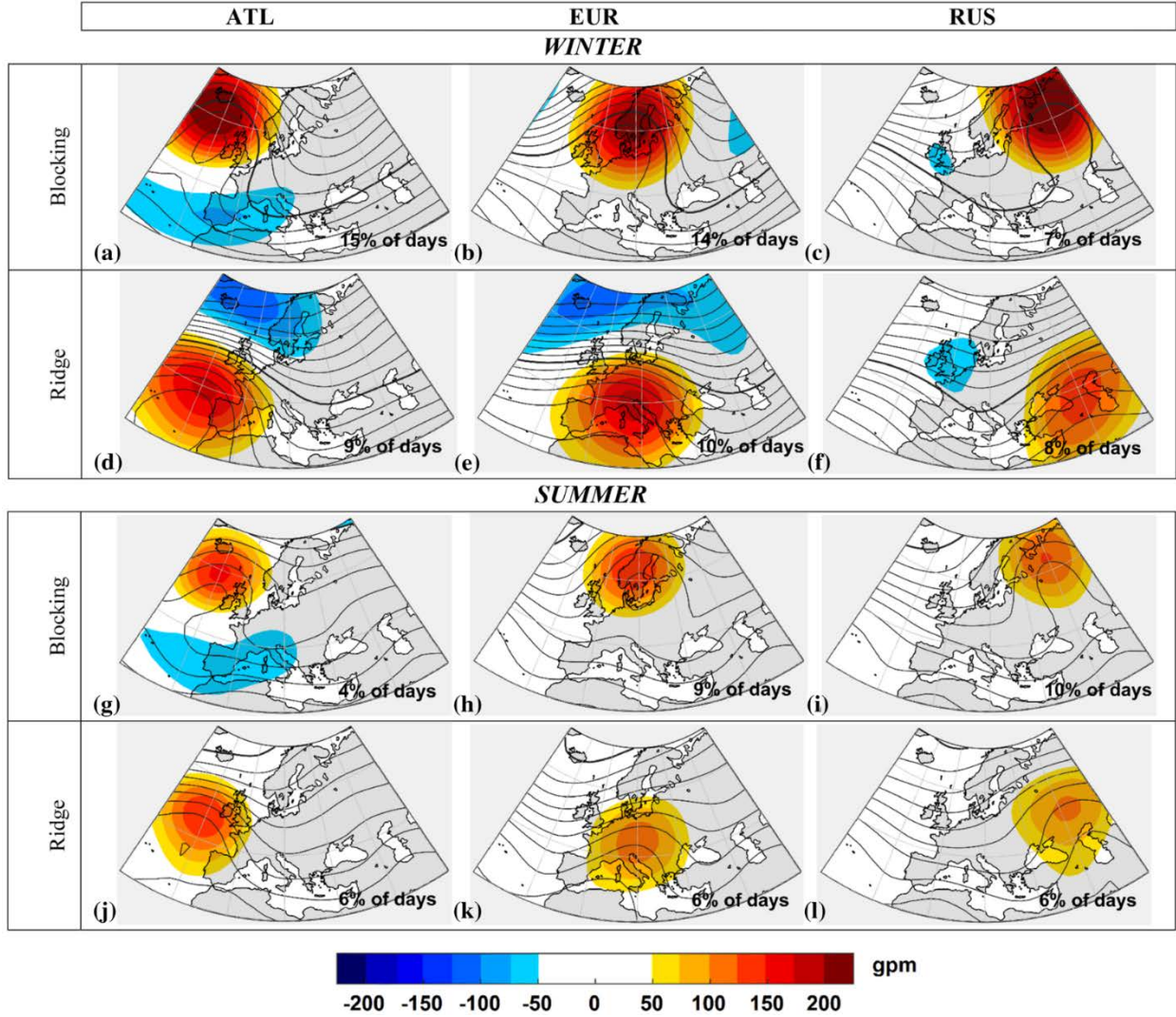


**Fig. 2.2** Composites of the daily anomalies (shaded areas) and absolute values (contours) of 500 hPa geopotential height for blocking centers and ridges in each sector, during winter (upper panels, a-c and d-f, respectively) and summer (lower panels, g-i and j-l, respectively). All values are in gpm and the thick line represents the 5500 isohypse (the thinner contours are separated by 50 gpm). The seasonal frequencies of occurrence for each regime are shown in percentage.

In the following sub-sections, the specific surface temperature responses driven by each weather regime, as well as the corresponding synoptic environments, will be analyzed in more detail.

### 2.1.3.2 Seasonal temperature responses

Using the seasonal and regional catalogues of blocking and ridge days, we computed the corresponding composites for the maximum and minimum T2m anomalies. In Figs. 2.3 and 2.4 we present the maximum (TX) and minimum (TN) temperature anomalies for winter and summer, displaying only statistically significant anomalies at the 5% significance level.

## 2. European temperature responses to blocking

Overall, the geographical locations of the anomaly patterns undergo west-east shifts, in agreement with the positioning of the considered blocking or ridge structure (as presented in Fig. 2.2). Additionally, there is a clear seasonality in the responses to blocking and ridge patterns, as they typically extend over larger areas in winter than in summer. Furthermore, the temperature responses to blocking are opposite to those of ridges in winter, but not in summer. These distinctive signatures highlight the need of distinguishing between blocking and ridges, including their spatial scales and location.

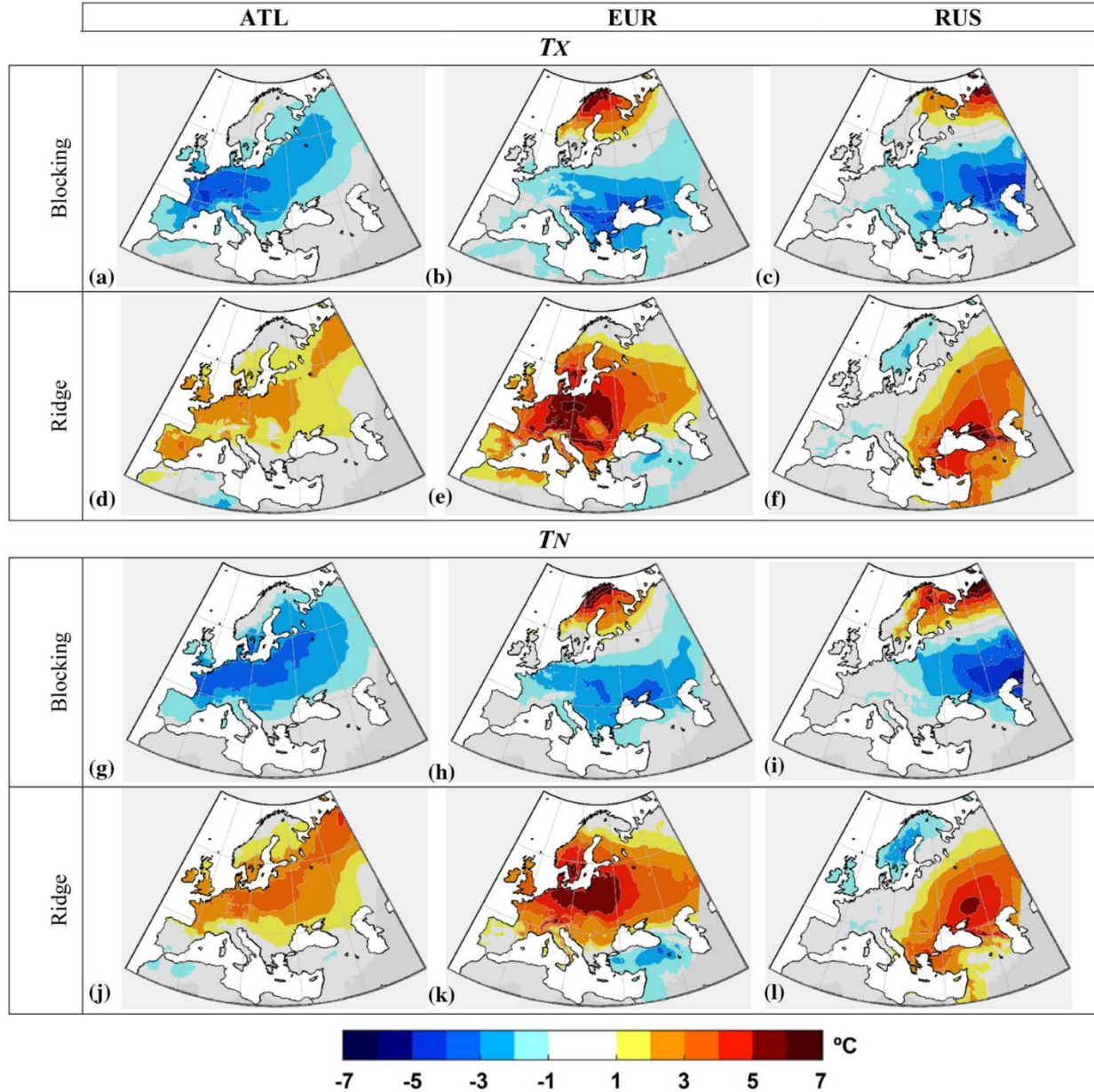


**Fig. 2.3** Composites for blocking and ridge days occurring in each sector (ATL, EUR and RUS) of winter 2 meters above ground maximum (upper panels – TX; a-c and d-f, respectively) and minimum temperature (lower panels – TN; g-i and j-l, respectively) anomalies (in °C). Only statistically significant anomalies at 5% significance level are depicted.

## 2. *European temperature responses to blocking*

---

The responses in TN and TX are generally coherent for all sectors and regimes during winter (Fig. 2.3) and reveal highly contrasting patterns between blocking and ridges (Fig. 2.3a-c versus 2.3d-f). While during blocking most of Europe experiences well below average temperatures, ridge days are characterized by extensive above average temperatures. Negative anomalies exceeding  $-3^{\circ}\text{C}$  tend to occur southward and eastward of the blocking centers, with ATL blocking (Fig. 2.3a) revealing the largest widespread signal over the continent. During blocking episodes, strong positive temperature anomalies are found in land areas under the highest Z500 anomalies (Fig. 2.2), i.e. northern half of Scandinavia for EUR blocks (Fig. 2.3b) and northern Russia and eastern Scandinavia for RUS blocks (Fig. 2.3c). Conversely, winter ridges in both ATL and EUR sectors (Fig. 2.3d-e) are responsible for anomalously warm conditions in almost all regions of Europe. These anomalies are particularly striking for EUR ridges (Fig. 2.3d), when Central Europe experiences positive TX anomalies reaching up to  $7^{\circ}\text{C}$ . There are some areas on the ridge's eastern and western flanks that experience slightly below average temperatures, mainly in Mediterranean regions. This is particularly noteworthy in Turkey during EUR ridges (Fig. 2.3k), though these negative anomalies are smaller in magnitude and spatial extension than their positive counterparts.

As previously mentioned, summer temperature anomalies (Fig. 2.4) are more spatially confined than in winter and the opposite temperature response to blocking and ridge patterns is no longer observed (Fig. 2.3). In the case of blocking systems, positive anomalies are again centered under the maximum Z500 anomaly area, but now affecting larger areas. In particular, during EUR (RUS) blocking, extensive areas of Central Europe and Scandinavia (Eastern Europe and Russia) experience anomalously warm conditions, with TX anomalies  $>5^{\circ}\text{C}$ , as seen in Fig. 2.4b (2.4c). Temperature anomalies for ATL blocking (Fig. 2.4a) are much less pronounced. As in winter, negative anomalies are found in the southern and eastern flanks of blocking systems, but they are small in magnitude, and mostly restricted to TX. Still, southern areas of Europe (e.g., Iberia, Balkans) display negative temperature anomalies associated to blocking in both winter and summer.

Summer ridges are associated with above normal temperatures over a more confined area than in winter. In particular, they do not have significant effects in temperature over northernmost areas of Europe during this season. The lack of opposite signed responses to blocking and ridges during summer is evident in some regions, such as Central Europe or Russia, which experience above average surface temperatures under both regimes, albeit at different latitudes. On the contrary, in southernmost areas, particularly the Iberian Peninsula for ATL regimes (Fig 2.4d and 2.4a), positive temperature anomalies during ridge days tend to be replaced by negative anomalies during blocking days. Furthermore, summer temperature anomalies over southern Europe critically depend on the specific location of ridge structures.

## 2. European temperature responses to blocking

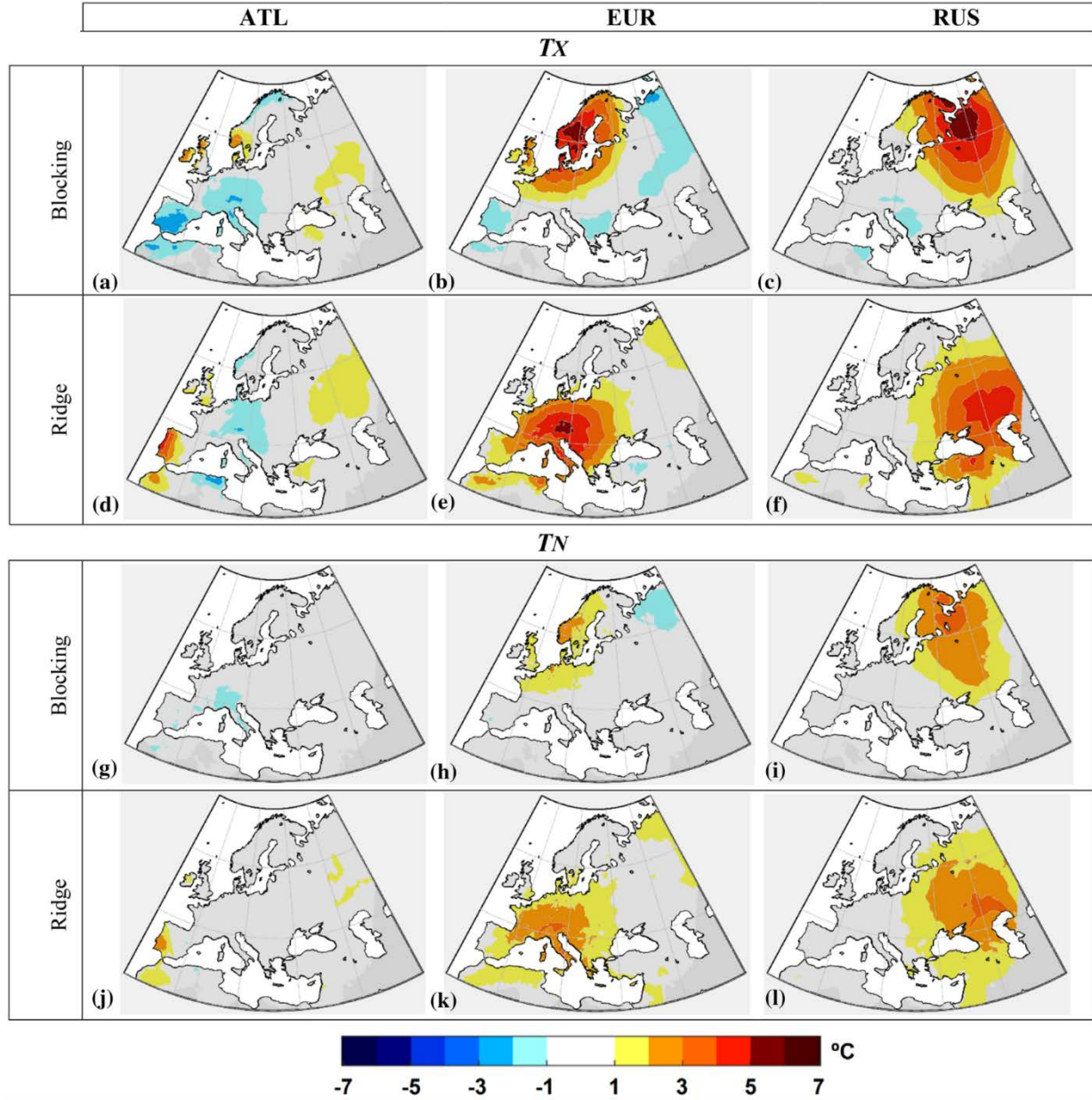


**Fig. 2.4** Same as in Fig. 2.3, but for summer.

Although their locations are similar, TX anomalies (Fig. 2.4d-f) are larger in magnitude than those of TN (Fig. 2.4j-l). This different amplitude in the day-time and night-time temperature responses is much more pronounced than during winter, which is also observed for blocking systems (Fig. 2.4a-c vs 2.4g-i). This is particularly relevant for the occurrence of extremely hot days in summer. In this sense, it is worth noticing that a given synoptic pattern can affect very differently areas situated relatively close, as shown by García-Herrera et al. (2005b) when comparing the weather regimes associated with local heatwaves in Lisbon and Madrid. Therefore, a finer-scale analysis using smaller regional sectors is required to address local extreme events. In

## 2. *European temperature responses to blocking*

---

Figs. 2.12 and 2.13 of the Supplementary Material we show the winter and summer composites of TX and TN, considering narrower longitudinal sub-sectors for blocking and ridge location (15° longitude-wide). Overall, the results are similar to those of Fig. 2.3 and 2.4, although the temperature responses to summertime ridges are more spatially restricted, especially in western Europe. As an illustration for the Iberian Peninsula, the exact areas under intense summer hot conditions are very dependent on small west-east shifts in the position of the sub-tropical ridge (Fig. 2.14g-i). Thus, some regional impacts can be smoothed out in the analysis using larger sectors. However, on the whole, the analysis based on three 30° longitudinal sectors is sufficient to identify the most relevant temperature responses to blocking and ridges, as well as the associated mechanisms, which are described in the following section.

### *2.1.3.3 Synoptic and forcing mechanisms*

In this section we apply the methodology described in Section 2 in order to assess the relative contribution of different processes to the local temperature anomalies associated with blocks and ridges, namely: 1) horizontal advection by the large-scale flow; 2) vertical advection - adiabatic heating/cooling; 3) diabatic processes. In most cases one dominant mechanism can be identified, though local temperature responses can also be due to a combination of the forcing terms, frequently involving a partial cancelation in the net temperature tendency. For the sake of succinctness, only the leading term is shown in Fig. 5, and the full analysis of the heating/cooling fraction due to each specific term is presented in the Supplementary Material (Figs. 2.14 and 2.15).

During winter (Fig. 2.5a-c) and summer (Fig. 2.5g-i) blocking days, horizontal advection by anomalous southerly flows appears responsible for a large fraction of the warming observed in the northwestern flank of the blocking systems, with the exception of winter RUS blocks. The negative temperature anomalies found in the southeastern flank of the blocking center, particularly striking during winter, are also predominantly a result of cold advection from higher latitudes under the northerly flow established along the eastern flank of the high-pressure system (see the anomalous wind fields in Fig. 2.5a-c). This colder air is carried towards southern Europe (e.g. north of the Black Sea), thus interacting with different air masses. As a result, other processes, such as diabatic cooling, and in particular, convective processes in warm seasons, can gain further importance in localized areas to the southeast of the blocking centers (Sousa et al. 2017a). This mixed contribution of different forcing terms at lower latitudes under blocking occurrence is confirmed by Fig. 2.14 and 2.15. In areas under the maximum geopotential height anomaly, warming due to reinforced subsidence and diabatic heating gains particular relevance, particularly for continental blocks. There are also differences in the relative contribution of each term depending on the season (Fig. 2.5a-c and 2.5g-i): warming due to horizontal advection is relevant during both winter and summer blocks, while anomalous downward motion is mostly relevant for winter blocking. On the other hand, significant diabatic heating dominates in summer, predominantly over continental areas (Fig. 2.5h-i). As shown later, the summer dominance of the diabatic term over land areas is well explained by changes in the radiative flux budgets.

## 2. European temperature responses to blocking

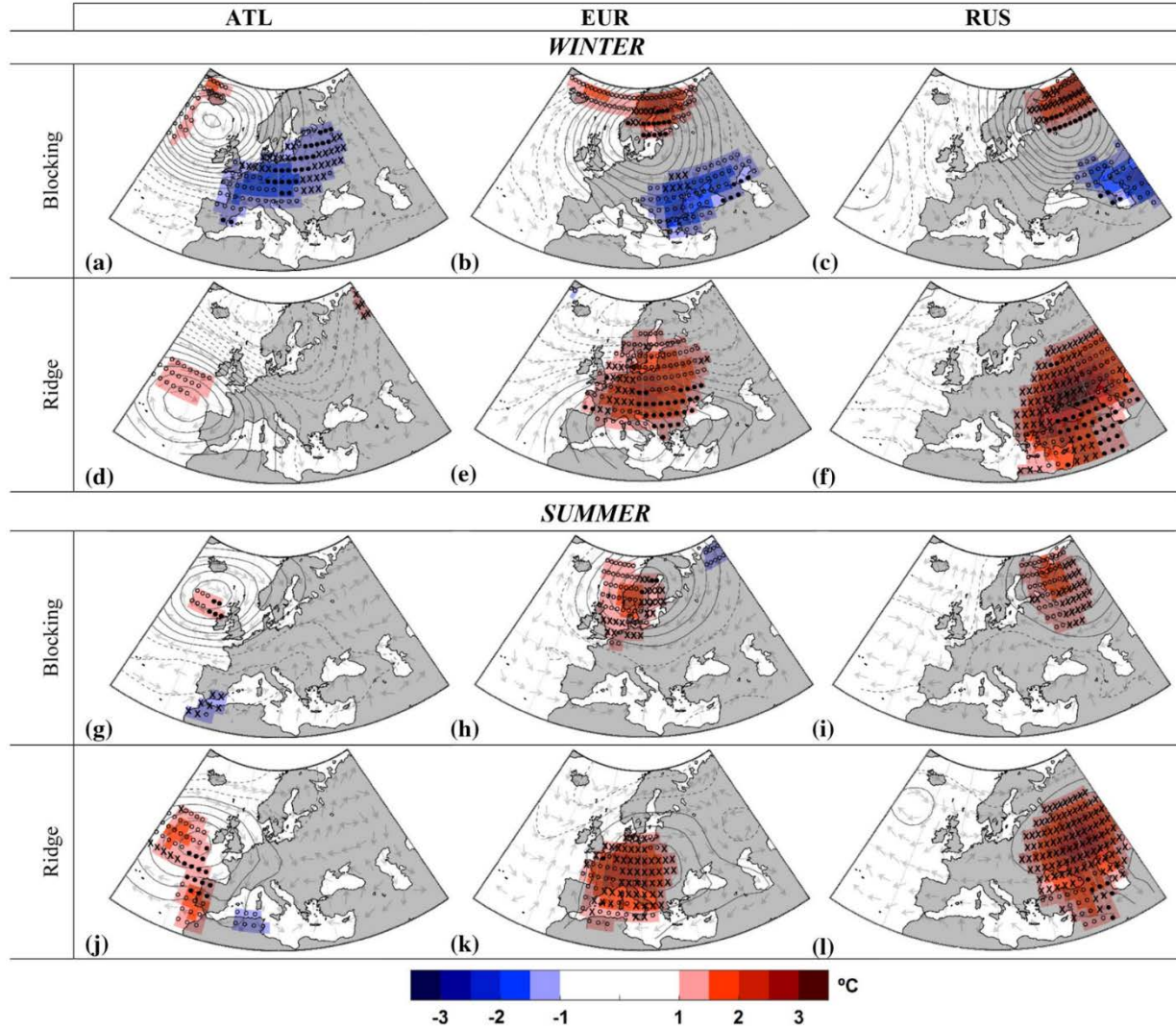


**Fig. 2.5** Mechanisms related to temperature anomalies in the lower troposphere (1000–850 hPa) during blocking and ridge days during winter (upper panels, a-c and d-f, respectively) and summer (lower panels, g-i and j-l, respectively). Color shadings depict anomalies in the mean daily temperature (in °C). Solid (dashed) contours represent positive (negative) 500 hPa geopotential height anomalies in 15 dam intervals. Light grey vectors show anomalies in the horizontal wind direction. Symbols denote the highest contributing mechanism for the observed temperature changes at each grid point: horizontal advection (○), vertical advection (●) and diabatic processes (X).

Regarding ridge days, warm horizontal advection from Atlantic air masses influences the temperature responses in the northern flank of the ridge, particularly during winter ATL and EUR ridges (Fig. 2.5d-e). This is associated with the passage of cyclones, but also with the corresponding changes in cloud cover and long-wave fluxes, as explained below. Similarly to blocking, subsidence and diabatic processes are crucial in continental areas under the influence of winter and summer sub-tropical ridges (Fig. 2.14m-r and 2.15m-r). Adiabatic heating due to strong subsidence extends over larger areas in winter than in summer, mostly eastwards of the maximum

## 2. *European temperature responses to blocking*

---

Z500 anomalies (Fig. 2.5e-f), while diabatic heating dominates the summer temperature responses (Fig. 2.5k-l). Over the Iberian Peninsula, subsidence and horizontal advection towards southwestern coasts are the main driver for above average summer temperatures during ATL ridges.

It should be stressed that NCEP/NCAR temperature anomalies for the considered layer do not fully overlap with the TX and TN anomalies of the E-OBS datasets in all areas and for all regimes, thus partially explaining some discrepancies between the areas highlighted in Fig. 2.5 and Figs. 2.3 and 2.4. Still, there are also some important dynamical features related to these discrepancies. For example, negative T2m anomalies during winter blocking (Fig. 2.3a-c, 2.3g-i) are more widespread than aloft (Fig. 2.5a-c). In particular, some areas with negative near-surface temperature anomalies display simultaneously positive anomalies in the highest level of the considered layer (850 hPa, not shown). This indicates a typical pattern of thermal inversion under high pressure systems, which extends westwards of the blocking center (see Fig. 2.16a-c). The thermal inversion and the corresponding imprisonment of cold air at lower levels are typical of enhanced long-wave radiative cooling, thus stressing the importance of diabatic processes for the near-surface temperature responses. During summer, the well-mixed boundary layer determines a better agreement between anomalies at surface and aloft, supporting the smaller role of horizontal advection when compared to other processes, particularly those associated to diabatic heating.

Up to now, we have shown that diabatic processes are key to determine the near-surface temperature responses to blocking and ridges, particularly in summer. The diabatic term includes different processes, such as radiative fluxes, latent and sensible heat fluxes and frictional dissipation. To better frame the observed temperature responses to the weather regimes and the seasonal-dependent role of the diabatic term, we computed composites of surface radiative fluxes for blocking and ridges in winter (Fig. 2.6) and summer (Fig. 2.7), along with composites of total cloud cover anomalies (Fig. 2.8).

The radiative forcing over Europe during winter blocking episodes is not remarkable, at least concerning short-wave fluxes (Fig. 2.6d-f), which are quite modest in high latitudes during months with reduced insolation. Anomalies are rather dominated by the gains (losses) in surface net long-wave fluxes, which in turn are strongly associated with above (below) average cloud cover (see also Fig. 2.8a-c). For example, near the blocking centers, the enhanced nocturnal long-wave losses (Fig. 2.6a-c) under clear sky conditions are partly offset by diurnal short-wave gains (Fig. 2.6d-f). This winter radiative surface cooling signal is in agreement with that in the 1000-850 hPa layer due to the diabatic term (Fig. 2.14g-i), which is the leading process in areas to the southeast of the ATL and EUR blocking centers (Fig. 2.5a-b).

## 2. European temperature responses to blocking

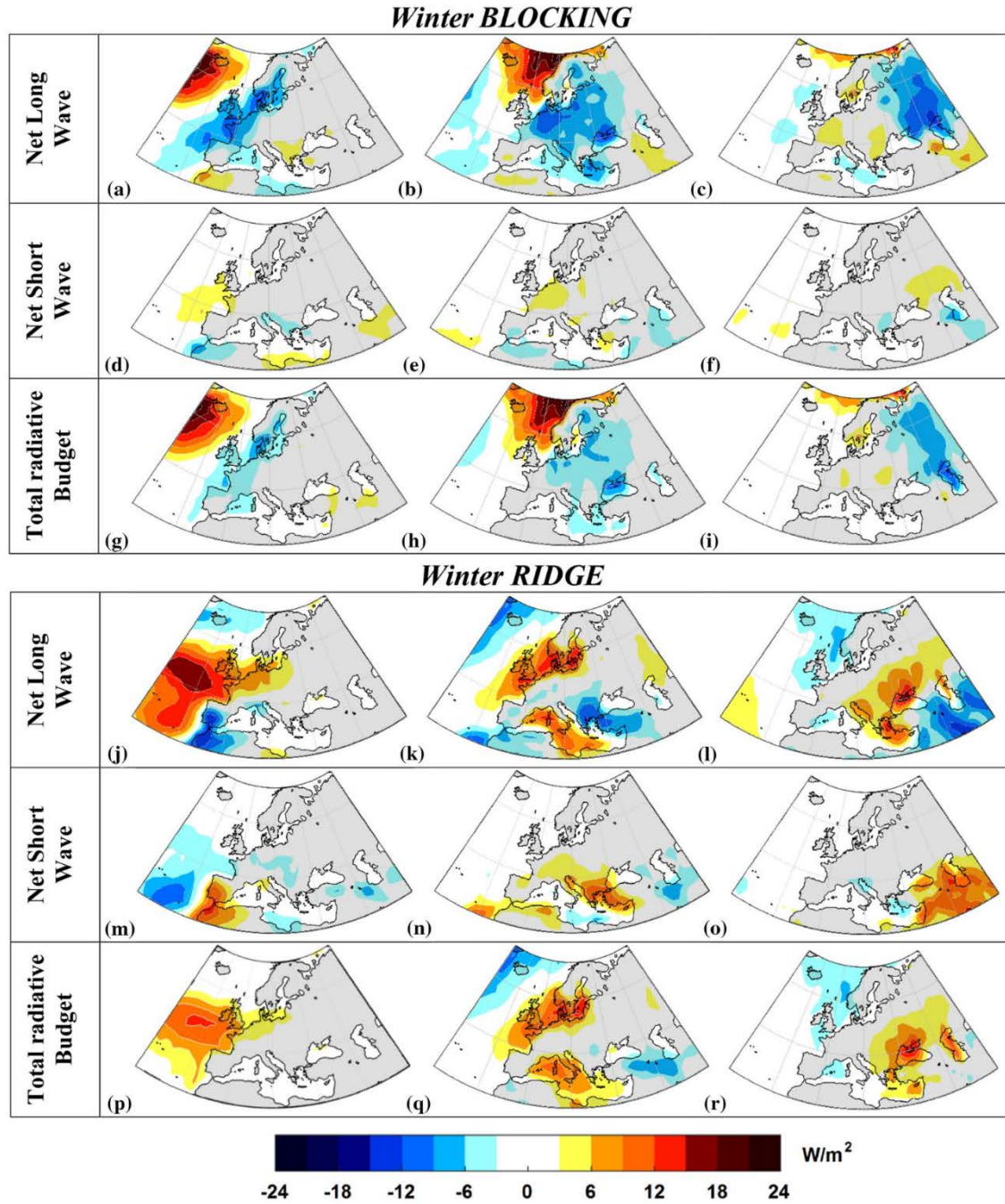


**Fig. 2.6** Composites of net surface longwave and shortwave radiative flux anomalies and corresponding total radiative budget ( $\text{Wm}^{-2}$ ) for blocking (upper panel; a-c, d-f and g-i, respectively) and ridge (lower panel; j-l, m-o and p-r, respectively) days during winter. Reddish (bluish) colors correspond to positive (negative) fluxes towards the surface.

## 2. *European temperature responses to blocking*

---

The radiative fluxes anomalies during winter ridges reveal an increase in diurnal radiative heating near the Z500 maximum (Fig. 2.6m-o), due to positive net short-wave fluxes under enhanced clear sky conditions over Iberia (ATL), Balkans (EUR) and Middle East (RUS). However, this signal is offset by the opposite negative long-wave fluxes (Fig. 2.6j-l) over the same southern regions, as reflected in the total radiative budget (Fig. 2.6p-r). In contrast, areas north of the ridge structures exhibit significant increases in cloud cover (Fig. 2.8d-f), which lead to positive anomalies in the surface long-wave (Fig. 2.6j-l) and total (Fig. 2.6p-r) radiative budgets. A similar increase in long-wave and total radiative fluxes is found north of the blocking systems, but restricted to very high latitudes (Fig. 2.6a-c, 2.6g-i). The winter radiative heating is particularly relevant for the UK and coastal areas of central Europe under ATL or EUR ridges (Fig. 2.6j-k), as well as some Mediterranean areas during EUR and RUS ridges (Fig. 2.6k-l). Its combined effect with the advection of mild Atlantic air masses explains the large positive near-surface temperature responses during ridge days (Fig. 2.3d-f). However, as long-wave radiative fluxes tend to cancel out the short-wave fluxes, on the overall diabatic processes are less important in the 1000-850 hPa layer than subsidence or advection, with the exception made for northern Russia (Fig. 2.5d-f).

During summer, anomalies in radiative fluxes are larger than in winter, in accordance with the stronger contribution from diabatic processes (Fig. 2.5g-l) and an increase in insolation hours. Like in winter, below average cloud cover (Fig. 2.8g-l) over the centers' systems results in simultaneous warming by diurnal radiative gains (Fig. 2.7d-f and Fig. 2.7m-o) and cooling by nocturnal radiative losses (Fig. 2.7a-c and Fig. 2.7j-l). Nonetheless, and different to winter, the summer increases in short-wave income are stronger in magnitude than the enhanced nocturnal surface long-wave losses over areas under the blocking and ridges centers. Thus, short-wave gains clearly dominate in summer, and the resulting net radiative balance (Fig. 2.7g-i and Fig. 2.7p-r) explains well the larger anomalies for TX than for TN. The subsequent increase in daily temperature range can be found for both blocking and ridge regimes, being particularly remarkable at higher latitudes for blocking episodes, and also for central Mediterranean areas during EUR ridges. On the other hand, areas south of blocking and north of ridges experience losses in net short-wave fluxes and gains in long-wave radiation. This is in agreement with increases in cloud cover (Fig. 2.8g-l) due to the deflection of humid Atlantic westerly flows around the high pressure centers (e.g., Trigo et al., 2004; Sousa et al. 2017a). This effect on the radiative budget due to increased cloudiness is particularly evident for Atlantic areas in summer, when comparing ATL ridges to those located in EUR or RUS (Fig. 2.7p-r).

## 2. European temperature responses to blocking

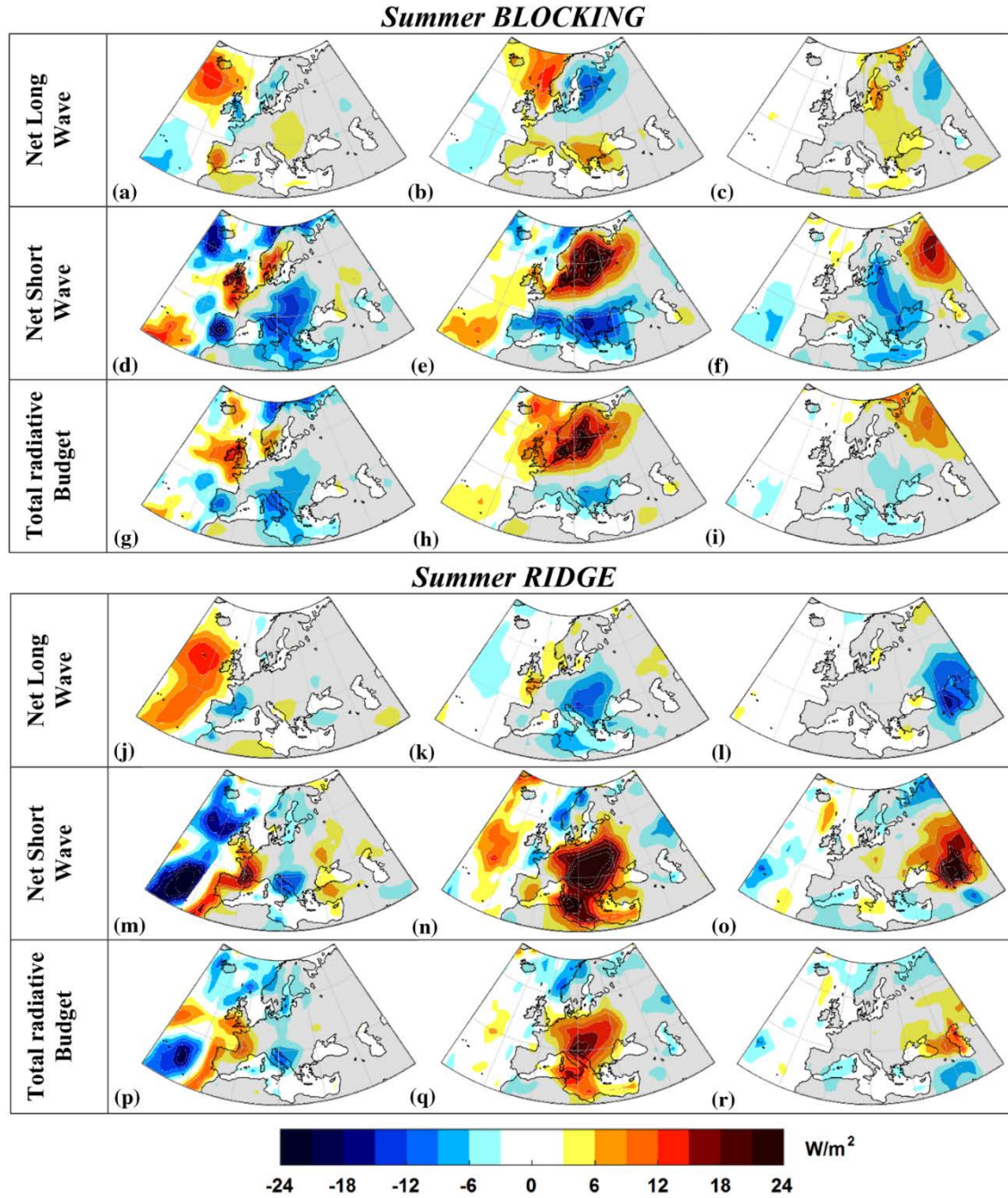
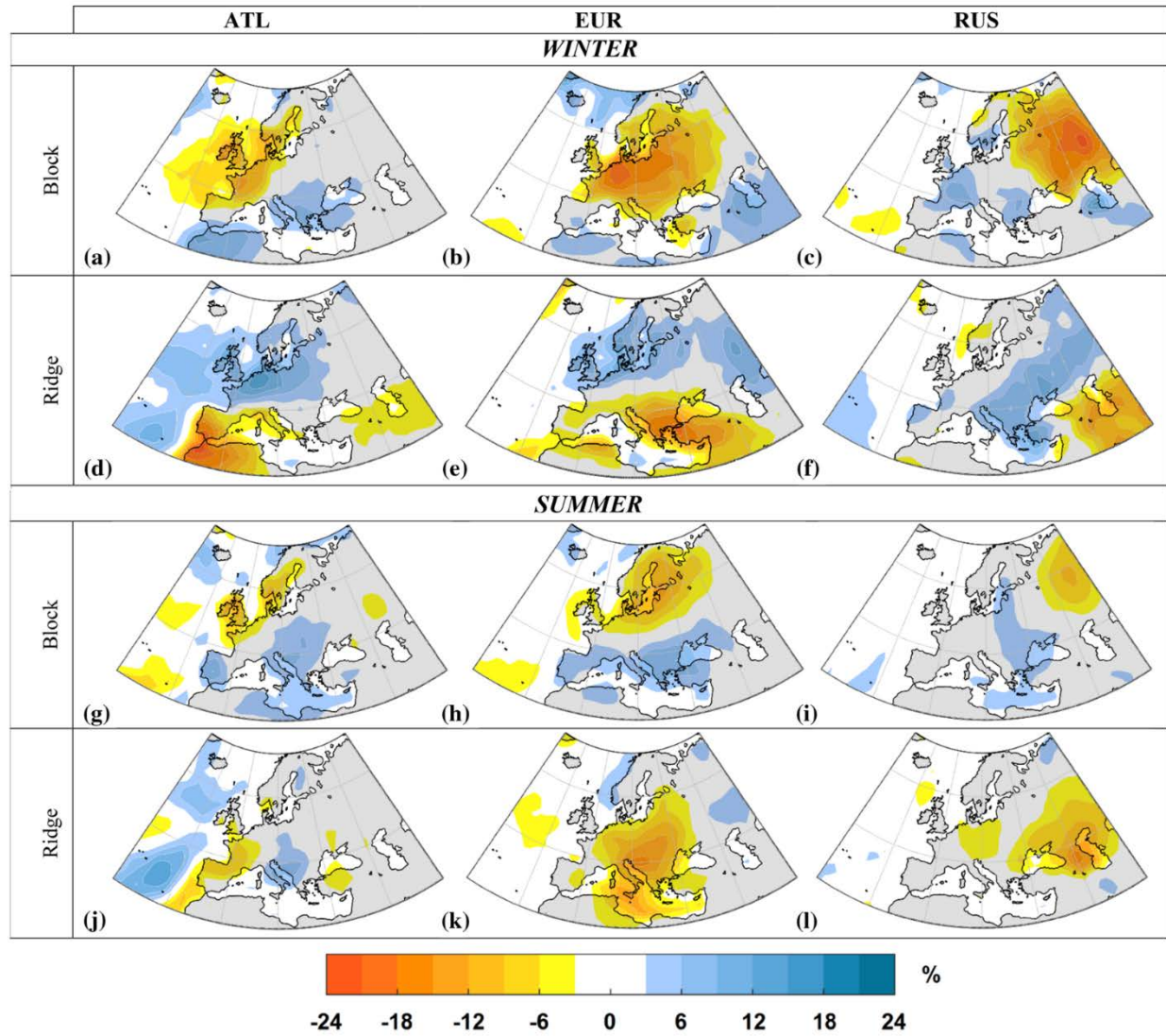


Fig. 2.7 Same as Fig. 2.6, but during summer.

## 2. European temperature responses to blocking



**Fig. 2.8** Composites of the total cloud cover anomalies (%) for blocking and ridge days occurring in each sector during winter (upper panel; a-c and d-f, respectively) and summer (lower panel; g-i and j-l, respectively).

### 2.1.3.4 Changes in regional temperature distribution

In this section we will analyze regional changes in the Probability Density Function (PDF) of daily TX and TN for each weather regime. These regional temperature responses will also be related to the previously discussed forcing mechanisms. The PDF analysis was performed using all grid point series of each region highlighted in magenta in Fig. 2.1. We computed regional PDFs for all days of each season and for each regime separately (Figs. 2.9 and 2.10), along with the corresponding changes in mean TN and TX and in their temporal variance. We also measured the degree of homogeneity inside each region ( $\sigma_T$ ), by computing the standard deviation of the mean local temperatures of all grid points, thus accounting for the dispersion of the climatological TX and TN values within each region. As it can be seen in Figs. 2.9 and 2.10 the regions with larger values of  $\sigma_T$  comprise important orographic barriers (Iberia, Italy and Turkey).

Figure 2.9 indicates that wintertime PDF temperature distributions over the considered regions are generally shifted towards lower values for blocking, and higher values for ridge patterns. Warming due to the presence of ridge structures is on the overall larger than cooling due to blocking. The anomalous warming driven by winter ridges may lead to high temperatures over large parts of Europe, such as the Central European region (Figs. 2.9e-f). For this region, EUR ridges (red dashed lines in Fig. 2.9) result in a mean increase in TX of almost 6°C, and of about 4°C in TN, as well as abnormally high frequencies of extremely warm winter days, while nights with TN below -10°C are almost nonexistent. In the UK, the frequency of days with TX below freezing during ATL (blue dashed lines) and EUR ridge patterns becomes almost negligible (Fig. 2.9b). While ATL and EUR ridges result in well above average temperatures over most of Europe, the same is not true for RUS ridges (green dashed lines, Fig. 2.9). In this case, well above average temperatures are restricted to the easternmost areas of Europe (cf. Fig. S6a-d for Russia and Turkey). However, in areas distant enough to the west of such structures (e.g., UK and Iberia) slightly negative temperature anomalies are found due to the presence of a trough westwards of the RUS ridge (Fig. 2.2f).

During winter blocking, there is a shift towards colder TX and TN in all regions, which is particularly pronounced for ATL and EUR blocks (blue and red solid lines, Fig. 2.9). Furthermore, blocking promotes wintertime extreme cold days and nights over large parts of Europe, as inferred from the regional shifts towards the left end tails of the PDF distributions. In particular, ATL blocks are the main drivers of cold days in all regions, since the location of the high pressure center favors cold advection over large areas of the continent (as previously shown in Fig. 2.5a). For the same reason, during EUR blocks, colder than average temperatures are observed in Central Europe (Fig. 2.9e-f) and Italy (Fig. 2.9g-h), extending towards Russia and Turkey (Fig. 2.17a-d). Remarkable PDF changes during winter RUS blocking are mostly restricted to the easternmost areas, as it was found for RUS ridges.

## 2. European temperature responses to blocking

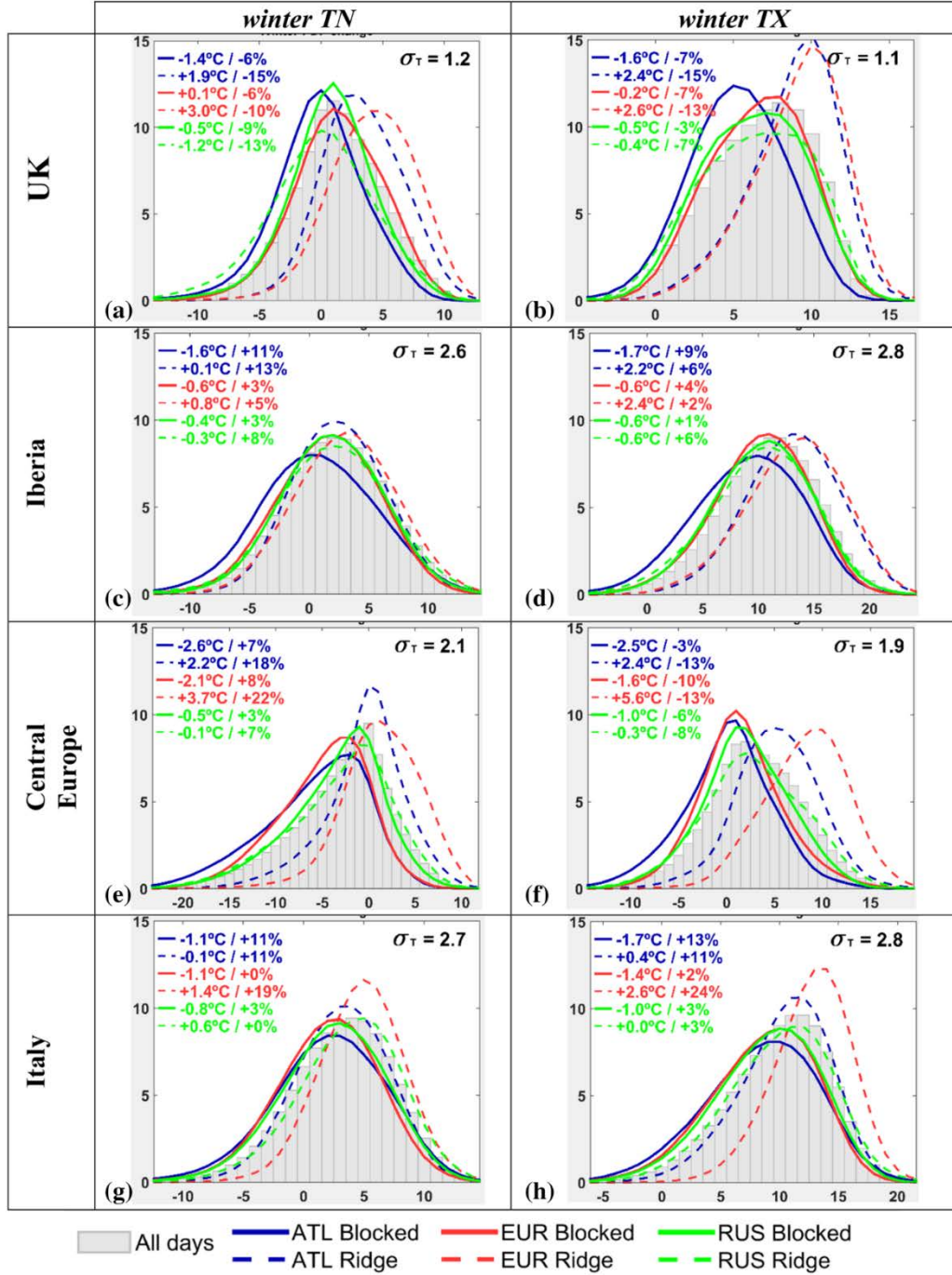


**Fig. 2.9** Distributions for winter minimum (left panels – TN) and maximum (right panels – TX) 2 meters above ground temperature frequency (%) for blocking and ridge days and for the four regional sectors depicted in magenta in Fig. 2.1 (UK a-b; Iberia c-d; Central Europe e-f and Italy g-h). Grey bars denote seasonal climatology, solid lines correspond to blocking days and dashed lines to ridge days. Upper left values represent the corresponding changes in mean temperature (°C) and variance (%) with respect to the full distribution parameters, while  $\sigma_T$  shows standard deviations of area-mean temperatures.

## 2. *European temperature responses to blocking*

---

Winter ridges in the ATL and EUR sectors reduce the variance of TX and TN in the UK (Fig. 2.9a-b) by more than 10%, while in Central Europe they are associated with smaller (larger) variability in TX (TN), as shown in Fig. 2.9f (2.9e). On the overall, winter blocking patterns result in qualitatively similar, but smaller changes in variance. For southern sectors, most weather regimes concur with larger wintertime variance in TX and TN. This is particularly clear for the Italian sector (Fig. 2.9g-h), where TX displays around 25% more variability during EUR ridges.

During summer (Fig. 2.10), the regional PDF responses to blocking and ridges are no longer opposite in sign for all regions. While ridges (blocks) are still associated with warmer (colder) than average temperatures in the southernmost regions (Figs. 2.10c-d and 2.10g-h), both regimes cause shifts towards higher temperatures in the northernmost regions (Figs. 2.10 a-b and 2.10e-f). Larger PDF changes are observed for ridges than for blocks, and in TX than in TN, in agreement with Fig. 2.4 and the dominant role of short-wave over long-wave radiative fluxes in summer (Fig. 2.7). In the Iberian Peninsula, there is a very clear rise in the number of days with TX above 35°C for ATL and EUR ridges when compared to other regimes (Fig. 2.10d). In Central Europe, EUR blocking and ridge patterns result in an impressive increase in the frequency of days above 30 and 35°C (Fig. 2.10f), respectively. As we move to eastern Europe, the RUS patterns become more relevant (see PDF changes for Russia and Turkey in Fig. 2.17). Concerning summer changes in variance, we found a slight increase for almost all patterns and regions, particularly pronounced in Italy (Fig. 2.10g-h) during EUR ridges.

## 2. European temperature responses to blocking

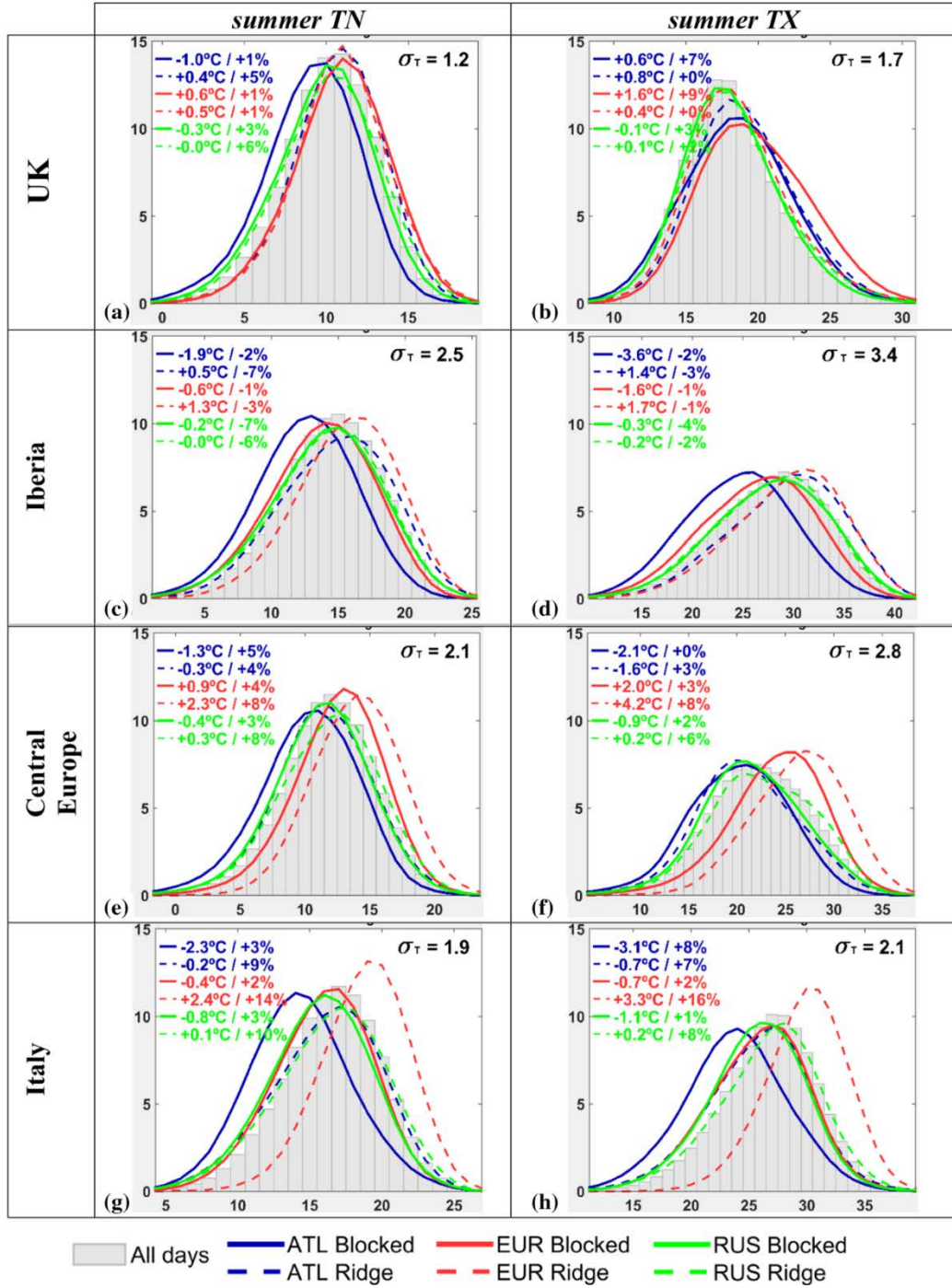


**Fig. 2.10** Same as Fig. 2.9, but for summer.

Changes in extreme temperatures associated with blocking and ridges were also investigated for each region of Fig. 2.1. To do so, we computed for each grid point the number of days below the 10th percentile of winter TN (TN10, hereafter) and above the 90th percentile of summer TX (TX90, hereafter). The percentiles, which were derived from all seasonal days of the period 1950–2012, the occurrence of exceedances and their changes during blocking and ridges were spatially

## 2. *European temperature responses to blocking*

---

averaged for all grid points of each region. The relative changes in these extreme indices associated with each weather regime are presented in Fig. 2.11 (expressed in % with respect to that expected from the full 1950-2012 climatology).

Changes in TN10 confirm the previously described opposite responses for blocking and ridge patterns during winter. On the overall, there is an increase in cold winter extremes during blocking (filled triangle symbols in Fig. 2.11). In particular, the increases in TN10 exceed 10% over Iberia (Fig. 2.11c) and Central Europe (Fig. 2.11b) during ATL blocks. On the other hand, ridges (open triangle symbols), especially those occurring in the ATL and EUR sectors, reduce the occurrence of winter cold extremes in all regions. Similar responses to blocking and ridges are found in winter TN10 for easternmost areas (cf. Fig. 2.18 for Russia and Turkey), but being the RUS patterns more relevant here.

During summer, blocking (filled circles) and ridges (open circles) cause opposite changes in the frequency of extremely hot days in southern Europe (Iberia and Italy, Fig. 2.11c-d). However, in areas further north (UK and Central Europe, Fig. 2.11a-b), both weather regimes promote substantial increases in TX90. Thus, while ridging is associated to a rise in the frequency of extremely hot days in almost all regions, the same is not true for blocks, which decrease (increase) TX90 in southern (northern) regions. In particular, nearly 30% more extremely hot days occur in Central Europe and Italy under EUR ridges (Fig. 2.11b and 2.11d, respectively), while in Iberia TX90 increases by around 10% during ATL and EUR ridges (Fig. 2.11b). Differently, the most important regimes for the occurrence of hot days in the UK are ATL and EUR blocks (Fig. 2.11a), which cause TX90 increases of around 10% and 15%, respectively. Again, for easternmost areas, weather regimes centered in the RUS sector trigger the largest changes in TX90. Thus, in Turkey (Fig. 2.18b), extremely hot conditions are driven essentially by RUS ridges, whereas in Russia (Fig. 2.18a) both RUS ridges and blocks result in a 15-20% increase in TX90. In fact, the impact of anomalous Z500 fields in the Russian area has been widely discussed due to recent events, such as the 2010 Russian mega-heatwave (e.g., Barriopedro et al. 2011).

## 2. European temperature responses to blocking

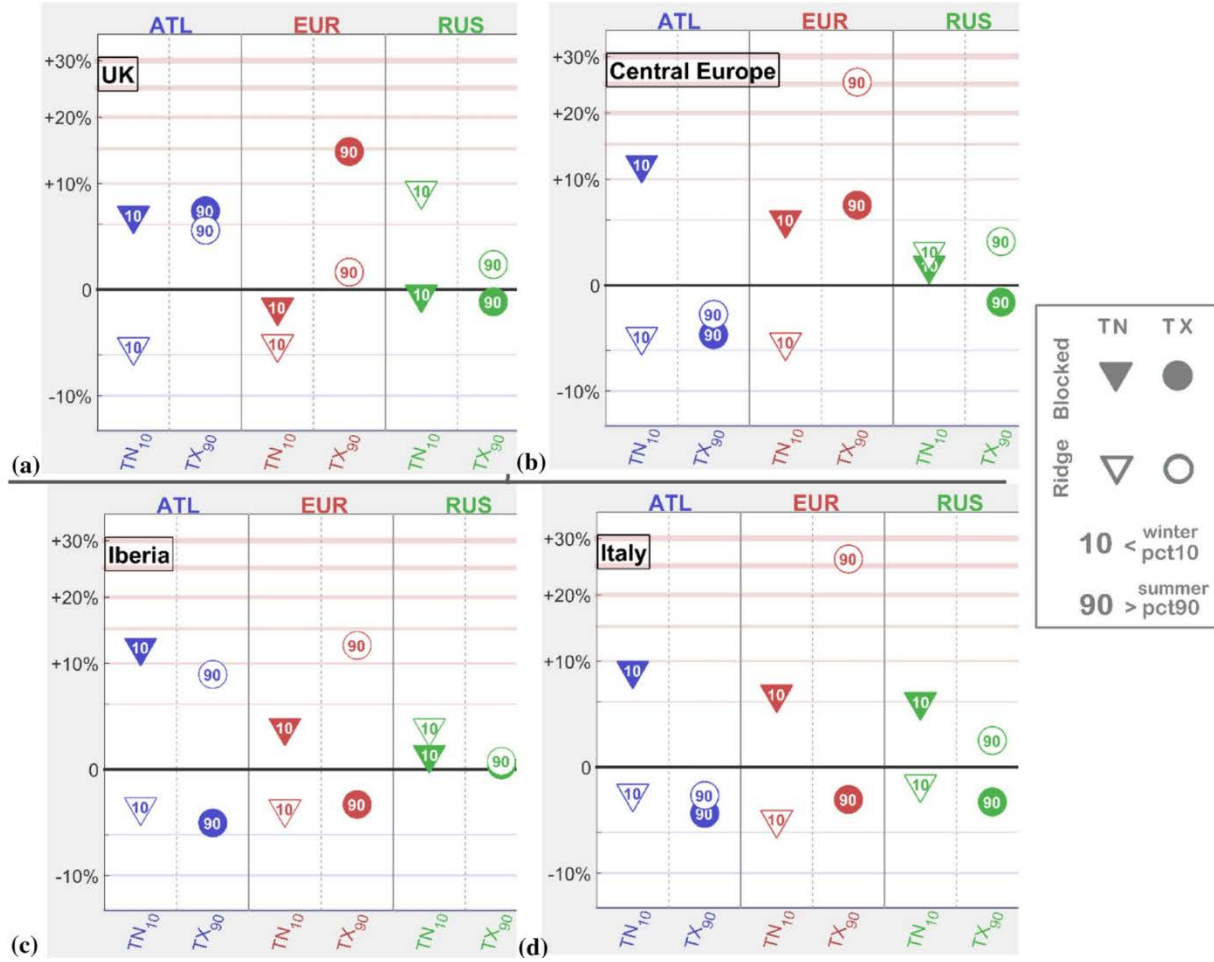


**Fig. 2.11** Relative changes (%) in the frequencies of extreme temperature during blocking and ridge patterns in the regional sectors presented in Fig. 2.1 (UK a, Iberia b, Central Europe c and Italy d), using the winter TN10 and summer TX90 indices. Circles (triangles) represent maximum (minimum) temperature, and filled (open) symbols represent blocking (ridge) patterns.

### 2.1.4 Discussion and Conclusions

In this work we introduced a clear separation between high-latitude blocking structures and sub-tropical ridges occurring in different sectors of the Euro-Atlantic area (30 °W-60 °E), both in terms of climatology and seasonal impacts on temperature in the European continent. While winter blocking characteristics have been extensively studied, our work also focuses on the characterization of blocking impacts on European summer temperature, which has been much less investigated. Furthermore, the extension of this comprehensive analysis towards the sub-tropical ridge phenomenology is a significant novelty. In this sense, this systematical separation between high- and low-latitude structures may be used in other climatological and dynamical applications, besides the one presented in this work.

## 2. *European temperature responses to blocking*

---

We introduced an objective separation of the different forcing mechanisms behind the temperature responses associated to each considered weather regime. This approach enabled quantifying the importance of the following forcing factors: horizontal advection, vertical advection and diabatic heating. Particular attention was devoted to the radiative contribution to the diabatic term. To our knowledge, this systematic quantification of the different contributing factors to the temperature responses represents an innovation in the literature of climatological impacts related to blocking and ridge phenomenology – Seo et al. (2016) used a similar approach to link temperature anomalies with the Madden-Julian Oscillation. Despite the limitations in the methodology, the results are in agreement with previous studies which have analyzed air parcel trajectories over Europe and the associated surface temperature responses for some specific case studies or regional weather systems. Thus, our approach corroborates these results from another perspective, and also distinguishes between the physical mechanisms associated with blocking and ridges, and to what extent they critically depend on their exact locations.

Finally, we complemented our analysis by evaluating changes in the PDF distributions of seasonal maximum and minimum temperature for different European regions, and in the frequency of extremely cold nights in winter and hot days in summer. This assessment allowed a finer look at regional impacts, framing smaller scale responses into the previous larger scale analysis. The main results of this study can be summarized as follows:

1) In winter, the synoptic signatures and near-surface temperature responses are generally opposite between blocking and ridge patterns. In particular, most of Europe experiences colder (warmer) than average winter conditions during blocking (ridge) days. On the contrary, the summer temperature responses to blocking and ridges are more regional and not so dissimilar, with above average regional temperatures for both patterns. Negative temperature anomalies are essentially restricted to southern Europe during blocking episodes. The spring transition in the blocking signatures from winter cold to summer warm anomalies in central and northern areas of Europe has been noted recently by Brunner et al (2017).

2) Concerning the regional classification of blocking and ridges, the largest impacts associated to the weather regimes of each specific sector follow the specific longitudinal locations of the maximum 500 hPa geopotential height anomalies. Nevertheless, blocking and ridge structures located over central and western Europe are usually the ones with larger and more extensive temperature anomalies, as they cause the largest disruption of the Atlantic jet stream.

3) During winter, the horizontal advection by the anomalous flow plays a dominant role in shaping the lower-tropospheric temperature responses to blocking and ridge systems. In particular, the cold advection of high-latitude air masses towards central and southern Europe during blocking episodes and the transport of Atlantic moist and warm air towards the continent during sub-tropical ridges are key processes. Over continental areas, long-wave radiative losses associated to blocking and ridges tend to offset the near-surface temperature anomalies induced by changes in short-wave radiation fluxes. In summer, diabatic heating is the most important factor in determining warm temperature anomalies during blocking and ridge regimes. Different to winter, the induced anomalies in short-wave radiative fluxes overwhelm those in long-wave radiative fluxes due to the summer increase in insolation hours. As a consequence, blocking and ridges prompt larger

## 2. *European temperature responses to blocking*

---

responses in maximum than in minimum temperatures, and a resulting increase in the temperature daily range. The adiabatic heating triggered by reinforced subsidence during blocking and ridges plays a secondary role in rising lower-tropospheric temperatures, being more relevant during winter, and particularly important near the central locations of the anticyclonic circulation.

4) This process-oriented attribution has enabled more detailed regional and seasonal analyses, additionally reporting some smaller-scale exceptions. However, some limitations must be acknowledged. For example, although a dominant forcing factor has often been identified, in some cases there is a similar contribution or a partial cancelation between the considered forcings. In spite of this, our results are in agreement with Lagrangian-based studies (Pfahl et al., 2015; Bieli et al., 2015; Santos et al., 2015), which have noticed that winter cold events are associated to long air mass trajectories, whereas summer events are more related to in situ warming due to enhanced radiation and surface heat fluxes.

5) On the overall, winter changes in extremely cold temperatures are spatially coherent, with generalized increases (decreases) in the frequency of TN10 during blocking (ridge) occurrence. Summer changes in extremely hot days are more regionally focused during blocking and ridge regimes. This is particularly evident in southern Europe, where we show a clear dissociation between the impacts of blocking (decreases in TX90) and ridges (increases in TX90). Further, the impact of ridges is particularly dependent on the exact longitudinal location of northwards extensions of the sub-tropical ridge belt.

In summary, we have clarified the very distinct role of blocking and ridges in European temperature. This gains particular relevance for summer extreme temperatures in southern Europe, which has been affected by major heatwaves such as the episodes of 2003 and 2007 and is bound to suffer even more frequent heatwaves in coming decades (Christensen et al., 2013). In this sense, there has been some misperception and imprecise attribution of heat episodes in these areas to classical blocking definitions (e.g. Trigo et al., 2005). We are confident to have achieved a more complete and consistent phenomenological description of the distinctive impacts of blocking and ridges on European winter and summer temperature. Finally, we must acknowledge the relevance of performing further sensitivity analyses using different reanalyses datasets when carrying out specific methodologies as the one performed in this work, namely the temperature tendency diagnostic.

### **Acknowledgments**

Pedro M. Sousa was supported by the Portuguese Science Foundation (FCT) through a doctoral grant (SFRH/BD/84395/2012).

We acknowledge the E-OBS dataset from the EU-FP6 project ENSEMBLES (<http://ensembles-eu.metoffice.com>) and the data providers in the ECA&D project (<http://www.ecad.eu>).

### 2.1.5 Supplementary Material

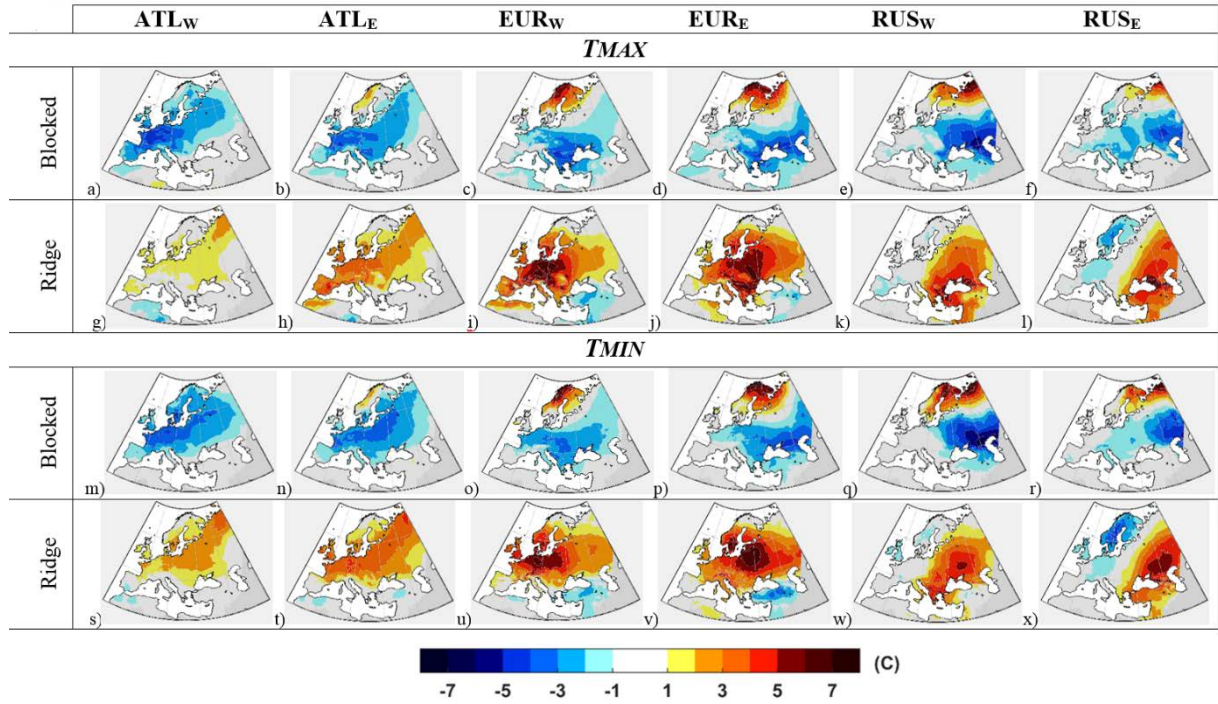


**Fig. 2.12** Seasonal composites for the winter 2 meters maximum (upper panels, a-l) and minimum temperature (lower panels, m-x) absolute anomalies during blocked and ridge patterns in each considered sector. All values are in Celsius and only statistically significant anomalies at the 5% level are shown.

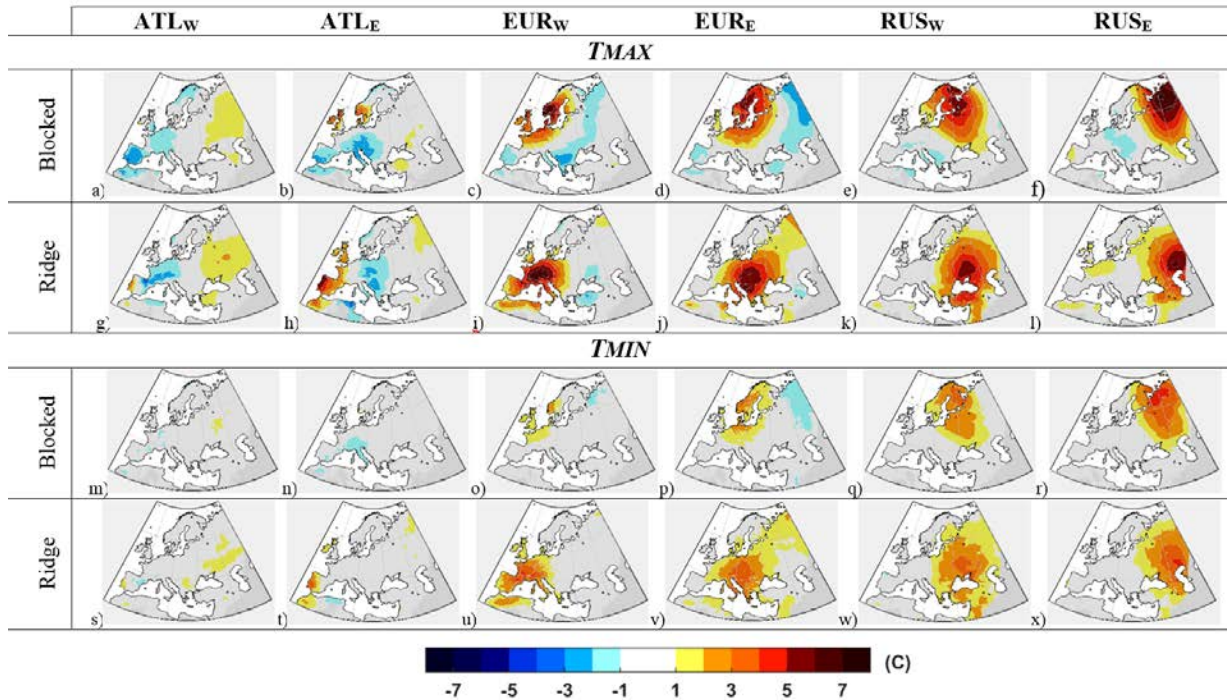


**Fig. 2.13** Same as Fig. 2.12, but during summer.

## 2. European temperature responses to blocking

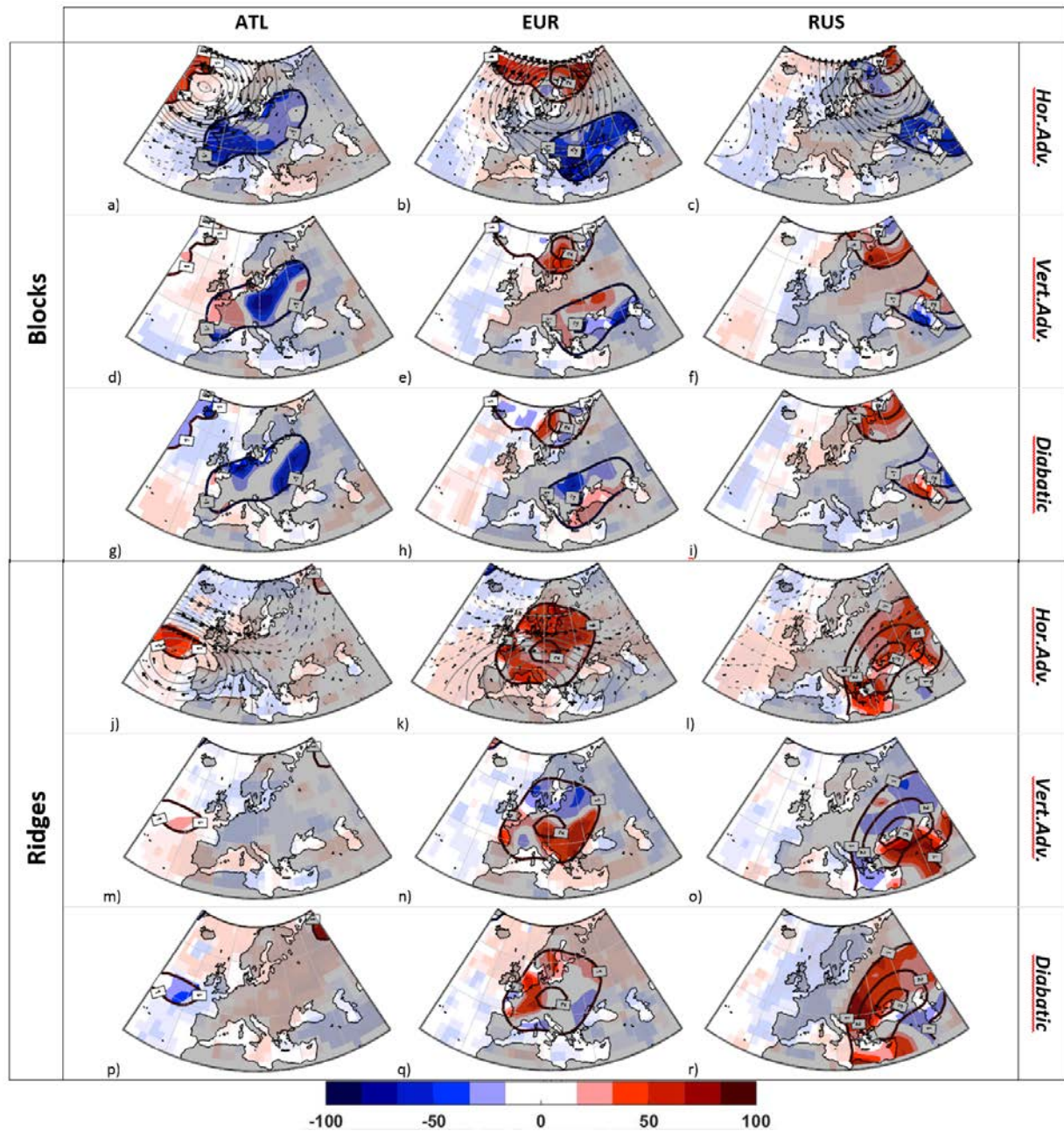


**Fig. 2.14** Contributions of the different forcing terms for temperature changes during winter in the lower troposphere (1000-850 hPa) during block (three upper rows, a-i) and ridge (three lower rows, j-r) days: horizontal advection, vertical advection and diabatic processes. Warming (cooling) contribution of each term is represented in red (blue) shadings and in percentage. Solid lines correspond to the changes in mean daily temperature (as in the previous figures) and the shadings in term contributions for areas with irrelevant temperature change (below 1°C) have been lightened.

## 2. European temperature responses to blocking

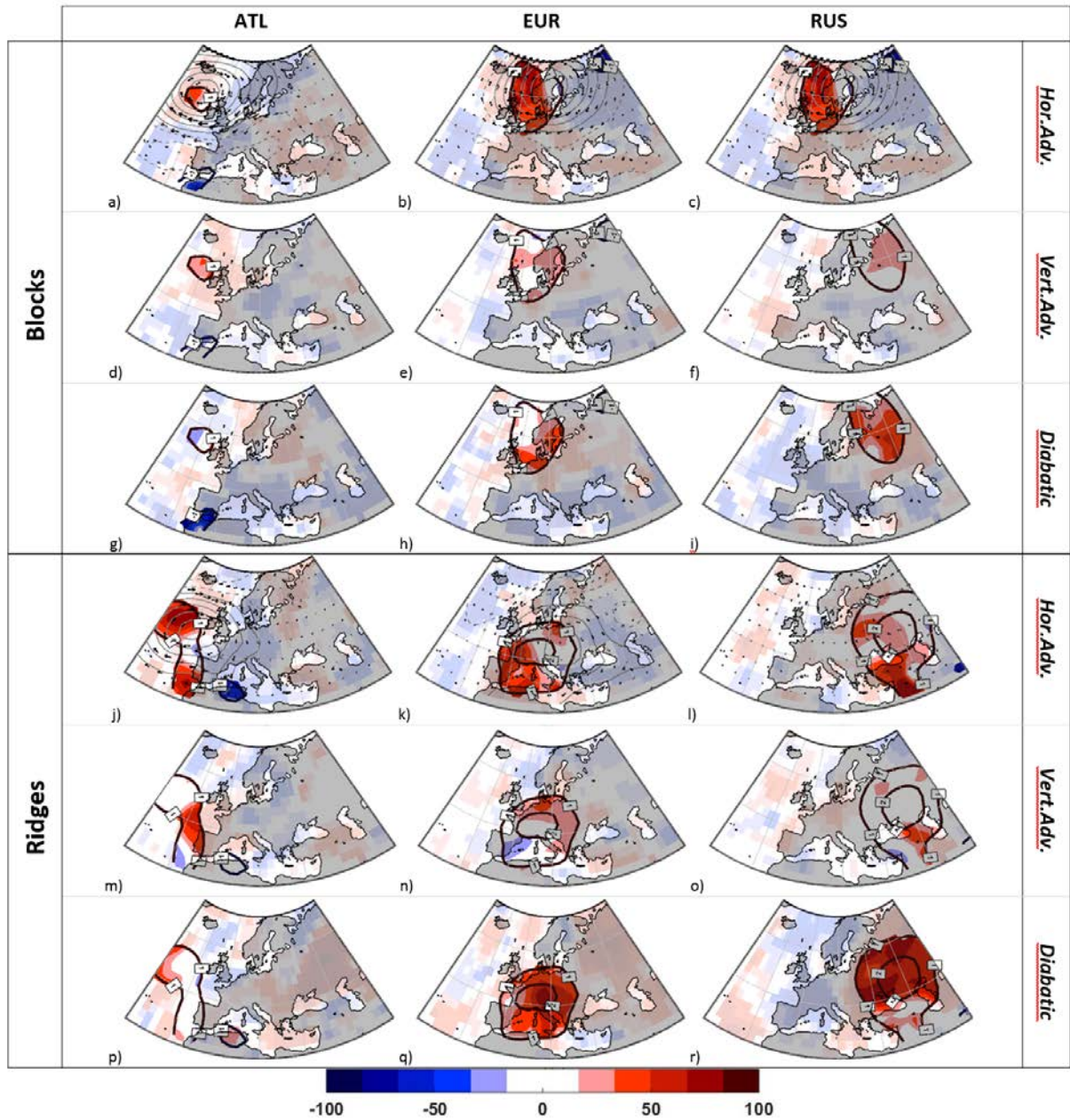


**Fig. 2.15** Same as Fig. 2.14, but during summer.

## 2. European temperature responses to blocking

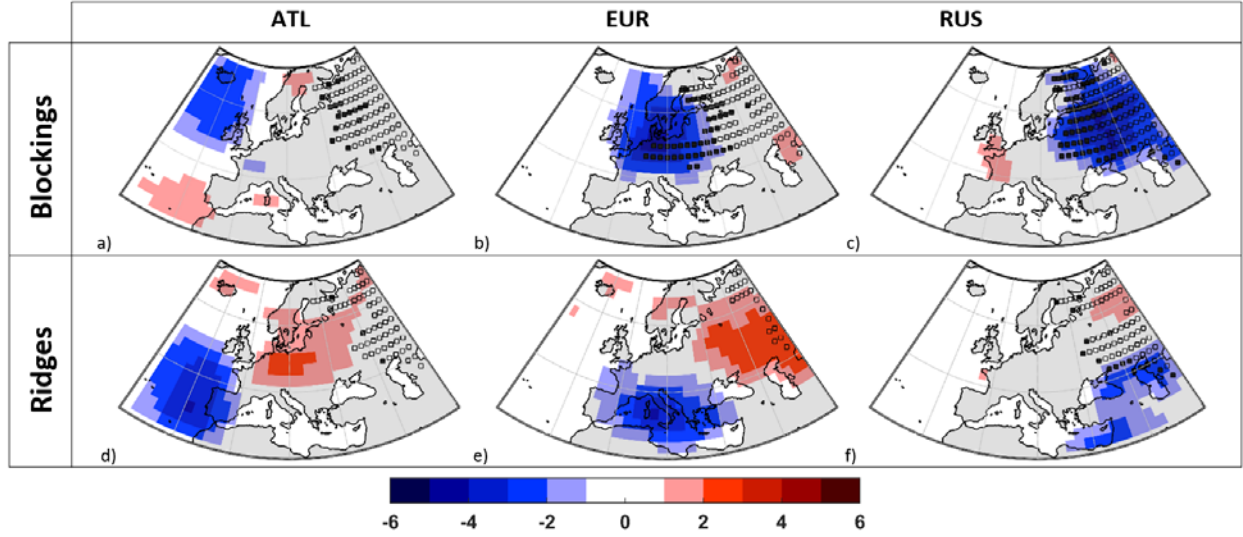


**Fig. 2.16** Anomalies in the winter mean lapse-rate ( $-dT/dp$ , in  $^\circ\text{C/km}$ ) for the 1000-850 hPa layer during each regime (blocking a-c and ridges f-g) against the climatological mean are shown in color shadings. All squares represent areas with thermal inversion in this layer ( $-dT/dp < 0^\circ\text{C/km}$ ) under each specific regime, being the gridpoints where usually there is no thermal inversion (considering the mean climatological series) represented by the black filled squares.

## 2. European temperature responses to blocking

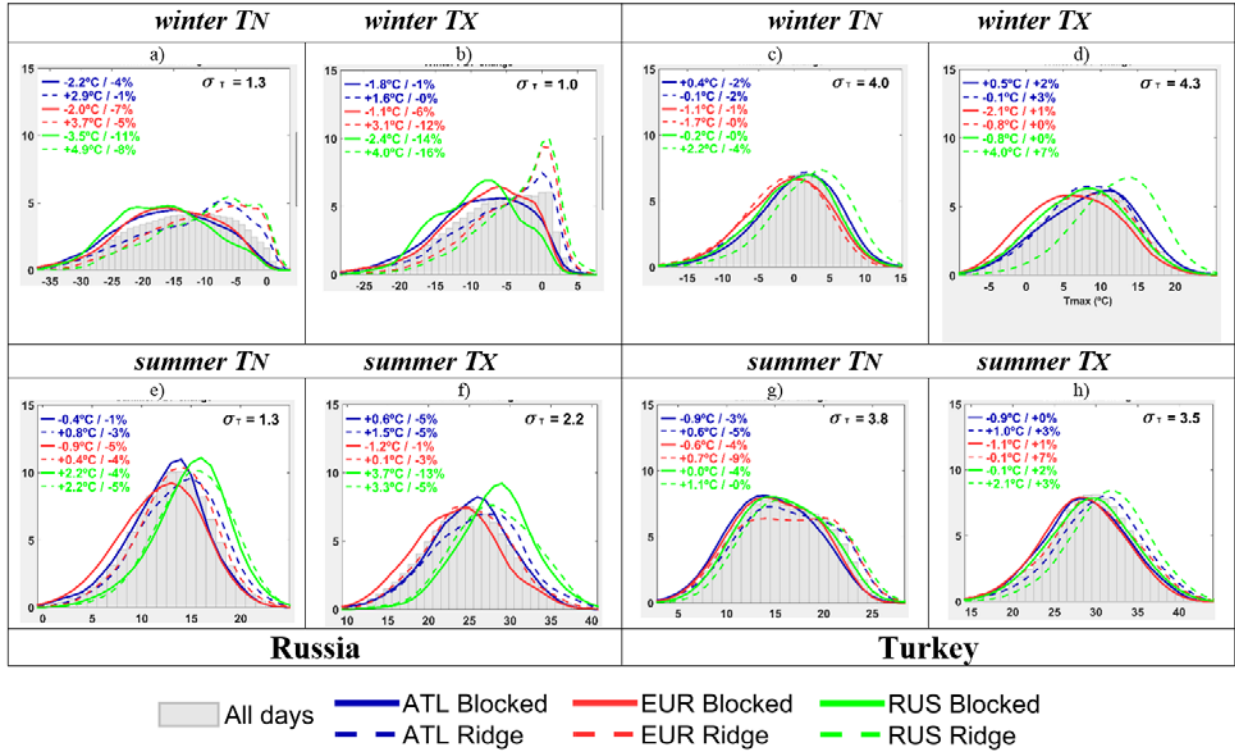


**Fig. 2.17** Changes in the minimum (TN) and maximum (TX) 2m temperature frequency (%) for the different considered synoptic patterns in the Russian (left panels, a-b and e-f, respectively) and Turkish (right panels, c-d and g-h, respectively) regional boxes presented in Fig. 2.1. Grey bars denote seasonal climatology, solid lines correspond to blocked days and dashed lines to ridge days. Upper left values represent changes in the mean (C) and variance (%) for each pattern, while  $\sigma_T$  shows the standard deviation in the means of all the box's gridpoints.

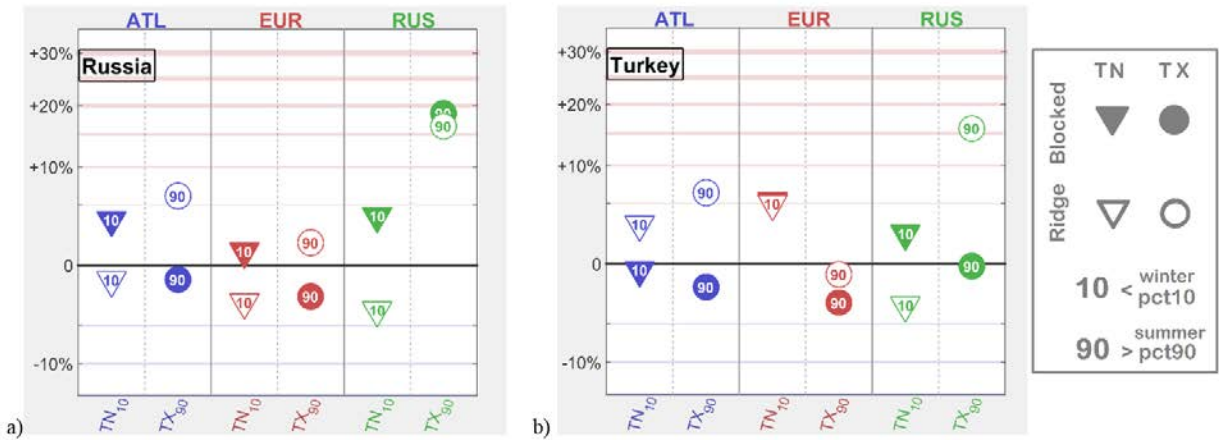


**Fig. 2.18** Relative changes (%) in the frequencies of extreme temperature during blocking and ridge patterns in the Russian (left panel, a) and Turkish (right panel, b) sectors presented in Fig.1, using the winter TN10 and summer TX90 indices. Circles (triangles) represent maximum (minimum) temperature, and filled (empty) symbols represent blocking (ridge) patterns.

## Chapter 3

### Blocking impacts on European precipitation regimes

#### Contents

---

#### **3.1 Paper in *Climate Dynamics***

*3.1.1 Introduction*

*3.1.2 Data and Methods*

*3.1.3 Changes in mean precipitation rates*

*3.1.4 Synoptic and dynamics associated to different blocking locations*

*3.1.5 Shifts in precipitation distributions*

*3.1.6 Discussion and Conclusions*

*3.1.7 Supplementary material*

#### **3.2 Dry fingerprint of ridge patterns in southern Europe**

#### **3.3 Impacts in European snow-cover**

---

## Summary

### **Context and objectives**

In this chapter the main effects of blocking activity in European precipitation regimes are analyzed, as presented in Sousa et al. (2017a). Section 3.1 describes the contrasting signals of blocked and strong zonal flow regimes. The E-OBS precipitation dataset is used to analyze the impacts of blocking/zonal regimes in European precipitation regimes. The regional impacts of blocking occurrence in different sectors aims a more comprehensive assessment than previously performed in the literature. Special attention is devoted to some synoptic/dynamical processes and shifts in precipitation regimes associated to each considered atmospheric pattern. Based on the methodology presented in Chapter 2, the separation of impacts in European precipitation associated to high- and low-latitude high pressure structures (blocks and ridges, respectively) is performed in Section 3.2. The regional impacts of blocking and ridge occurrence in winter European solid precipitation (snow-cover) are also addressed (Section 3.3).

### **Methods**

We computed composites of daily precipitation and winter snow-cover anomalies occurring during blocked and zonal flow days in three longitudinal sectors (ATL, EUR and RUS). To further characterize the synoptic environment, a subset of variables derived from the NCEP/NCAR dataset was examined: Integrated Vapor Transport (IVT), an instability index (Lifted Index – LI) and extratropical cyclone activity. The changes in the Probability Density Functions (PDFs) of precipitation distributions in several subcontinental areas over northern and southern Europe were also computed.

### **Results**

Our results show a clear north-south dipole in the precipitation regime responses. Blocking occurrence leads to below average precipitation in the northern half of Europe (more than 50%), due to the ceasing of moist westerly Atlantic flows, and to increased precipitation in southernmost areas, which is in agreement with increased atmospheric instability. A reversal of these anomalies is found for strong zonal flow days, which are responsible for precipitation deficits in southernmost countries of Europe, and precipitation increases further north. Within strong zonal flow regimes, we find that subtropical ridges are associated with particularly dry conditions in the Mediterranean. On the contrary, the analysis of changes in precipitation distributions shows a clear shift towards more torrential regimes in the Mediterranean environment during blocking episodes.

Winter snow-cover is shown to be enhanced during blocking occurrence in large areas of Europe (including southernmost areas), particularly for ATL patterns, which increase by ~50% the number of days with snow covered surface in central Europe. This impact is related with much colder than average conditions under northerly advection. On the other hand, ATL and EUR ridge regimes impose a much lower frequency of days with snowed soils in large parts of the continent, due to a predominantly mild zonal flow.

## 3.1 Paper in *Climate Dynamics*

*Pedro M. Sousa, Ricardo M. Trigo, David Barriopedro, Pedro M. M. Soares, Alexandre M. Ramos, Margarida L. R. Liberato*

*Paper published in Climate Dynamics (2017a)*

In this work we performed an analysis on the impacts of blocking episodes on seasonal and annual European precipitation and the associated physical mechanisms. Distinct domains were considered in detail taking into account different blocking center positions spanning between the Atlantic and western Russia. Significant positive precipitation anomalies are found for southernmost areas while generalized negative anomalies (up to 75 % in some areas) occur in large areas of central and northern Europe. This dipole of anomalies is reversed when compared to that observed during episodes of strong zonal flow conditions. We illustrate that the location of the maximum precipitation anomalies follows quite well the longitudinal positioning of the blocking centers and discuss regional and seasonal differences in the precipitation responses. To better understand the precipitation anomalies, we explore the blocking influence on cyclonic activity. The results indicate a split of the storm-tracks north and south of blocking systems, leading to an almost complete reduction of cyclonic centers in northern and central Europe and increases in southern areas, where cyclone frequency doubles during blocking episodes. However, the underlying processes conducive to the precipitation anomalies are distinct between northern and southern European regions, with a significant role of atmospheric instability in southern Europe, and moisture availability as the major driver at higher latitudes. This distinctive underlying process is coherent with the characteristic patterns of latent heat release from the ocean associated with blocked and strong zonal flow patterns. We also analyzed changes in the full range of the precipitation distribution of several regional sectors during blocked and zonal days. Results show that precipitation reductions in the areas under direct blocking influence are driven by a substantial drop in the frequency of moderate rainfall classes. Contrarily, southwards of blocking systems, frequency increases in moderate to extreme rainfall classes largely determine the precipitation anomaly in the accumulated totals. In this context, we show the close relationship between the more intrinsic torrential nature of Mediterranean precipitation regimes and the role of blocking systems in increasing the probability of extreme events.

#### 3.1.1 Introduction

Blocking systems wield a significant role on the atmospheric dynamics of mid-latitude regions, and their frequency and variability impinge on the climatology of large continental areas. As a result, these high latitude quasi-stationary anticyclones have been frequently studied throughout the last decades, regarding their climatology and characterization (e.g., Rex, 1950b, 1951; Treidl et al., 1981; Barriopedro et al., 2006, 2010a; Croci-Maspoli et al., 2007; Davini et al., 2012a), their specific impacts (e.g., Trigo et al., 2004; Sillmann and Croci-Maspoli, 2009; Buehler et al., 2011; Barriopedro et al., 2011; Ruti et al., 2014; Sousa et al., 2016), as well as their representation in General Circulation Models (Barriopedro et al., 2010a, b, Matsueda et al., 2009; Scaife et al., 2010; Barnes et al., 2012; Vial and Osborn, 2012; Anstey et al., 2013; Dunn-Sigouin and Son, 2013; Masato et al., 2013). Previous studies have found that, over the Euro-Atlantic sector, the occurrence of winter blocking systems disrupts the dominant zonal circulation that affects the European continent, often leading to a reversal of this prevailing westerly flux. As a consequence, low-pressure systems travelling from the Atlantic towards Europe are diverted from their usual paths, resulting in a large decrease of rainfall for most of the European countries. An exception can be found for southernmost and northernmost sectors of Europe, which experience increased precipitation due to a bifurcation of the storm-track around the blocking high structure (Trigo et al., 2004; Nieto et al., 2007; Sousa et al., 2016).

It is worth mentioning the differences between a blocking pattern and a subtropical ridge (Barriopedro et al., 2010a) although sometimes they can induce similar anomalies in surface climate variables (García-Herrera et al., 2010). Some authors have shown that northward strengthening's of sub-tropical ridges in the Eastern Atlantic during the wet season have opposite precipitation responses in Western and Southern Europe to those associated with blocking (e.g. Santos et al., 2009, 2013). Such separation of phenomena should be kept in mind to stress how important is the distinction between the impacts of this type of ridge patterns and those caused by high latitude blocking, which we are concerned about in this particular study. In fact, the balance between strong westerly zonal flows and their interruption at higher (lower) latitudes during blocking (ridge) episodes tend to dominate a large fraction of the variability of European rainfall (Hoy et al., 2014). Teleconnection indices associated with major large-scale patterns affecting the North-Atlantic and European sectors (particularly the North Atlantic Oscillation, the Eastern Atlantic and the Scandinavian pattern) are frequently used in order to explain the intra and inter-annual fluctuations of the intensity of zonal flow, and consequently of precipitation series (e.g. Trigo et al., 2008; Vicente-Serrano et al., 2009; Altava-Ortiz et al., 2010; Casanueva et al., 2014). Still, such one-dimensional monthly-based approaches hamper a deeper comprehension of more complex spatial patterns occurring at intra-monthly time scales, such as blocking systems, reinforcing the need of using more objective blocking detection schemes.

Previous studies based on these algorithms have shown that the impacts of Euro-Atlantic blocks in terms of winter precipitation regimes essentially change with latitude, with a general decrease in most of central areas of Europe, and increases at lower and higher latitudes, albeit over less extensive areas. Such changes may have significant relevance on the annual total during years with highly anomalous frequency of blocking occurrence. However, studies of

### 3. *Blocking impacts on European precipitation regimes*

---

European precipitation changes associated with blocking have been restricted to the winter season. In this regard, most of the European continent lacks a comprehensive and all year-round analysis on changes in precipitation due to blocking occurrence. This analysis is of particular relevance in southern areas of Europe with Mediterranean climates, where precipitation regimes during the warm season tend to be more torrential, i.e., with a higher contribution of intense and more isolated rainfall episodes to annual totals (e.g. Kutiel et al., 1996; Peñarrocha et al., 2002; Burgueno et al., 2010; Cortesi et al., 2013). Therefore, in this perspective, linking precipitation anomalies with blocking occurrence throughout the use of objective detection methods acquires particular importance. An additional asset of these methods is their versatility to address changes in surface impacts as a function of the blocking location. In this sense, previous works have shown that the distinction of separate (yet large) blocking sectors in the Euro-Atlantic sector still results in considerably different impacts at finer scales inside the Euro-Atlantic sector (Yao and Luo, 2014a, b), and even in smaller areas such as the Iberian Peninsula (Sousa et al., 2016). Accordingly, the relevance of the specific longitudinal position of the center of a blocking system cannot be disregarded when analyzing impacts at such a large scale as for the European continent.

On the other hand, blocking impacts on European precipitation regimes have been generally characterized throughout the use of composites of either absolute or relative precipitation anomalies (e.g. Trigo et al., 2004; Masato et al., 2011). This approach focuses on changes in the mean and hence, has neglected to a large extent the importance of shifts in precipitation distributions which arise from these particular synoptic patterns. Extreme Values theory has been used to identify either changes in precipitation and temperature extremes over very confined regions (e.g., Buehler et al., 2011; Sousa et al., 2016) or shifts in temperature distributions (Sillmann et al., 2011). To the best of our knowledge, the assessment of the impact of blocking patterns on the entire precipitation distribution has only been addressed outside of Europe in regions such as California (Hughes et al. 2009). The investigation of these precipitation changes can be assessed through rather simple methodologies, like the one used by Soares et al. (2014), which analyzed changes in Probability Density Functions (PDFs) of precipitation series for Portugal, in the scope of Regional Climate Models performance and future scenarios evaluation. This method follows the works of Perkins et al. (2007) and Boberg et al. (2009, 2010).

Works such as Trigo et al. (2004), Michel et al. (2012), Pfahl (2014) or Sousa et al. (2016) have also shown that the precipitation increases found in southern sectors of Europe during blocking episodes are mainly driven by dynamical features. These factors include synoptic scale processes such as increases in cyclone frequency, but there are also other thermodynamical factors which can enhance atmospheric instability at the local or mesoscale (Lolis et al., 2004; Ricard et al., 2012). Hence, smaller scale processes (e.g. latent heat fluxes) must be addressed to understand regional impacts of blocking occurrence, in line with the distinct shaping of precipitation Probability Density Functions associated to blocking occurrence in specific sectors of the European domain.

The main objective of this work is to characterize the distinct impacts on European precipitation regimes of blocking occurrence in three different sectors, taking into account the

entire distribution of precipitation series, which allows evaluating the net changes as well as the responses in precipitation intensity. The changes in the precipitation regimes of several regions will be supported by a comparison between blocked and strong zonal patterns occurring over different longitudinal sectors of the target domain. Finally, the precipitation responses will be interpreted in terms of dynamical and thermodynamical processes. The work is structured as follows: in Sect. 3.1.2, the datasets are presented, along with a characterization of typical atmospheric patterns during blocking episodes; in Sect. 3.1.3 the precipitation anomalies registered during blocked and zonal patterns are presented, followed by the main dynamical drivers associated to these atmospheric patterns in Sect. 3.1.4; the different responses in terms of changes in precipitation distributions due to blocked and zonal patterns are presented in Sect. 3.1.5; finally, a summary and discussion of the obtained results is offered in Sect. 3.1.6.

#### **3.1.2 Data and Methods**

We used daily precipitation data for Europe from the E-OBS dataset during the period 1950–2012 (Haylock et al. 2008). This European land-only daily high-resolution gridded dataset is accessible throughout the European Climate Assessment and Dataset (ECA&D), and is available on a grid with a horizontal resolution of  $0.25^\circ \times 0.25^\circ$ , based on the interpolation of daily observations from meteorological stations. Despite the overall good quality of this dataset we must acknowledge that this dataset has caveats in areas where the spatial distribution of stations is sparser, such as biased and over smoothed precipitation fields in some cases, as well as possible effects in extremes (e.g., Hofstra et al. 2009, 2010).

The dataset from the NCEP/NCAR reanalysis (Kalnay et al., 1996), on a horizontal resolution of  $2.5^\circ \times 2.5^\circ$  for the 1950–2012 period is also used. The variables explicitly considered were: daily fields of 500 hPa geopotential height (Z500), Lifted Index (LI) and Latent Heat Flux (LHF). In addition, several fields also from the NCEP/NCAR reanalysis were employed to compute the Integrated Water Vapor Transport between 1000 and 300 hPa (IVT, Ramos et al., 2015) and the following catalogues of weather systems: (i) blocking events (Barriopedro et al., 2006); (ii) strong zonal flow days (Sousa et al., 2016); (iii) extratropical cyclones for the northern hemisphere obtained by using the methodology described in Trigo (2006a). These derived datasets are used to explore the blocking signatures in precipitation regimes and to interpret the role of the associated dynamical and thermodynamical processes.

The particular characteristics of the blocked and zonal days catalogues are described next. We distinguish synoptic conditions characterized by blocked patterns and strong zonal flows by objectively identifying days under such atmospheric conditions in the Eurasian sector. These methods rely on the Z500 field from the NCEP/NCAR reanalysis. The catalogue of blocked days was developed by Barriopedro et al. (2006) - further information on the methodology can be found in that work. The authors have used this and other similar blocking datasets extensively for different applications, such as to characterize blocking effects on total ozone (Barriopedro et al., 2010c) and stratospheric variability (Barriopedro and Calvo, 2014), and in evaluating the impact

### 3. Blocking impacts on European precipitation regimes

of blocking patterns in the Iberian Peninsula using a high-resolution precipitation dataset (Sousa et al. 2016).

Following the latter work, the locations of the maximum Z500 for each identified blocking pattern will hereafter be called blocking centers. The reduction of the large-scale blocked pattern to a single central gridpoint (representative of the entire blocking system) enables an objective separation of blocking in different spatial sectors. Thus, three sectors were defined: the Atlantic sector (ATL) which includes all blocking centers located in  $30^{\circ}$ – $0^{\circ}$ W, the European sector (EUR), spanning  $0^{\circ}$ – $30^{\circ}$ E and the Russian sector (RUS), including blocking centers positioned between  $30$  and  $60^{\circ}$ E. Figure 3.1 presents the annual mean frequency of blocking center locations in each gridpoint. We must stress that this classification of blocks into ATL, EUR and RUS types intends to assess different precipitation responses and changes in precipitation regimes purely based on the geographical location of the considered high pressure system, which strongly influences the synoptic environment associated to blocking occurrence in each considered sector. The selection of these blocking sectors is based on previous studies that have already identified distinctive features in the resulting blocking signatures (Wang et al., 2010; Masato et al., 2011; Sousa et al., 2016).

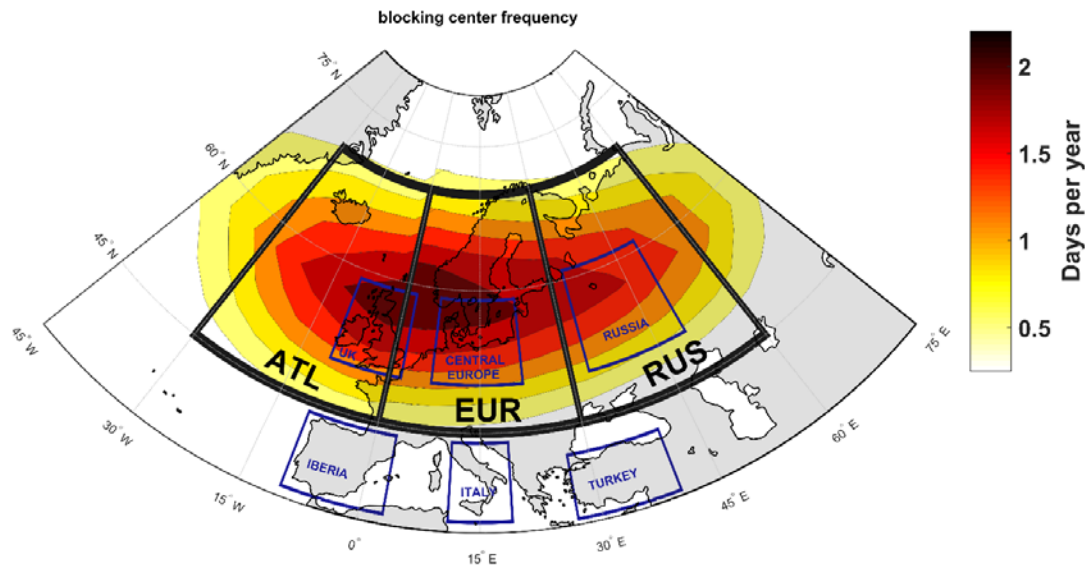


**Fig. 3.1** Thick black boxes identify the considered sectors for blocking center location: Atlantic (ATL)-from  $30^{\circ}$  W to  $0^{\circ}$  W; European (EUR)-from  $0^{\circ}$ E to  $30^{\circ}$ E; Russian (RUS)-from  $30^{\circ}$ E to  $60^{\circ}$ E. The shadings indicate the annual mean frequency of blocking center locations in each gridpoint. Blocks outside the  $45^{\circ}$  N to  $70^{\circ}$  N latitude strip were discarded in both sectors. Thin blue boxes identify areas which were considered in the regional assessment performed in Section 3.1.5.

Seasonal composites of Z500 anomalies during blocking days in each sector are shown in Fig. 3.2. Positive Z500 anomalies centered in the respective blocking sector dominate the northern latitudes, being larger in the colder seasons for all sectors. They capture well the canonical signatures associated with blocking over its climatologically preferred sectors of occurrence in the Eurasian sector, which include eastern Atlantic, Scandinavian and the Urals, respectively.

### 3. Blocking impacts on European precipitation regimes

Negative anomalies of the Z500 fields are less pronounced and usually found southwards and northwards of the blocking centers, mainly during ATL blocks. Also, in this region, summer blocks display a northward extension of subtropical wave-breaking systems near the Azores high. It is important to note that some blocking events contribute to the composites of more than one sector during their lifecycle, since they tend to evolve eastwards towards Europe (Crocini-Maspoli et al., 2007; Barriopedro et al., 2010a; Sousa et al., 2016).

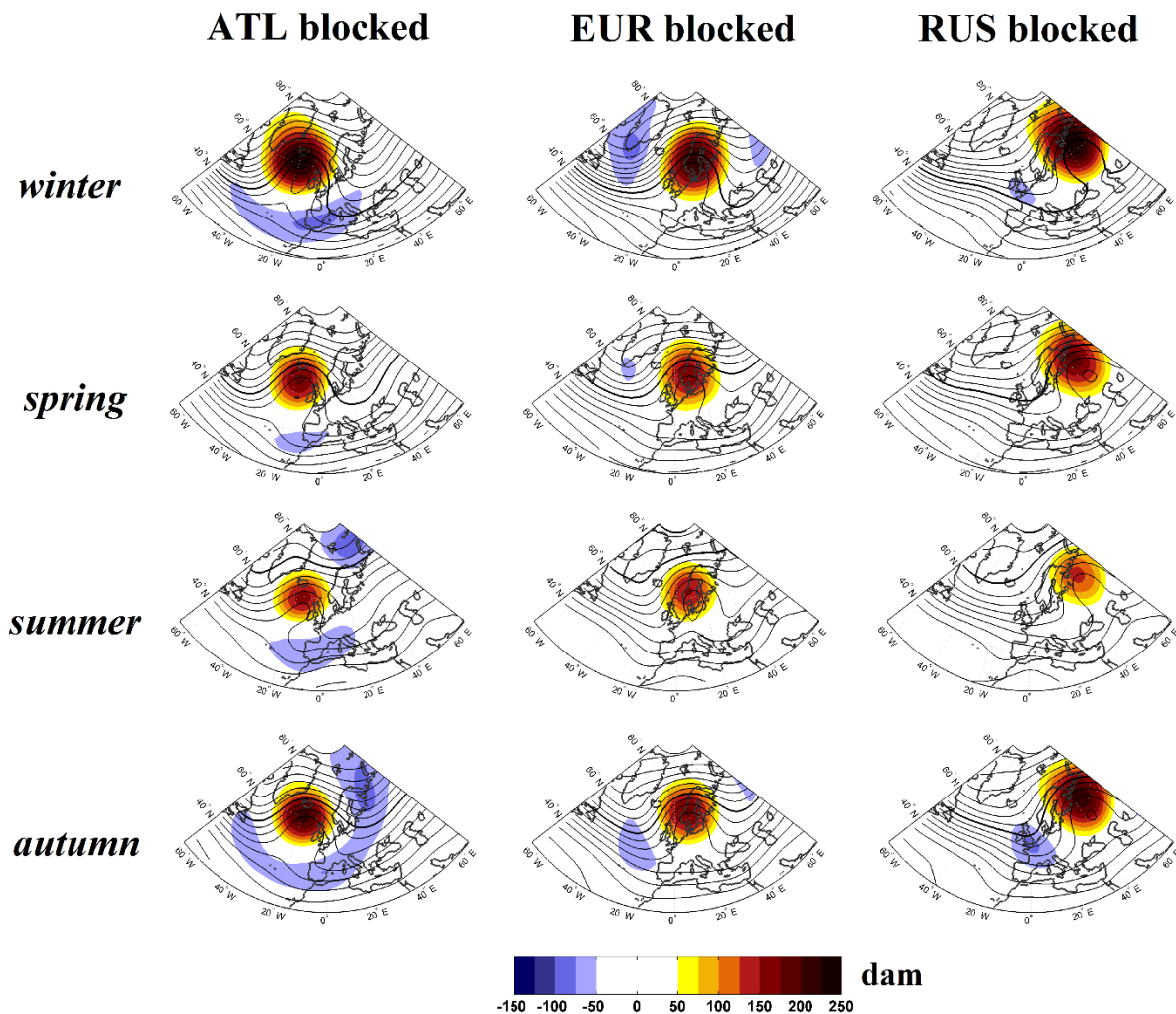


**Fig. 3.2** Composites of the daily anomalies (shaded areas) and absolute values (isolines) of 500 hPa geopotential height for blocking centers in each sector and for all seasons. All values are in decameters (dam) and the thick line represents the 550 dam isohypse.

As a complement to highlight the large impacts resulting from zonal flow reversals which occur during blocking episodes, we also computed a catalogue of days were strong zonal flow conditions occur in the same three sectors (ATL, EUR and RUS). They represent strong westerly flows and hence a large-scale atmospheric pattern that is nearly opposite to that of blocking.

### **3. *Blocking impacts on European precipitation regimes***

---

They were computed following very simple criteria based on several empirical thresholds imposed on the meridional mid-latitude Z500 gradients to ensure a strong westerly flow. See Trigo et al. (2004) for further details on the methodology.

Extratropical cyclones for the northern hemisphere were obtained by adapting the methodology described in Trigo (2006a) and recently used to assess and intercompare the most common features of mid-latitude cyclones, including the most active regions, the most common trajectories, inter-annual variability and trends (e.g. Vicente-Serrano et al. 2011; Neu et al. 2013), cyclone formation mechanisms and impacts (e.g. Liberato et al., 2012, 2013). The objective cyclone identification is based on the detection of local minima in 1000 hPa geopotential height. The cyclone tracking consists on a nearest neighbor search in the previous Z1000 field, considering several thresholds: (i) within a certain area, the cyclone speed should not exceed 50 km/h in the westward direction and 160 km/h in any other. Additionally, the cyclone speed should be higher than 12 km/h. These criteria allow to include the most rapidly deepening cyclones (e.g. Xynthia, Liberato et al., 2013) and to filter the stationary cyclones; (ii) during the lifecycle the cyclone should reach a minimum central pressure corresponding to a sea level pressure below 1020 hPa; (iii) a minimum lifetime of 24 h.

#### **3.1.3 Changes in mean precipitation rates**

In order to evaluate the distinct impacts of the different blocking locations on precipitation regimes, we computed the composites for absolute and relative anomalies of daily precipitation, during blocked and zonal days, in each of the three considered sectors, at the annual and seasonal temporal scales (Figs. 3.3, 3.4). When evaluating the resulting relative anomaly composites one must bear in mind the large range of precipitation values that coexist within such a large domain as the European continent. Thus, one must take into account that similar absolute anomalies in regions with very distinct total annual precipitation climatologies have different relevance. Consequently, to ensure this distinction we first considered the annual composites for the relative changes in precipitation during blocked and zonal days, as presented in Fig. 3.3.

### 3. Blocking impacts on European precipitation regimes

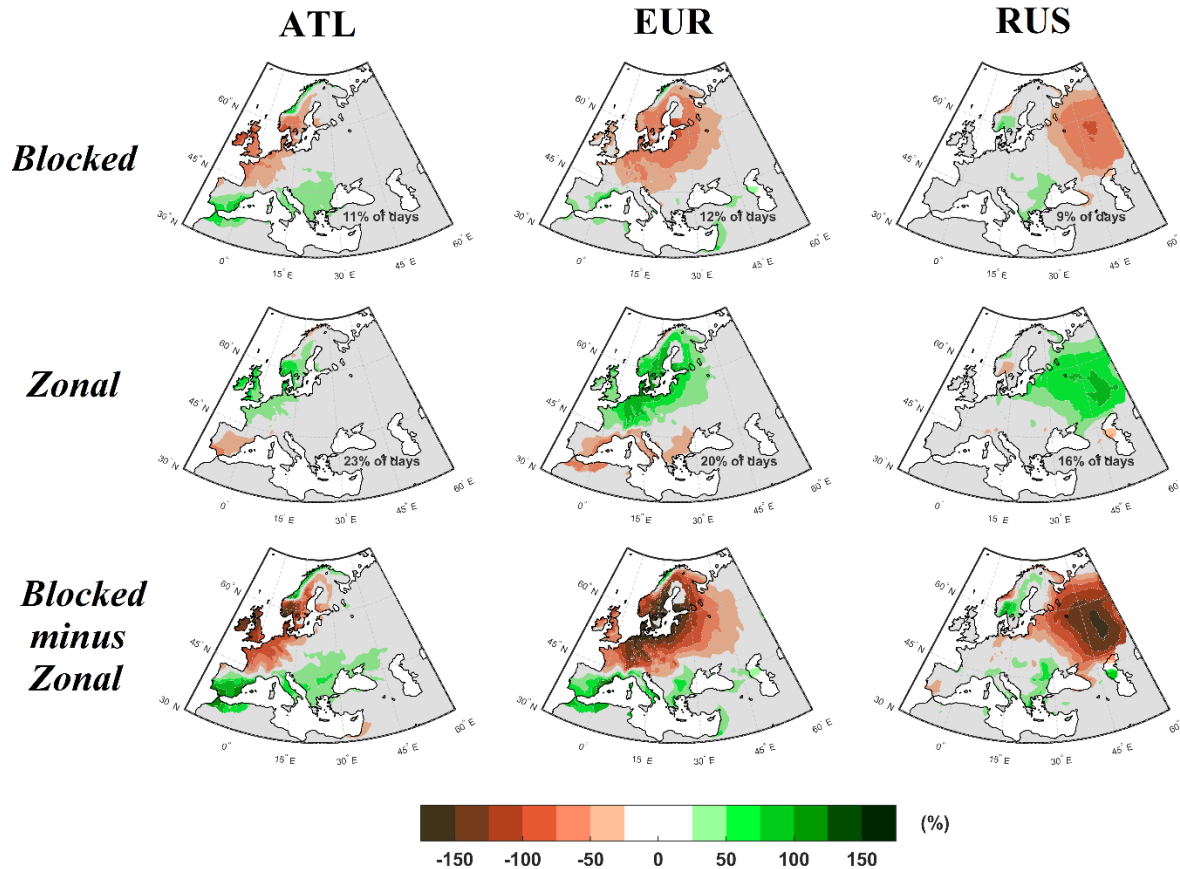


**Fig. 3.3** Annual composites for daily precipitation anomalies (%) in Europe during blocking (upper row) and strong zonal flow (middle row) days in the ATL (left column), EUR (central column) and RUS (right column) sectors. The difference between the regional blocking and strong zonal flow composites is presented in the bottom row. Only statistically significant anomalies at the 5 % level are shown (two-sample Kolmogorov-Smirnov test).

Figure 3.3 clearly shows that for the three considered sectors, the presence of blocking systems leads to well below average precipitation in a wide region under direct influence of the anticyclonic circulation. Maximum decreases of near 75 % are recorded in northern Europe near the blocking centers, which corresponds to an almost complete cease of precipitating days. The maximum negative anomaly is well collocated with the maximum Z500 anomaly of the respective sector (Fig. 3.2), being more extensive for EUR blocking. On the other hand, the increase in precipitation in southern areas of Europe, as well as in the Atlantic strip of Scandinavia matches well with the negative Z500 anomalies, which arise northward and southward of blocking systems (as shown in Fig. 3.2). These positive precipitation anomalies shift eastwards with the considered blocking sector, thus following the relative west-east migration of the maximum Z500 positive anomaly (blocking center). At the annual scale, the widest positive anomalies are found for ATL blocks, during which a large portion of Iberia, Italy, and the Balkans region experience wetter than usual conditions. In particular, daily precipitation rates in southeastern Iberia almost double.

### 3. *Blocking impacts on European precipitation regimes*

---

During strong zonal westerly flows these anomalies are essentially inverted, with a significant reduction in precipitation amounts at lower latitudes, particularly around the Mediterranean basin. Much less significant losses are also found for northernmost areas of Scandinavia. On the contrary, sharp increases in precipitation rates are found in most central and northern Europe, with gains close to 100 % in Benelux, Germany and southern Scandinavia during strong zonal flows in the EUR sector. The difference between composites for blocked and zonal flows sharpens their opposite responses in daily precipitation anomalies, thus illustrating the very significant impacts of zonal flow reversals.

The presented changes in precipitation are in general good agreement with those in the frequency of dry days (below 1 mm) - see Fig. 3.13 from the Supplementary Material. In Sect. 3.5, we will address in more detail how the changes in the number of wet days are distributed for different precipitation intensities.

As stated before, annual rainfall totals in the European domain range from a few hundred mm in dryer regions to several thousand mm in mountainous regions, particularly in Atlantic coastal areas (Haylock et al. 2008). This must be taken into account when analyzing relative anomalies, as a change of 50 % per day in a dry region/season corresponds to a much lower absolute precipitation anomaly than in a corresponding wet region. Therefore, we now present (Fig. 3.4) the corresponding seasonal analysis of Fig. 3.3 but based on the precipitation absolute anomalies at the seasonal scale. In this case, we summarize the results presenting the difference in daily rates between blocking and strong zonal flow days.

When using absolute anomalies, the relative changes are emphasized in regions where seasonal precipitation amounts are high, as for example in central and northern Europe during most of the year, or in easternmost interior areas during the warm seasons. Nevertheless, increases of 2-3 mm per day are significant in relatively dry areas (such as southernmost Europe), as previously depicted in Fig. 3.3. When blocked conditions prevail, precipitation losses in the UK and central Europe are quite striking throughout the year. Summer precipitation responses often embrace lower spatial extensions; however, in some regions such as the northernmost countries and Russia—where precipitation in form of snow is often recorded in colder months—the summer deficits represent the largest changes.

This seasonal analysis also helps distinguish seasonal precipitation responses that are masked at the annual scale. For example, during summer, blocking systems and their associated impacts shift north, and rainfall increases in parts of continental Europe—suggesting a rise in convective precipitation during summer blocks, as it will be discussed further ahead.

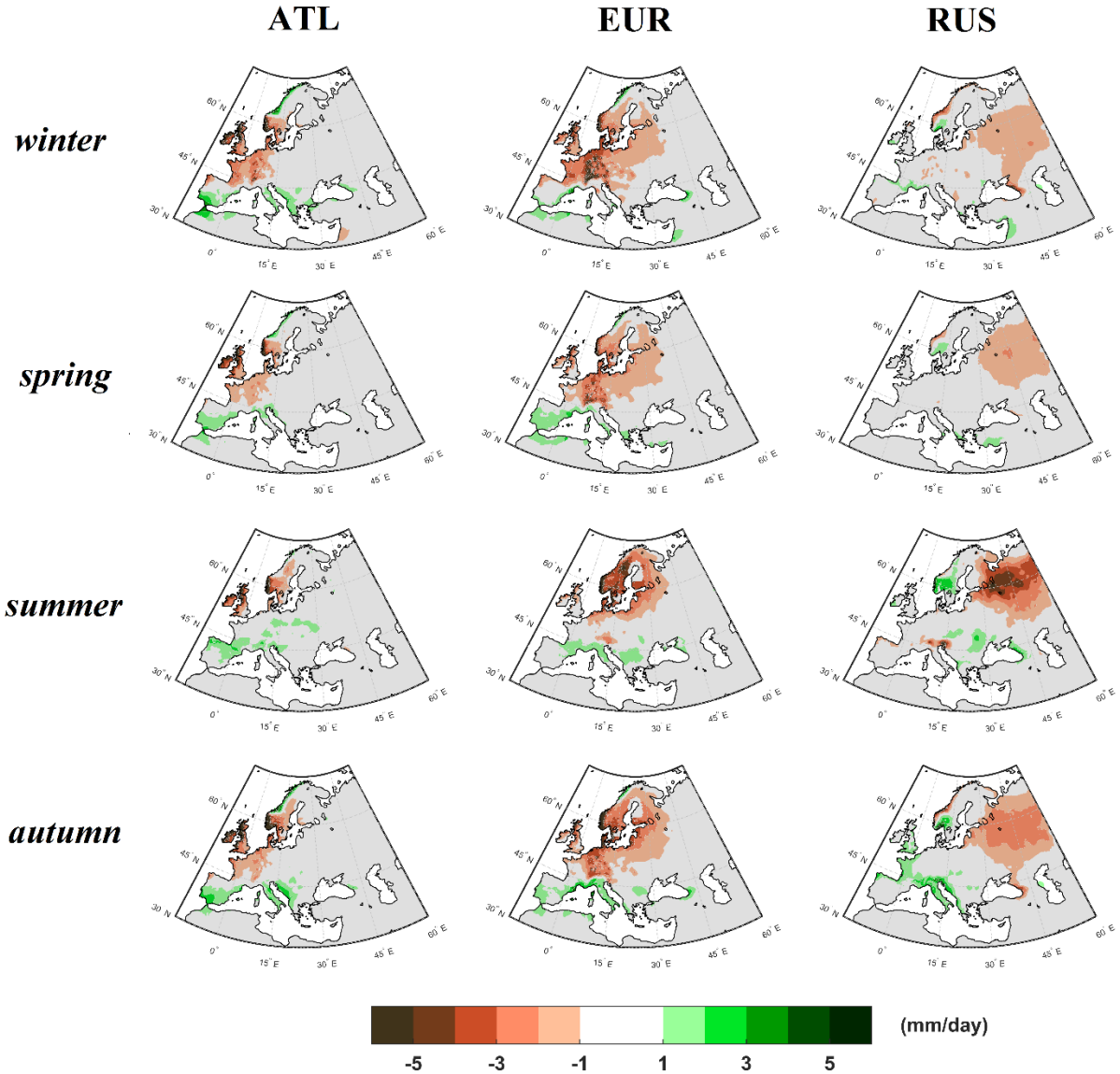


**Fig. 3.4** Seasonal composites for the differences in absolute anomalies of daily precipitation (mm/day) between blocking and strong zonal flow patterns in the ATL (left column), EUR (central column) and RUS (right column) sectors. Only statistically significant anomalies at the 5 % level are shown.

#### 3.1.4 Synoptic and dynamics associated to different blocking locations

To better understand the processes triggering the precipitation anomalies associated with blocking (particularly relevant in southern Europe) we analyzed the changes in the frequency of extratropical cyclonic activity occurring during blocked and zonal regimes. According to Neu et al. (2013) a cyclone refers to a point (the cyclone center) identified on the Earth's surface at a certain time using a certain methodology. The annual mean climatological frequency of

### 3. Blocking impacts on European precipitation regimes

extratropical cyclone center locations in the Euro-Atlantic-Russian sectors is shown in the top panel of Fig. 3.5, along with their relative anomalies (in %) during blocked and zonal events in each sector.

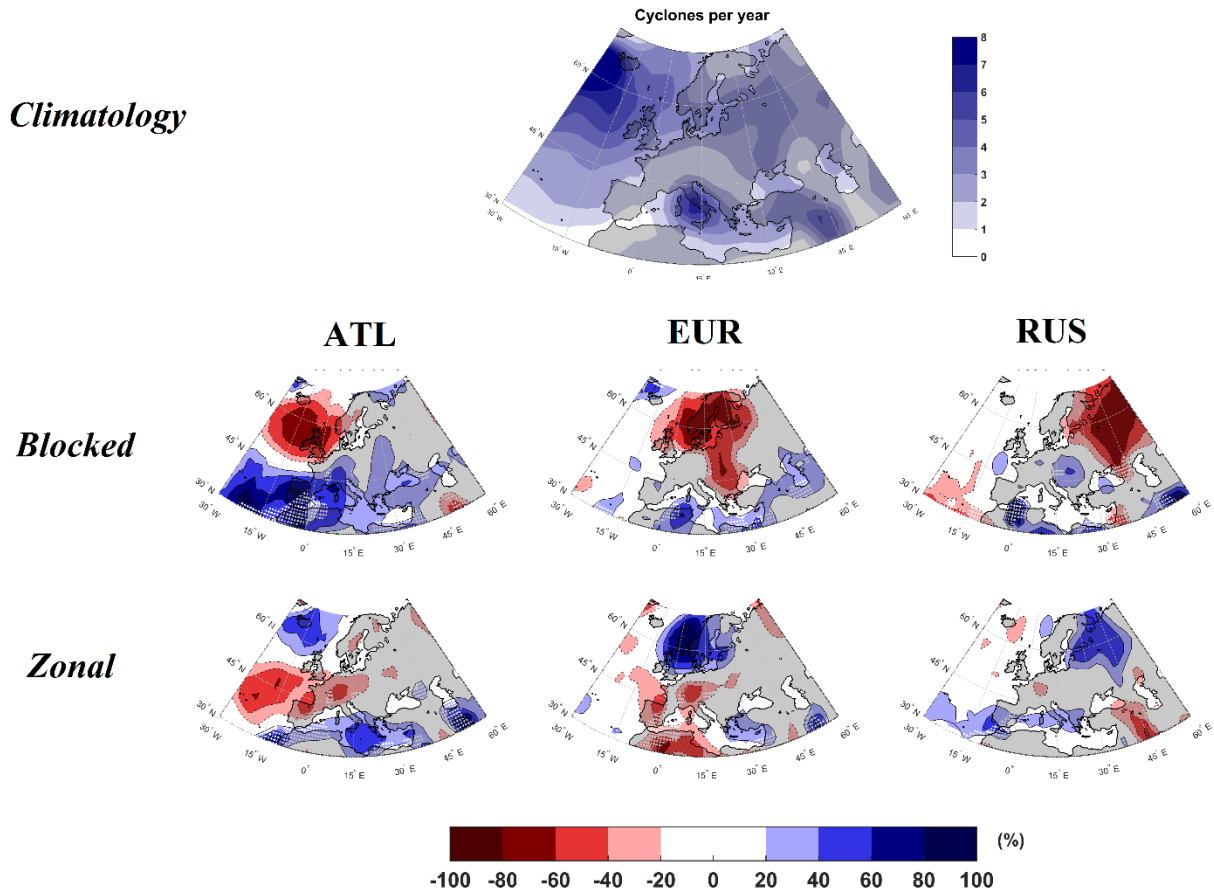


**Fig. 3.5** Top: annual mean frequency of non-stationary cyclone centers (counted in  $2.5^\circ \times 2.5^\circ$  boxes). Middle: row annual mean changes (in %) in the cyclone frequency during blocking episodes in the ATL (middle left), EUR (middle center) and RUS (middle right) sectors. Bottom: row annual mean changes (in %) in the cyclone frequency during strong zonal flow episodes in the ATL (bottom left), EUR (bottom center) and RUS (bottom right) sectors. Increases are shown with blue shading and decreases with red shading. Stippling corresponds to areas with very low mean annual frequency of cyclone occurrence (below 0.5 per year).

A clear increase in cyclonic activity (non-stationary near-surface systems) in southwestern Europe is found during ATL blocks (Fig. 3.5, middle left), contrasting with an almost complete cutback in the UK area, where cyclonic activity is almost non-existent during blocking patterns (relative changes near 100 %). This decrease shifts eastwards as we consider blocking sectors further east. In the particular cases of EUR and RUS blocks, increases in cyclone frequency are also found south of the blocking structures, although more spatially confined and much less pronounced. These changes are in agreement with the well-known blocking effect on storm-tracks and the resulting split in two branches—north and south of the blocking high. During zonal

### 3. *Blocking impacts on European precipitation regimes*

---

patterns consistent increases in cyclone activity are found at higher latitudes, ranging from Iceland to eastern areas of Scandinavia and northern Russia, along with an eastward extension of the strongest branch of the Jetstream. On the southern flank of the Jetstream mean location we find negative anomalies in the frequency of cyclones. These occur over large portions of western and central Europe during strong westerly flows in the ATL and EUR, which in the specific case of the former synoptic pattern contrast with simultaneous increases (reaching 50 %) in eastern Mediterranean areas. Modest increases in extratropical cyclone paths at lower latitudes are also found during strong westerly flow regimes. Nevertheless, these changes tend to be comparatively smaller than those during blocking. Similar spatial patterns have been found for the changes in cut-off lows frequency during blocked/zonal conditions (Sousa et al., 2016; Nieto et al., 2007).

As expected, the southward shift in cyclonic activity during blocking episodes is in fair agreement with the decrease (increase) in precipitation in northern (southern) Europe. This impact is particularly striking during ATL blocks, which exert the largest influence on the track of storms approaching Europe, and accordingly, on the European moisture sources of the Atlantic Ocean, as it will be detailed further ahead. On the other hand, the modest increases in cyclone frequency over some Mediterranean areas during zonal flows are not accompanied by significant rises in precipitation rates (Fig. 3.3).

To complement the obtained changes in cyclonic activity and deep further in the processes behind the precipitation responses, we computed composites of Z500, LI, and IVT (and the corresponding mean horizontal transport of IVT) for blocked and zonal days. The anomalous fields of these variables are shown simultaneously in Fig. 3.6, in order to evaluate concurrently the dynamic and thermodynamical processes (including moisture fluxes and atmospheric instability).

### 3. Blocking impacts on European precipitation regimes

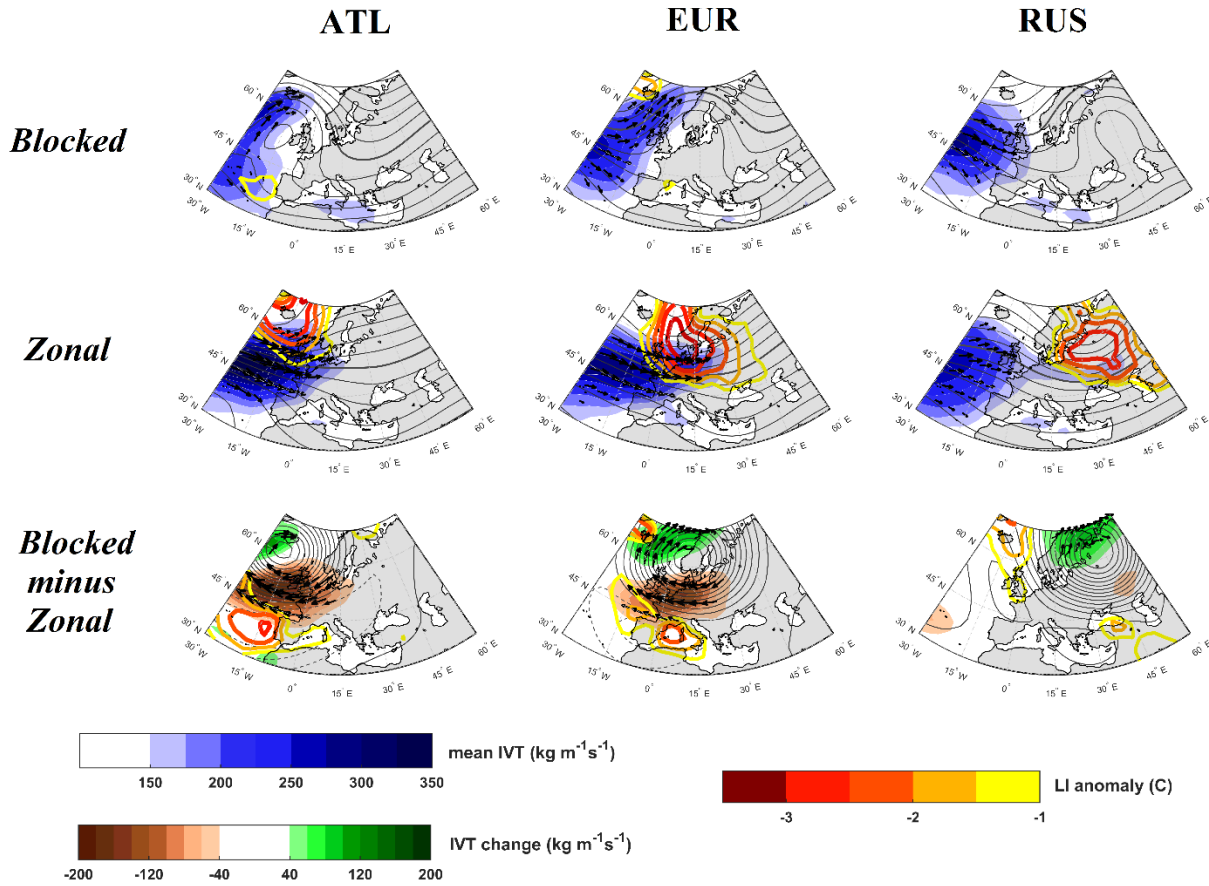


**Fig. 3.6** Annual composites of the daily Integrated Vapor Transport (IVT, in  $\text{kg m}^{-1} \text{s}^{-1}$ , blue shading), and its anomaly in the bottom panels (brown to green shading), the Lifted Index anomaly (LI, in C, reddish thick lines), 500 hPa geopotential height (Z500, in dam, thin grey lines – the thicker grey line corresponds to the 550 dam isohypse) and mean horizontal transport (black arrows,  $\text{kg m}^{-1} \text{s}^{-1}$ ) for blocking (upper row) days, strong zonal flow days (middle row) days and their difference (bottom row). Left, center and right columns correspond to composites for weather patterns occurring in the ATL, EUR and RUS sectors, respectively.

The composites during strong zonal flow days (Fig. 3.6, middle row) reveal a stretching of the high moisture content corridor from the Atlantic towards each considered sector, although in the case of the RUS sector, moisture income towards this area is relatively modest. These extensions towards each sector are on the overall quite coherent with the cyclonic signatures and the precipitation anomalies during zonal days previously shown (Fig. 3.3). On the other hand, blocking structures obstruct these moisture fluxes (Fig. 3.6, upper row), being most of the moisture transport deflected northwards. In the case of ATL blocks, these fluxes are diverted far from continental Europe and the UK, while during EUR blocks the northward deflection of the moisture corridor occurs over Ireland towards Scandinavia. Moisture transport anomalies during RUS blocks are less striking, which agrees with the fact that larger precipitation anomalies in this sector are confined to summer (Fig. 3.4), when moisture fluxes are reduced. For the three

### 3. *Blocking impacts on European precipitation regimes*

---

blocking sectors, there is also a modest transport towards lower latitudes (Mediterranean areas) through the southern flank of the blocking systems. In agreement with the precipitation differences between blocked and zonal patterns, the corresponding difference in moisture fluxes at the annual scale (Fig. 3.6, lower row) clearly shows that a shift from a westerly flow to blocked pattern results in an overall substantial decrease in moisture availability over western and central areas of Europe, and in a significant increase in northernmost Scandinavian areas.

The precipitation increases in southern Europe during blocking episodes do not reflect significant anomalies in available moisture. Instead, for southernmost latitudes, atmospheric instability (depicted by the Lifted Index) appears to relate better with precipitation anomalies, as evidenced in the blocking minus zonal flow composites (bottom panels of Fig. 3.6). Moreover, these changes in LI are spatially consistent with the changes in cyclonic activity frequency, suggesting potential effects in the frequency of extreme precipitation days (as it will be analyzed in Sect. 3.5) in the regions located at the southern flank of blocking structures (i.e. in Mediterranean areas). Thus, moisture availability is not a major constrain to the occurrence of significant precipitation events in southern Europe, at least at the annual scale. On the other hand, the small increases in cyclonic activity in the Mediterranean area which are found during zonal days (Fig. 3.5) are not collocated with the positive LI changes (located further north), therefore supporting the weak precipitation effectiveness of low-latitude weather systems under zonal flows. All these facts reinforce the major role played by atmospheric instability on the precipitation regimes of southern Europe, and its gradual loss of importance as we move north, where stratiform precipitation and moisture availability tend to dominate.

Despite cyclonic activity increases in northern Europe extend to parts of central Europe during ATL blocks (Fig. 3.5), the simultaneous reduction in moisture fluxes at these latitudes explains the decrease in precipitation that can be found in areas such as southern France, parts of central Europe, or even northwestern sectors of the Iberian Peninsula. In this sense, it is important to stress that frontal precipitation associated to extratropical cyclones tends to occur to the south of the cyclone center. As an example concerning the latter region, Sousa et al. (2016) noted that a large fraction of the precipitation that occurs in this area depends on frontal systems linked to cyclone centers located at higher latitudes, and whose frequency is strongly reduced during blocking situations. The same rationale can be applied to other regions as France and central parts of Europe during blocking events in the EUR sector. Thus, while at higher latitudes, the blocking-related decreases in precipitation are in good agreement with an obstruction of storm-tracks and associated moisture corridors, in southern areas, the agreement between blocking-related rainfall increases (Fig. 3.4) and above average atmospheric instability suggests a shift towards more extreme precipitation regimes.

### 3. Blocking impacts on European precipitation regimes

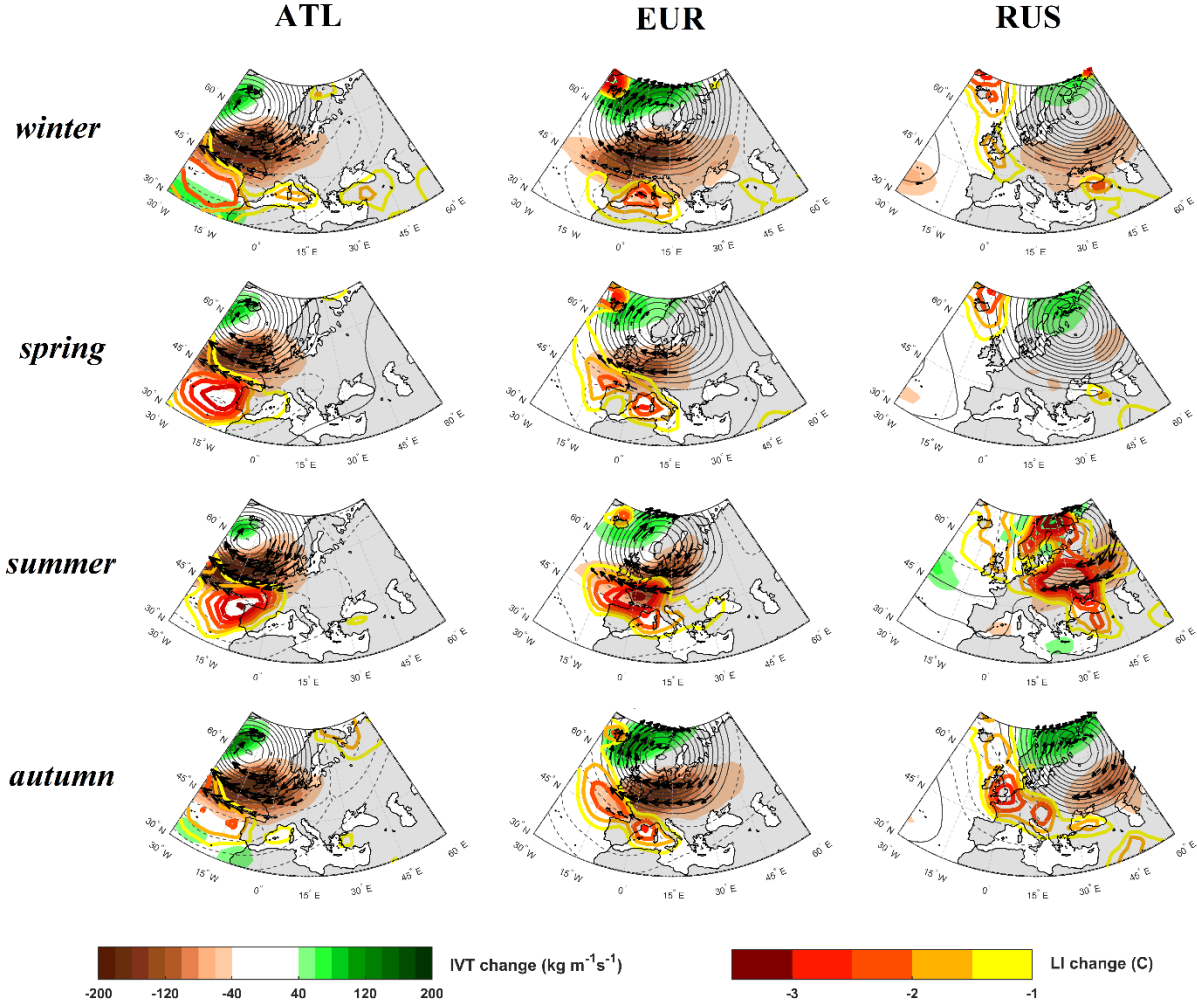


**Fig. 3.7** Seasonal composites for the positive (negative) changes in the daily Integrated Vapor Transport (IVT, in  $\text{kg m}^{-1} \text{s}^{-1}$ ) in green (brown) shading, the increment in atmospheric instability using the Lifted Index (LI, in  $^{\circ}\text{C}$ ) in reddish thick lines, the positive (negative) changes in the 500 hPa geopotential height ( $Z_{500}$ , in dam) in solid (dashed) thin grey, when shifting from strong zonal flow to blocked patterns in the ATL (left column), EUR (central column) and RUS (right column) sectors. Arrows represent the mean horizontal transport of specific humidity.

Overall, the seasonal composites (Fig. 3.7) resemble the annual, although a generalized northward shift can be noted during the warm season—in good agreement with the corresponding migration of the seasonal precipitation anomalies (Fig. 3.4). The pattern of enhanced atmospheric instability in the areas southwards of blocking systems is considerably larger in warmer months. During spring and summer the increase in instability is quite striking west of Iberia (during ATL blocks), as well as in southern France and western Mediterranean areas (during EUR blocks). Interestingly, during summer, an outstanding rise in atmospheric instability during RUS blocks covers a wide domain spanning from Turkey to Scandinavia. The fact that this pattern is essentially restricted to summer explains its absence at the previous annual scale.

### 3. *Blocking impacts on European precipitation regimes*

---

analysis. In effect, during summer some continental areas display precipitation decreases under blocked conditions, despite significant increases in atmospheric instability. We hypothesize that the summer enhancement in atmospheric instability during blocked days must be insufficient to overwhelm the moisture inflow reduction associated with this atmospheric pattern. Thus, once again we find that the precipitation responses in northern areas of Europe are well explained by changes in moisture availability. Nevertheless, some mid-latitude continental areas show a seasonal shift towards wetter conditions during summer and autumn blocks, despite the overall reduction in moisture inflow. These regional warm season changes are concurrent with remarkable increases in LI and hence, the reasoning could be quite comparable to the one presented for southern Europe (essentially driven by atmospheric instability). In summary, this balance between contrasting responses in terms of moisture flows and atmospheric instability between northern and southern Europe is, overall, well explained by a dominant role of moisture fluxes in the former, and of atmospheric instability in the latter, whose influence extends further north into continental Europe during the warmer months.

The atmosphere–ocean coupling must be also considered in this context. In fact, variables such as Sea Surface Temperature anomalies and Latent Heat Fluxes (hereafter LHF) may play a role on thermodynamic processes at both local scale (such as small scale convective systems), and synoptic scale, such as cyclone life-cycles (Grams et al., 2011). As previously shown, LI changes are not always associated to concurrent changes in atmospheric circulation (e.g. cyclones), and hence, the underlying processes behind these LI changes (particularly important in southern areas) should be explored. Thus, we have analyzed changes in LHF during blocked and zonal patterns, as presented in Fig. 3.8.

As it can be observed in the top panel of Fig. 3.8, the highest mean values of LHF (at the annual scale) are observed over the equatorial areas and the Gulf Stream in the Western Atlantic. These areas with high rates of oceanic evaporation are the main large-scale sources of moisture content originated in the Atlantic which are carried towards Europe by typical westerly flows (Gimeno et al., 2013). Other regions, such as the Mediterranean area, may also be important sources of moisture for regional precipitation throughout evaporative processes (Gimeno et al., 2010, 2012). Subsequently, we analyzed LHF anomalies during blocked or zonal synoptic patterns, as changes in evaporative rates should not be disconnected from the thermodynamic processes related with precipitation (particularly convection).

As shown in Fig. 3.8, strong zonal flows are related to above average LHF at higher latitudes, particularly notable in the vicinity of the UK during ATL events, but also in the North Sea and Baltic Sea during EUR and RUS zonal flow episodes, respectively. On the contrary, at lower latitudes, these zonal regimes result in below average LHF. During blocked conditions, there is an overall opposite response in terms of LHF anomalies. For example, during ATL blocks, a large area surrounding Iberia shows higher values of LHF (with maximum expression in the Gulf of Biscay). During EUR blocks this pattern shifts eastwards towards the eastern Mediterranean (particularly in the Aegian Sea), while during RUS blocks positive anomalies are restricted to the Black Sea.

### 3. Blocking impacts on European precipitation regimes

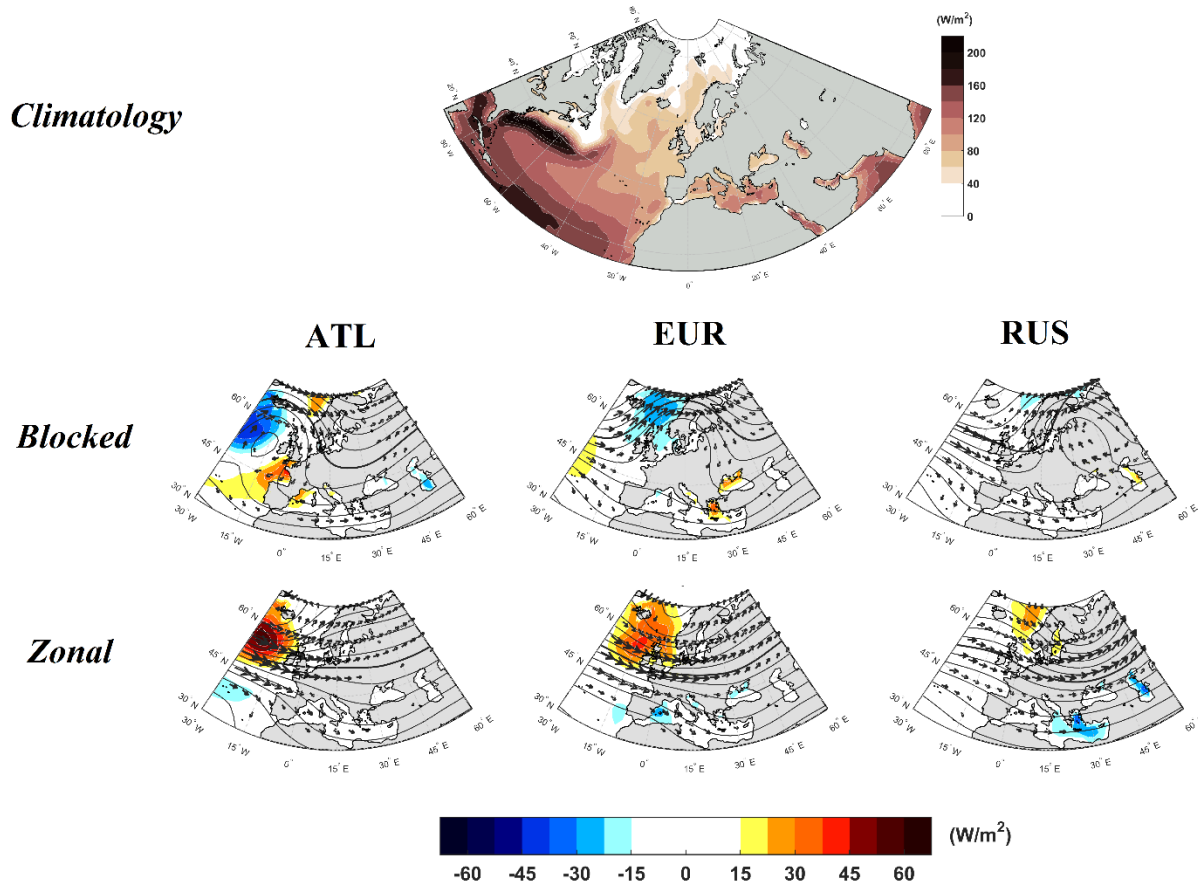


**Fig. 3.8** Top: annual mean latent heat flux (counted in  $2.5^\circ \times 2.5^\circ$  boxes). Middle: row annual mean changes (in  $\text{W/m}^2$ ) in the latent heat fluxes during blocking episodes in the ATL (middle left), EUR (middle center) and RUS (middle right) sectors. Bottom: row annual mean changes (in  $\text{W/m}^2$ ) in latent heat fluxes during strong zonal flow episodes in the ATL (bottom left), EUR (bottom middle) and RUS (bottom right) sectors. Increases are shown with red shading (solid white lines) and decreases with blue shading (dotted white lines).

This pattern of above average LHF in the southern flank of blocking systems may reflect enhanced evaporative processes under the advection of cooler air from higher latitudes due to the easterly/northeasterly synoptic flow. On the other hand, strong westerly flows extending to the surface level may explain the increased LHF at higher latitudes during zonal regimes. Note that the regions of increased LHF during blocked conditions do not display concurrent changes in atmospheric circulation, but they agree with the regions experiencing increased precipitation. In this context, positive LHF anomalies could help explain thermodynamic processes which regionally enhance atmospheric instability in southern areas of Europe during blocking episodes. Taking the Iberian Peninsula as an example, in Fig. 3.14 of the Supplementary Material we present the forward trajectories of air parcels (at different altitudes) originated in areas where the maximum LHF anomaly was found (e.g., the Gulf of Biscay) for a subset of days under ATL blocking. This pattern favors the transport and elevation of air parcels (originally at lower levels in the region with above normal evaporation) towards Iberia, thus possibly establishing a positive

feedback process between evaporative and convective processes, and contributing, at least partially, to the observed rainfall increases in the region.

#### 3.1.5 Shifts in precipitation distributions

In the previous sections we analyzed net precipitation changes in Europe associated to distinct atmospheric circulation patterns. Still, it is important to understand the underlying shifts in different precipitation regimes (or intensities), which can be addressed looking at precipitation distributions, or commonly designated PDF changes. In this section we perform a comprehensive assessment of modifications in precipitation distributions in some representative areas (identified in the boxes in Fig. 3.1) following a similar scheme as the one presented in Soares et al. (2014), and consisting in the next steps:

- (i) For each box presented in Fig. 3.1, we pooled together all the gridpoints, and then computed frequency histograms for wet days (days with rainfall above 1 mm) for 1 mm bins, without distinguishing weather regimes ( $HIST_{ALL}$ );
- (ii) The frequency of each of these bins has been multiplied by its precipitation value, in order to obtain its relative contribution to the total precipitation climatology ( $CONT_{ALL}$ ) of each box;
- (iii) The previous procedure was also applied to wet days under each specific weather regime and for each sector (thus obtaining  $CONT_{BLOCK}$  and  $CONT_{ZONAL}$ );
- (iv) The difference between the bin contributions under each weather regime and the corresponding all-days bin was then computed, in order to obtain the relative change in the contribution of different daily precipitation intensities to the total precipitation anomaly ascribed to the specific weather regime, according to:

$$(CHANGE_{Block}) = \frac{CONT_{BLOCK} - CONT_{ALL}}{NDAYS_{BLOCK}} \quad (1)$$

$$(CHANGE_{Zonal}) = \frac{CONT_{ZONAL} - CONT_{ALL}}{NDAYS_{ZONAL}} \quad (2)$$

The computation described in Eqs. (1) and (2) has been performed for all three sectors considered previously (ATL, EUR and RUS), and  $NDAYS$  represents the number of wet days occurring in each of these specific weather regimes.

Since the sample sizes for each specific weather regime and for each sector are different (and much smaller than the all-days sample size) we have applied a bootstrapping technique to enable a fair comparison between them. For each weather regime, the method estimates  $HIST_{ALL}$  for subsamples of days with the same size as that of the specific weather regime. Thus, for a given weather regime having  $NDAYS$  as sample size, we randomly selected  $NDAYS$  from the complete series and obtained the corresponding histogram, to perform an unbiased comparison.

### 3. Blocking impacts on European precipitation regimes

This random process was repeated 1000 times, and the average of the resulting histograms was taken as the final  $HIST_{ALL}$ .

The precipitation distributions of the four selected European regions and their shifts associated with the occurrence of blocking and strong westerly flows over each sector are shown in Figs. 3.9, 3.10, 3.11 and 3.12. In these figures, the upper panel shows the histogram of daily precipitation for all wet days (above 1 mm,  $HIST_{ALL}$ ) and the black curves show the contribution of each bin to the total precipitation ( $CONT_{ALL}$ ), thus highlighting the daily intensities that are more relevant to the total rainfall of each specific region. The middle panels show the relative changes for each bin under each specific weather regime ( $CHANGE_{Block}$  and  $CHANGE_{Zonal}$ , distinguishing between the three sectors considered), in order to compare the impacts that each atmospheric pattern promotes in different precipitation intensities. Finally, the lower panels show the cumulative relative changes from the previous panels, with the impacts of each considered weather pattern on the total precipitation distribution of the considered location. Please note the different y-axis scales in Figs. 3.9, 3.10, 3.11 and 3.12.

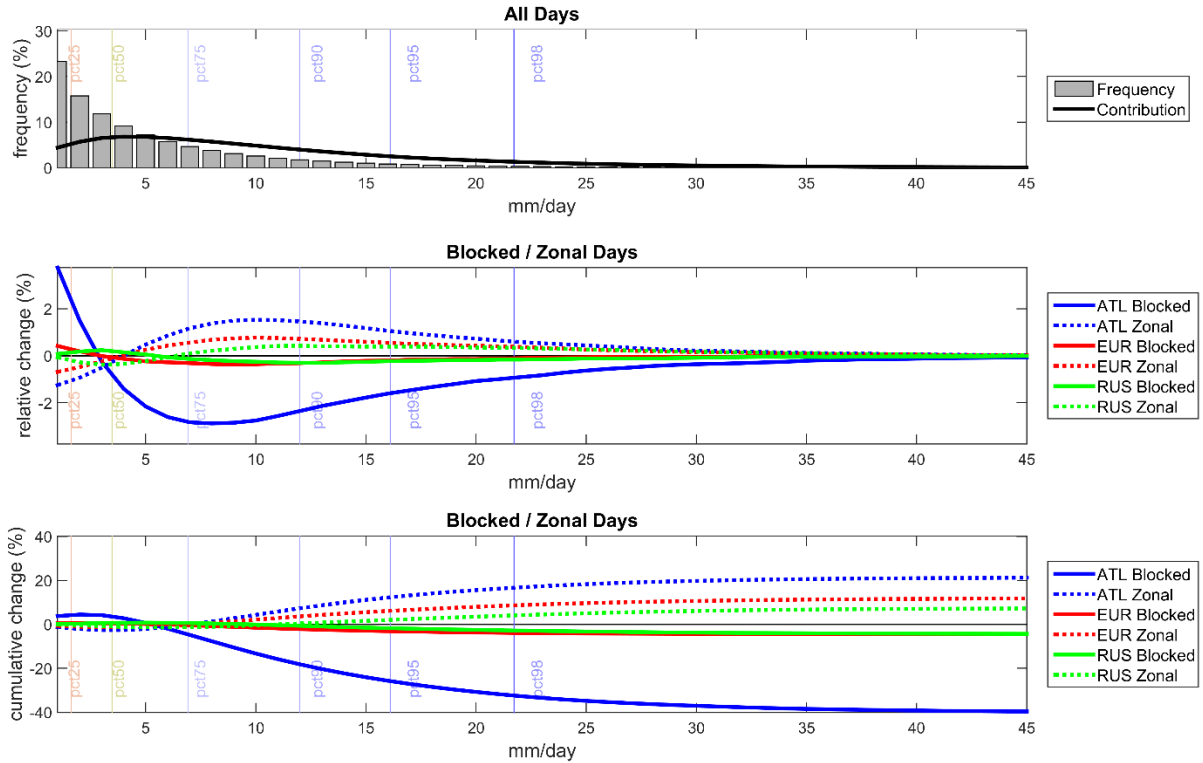


**Fig. 3.9** Shifts in the precipitation distribution for the UK during the different considered synoptic patterns. Top: relative frequency of days with precipitation totals considering 1 mm bins (grey bars) and the corresponding contribution of each bin to the total annual precipitation (solid black line). Middle: relative change in the contribution of each bin to the total annual precipitation for blocked (solid lines) and zonal (dashed lines) patterns in the three considered sectors (colored lines). Bottom: cumulative change resulting from the relative changes in the precipitation distribution associated to each blocked (solid lines) and zonal (dashed lines) pattern. The thin vertical lines represent different percentiles of total daily precipitation (considering only days above 1 mm).

### 3. *Blocking impacts on European precipitation regimes*

---

This approach enables a deeper assessment of the contrasting anomalies found in the precipitation composites (Figs. 3.3, 3.4) for areas such as the UK (Fig. 3.9) or the Iberian Peninsula (Fig. 3.10). As stated before, ATL and EUR blocked patterns reduce daily precipitation rates in the UK and foster them on most of the Iberian Peninsula, while the opposite result is found for strong zonal flow days. The analysis of Fig. 3.9 provides a more detailed view of these differences, as it clarifies that blocked patterns in the ATL sector drastically reduce the number of moderate rainfall days in the UK region (below the 90<sup>th</sup> percentile), and increase the frequency of low precipitation days, as compared to the climatology. The latter have a relatively minor contribution for the precipitation totals, while the former impinge a very large impact on the accumulated relative changes of the precipitation distribution (Fig. 3.9, lower panel), with the total effect being a reduction of 40 % in annual precipitation. On the contrary, strong zonal patterns (particularly in the ATL and EUR sectors) induce an increase of the highly-contributing precipitation bins (those near the median of the distribution), resulting in positive cumulative changes, in clear agreement with the composites of the previous section. Thus, ATL patterns are the most efficient in triggering shifts in precipitation distributions in the UK.

On the other hand, the differences in Iberian precipitation (Fig. 3.3) during blocked (zonal) days in the ATL and EUR sectors are associated to an increase (decrease) in days with precipitation amounts above the 50th percentile (Fig. 3.10). Contrarily to the UK, where blocked and zonal flows have minor impacts in the occurrence of extreme precipitating events, in the Iberian Peninsula ATL and mainly EUR blocks are associated with a substantial shift in extreme events (Fig. 3.10, middle panel), which largely influences the annual total differences in precipitation (Fig. 3.10, lower panel). This is a strong evidence of the impact that blocked patterns have on the occurrence of intense to extreme precipitation days in this area, which are essentially driven by atmospheric instability, as referred in Sect. 3.4. These results help distinguish the utterly different precipitation regimes, and the underlying processes, that dominate annual rainfall totals at different European latitudes. Still, we must bear in mind the existence of large gradients in precipitation regimes that characterize some areas (particularly in southern Europe). Such different responses across regions and seasons, result in a smoothed signal in the annual balance for the entire region. In the particular case of the Iberian Peninsula, different local responses from the overall region's signals are found in northwestern areas during the wet season (Sousa et al., 2016), as shown in Fig. 3.15 and 3.16 of the Supplementary Material.

### 3. Blocking impacts on European precipitation regimes

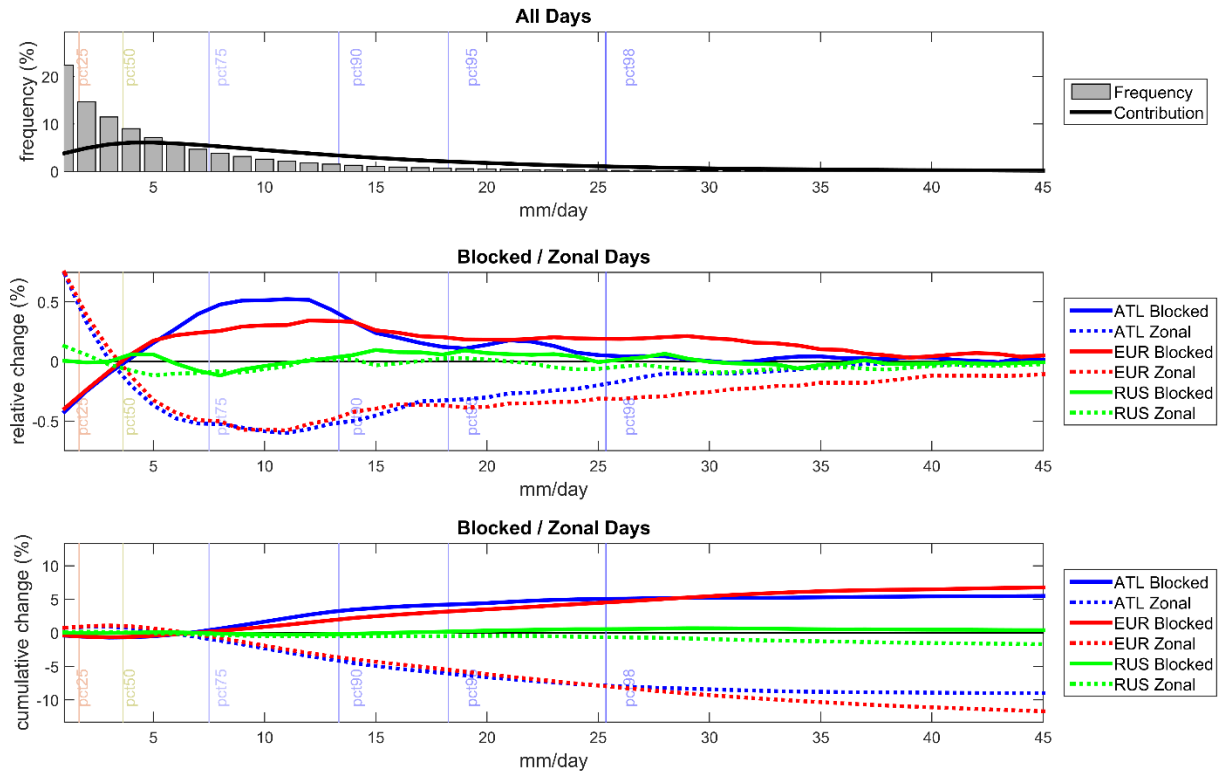


**Fig. 3.10** Same as Fig. 3.9, but for the Iberian Peninsula.

The contrasting results between the UK and Iberian Peninsula shifts in the precipitation distributions are similar to those found between central/northern Europe against the central Mediterranean areas, the main difference residing on the zonal (blocking) sector with most important differences, which in the latter cases correspond to the EUR sector. Thus, zonal (blocked) conditions relate to an overall increase (decrease) in the number of moderate rainfall days (largest differences around 5 mm/day rates) in most of central/northern Europe, while the opposite response is found at lower latitudes, where differences are more associated to the higher percentiles of daily precipitation intensity. Taking into account the similarity with the previous cases, we opted to remit the corresponding figures (3.17 and 3.18) to the Supplementary Material.

We also explored the shifts in the seasonal distributions. Overall, the results indicate a latitudinal dependent behavior. Northern regions of Europe exhibit qualitatively coherent responses to weather systems through the year, although the cumulative changes can display seasonal variations, following the seasonal cycle of precipitation and the factors that cause precipitation anomalies therein (cyclonic activity and moisture availability). As an example, we decided to present the differences in the summer precipitation distribution of the Russian box to emphasize the huge impact that summer blocking episodes exert on the climate of this region (Fig. 3.11). As in other northern/central European areas, the positive (negative) cumulative

### 3. Blocking impacts on European precipitation regimes

changes that arise from zonal (blocked) flows over this region are strongly influenced by variations in the number of moderate rainfall days.

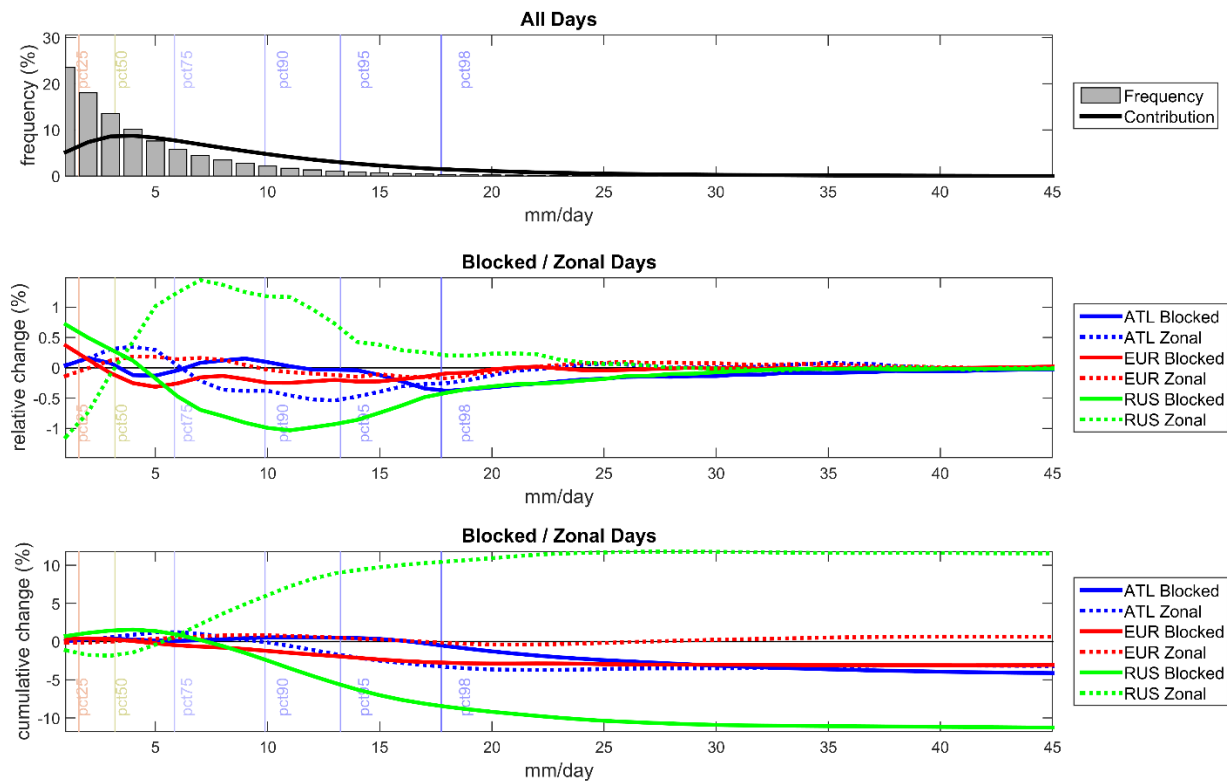


**Fig. 3.11** Same as the previous, but for Russia, and considering only summer days.

On the other hand, the shifts in the precipitation distribution of southern European areas are more likely to be seasonal dependent, as the seasonal cycle in precipitation is larger and the relative contribution of extreme precipitation to the annual total is more important than in northern Europe. Figure 3.12 shows the PDF changes at the annual scale for Turkey. Significant differences occur in a wide range of percentiles, including the highest ones (above the 95th). However, there are clearly contrasting responses between winter and summer weather patterns (see Figs. 3.19 and 3.20 from the Supplementary material). There is not a clear opposite response to zonal or blocked flows, nor a coherent signal through the year. This fact suggests an important heterogeneity in precipitation regimes at both intra-annual and spatial scales in the region, when compared to other European areas, and in particular with other Mediterranean sectors (Sousa et al., 2011). The fact that some other European areas do not show significant differences in the annual mean precipitation responses to blocked/zonal may be due to the co-existence of similar contrasting signals, either in different seasons, or at different precipitation intensities of the distribution.

### 3. Blocking impacts on European precipitation regimes

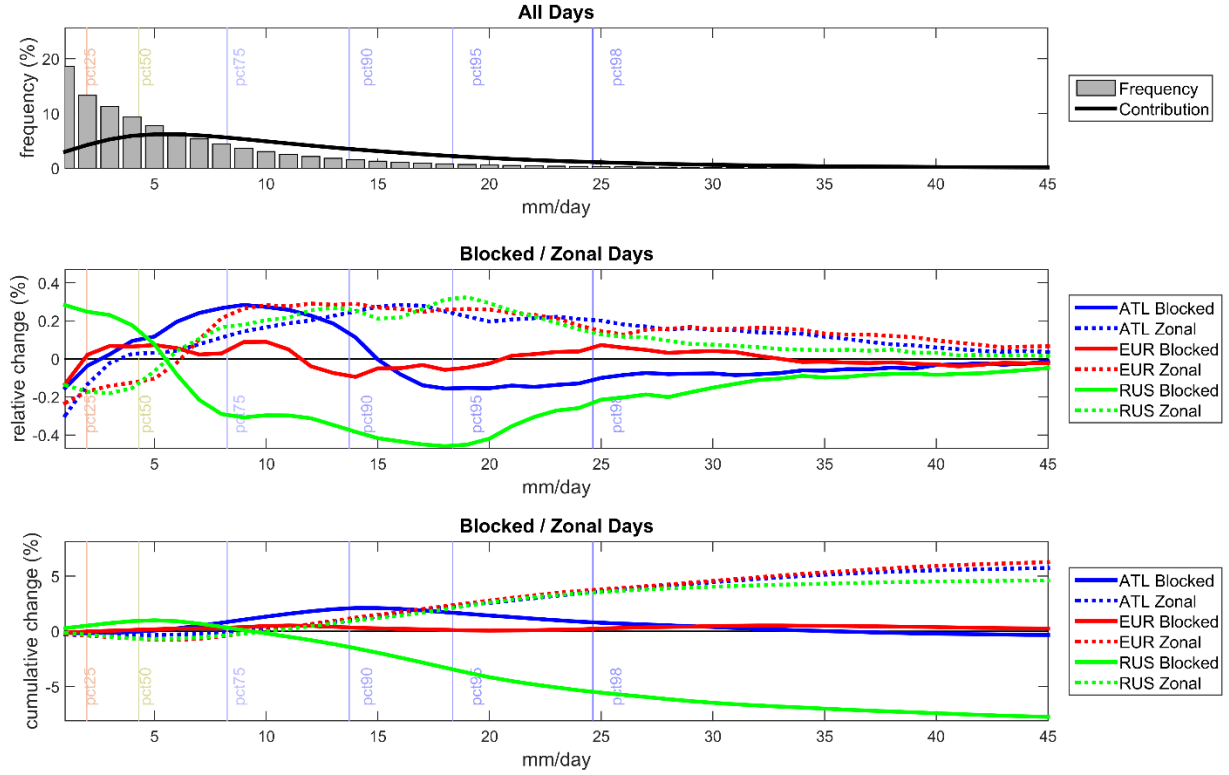


**Fig. 3.12** Same as the previous, but for Turkey.

In summary, the presented cases denote that precipitation regimes in southern Europe are more dependent (than those at higher latitudes) of shifts in the higher percentiles of the daily rainfall intensity. In addition, heterogeneities at both spatial and temporal scales are also much more important than in northern Europe, where distributions tend to be qualitatively similar throughout the year. Consequently, in northern regions, annual analyses of the precipitation distribution shifts are generally sufficient to examine the distinct impacts of blocked and zonal episodes, as the shifts in highly-contributing moderate rainfall days prevail in these regions throughout the year.

#### 3.1.6 Discussion and conclusions

We have performed a pan-European analysis on the impacts of blocking episodes and strong zonal flows on European precipitation regimes and the physical mechanisms associated. Unlike previous studies, we have described the impact in annual and seasonal precipitation, thus including seasons other than winter, which has been the focus of previous assessments. We first analyzed composites for precipitation anomalies, and afterwards, the precipitation distribution shifts over major regional domains, considering in all cases the effects of large scale circulation anomalies over three different areas of occurrence (mid-Atlantic, Europe and Russia).

### 3. *Blocking impacts on European precipitation regimes*

---

Overall, the results indicate significant opposite precipitation responses to blocking occurrence between northern and southern regions of the continent. Positive net changes are found in southernmost areas, while negative net changes occur in most central and northern regions of Europe - exception made for the Atlantic strip of Scandinavia where variations in precipitation present the same signal response as in southern Europe. The location of the largest precipitation anomalies follows well the positioning of the blocking centers, migrating eastward as we move from the Atlantic to the Russian sector. On the other hand, during strong westerly flows, the anomalies of this north-south dipole are reversed, resulting in precipitation gains (decreases) at higher (lower) latitudes. In the areas under direct blocking influence, the substantial decrease in precipitation rates (reaching in some cases around 75 %) extends throughout the year, including areas where annual rainfall totals depend more on warm season's precipitation. In particular, the dramatic decrease in Russian precipitation during spring and summer blocking episodes gains particular relevance under the scope of recent noticeable events, such as the mega-heatwave of 2010 (Barriopedro et al., 2011). Our results reinforce the potentially outstanding impact of prolonged blocking episodes occurring over continental areas in terms of water availability (e.g., the role of Russian blocks on the complex feedback processes between pre-conditioning soil moisture deficits and summer heatwaves enhancement, Miralles et al., 2014; García-Herrera et al., 2010).

The presence of blocking systems results in a bifurcation of storm-tracks north and south of their usual paths, as already described by Trigo et al. (2004) or Walter and Graf (2005). In large parts of central and northern Europe, where frontal systems associated to synoptic-scale disturbances usually prevail, these storm-track shifts are responsible for the previously referred rainfall deficit due to the subsequent significant decreases in cyclone frequencies and moisture transport. Contrariwise, during days characterized by strong zonal flow, our results demonstrate an increase in cyclonic activity and moisture transport towards northern and central Europe, concurring with a rise in rainfall totals, associated to a stronger than usual Jetstream. In agreement with this main driver of precipitation anomalies in northern and central Europe, the strongest effects are observed under the occurrence of circulation anomalies centered in the Atlantic and European sectors, which exert a major influence on the storm-tracks and moisture advection inland.

On the other hand, in southern Europe, the branch of storm-tracks deflected southwards due to blocking occurrence is responsible for above average cyclonic activity. Again, this effect is particularly relevant for blocking centers located in the Atlantic sector, resulting in twice as much cyclonic activity in the Iberian Peninsula area. Although not so striking, increases in cyclone frequency extend throughout many Mediterranean areas for other blocking locations. Quite the opposite, rainfall deficits in southern Europe are found for strong westerly flows, particularly in western and central Mediterranean areas.

While the rainfall increases over southern Europe during blocking agree with cyclonic activity anomalies, we have shown that they are better explained by increases in atmospheric instability, which are particularly notable in the southern flank of blocking systems. This process is not particularly dependent of high moisture contents, as our analysis shows that these blocking-

### 3. *Blocking impacts on European precipitation regimes*

---

related rainfall increases are concurrent with below average moisture influxes towards Europe. This emphasizes the more convective nature of precipitation regimes of southern European countries, when compared to a much more relevant contribution of frontal/stratiform systems at higher latitudes. These results lead us to perform a more regionalized assessment of precipitation changes and to highlight the meridional variation in precipitation responses and associated mechanisms. In this regard, we went further than previous studies by analyzing changes in the seasonal and annual precipitation distributions for a number of boxes in northern and southern Europe, during blocked and zonal regimes.

We show that the overall negative net changes in precipitation in most sectors of central/northern Europe are essentially driven by the substantial drop in the mid-percentiles of the distribution (i.e., moderate rainfall days), which strongly contribute to the cumulative totals. Inversely, during days characterized by intense zonal flow, an increase in the mid-percentiles of daily precipitation rates highlights the vital role of synoptic-scale frontal systems and their association to a stronger Jetstream and the Atlantic moisture inflow. In contrast, in southern European areas, the increases in precipitation rates during blocking episodes are mostly related with increases in the mid to high percentiles of the precipitation distribution, in some cases particularly striking above the 90th and 95th percentiles. This clearly shows an increase in the probability of heavy to extreme precipitation days during blocked patterns, confirming the role of convective processes in the blocking-related precipitation anomalies of southern Europe. Given the significant contribution of heavy precipitation days to annual totals in this region, our results highlight an outstanding role of blocked patterns on the inter-annual variability of southern European rainfall regimes.

In most areas, the synoptic patterns and precipitation responses are quite coherent throughout the year. However, the involved mechanisms differ in magnitude and spatial extent from season to season and affected areas. In particular, blocking occurrence and the associated increase in atmospheric instability (and consequently in convective processes) to the south/southeast of blocking centers shift northward during summer, and as a consequence, positive precipitation anomalies also extend further north than during other seasons. Besides, we have also verified that while precipitation responses during blocked/zonal regimes are spatially coherent in central and northern Europe, the responses in southern regions are more complex. In this area, opposite responses within relatively small domains (and/or between different seasons) can be masked on the annual analysis (e.g. Iberia and Turkey).

Finally, we discussed how processes such as latent-heat-fluxes may be determinant to both cyclogenesis and local feedback processes. In fact, blocked atmospheric patterns are associated with above average evaporation in specific sectors, which may enhance atmospheric instability and/or provide a local moisture source for precipitation. In this context, parcel tracing and other ocean-atmosphere processes should be analyzed in more depth for a deeper assessment of local-scale processes, which may be particularly relevant in southern European areas.

### 3. Blocking impacts on European precipitation regimes

**Acknowledgments** Pedro M. Sousa was supported by the Portuguese Science Foundation (FCT) through a doctoral grant (SFRH/ BD/84395/2012). Alexandre M. Ramos was also supported by FCT in a postdoctoral grant (FCT/DFRH/SFRH/BPD/84328/2012). Pedro M.M. Soares thanks the Portuguese Science Foundation (FCT) for funding under Project SOLAR-PTDC/GEOMET/7078/2014 This work was partially supported by FEDER funds through the COMPETE (Programa Operacional Factores de Competitividade) Programme and by national funds through FCT (Fundação para a Ciência e a Tecnologia, Portugal) through Project STORMEx FCOMP-01-0124-FEDER-019524 (PTDC/AAC-CLI/121339/2010). We acknowledge the E-OBS dataset from the EU-FP6 Project ENSEMBLES (<http://ensembles-eu.metoffice.com>) and the data providers in the ECA&D Project (<http://www.ecad.eu>). The authors gratefully acknowledge the NOAA Air Resources Laboratory (ARL) for the provision of the HYSPLIT transport and dispersion model and/or READY website (<http://www.ready.noaa.gov>) used in this publication.

#### 3.1.7 Supplementary Material

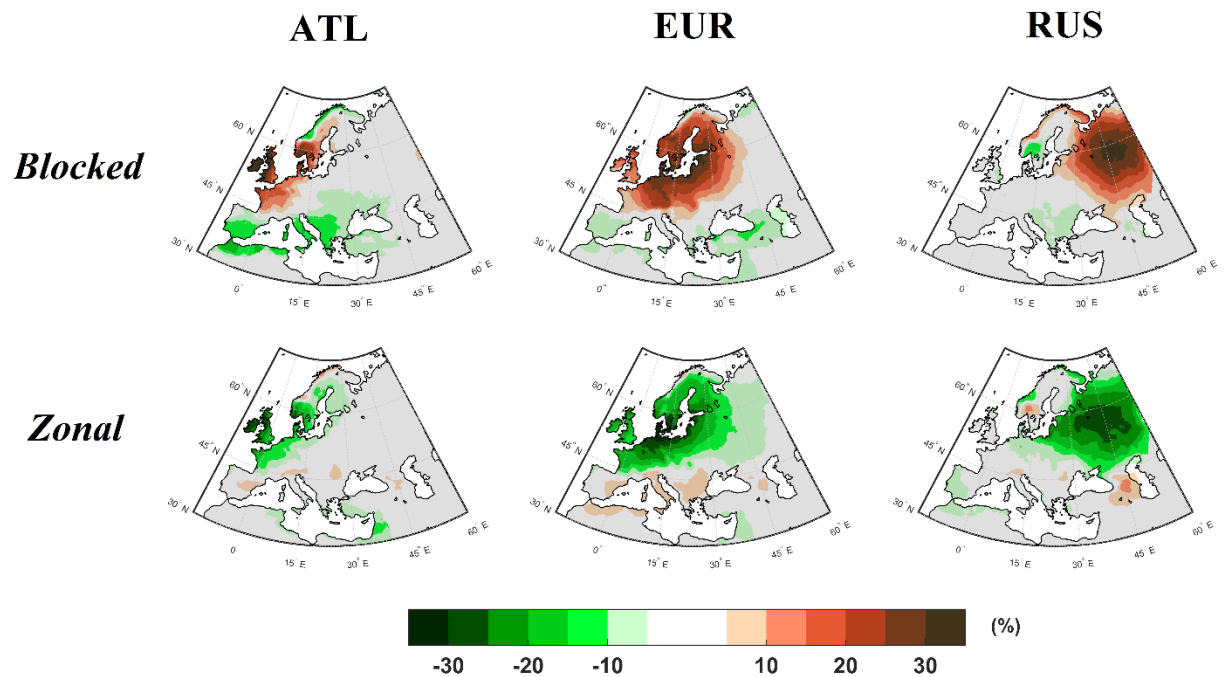


**Fig. 3.13** Change in the number of dry days (%) in Europe during blocking (upper row) and strong zonal flow (bottom row) days in the ATL (left column), EUR (central column) and RUS (right column) sectors, relative to the complete series.

### 3. Blocking impacts on European precipitation regimes

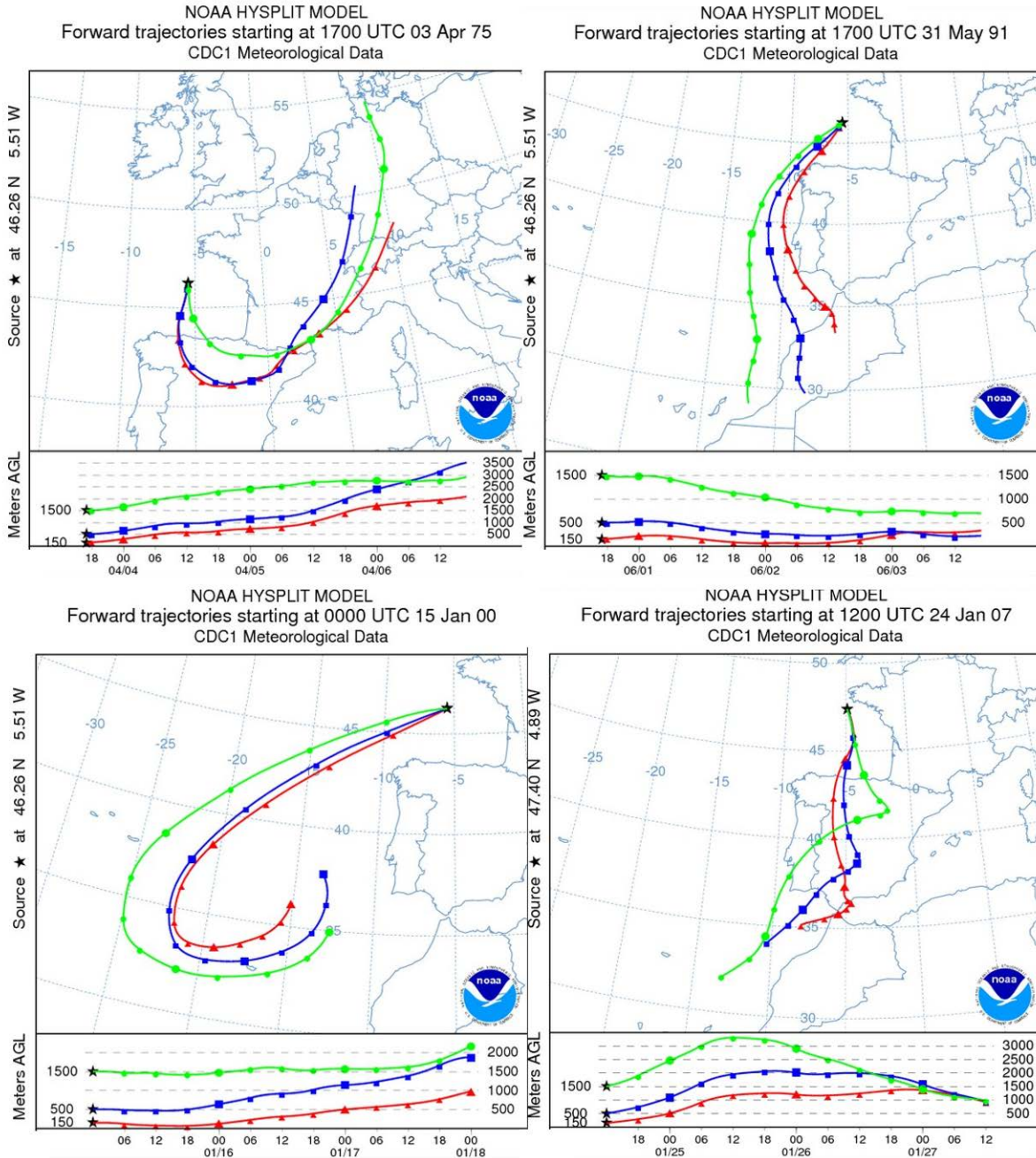


**Fig. 3.14** Forward trajectories of air parcels (starting at 3 different altitudes) originated where the maximum LHF anomaly was found (the Gulf of Biscay) for a subset of 4 ATL blocking days. Plots were originated with the tool available from the NOAA Air Resources Laboratory website ([https://ready.arl.noaa.gov/HYSPLIT\\_traj.php](https://ready.arl.noaa.gov/HYSPLIT_traj.php)) and which uses the HYSPLIT Trajectory Model (Draxler and Rolph, 2003; Rolph, 2003).

### 3. Blocking impacts on European precipitation regimes

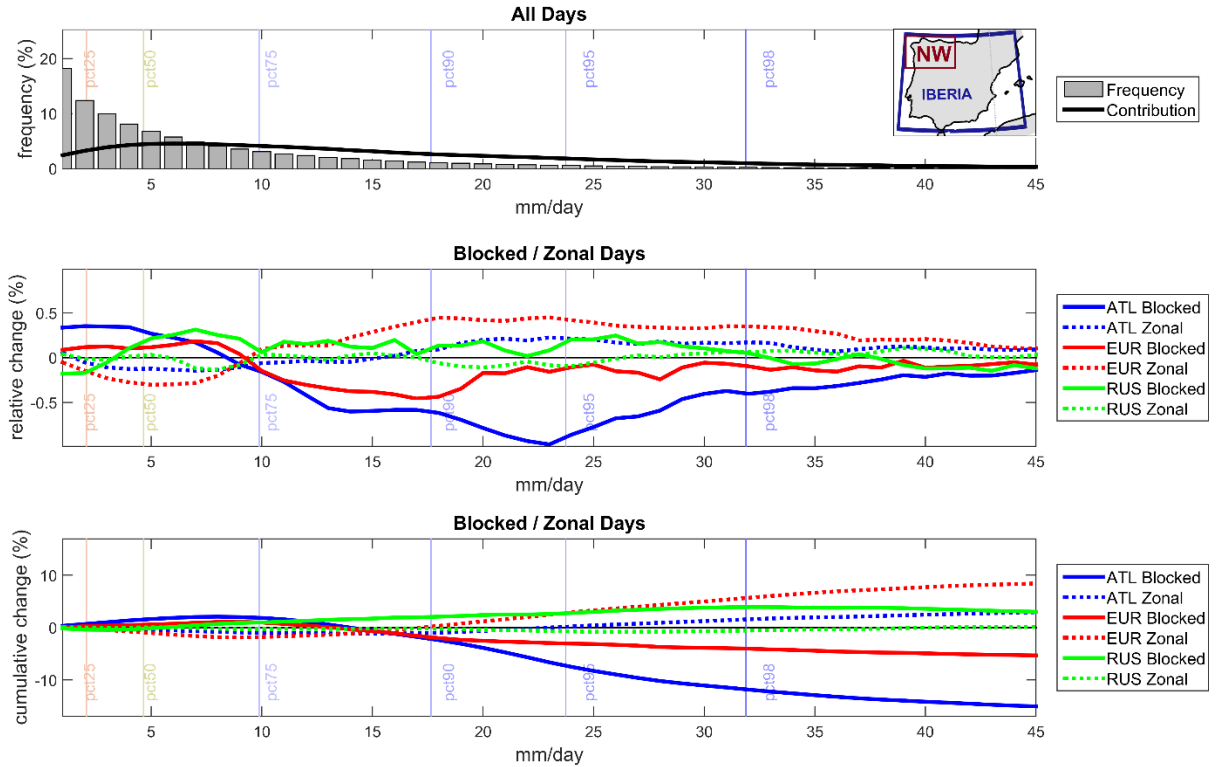


**Fig. 3.15** Changes in precipitation distributions in the northwestern sector of the Iberian Peninsula during winter months and for the different considered synoptic patterns. Top: Relative frequency of daily precipitation totals considering 1mm bins (grey bars) and the corresponding contribution of each bin for the total annual precipitation (solid black line). Middle: Relative change in the contribution of each bin for blocked (solid lines) and zonal (dashed lines) patterns in the three considered sectors. Bottom: Cumulative change resulting from the changes in distributions associated to each blocked (solid lines) and zonal (dashed lines) pattern. The thin vertical lines represent different percentiles of total daily precipitation (considering only days above 1mm).

### 3. Blocking impacts on European precipitation regimes

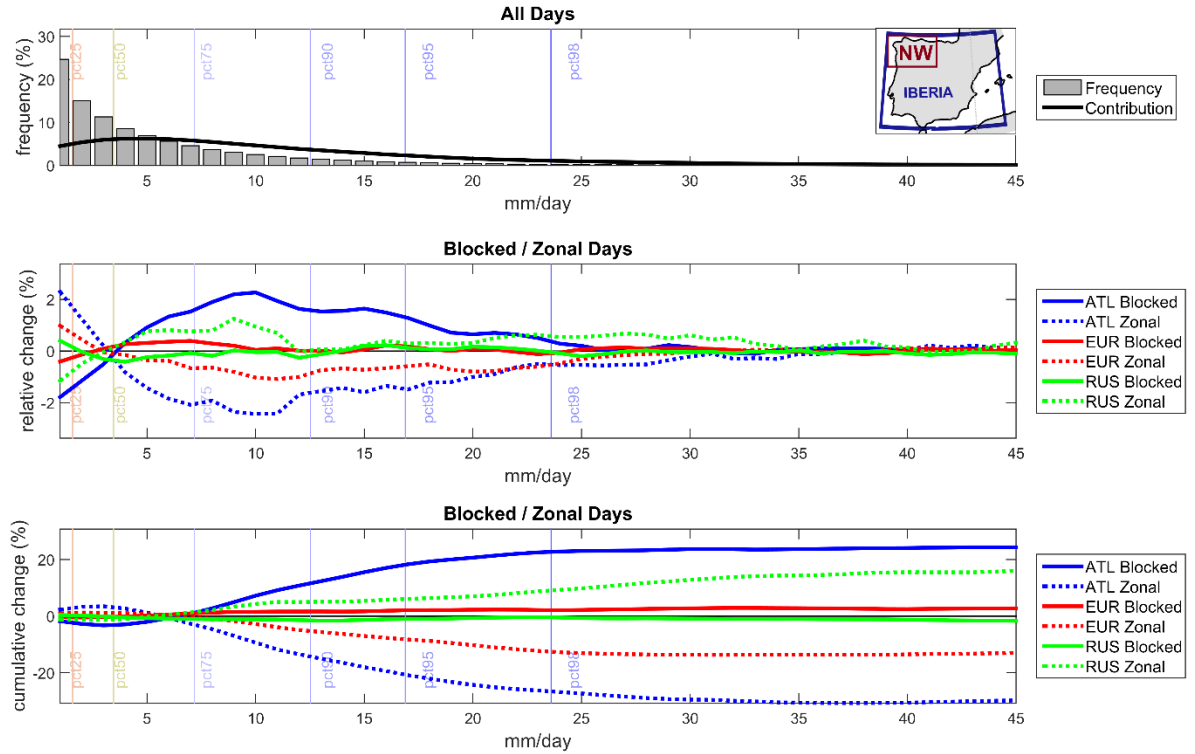


**Fig. 3.16** Same as the previous, for the northwestern sector of Iberia, but only during summer months.

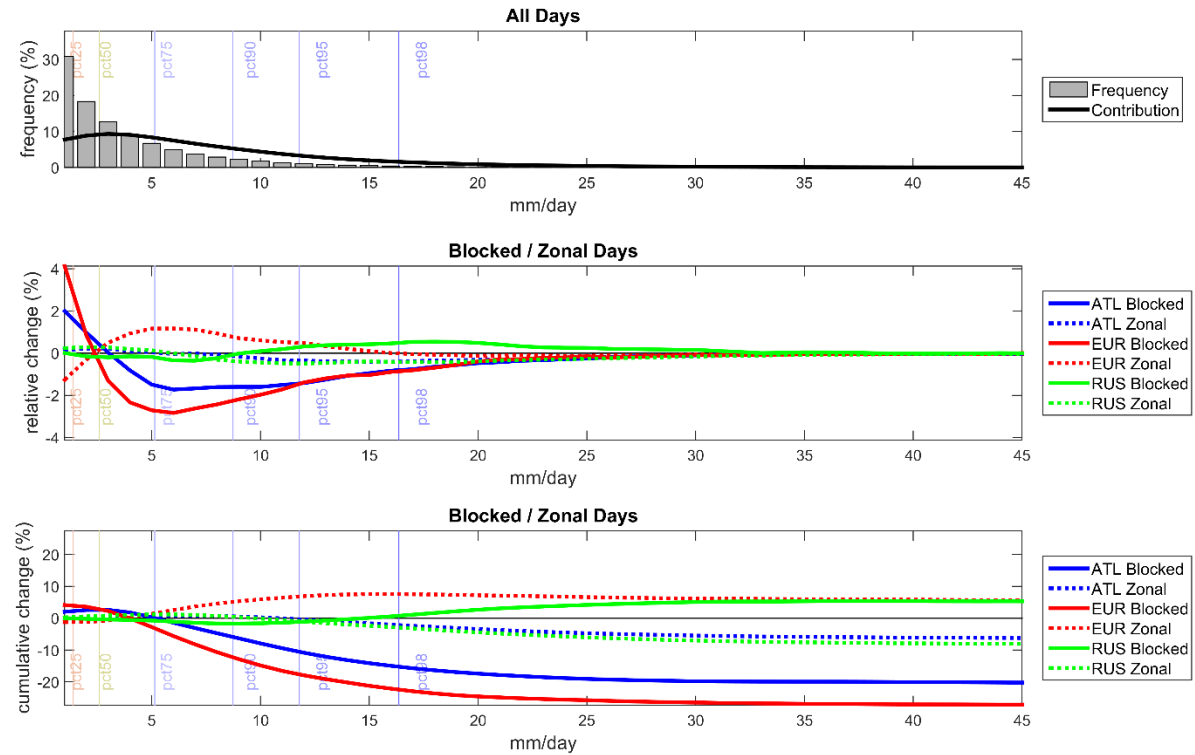


**Fig. 3.17** Same as the previous, but for Central Europe (entire year).

### 3. Blocking impacts on European precipitation regimes

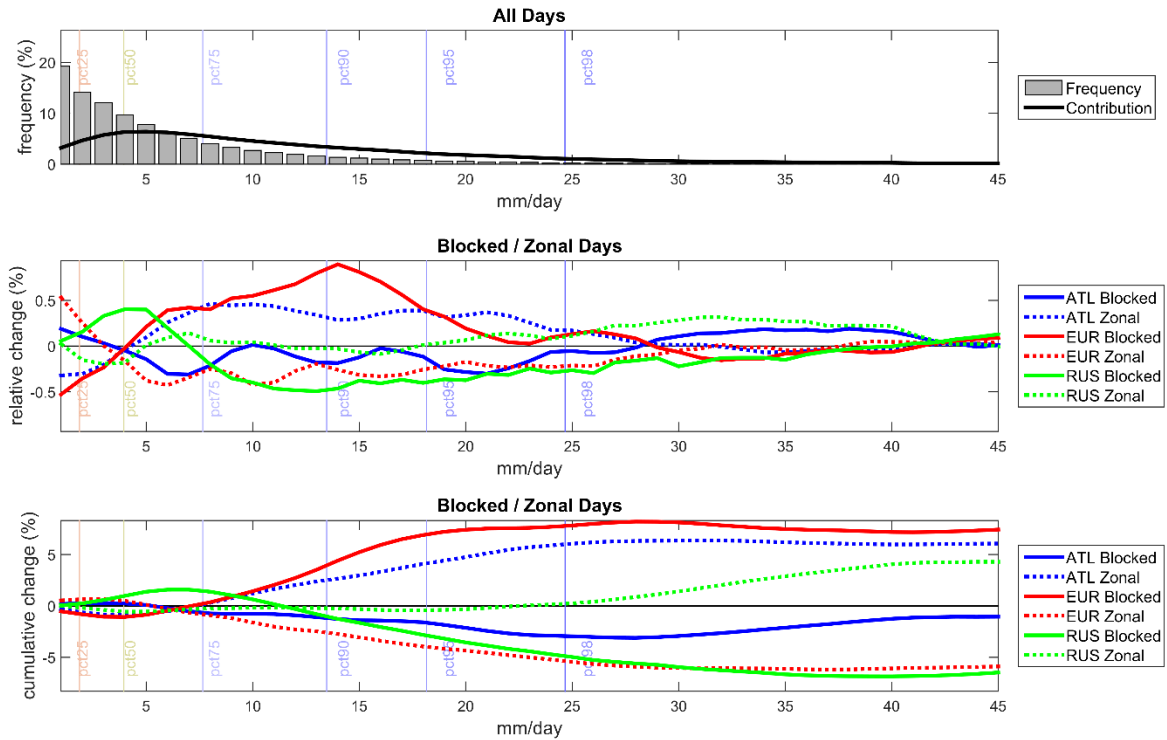


**Fig. 3.18** Same as the previous, but for Italy (entire year).

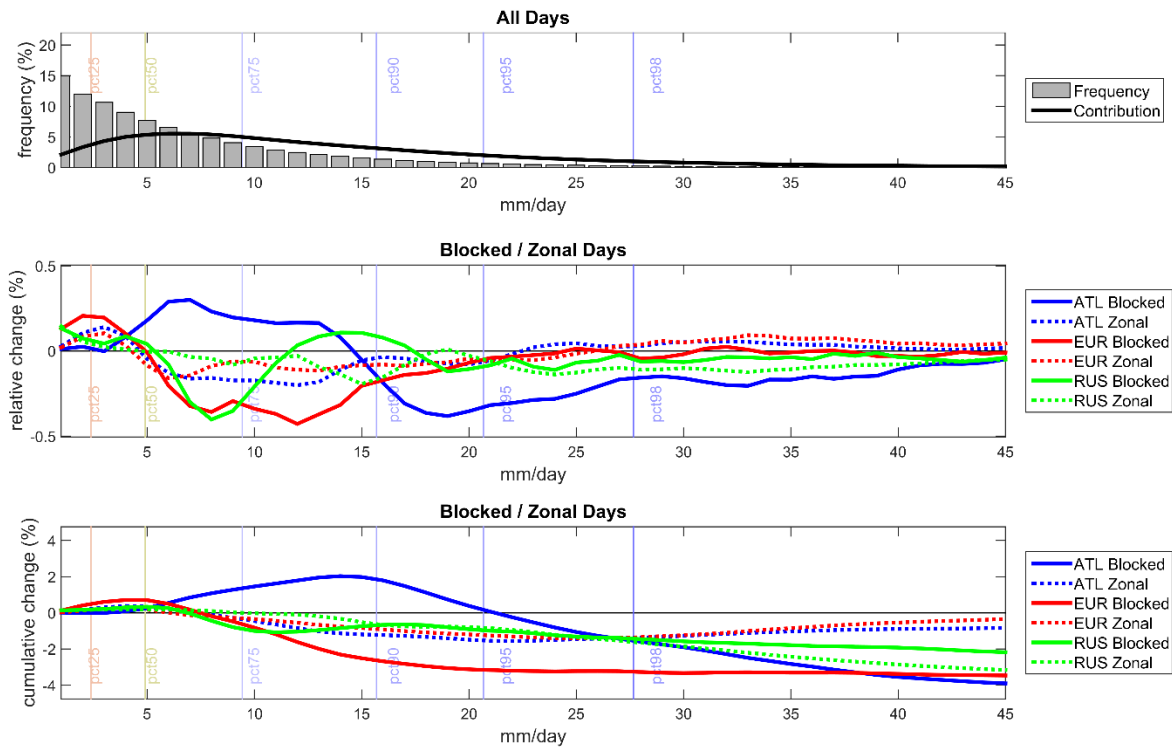


**Fig. 3.19** Same as the previous, but for Turkey, and only during winter months.

### 3. Blocking impacts on European precipitation regimes

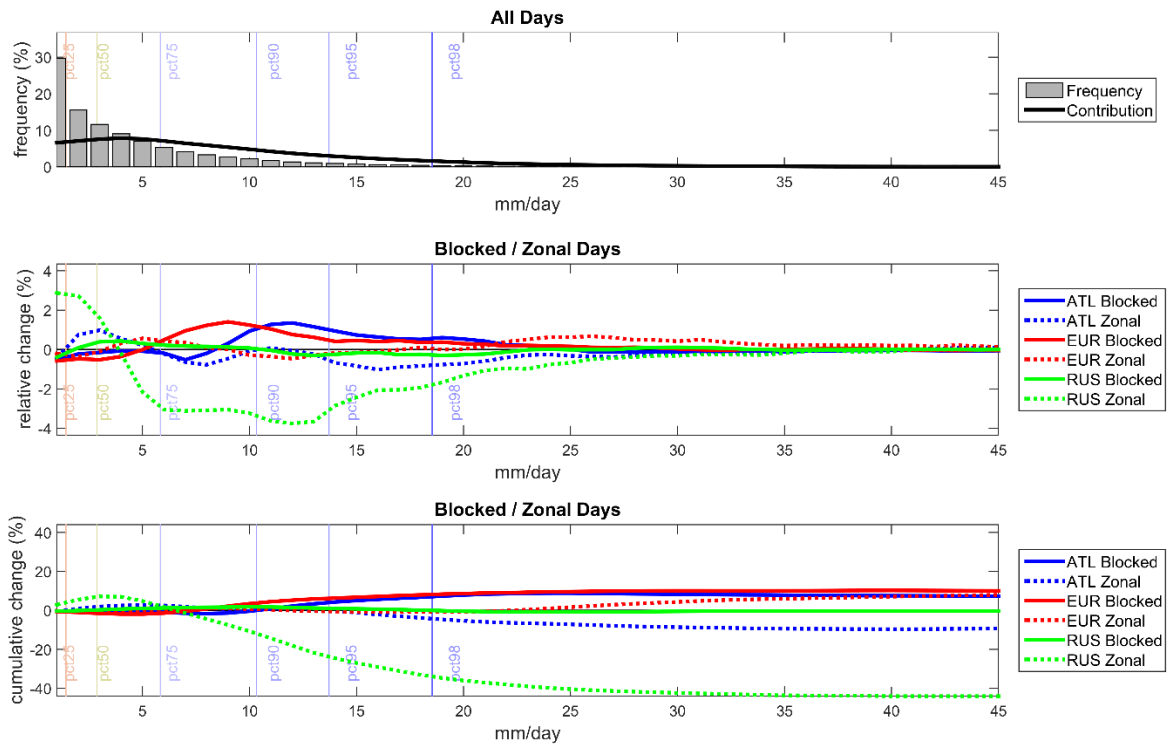


**Fig. 3.20** Same as the previous, but for Turkey, and only during summer months.

## 3.2 Dry fingerprint of ridge patterns in southern Europe

As discussed in Section 3.2, dry episodes are recurrent in southern European areas, particularly in the Mediterranean. In Section 3.3, we demonstrated that the variability in rainfall regimes and particularly heavy precipitation events in southern Europe are closely related to the occurrence of high-latitude blocking. On the other hand, precipitation deficits in this area are related to anomalous high pressure systems at lower latitudes (e.g. Xoplaki et al., 2004). Santos et al. (2009) already associated very dry winters in Portugal to the occurrence of persistent sub-tropical ridge episodes in the eastern Atlantic, which reduce the number of frontal systems in the vicinity of northwestern Iberia, thus resulting in well below average rainfall during the wet season.

Taking this into account, and making use of the developed catalogue of sub-tropical ridges, we also explored the impacts on European precipitation during ridges in the ATL, EUR and RUS sectors. The composites for the seasonal precipitation relative anomalies (in %) are shown in Fig. 3.21.

### 3. Blocking impacts on European precipitation regimes

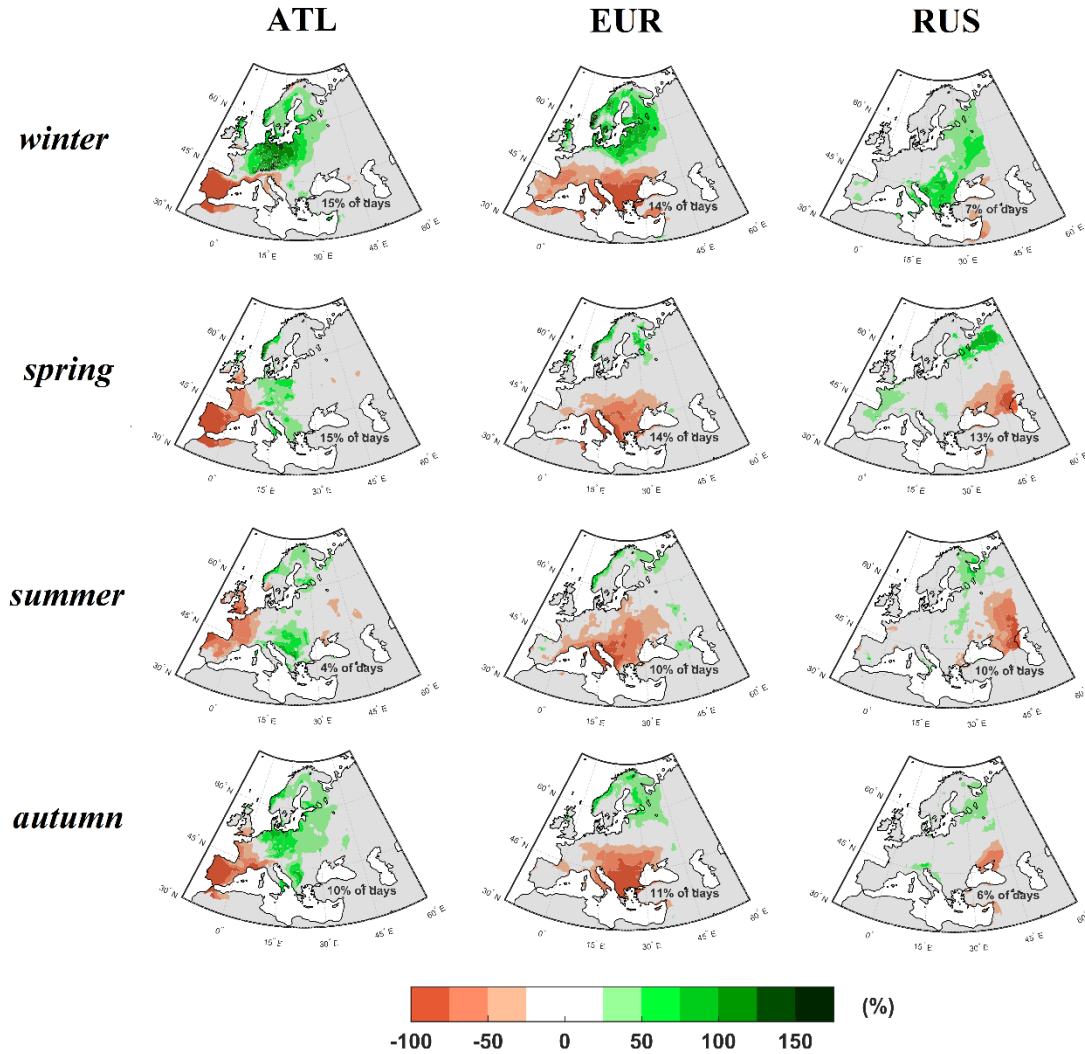


**Fig. 3.21** Seasonal composites of daily precipitation anomalies (%) in Europe for ridges in the ATL (left column), EUR (central column) and RUS (right column) sector. Only statistically significant anomalies at the 5 % level are shown (two-sample Kolmogorov-Smirnov test).

Similar to the temperature anomalies (particularly during winter) presented in Chapter 2, the precipitation changes during ridge days are essentially opposite to those found for blocking days (Fig. 3.4). Consequently, ridge patterns are associated with well below average precipitation in most of southern areas, where the maximum geopotential height anomalies of the ridge structure are located (see Fig. 2.2). The exception can be found during RUS ridges, which are located sufficiently to the east to still allow the penetration of Atlantic frontal systems towards the Mediterranean area. It should be noted the similarities of the ridge signals in precipitation (particularly in winter and for central and northern Europe) with the corresponding patterns obtained for the zonal flows as shown in Fig. 3.22.

### 3. Blocking impacts on European precipitation regimes

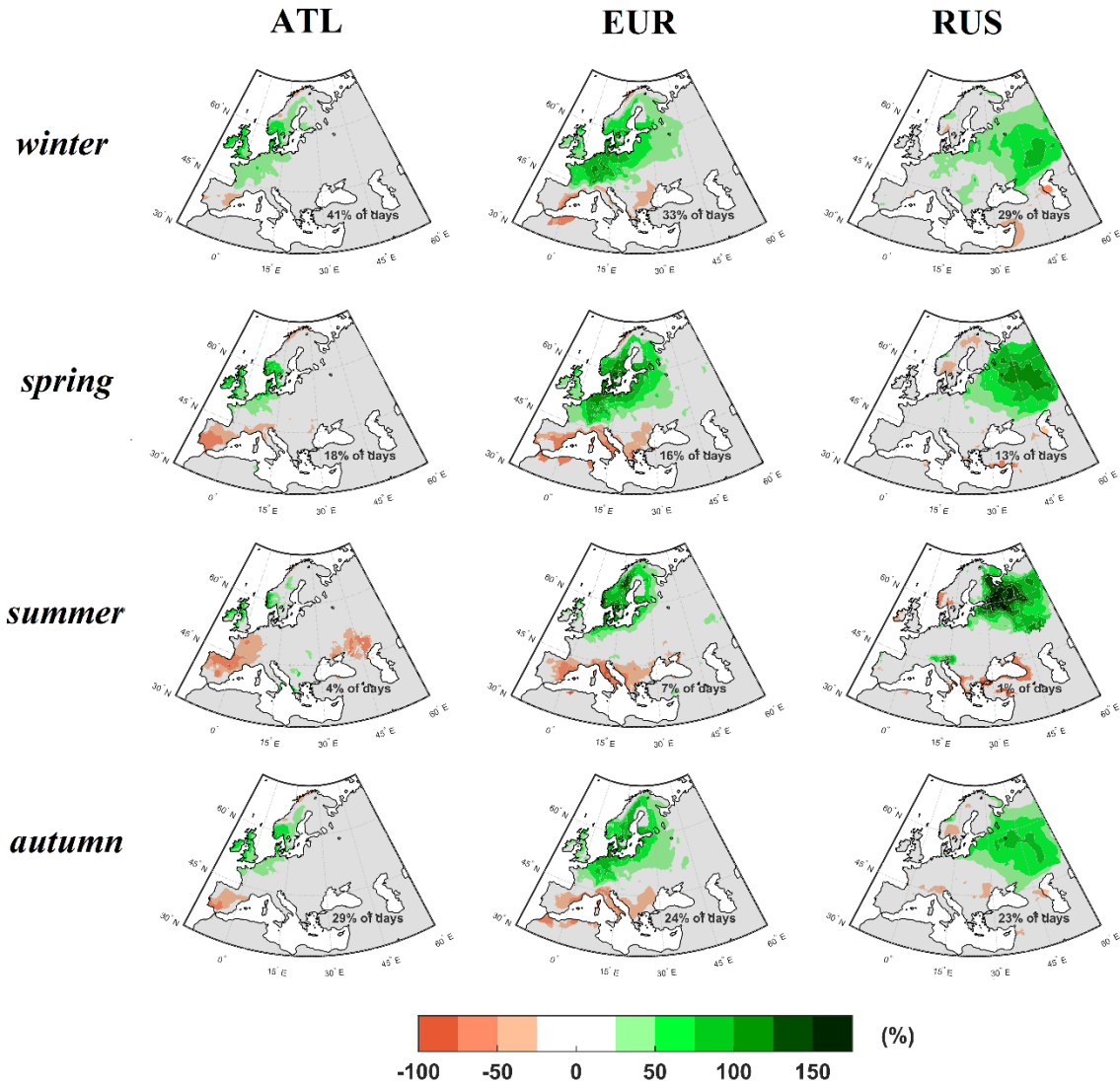


**Fig. 3.22** Same as Fig. 3.21, but for strong zonal flows.

Interestingly, ridges promote the lack of rainfall over some areas. For example, most of Iberia is completely dry during ATL ridges. The same is true in southern Italy and most of the Balkans area during EUR ridges. The precipitation responses to ridges are quite coherent throughout the year, although during summer the dry fingerprint of subtropical ridges extends further north, reaching central Europe and even the UK (particularly during spring and summer ATL ridges).

Contrarily, central and northern areas of Europe are, on the overall, much wetter during ridge occurrence. During winter ATL ridges the Alpine region receives about 150% of the usual rainfall. Indeed, this natural barrier marks a clear separation in the north-south dipole of the precipitation responses to ridges. These increases northwards of the ridge location agree with an enhanced zonal flow at higher latitudes, thus corroborating the similar composites found in Figs. 3.21 and 3.22. These patterns are not detached at all, as a ridge structure and its corresponding

### 3. Blocking impacts on European precipitation regimes

positive Z500 anomaly at low latitudes sharpens the north-south pressure gradient, thus favoring above average zonal flow.

In this sense, while blocking events are related to precipitation scarceness in the northern half of Europe, ridges are a key driver of precipitation deficits in the southern half, and particularly on the Mediterranean. This fact gains relevance in climates where water availability depends a lot on winter rainfall totals, being winter ridges a major drawback for annual precipitation totals.

## 3.3 Impacts in European snow-cover

Snow cover represents an important contributor to soil moisture in mid-to-high latitudes and mountainous regions. While accumulations at higher elevations (e.g. the Alps - Beniston, 2012) depend mostly on the amount of precipitation, at lower altitudes, where snowfall is scarcer, temperature anomalies will tend to dominate the anomalous snowfall patterns (Henderson and Leathers, 2009). As shown previously in Chapter 2, blocking events are often associated with significant cold spells in the European continent. Thus, it is reasonable to assume that blocking patterns will also play a significant role on the anomalous snowfall regimes of Europe (e.g., García-Herrera and Barriopedro, 2006).

In this section, the associated impacts in snow cover are explored by using the Global Snow Lab from the Rutgers University Climate Lab (RUCL) dataset (Robinson et al., 2012), covering the 1974-2012 period. The climatological frequency of winter days with snow covered soil is presented in Fig. 3.23, while the correlation between the anomalies of snow covered soil days and blocking/ridges frequency during winter for the three main 30° width sectors of the Euro-Atlantic region is represented in Fig. 3.24.

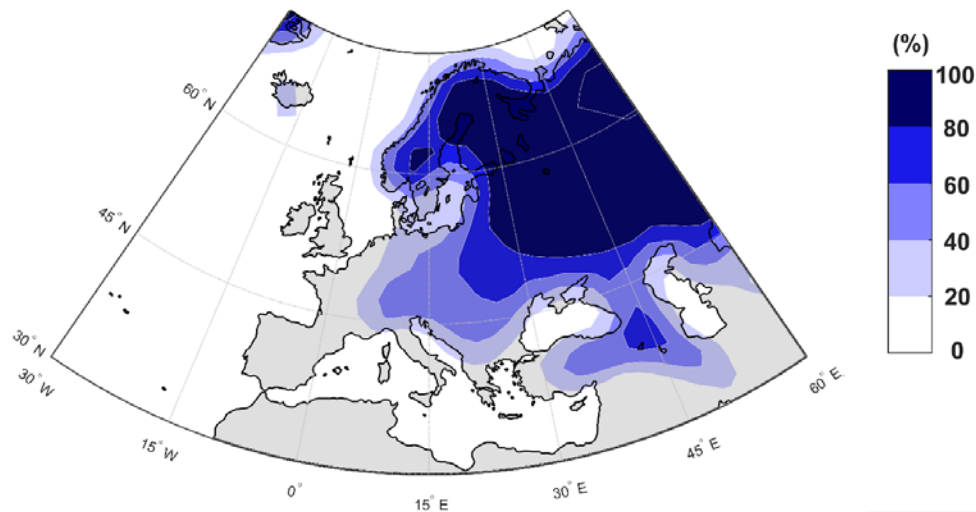


**Fig. 3.23** Climatological mean winter (December-February) frequency of days with snow covered soil (expressed in percentage with respect to the total number of winter days) for the 1974-2012 period.

### 3. Blocking impacts on European precipitation regimes

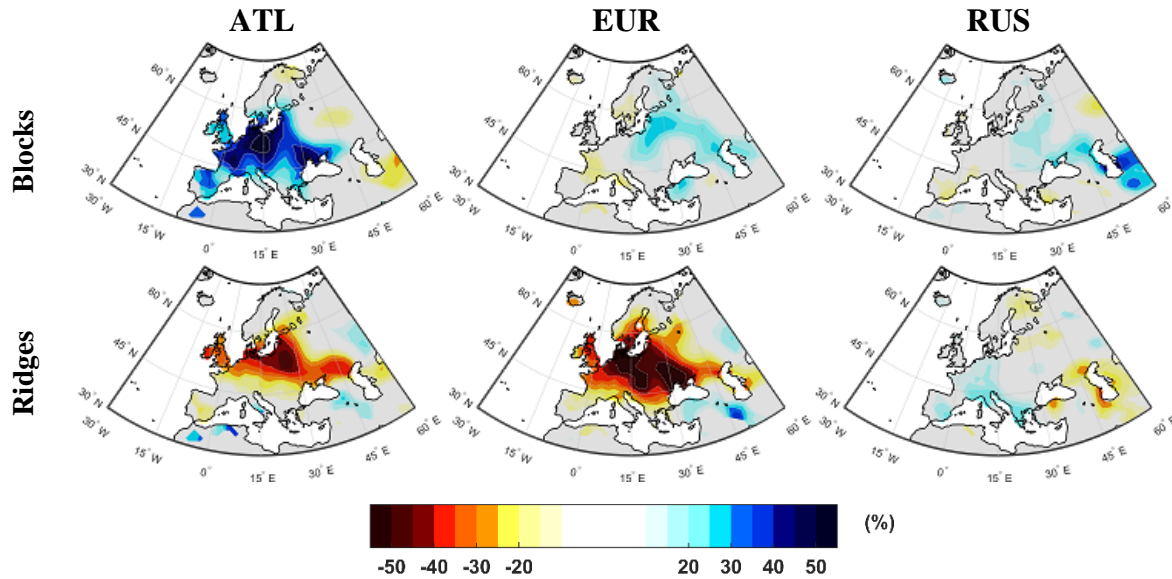


**Fig. 3.24** Winter correlation coefficients (in percentage) between the frequency anomalies of snow covered soil and blocking (upper panels) and ridge (lower panels) occurrence in the three longitudinal sectors: ATL, EUR and RUS. Only statistically significant correlations (at the 5% level) are shown.

The upper panel of Fig. 3.24 shows that ATL blocks are associated with higher than average snow cover days throughout most of Europe. As illustrated previously in Section 2.3, this pattern is related with significant cold advection of polar air masses towards the south of Europe (Fig. 2.5). Such conditions lead to increases up to 50% in days with snow cover in central Europe, despite the concurrent decreases in precipitation (Fig. 3.4), meaning that a larger fraction of the precipitation occurs in the form of snow. The impacts even extend over large parts of Iberia, Italy and the Balkans. During EUR and RUS blocks, the anomalies are less significant, and located further east, in areas where snowfall days represent winter standard conditions (Fig. 3.23), thus being their frequency just slightly enhanced by blocking action.

An almost completely opposite correlation is found for ATL and EUR ridges, resulting in much less days with snow cover in central Europe and the UK (lower panel in Fig. 3.24). This result is anticipated, as ATL and EUR ridges are related to significantly warmer temperatures in most regions (see Section 2.1). As a result, although precipitation totals are enhanced during these regimes, snowfall becomes scarcer. Furthermore, the associated positive temperature anomalies (in the order of 5-10°C) contribute to enhanced snow melting. Interestingly, during ATL (EUR) ridges some Mediterranean areas, such as Italy (Turkey), present slightly increased snow cover days, as some colder air masses plunge southwards in the eastern flank of the ridge structures. During RUS ridges some appreciable increases can be found in western and central Europe, although not comparable in magnitude to those occurring during ATL blocks. As shown in Fig. 2.2, ridges located in easternmost areas of Europe allow an atmospheric pattern characterized by slightly increased northerly flow and below average Z500 in western Europe.



## **Chapter 4**

# **Blocking impacts on Iberian precipitation and temperature**

### **Contents**

---

#### **4.1 Paper in Climate Dynamics**

*4.1.1 Introduction*

*4.1.2 Data*

*4.1.3 Seasonal impacts of blocking in Iberian precipitation*

*4.1.4 Synoptic forcing*

*4.1.5 Extreme Value Analysis*

*4.1.6 Discussion*

*4.1.7 Supplementary material*

#### **4.2 High-resolution Iberian rainfall deficits during ridge patterns**

#### **4.3 High-resolution Iberian temperature responses at a finer scale**

---

## Summary

### Context and objectives

As illustrated in Chapters 2 and 3, there is a significant contribution of blocking (ridges) for cold (warm) and wet (dry) spells in the Mediterranean region. This chapter will focus on Iberian precipitation and temperature responses to blocking and ridge patterns occurring in the ATL and EUR sectors, as these regional systems wield the largest impacts in the Iberian climate. To perform this finer scale regional analysis, it was necessary to employ high-resolution precipitation and temperature datasets. A thorough assessment of the high-resolution precipitation responses to blocking in Iberia, which includes a comprehensive Extreme Value Analysis can be found in Section 4.1 (as published in Sousa et al., 2016). Additional results on the rainfall signatures during ridge patterns are described in Section 4.2, while Section 4.3 is devoted to regional temperature responses in Iberia under blocking and ridge patterns.

### Methods

We use the IBERIA02 (precipitation) and SPAIN02 (temperature) datasets, at  $0.2^\circ \times 0.2^\circ$  horizontal resolution, and analyze the corresponding anomalies for each atmospheric pattern in each sector. Integrated Vapor Transport, the instability, as measured by the Lifted Index, cyclones and cut-off lows catalogues are used to characterize the synoptic environment. Changes in Probability Density Functions and an Extreme Value Analysis are performed to explore the relationships between blocking occurrence and precipitation regimes, including extreme rainfall events in different regions of the Iberian Peninsula.

### Results

Similarly to other Mediterranean areas, blocking is associated with increased precipitation in most of Iberia, except in the northwestern tip of the Peninsula. Despite the large-scale reductions in moisture availability, the generalized rainfall increases are well explained by enhanced atmospheric instability, partially driven by a southward deviation of the storm-track and increases in cut-off lows. These changes are not concurrent with increases in the number of precipitation days, thus highlighting the heavier behavior of precipitation regimes during blocking, which is particularly notable on the eastern shores of Iberia. Conversely, strong zonal flows, and especially sub-tropical ridges in the Euro-Atlantic sector result in more stable conditions and precipitation scarceness in Iberia (except in the northernmost regions).

An opposite response to blocks and ridges is also found in temperature, with blocking events favoring cold days in most areas (with temperature anomalies below  $-3^\circ\text{C}$  in winter), along with increased cloudiness and wetter than average conditions. On the contrary, dryer and sunnier weather conditions associated with ridges enhance sensible and short-wave radiative heating, thus promoting above average temperatures during both winter and summer. The specific location of the ridge is determinant for regional extreme summer temperature events, with subtropical ridges over Iberia triggering the largest anomalies in maximum temperature.

### 4.1 Paper in *Climate Dynamics*

*Pedro M. Sousa, David Barriopedro, Ricardo M. Trigo, Alexandre M. Ramos, Raquel Nieto, Luis Gimeno, K. F. Turkman, Margarida L. R. Liberato*

*Paper published in Climate Dynamics (2016)*

In this work we reassess the impacts of blocking patterns on precipitation regimes in the Iberian Peninsula, distinguishing between north Atlantic and European blocking. For this we take full advantage of the recently developed high-resolution datasets for the Iberian countries. Precipitation anomalies during blocking events obtained with this dataset allow a much finer regional characterization of the impacts in both average and extreme daily precipitation, particularly when compared to widely used low-resolution reanalysis datasets. Blocked patterns induce a negative-positive dipole of precipitation anomalies from northwest to southeast Iberia. Increases are widespread during Atlantic blocks and pronounced in southern and eastern areas of Iberia, while during European blocks they are more spatially restricted, with increases above 50 % in coastal Mediterranean areas, which represents a considerable fraction of the annual precipitation. Blocking impacts in precipitation are nearly opposite to those found during strong zonal flow situations, but there are also some asymmetries in the precipitation responses. A significant increase in cyclones and cut-off lows frequency southwards of blocking structures is related to precipitation excesses over southern and eastern areas, where dynamical factors and local processes play a crucial role. On the contrary, precipitation deficits in northwest Iberia during blocking episodes are better explained by a reduction in north Atlantic frontal activity and simultaneous decreases in large-scale moisture advection towards northern Iberia. We show that these anomalies during blocking result from changes in precipitation amount rather than from increases in rainy days, pointing to more extreme rainfall regimes, particularly in southeastern Iberia. Finally, an Extreme Value Analysis was performed, fitting Generalized Pareto Distributions to precipitation extremes. Results show that the different extreme precipitation regimes of northwest and Mediterranean regions are partially determined by opposite anomalies of the zonal flow. Thus, heavy precipitation events in Mediterranean areas are usually short-lived and frequently associated with blocking conditions, while in northwest Iberia the total accumulations during rainfall episodes are more important for triggering extreme events and they are mainly related to strong westerly flows.

### 4.1.1 Introduction

The climate of Europe is controlled to a large extent by the usual sequence of low-pressure systems travelling from the west and associated with the jet stream. These mid-latitude cyclones leave their fingerprint on spells of varying precipitation amount, alternating with dry periods that range from weekly to monthly scales. With the advent of upper level observations in the wake of the WWII, it was found that this pattern of predominantly zonal circulation is often disrupted by a temporary change to a situation of strong meridional flow (e.g., Rex, 1950a, b). This meridional component favors the formation of quasi-stationary anticyclones at high latitudes, coined as blocking highs (Rex, 1950a, b), which are often accompanied by low-pressure areas at lower latitudes (Treidl et al., 1981).

The influence of blocking systems on the climate of mid latitudes is well known. The first climate assessments of the impact of blocking were based on very few cases (e.g., Rex, 1951), or on particular anomalous seasons (e.g., Quiroz, 1984). More recently, the longer reanalysis datasets have been used to characterize blocking (e.g., Barriopedro et al., 2006, 2010a; Croci-Maspoli et al., 2007; Davini et al., 2012a) and their associated impacts (e.g., Trigo et al., 2004; Masato et al., 2011), including extreme events (e.g., Sillmann and Croci-Maspoli, 2009; Buehler et al., 2011), such as the drought events in the Iberian Peninsula (IP) during 2004–2005 (García-Herrera et al., 2007) and 2011–2012 (Trigo et al., 2013a), or the more recent outstanding heatwaves in the Euro-Russian area (Barriopedro et al., 2011; Ruti et al., 2014). The specific role of atmospheric blocking on precipitation regimes has been widely studied, although there is some tendency to focus on the climate of the area more directly affected by the anomalous stationary ridge. In this restricted spatial context, blocking occurrence causes precipitation scarceness. Nevertheless, blocking episodes may also increase precipitation in remote regions, since storm tracks tend to be deflected north and south of the blocking systems. Trigo et al. (2004) found that blocking episodes in the Euro-Atlantic sector reduce the precipitation rate at higher latitudes, and increase it in southernmost areas of Europe. In addition, blocking can be favorable for strangling upper level cold air pools (usually referred as cutoff lows), which may produce severe weather and flooding (Nieto et al., 2007). Cut-off lows are more frequent in spring and summer seasons, and in mid and low latitudes, with the European sector being a preferred sector of occurrence. In particular, Nieto et al. (2007) has shown that the southern flank of blocking systems is a favorable location for cut-off occurrence. This is crucial for the climate of the IP, where some of the most torrential rainfall episodes can arise from relatively small-scaled low-pressure systems. Some examples of cut-off low systems occurring under large-scale blocked conditions are the exceptional rainfall event in the Lisbon area in 18 February 2008 (Fragoso et al., 2010), or the October 2000 torrential precipitation event in eastern Spain (Homar et al., 2002). In addition, and particularly during late summer and early autumn, cut-off lows can trigger Mesoscale Convective Systems affecting the eastern coast of Spain and the Balearic Islands (García-Herrera et al., 2005a).

Within the context of blocking-related impacts, it is imperative to distinguish the disruption of the prevailing westerly circumpolar flow by a blocking episode from the strengthening of the North Atlantic ridge at lower latitudes (40°N–50°N—sometimes called low-latitude blocking), which is frequently linked with sub-tropical high pressure systems. Santos et al. (2008, 2009) have studied

the latter, and linked such events with the occurrence of severe droughts in the IP, particularly in the western half, since these patterns prevent storms from reaching that region. On the contrary, closed and persistent blocking systems located at higher latitudes leave a margin for the occurrence of synoptic eddies at lower latitudes (e.g., Pfahl, 2014). More specifically, the blocking pattern induces a shift of the usual storm-track paths that can interact with the sub-tropical jet stream, enhancing large-scale ascending motions, instability and the development of severe precipitation events (Toreti et al., 2010). Thus, unlike strong ridges, which tend to deprive the IP of rains, blocking episodes can promote either dry periods or wet spells therein, depending on the location of the blocking pattern.

The strong spatial and temporal variability of precipitation regimes in the IP, with the relatively high frequency of blocking patterns (Barriopedro et al., 2006; Woollings et al., 2010a) and cut-off-lows (Nieto et al., 2007) in western Europe converts the IP in an excellent “laboratory” to evaluate the impacts of blocking episodes. However, blocking induced low pressure systems may produce very distinct signatures in precipitation at the regional scale. This underlines the need of high-resolution precipitation datasets to obtain a more comprehensive assessment on the impacts of blocking episodes on the IP precipitation regimes. Previous studies have used gridded precipitation datasets with poor spatial horizontal resolutions to address blocking effects on precipitation (e.g., Trigo et al., 2004), thus possibly losing crucial spatial details. Additionally, Trigo et al. (2004) found that the blocking signals in precipitation are relatively unconnected from those in precipitable water, which are rather controlled by blocking-induced temperature anomalies. This fact suggests that the precipitation anomalies in IP during blocking situations are mainly driven by dynamical factors, such as higher-than-usual cyclonic activity, albeit the importance of thermodynamic factors in the precipitation responses to blocking cannot be disregarded. This fact stresses the need to explore the blocking influence on cyclone paths, and cut-off lows in the region.

In this study we perform a reassessment of blocking impacts on precipitation using the recently developed Iberian high-resolution gridded precipitation datasets (Belo-Pereira et al., 2011; Herrera et al., 2012). Moreover, we assess in detail how precipitation anomalies and associated atmospheric circulation change with respect to the specific location of the blocking high patterns. This spatial dependence may be crucial to determine the local impacts and extremeness of precipitating systems like cyclones and cutoff lows. Finally, we also explore the relationship between blocking and the occurrence of extreme precipitation. In summary, the main objectives of this work are: (1) to examine blocking impacts, in terms of precipitation anomalies and physical forcings (instability and moisture fluxes), distinguishing the sector of blocking occurrence; (2) to identify changes in cyclonic activity and cut-off lows frequency during blocking episodes; (3) to perform an Extreme Values Analysis for Iberian precipitation during blocking episodes.

This work is structured as follows. In Sect. 4.1.2, the data used in this work is described, and a brief overview of the blocking climatology in the target domain is presented. In Sect. 4.1.3, we analyze the impacts of different weather patterns (namely blocked and strong zonal flow) on the precipitation regimes, and compare them when using datasets of different spatial resolution. The synoptic patterns and forcings that promote these impacts are described in Sect. 4.1.4. An Extreme

Value Analysis is performed in Sect. 4.1.5, and finally, in Sect. 4.1.6, the main results of this work are discussed.

### 4.1.2 Data

#### *Reanalysis data*

We have used the following datasets for the purposes of our analysis:

(a) The recently developed high-resolution precipitation datasets for Portugal (PT02 - Belo-Pereira et al., 2011), and Spain (SPAIN02 - Herrera et al., 2012), which have a horizontal resolution of  $0.2^\circ \times 0.2^\circ$  and have been combined in a single dataset (IBERIA02) for the years spanning from 1950 until 2007. The average number of stations used by both datasets is very large (although not constant during the period), allowing its application for both climatological studies (e.g., Ramos et al. 2014), and characterization of extreme precipitation events (Ramos et al., 2015).

(b) The dataset from the NCEP/NCAR reanalysis (Kalnay et al., 1996) for the 1948–2007 period, at a  $2.5^\circ \times 2.5^\circ$  horizontal resolution. The variables explicitly considered were: daily fields of 500 hPa geopotential height (Z500) and Lifted Index (LI) - the latter is an instability index defined by the temperature difference between an air parcel lifted adiabatically and the temperature of the environment at Z500. Furthermore, we made use of several fields from the NCEP/NCAR data to compute the following data: (1) a catalogue of blocking events (Barriopedro et al., 2006); (2) a catalogue of cut-off lows (COL - Nieto et al., 2005); (3) Integrated Water Vapor Transport between 1000 and 300 hPa (IVT- Ramos et al., 2015); (4) a catalogue of cyclones for the northern hemisphere obtained by using the methodology described in Trigo (2006a). These datasets will be employed to explore the blocking signatures in precipitation regimes and interpret these responses in terms of dynamical (cyclones, COLs) and thermodynamical (IVT, LI) processes. The particular characteristics of the blocking catalogue are explored in more detail in the following sub-section.

#### *Blocking index catalogue*

The catalogue of blocked days was developed by Barriopedro et al. (2006) by using daily Z500 data on a  $2.5^\circ \times 2.5^\circ$  grid. It is an adapted version of the Tibaldi and Molteni (1990) index. Blocking events can be identified when the averaged zonal index, computed as the 500-hPa height difference between  $40^\circ$  and  $60^\circ\text{N}$ , is negative over  $30^\circ$  in longitude and during five or more days. To exclude spurious blocks due to the occurrence of cut-off lows, an additional negative height gradient northward of  $60^\circ\text{N}$  is demanded. A blocking event is detected when at least three consecutive longitudes appeared as blocked during at least five days. Two Z500 gradients (*GHGN* and *GHGS*) have been simultaneously computed for each longitude and for each day of study over the North Hemisphere:

#### 4. Blocking impacts on Iberian precipitation and temperature

---

$$GHGN = \frac{Z(\lambda, \phi N) - Z(\lambda, \phi 0)}{\phi N - \phi 0}$$

$$GHGS = \frac{Z(\lambda, \phi 0) - Z(\lambda, \phi S)}{\phi 0 - \phi S} \quad (1)$$

$$\phi N = 77.5^\circ \text{ N} + \Delta$$

$$\phi 0 = 60.0^\circ \text{ N} + \Delta$$

$$\phi S = 40.0^\circ \text{ N} + \Delta$$

$$\Delta = -5.0^\circ; -2.5^\circ, 0.0^\circ, 2.5^\circ, 5.0^\circ \quad (2)$$

where  $Z(\lambda, \phi)$  is the Z500 at a given latitude and longitude.  $GHGS$  is proportional to the zonal geostrophic wind component and provides a measure of the zonal flow intensity for each longitude, while  $GHGN$  is imposed in order to exclude non blocked flows. An arbitrary longitude is considered blocked when both  $GHGN$  and  $GHGS$  verify the condition expressed by Eq. (3) for at least one of the five  $\Delta$  values and simultaneously the  $\phi 0$  height anomaly is positive. The detection scheme also incorporates a procedure to detect the center of blocking events (maximum Z500 gridpoint within the anticyclonic flow), a blocking intensity index, and a spatial and temporal tracking algorithm.

In this study, we only considered daily blocking patterns for which the maximum Z500 anomaly is located between  $45^\circ\text{N}$  and  $70^\circ\text{N}$ , and these locations will hereafter be called blocking centers. We must stress that this definition has the purpose to enable an objective separation in blocking sectors by reducing the large-scale of the blocking pattern to a single gridpoint that is representative of the weather system, as the specific location of a blocking center plays a major role in defining the synoptic circulation of a much wider region. Thus, two main sectors are defined: the Atlantic sector (ATL) which includes all blocking centers located in  $30^\circ\text{W}$ – $0^\circ\text{W}$ , and the European sector (EUR), spanning  $0^\circ\text{E}$ – $30^\circ\text{E}$ . This regional classification is justified from previous works that have explored the relationship between blocking and the main modes of variability of the atmospheric circulation (e.g., Barriopedro et al., 2006; Scherrer et al., 2006). These studies have reported a tight link between blocking activity and the centers of variability of the leading modes in the Euro-Atlantic sector, with the North Atlantic Oscillation (NAO) and the Scandinavian Pattern (SCA) explaining most of the variability of ATL and EUR blocking, respectively. ATL and EUR blocking have also very distinct signals in European precipitation and temperature (e.g., Masato et al., 2011). Figure 4.1 (top) depicts the annual mean frequency of blocking center locations in each gridpoint ( $2.5^\circ \times 2.5^\circ$ ), as well as the seasonal frequency of blocking centers for each considered sector (bottom). It must remain clear that the main goal of classifying blocks into ATL and EUR types is to assess how the precipitation responses depend on the blocking location. Thus, this distinction between ATL and EUR blocks is purely based on their location, and does not necessarily involve different physical/dynamical processes in their lifecycles.

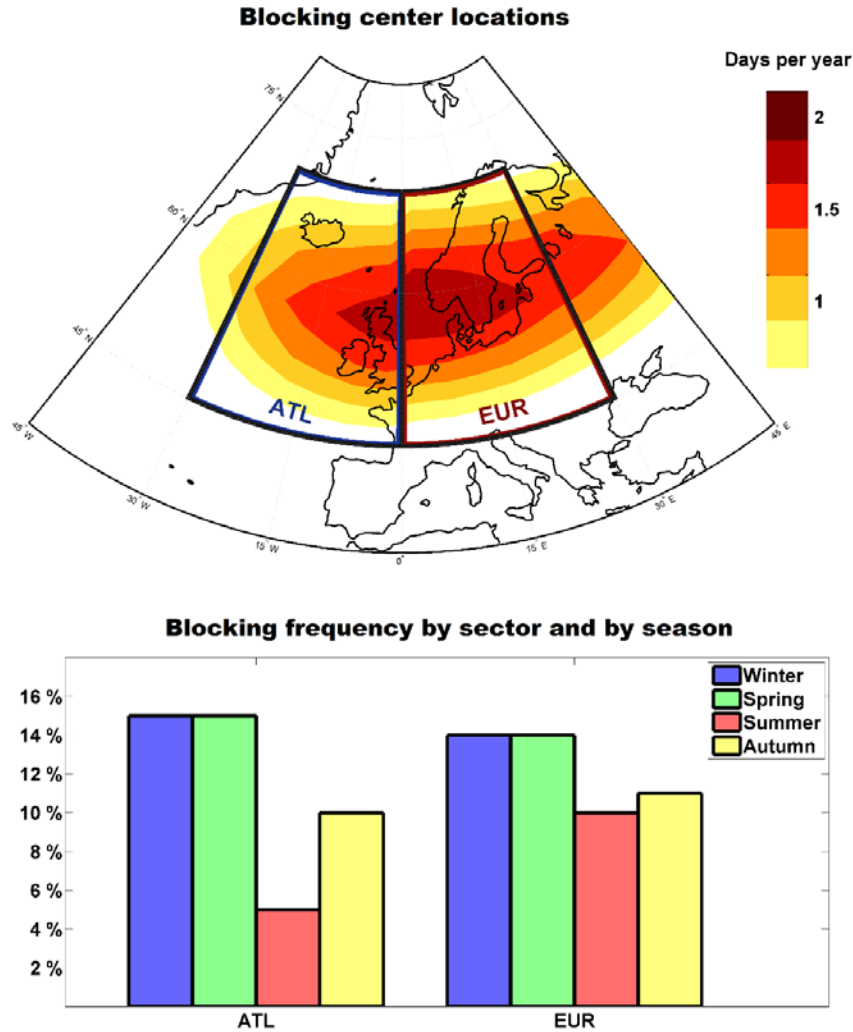


**Fig. 4.1** Top: boxes identifying the considered sectors for blocking center location: ATL - from 30°W to 0°W; EUR - from 0°E to 30°E. The shadings indicate the annual mean frequency of blocking center locations in each gridpoint. Blocks outside the 45°N–70°N latitude strip were discarded in both sectors. Bottom: Seasonal frequencies of blocking center location in each sector during 1950–2007 (in percentage relative to the total number of days in the season).

Before evaluating the regional impacts of blocking on the IP precipitation, it is important to briefly characterize the atmospheric circulation signatures associated with regional blocking occurrence. Figure 4.2 shows the composite of Z500 anomalies for blocking days in each sector and season. For both sectors, Z500 positive anomalies are larger in the cold seasons than in the warm seasons. The largest anomalies are associated with ATL blocking. In this region, summer blocks display a northward extension of subtropical wave-breaking systems near the Azores high. Regional blocking is also associated to negative Z500 anomalies in some of the surrounding areas, being more evident during ATL blocks and in colder seasons, but less pronounced than the positive ones. These negative anomalies display different intensity and location for ATL and EUR blocks, which suggest different impacts on precipitation, thus supporting the classification in blocking sectors

#### 4. Blocking impacts on Iberian precipitation and temperature

adopted herein. Note that some blocking events may contribute to the composites of both sectors, since ATL blocks tend to evolve eastwards towards Europe throughout their lifecycle (Crocimaspoli et al., 2007; Barriopedro et al., 2010a). This is supported by similar composites (see Supplementary Material – Fig.4.12) performed for blocking subsectors of 15° longitudinal extension within the ATL and EUR regions.

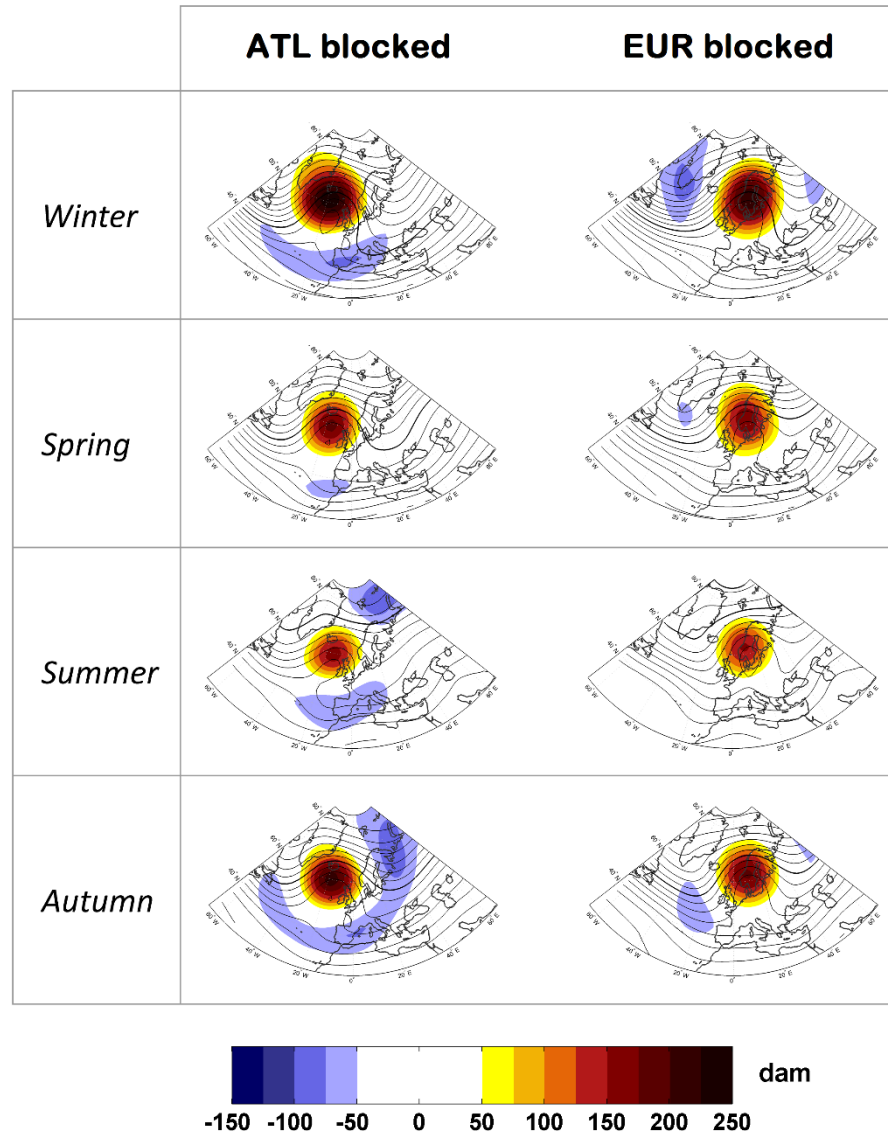


**Fig. 4.2** Composites of the daily anomalies (shaded areas) and absolute values (isolines) of 500 hPa geopotential height for blocking centers in each sector and for all seasons. All values are in decameters (dam) and the thick line represents the 550 dam isohypse.

#### 4.1.3 Seasonal impacts of blocking in Iberian precipitation

With the aim of evaluating the impacts of blocking on the IP precipitation, seasonal composites of daily precipitation anomalies were calculated for days with blocking centers in each sector. For

#### 4. Blocking impacts on Iberian precipitation and temperature

this purpose, daily anomaly series of precipitation in each gridpoint were computed, and then composited for blocking days of each season and sector. We opted to present the relative anomalies in the composites (in percentage relative to the climatological seasonal precipitation during 1950–2007), as seen in Fig. 4.3. Gridpoints where the climatological seasonal mean total precipitation is below 50 mm were discarded, since relative anomalies in dry areas may be misleading. This process excludes dryer regions in southern/central IP, where summer rainfall is usually scarce (Belo-Pereira et al. 2011), and the relevance of high anomalies would be doubtful. A two-sample Smirnov-Kolmogorov test (hereafter KStest) was applied to assess the statistical significance of these anomalies (Wilks, 2011).

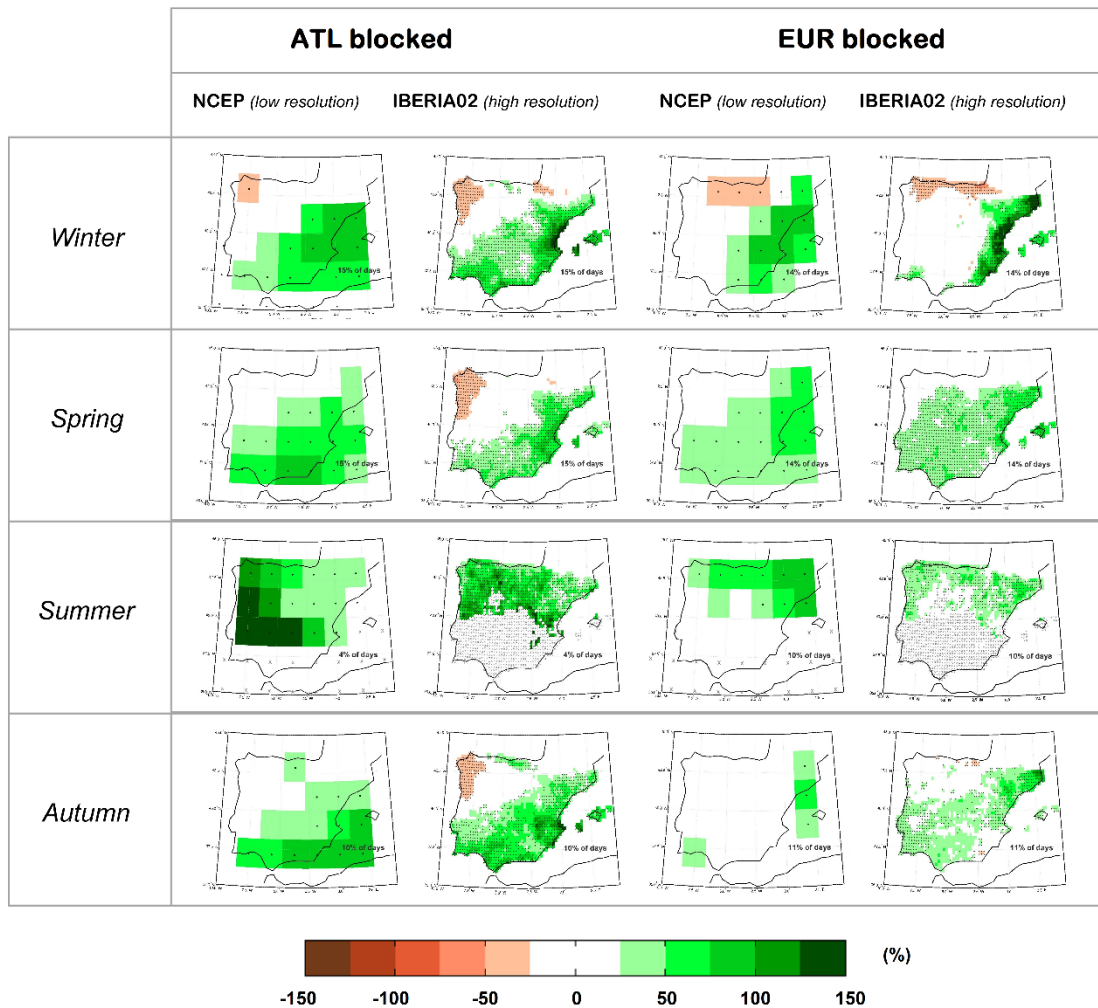


**Fig. 4.3** Seasonal composites of daily precipitation anomalies (%) in the Iberian Peninsula for blocking center days in each considered sector using (and comparing) the low-resolution NCEP/NCAR dataset with the high-resolution IBERIA02 dataset. Regions where the anomalies are statistically significant at the 5 % level are represented with dots. Anomalies for gridpoints with total seasonal precipitation below 50 mm were not considered (grey crosses).

#### 4. *Blocking impacts on Iberian precipitation and temperature*

---

The composites presented in Fig. 4.3 show that, with the exception of summer, the seasonal patterns of regional blocking signals in precipitation are reasonably coherent throughout the year, particularly for ATL blocks. The NCEP/NCAR reanalysis composites show a consistent positive precipitation anomaly in the Mediterranean coast associated with blocking occurrence in both sectors. In particular, during winter, the NCEP/NCAR reanalysis displays very minor differences between the impacts of ATL and EUR blocks. However, the high-resolution IBERIA02 dataset reveals specific regional details in these patterns and clear differences between ATL and EUR blocks. For example, significant negative precipitation anomalies are found in northwestern regions of the IP that cannot be clearly identified using the low-resolution dataset. In summer, the NCEP/NCAR reanalysis displays a SW–NE gradient response in precipitation anomalies that is absent in the high-resolution dataset. We must bear in mind that most of IP registers low mean precipitation values during these months and, consequently, one should refrain from overemphasizing summer anomalies.

Regarding the different impacts that arise from different blocking locations, it is found that for most of the year (with the exception made for spring), ATL blocks are associated with increased precipitation over wide areas of the IP, while EUR blocks tend to bring more localized positive anomalies, particularly in coastal Mediterranean strips. For instance, during autumn, ATL blocks lead to above average precipitation in almost the entire peninsula. Taking this example, once again, the impact of the different resolutions from the datasets appears very clear, as EUR blocking composite for the NCEP/NCAR dataset clearly miss most of the positive autumn precipitation anomalies that are depicted by the corresponding IBERIA02 composite.

Taking into account the tendency for eastward blocking migration mentioned above, we have also computed the precipitation anomaly composites occurring in the previous 5 days to EUR blocks. These composites show a quite similar pattern (see Supplementary Material – Fig. 4.13) to the one found for ATL blocking, thus confirming that the transition from the ATL to the EUR precipitation composites partially reflects the transient responses to an eastward blocking migration and hence, that the precipitation responses to blocking depend on the blocking location.

With the aim of summarizing the different impacts of regional blocking, we computed annual composites of daily precipitation anomalies for each blocking sector. Furthermore, to better interpret the blocking signatures we compared them with the corresponding composites obtained for days characterized by strong zonal flow, which represents a large-scale atmospheric pattern with nearly opposite anomalies to those associated with blocking. This procedure allows assessing the linear response in precipitation to opposite zonal flow regimes. For this purpose, we followed very simple criteria described in Trigo et al. (2004) to classify strong zonal flow days in the Atlantic and European sectors: (1) a given longitude is affected by strong zonal flow conditions if the meridional mid-latitude Z500 gradients exceed several empirical thresholds (see Trigo et al., 2004 for further details); (2) the entire sector is considered to be in strong zonal flow configuration if at least three adjacent longitudes satisfy (1). The KStest was applied to assess the statistical significance of these anomalies.

The annual composites of daily precipitation anomalies for regional blocking and strong zonal flow conditions are shown in Fig. 4.4. The existence of a negative–positive dipole in precipitation

#### 4. Blocking impacts on Iberian precipitation and temperature

anomalies under blocking action is again evidenced at the annual scale. For both blocking sectors, the positive precipitation anomalies found in eastern and southern coastal areas are considerably wider in spatial extension and larger in amplitude than the negative anomalies found in northwestern IP, which are essentially restricted to ATL blocks. During strong zonal episodes there is also a tendency for a northwest-southeast dipole in precipitation anomalies, but with the opposite signals to those found during blocking conditions. Strong westerly flows are related with below average precipitation in southern and eastern IP, and with near-normal or non-significant precipitation excess in the northwest. As a consequence, the differences between blocked and zonal conditions depict an even more contrasting dipole, which reflects the large relevance that blocking episodes wield on rainfall regimes in southern and eastern regions of Iberia, where we once again stress that mean annual rainfall totals are much lower than for northwestern sectors (Belo-Pereira et al. 2011).

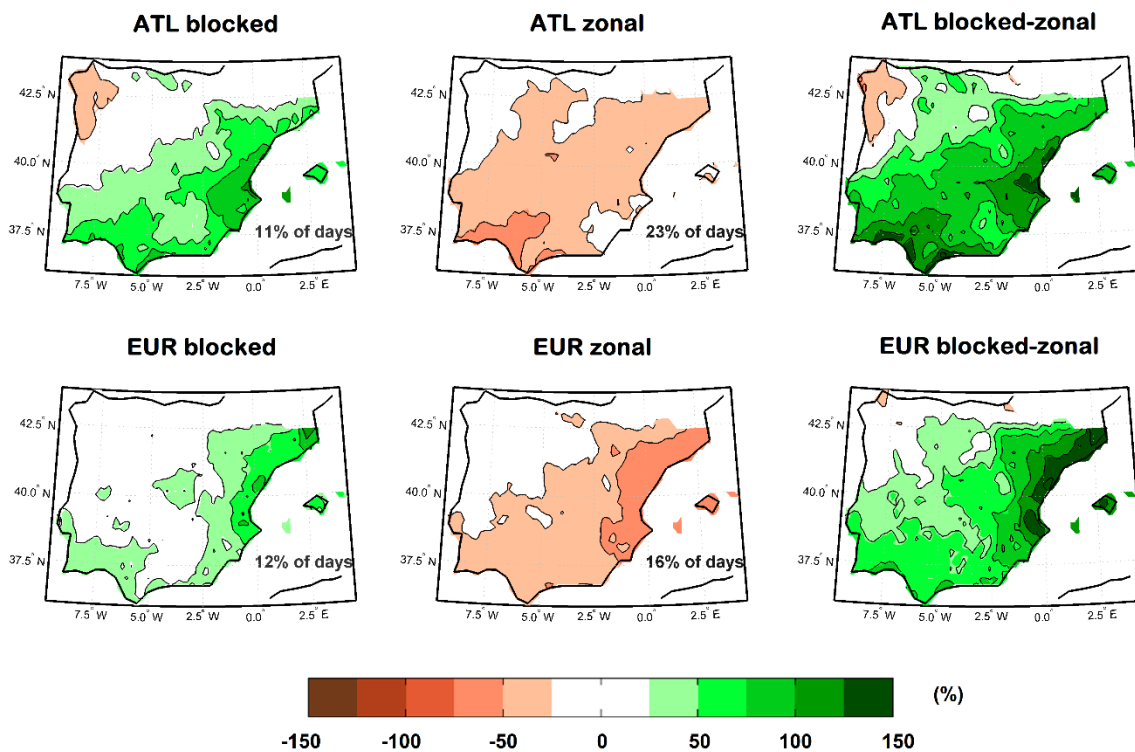


**Fig. 4.4** Annual composites of daily precipitation anomalies (%) in the Iberian Peninsula for blocking (left column) and strong zonal flow (center column) days in the Atlantic (upper row) and European (lower row) sectors. The difference between the regional blocking and strong zonal flow composites is presented in the right column. Only statistically significant anomalies at the 5 % level are shown.

As stated above, the high-resolution precipitation data set allows identifying important differences between the regional and local precipitation responses associated with ATL and EUR blocks that otherwise would be missed in a coarser grid. Thus, during ATL blocks positive anomalies cover a wider area than that affected by EUR blocks, and also the locations of the largest anomalies are different depending on the considered sector. In particular, during EUR blocks there is a particular emphasis on the coastal strip of eastern Spain, while under ATL blocks the highest

anomalies are found further south in eastern Spain, and also in southernmost areas of the IP and the Gibraltar area. On the other hand, a sharp northwest-southeast gradient is found for ATL blocks, while EUR blocks show a less pronounced gradient, and a slight northward shift of the associated maximum of precipitation, as compared to ATL blocks. Also, the deficit of precipitation in northwest IP is clearly identifiable for blocking located in the ATL sector, but it does not reach the 5 % statistical significance level in the EUR composite. The same regional differences are observed in the blocking minus strong zonal flow composite difference.

Another interesting difference between the ATL and EUR composites is their different linear response to blocked and zonal flows. Thus, the precipitation response to opposite anomalous conditions in the westerly flow over EUR is largely linear, while for the ATL sector there are important asymmetries. It should be noticed that part of these results may be due to a larger difference between the frequencies of blocked and zonal days for ATL when compared to EUR. In particular, the precipitation signals over eastern IP during ATL blocks are much larger than those observed during strong zonal flow conditions. This implies that the precipitation regimes of these areas are particularly sensitive to blocked conditions. Such asymmetric responses to circulation anomalies in the ATL sector are much more difficult to identify when relying on composites obtained using the NCEP/NCAR low-resolution dataset, once again reinforcing the convenience of the high-resolution dataset.

The impact of blocking events in the precipitation regimes of the eastern and southern sectors of IP (Fig. 4.4) coupled with the considerably lower climatological precipitation values observed in these regions necessarily imply a considerable contribution of blocking episodes on total yearly precipitation therein (solid lines, upper panels Fig. 4.5), which exceeds 10 % in eastern areas of the IP. We were also interested in checking if the precipitation anomalies during blocking patterns are derived from an equivalent change in the number of rainy days, or from changes in the precipitation amount during precipitating days. To address this question, we computed regional blocking composites of the anomalous number of days with total precipitation above 1 mm. The results (Fig. 4.5, shaded) indicate a large decrease in the number of rainy days over the northwestern half IP and much smaller changes elsewhere. The pronounced drop of rainy days in northwestern IP (in some areas above 20 %) only impinges a slight decrease in total precipitation (Fig. 4.4). We argue that this result could be due to blocking mainly inducing light precipitating days in the NW sector of IP, thus leading to small net changes. The decrease in the number of rainy days during blocking situations also affects other large portions of the IP, including regions where the precipitation composites showed significant increases in total precipitation. This suggests that the precipitation responses to blocking are largely attributable to changing rates of precipitation rather than to the number of precipitating days, especially in southeastern IP. Naturally, this also involves a higher frequency of intense or torrential precipitation days during blocked patterns in these regions, as it will be discussed further ahead.

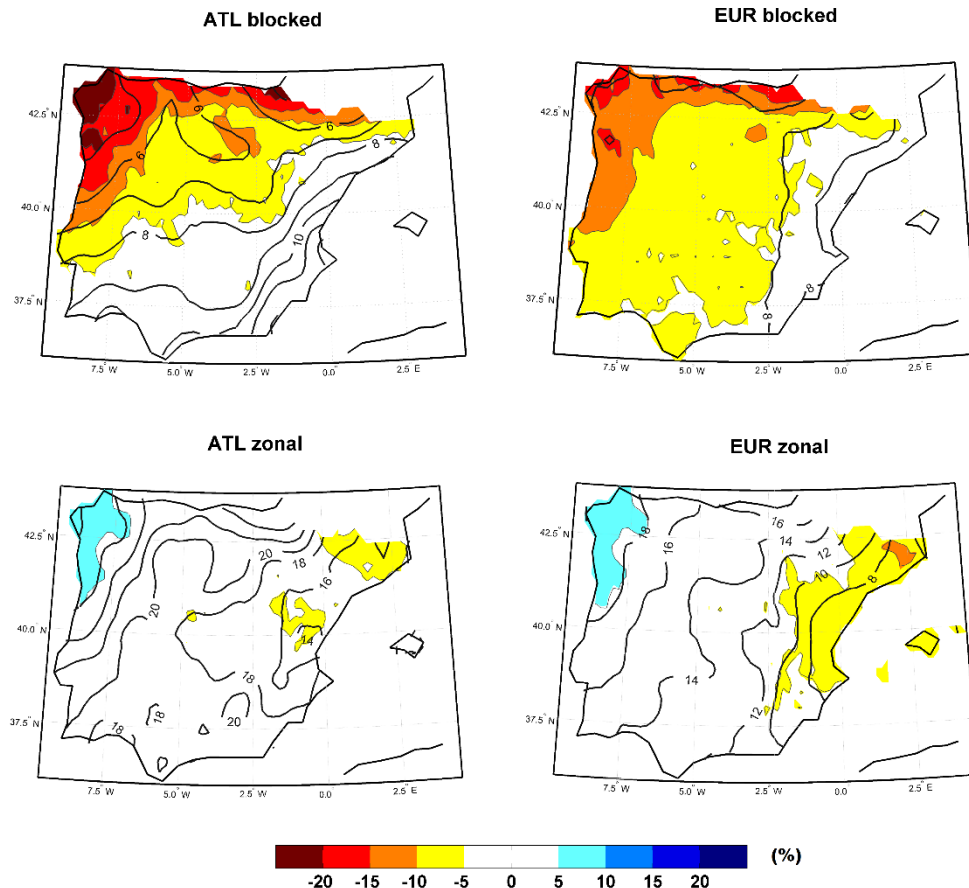


**Fig. 4.5** Increase (blue shades) or decrease (red shades) in the number of days with total precipitation above 1 mm during blocked patterns (upper panel) and strong zonal flows (lower panel), when compared with the complete 1950–2007 climatology (in percentage). Solid black lines represent the contribution (in percentage) of the corresponding synoptic pattern to the annual total precipitation.

### 4.1.4 Synoptic forcing

Once the impacts of regional anomalous zonal flow conditions on IP precipitation regimes are well characterized, it is important to understand the processes that drive them at the synoptic scale. As shown in previous works, blocking occurrence induces positive precipitation anomalies in several areas of southern Europe, but it does not promote higher values of precipitable water in the same areas (e.g., Trigo et al., 2004). Thus, it is mandatory to distinguish processes that enhance moisture availability from those that provide the favorable conditions for water condensation. For this purpose, we computed anomalous composites (for blocked and strong zonal flow situations) of Z500, LI, and IVT (and the corresponding mean horizontal transport of IVT). In this way, we were able to compare the distribution of moisture fluxes (throughout the use of the IVT) and simultaneously the anomalies in instability (LI). The former is related to moisture availability for precipitation and the latter measures whether the environmental conditions are prone to enhance condensation of water vapor. The composites have been performed for blocked and zonal days, and their difference, as depicted in Fig. 4.6.

#### 4. Blocking impacts on Iberian precipitation and temperature

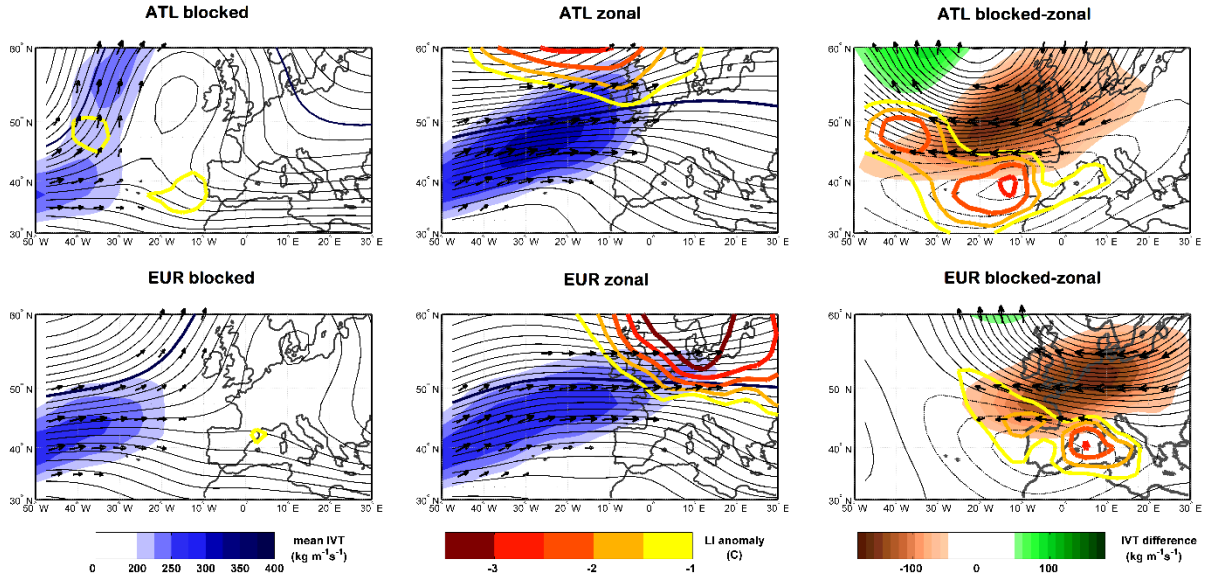


**Fig. 4.6** Annual composites of the daily Integrated Vapor Transport (IVT, in  $\text{kg m}^{-1} \text{s}^{-1}$ , blue shading), the Lifted Index anomaly (LI, in  $^{\circ}\text{C}$ , reddish thick lines), 500 hPa geopotential height (Z500, in dam, thin black lines - the thicker line corresponds to the 550 dam isohypse) and mean horizontal transport (black arrows,  $\text{kg m}^{-1} \text{s}^{-1}$ ) for blocking (left panel) days, zonal (middle panel) days and their difference (right panel). Upper (lower) row panels correspond to the Atlantic (European) sector composites.

The composites of Fig. 4.6 show that during strong zonal conditions there is a corridor of high moisture content transport extending towards the British Isles and affecting northwestern IP. This moist corridor is zonally elongated towards central Europe during strong zonal flow conditions over EUR, as compared to those occurring in ATL. Blocking patterns efficiently obstruct these moisture fluxes, which is in good agreement with the rainfall reductions observed in NW IP during blocking patterns, but not with the precipitation increases in southeastern IP. However, areas of positive LI anomalies are found in the IP during blocking episodes, with a dependence on the considered sector. Thus, atmospheric instability tends to be reinforced in western (eastern) IP during ATL (EUR) blocking days, in good agreement with the precipitation increases obtained in the previous section over southern (eastern) IP. Moreover, the difference between blocked and zonal flow composites shows a large increase in atmospheric instability over IP when we shift from zonal to blocked flows, despite their common reduction in moisture content at higher latitudes. This suggests that moisture availability is not a major limiting factor to explain the precipitation responses to anomalous zonal flow conditions over most of the IP. In fact, these composites show that the positive precipitation anomalies in south and eastern IP during blocking episodes are related with the increment of atmospheric instability in the target areas.

Additionally, we would like to explore whether the changes in moisture content and instability are triggered by specific weather systems. Trigo et al. (2004) already discussed the important role played by the southward deflection of the storm-tracks in the European precipitation responses to blocking episodes. Thus, taking into account the main synoptic patterns that trigger precipitation

events in the IP, we next explore changes in their frequency during blocking and strong zonal flow episodes for each considered sector. In this regard, we herein distinguish between near-surface cyclones and upper-level low-pressure systems such as COLs, both causing negative Z500 anomalies (as those found over the IP in the blocking minus strong zonal flow composites of Fig. 4.6). To achieve this, we first looked at the climatological frequency of cyclones and COL in the Euro-Atlantic area, as presented in the top panels of Figs. 4.7 and 4.8, respectively. The results reflect some well-known facts: (1) the North Atlantic is a preferred region for storm-tracks, with northwestern IP being commonly affected by them (Fig. 4.7); (2) the Mediterranean basin (and the IP in particular) are the regions in the Euro-Atlantic sector where COL activity is more frequent throughout the year (Fig. 4.8). We next check the amplitude and significance of eventual changes in their frequency (as compared to climatology) during blocking episodes for both the ATL and EUR sectors. We also explore if there is an agreement between cyclonic and COL blocking-related tracks and the already mentioned increases in atmospheric instability during these events.

The anomalies in cyclone activity (non-stationary near surface systems) show a clear increase in most areas close to the IP during ATL blocks (Fig. 4.7, middle left), in contrast with a sharp decrease in the UK, where cyclonic activity is almost non-existent during blocking patterns. For EUR blocks (Fig. 4.7, middle right) the cyclone frequency decrease is shifted eastwards (over the Scandinavia region), in good agreement with the location of the blocking high (Fig. 4.2), but the increase in cyclonic activity elsewhere is predominantly non-significant. Note that despite the cyclone increase over the IP there is also a reduction in moisture fluxes to the north of the IP during blocking conditions (Fig. 4.6), which may explain the decrease in precipitation found in NW IP. In this regard, it must also be reminded that a large fraction of the precipitation that occurs in this region is related to frontal systems that are linked to cyclone centers located at higher latitudes (Trigo et al., 2004) and whose frequency is strongly reduced during blocking situations. This is supported by the ATL blocking composites of Figs. 4.6 and 4.7, which show that the maximum decrease in cyclonic activity occurs to the north of the corresponding decrease in moisture content. Thus, the precipitation deficits in NW IP during ATL blocks can be attributed to a decrease on the frequency of efficient Atlantic low-pressure systems affecting high latitudes (and the subsequent decrease in moisture fluxes in the vicinity of northwest Iberia).

#### 4. Blocking impacts on Iberian precipitation and temperature

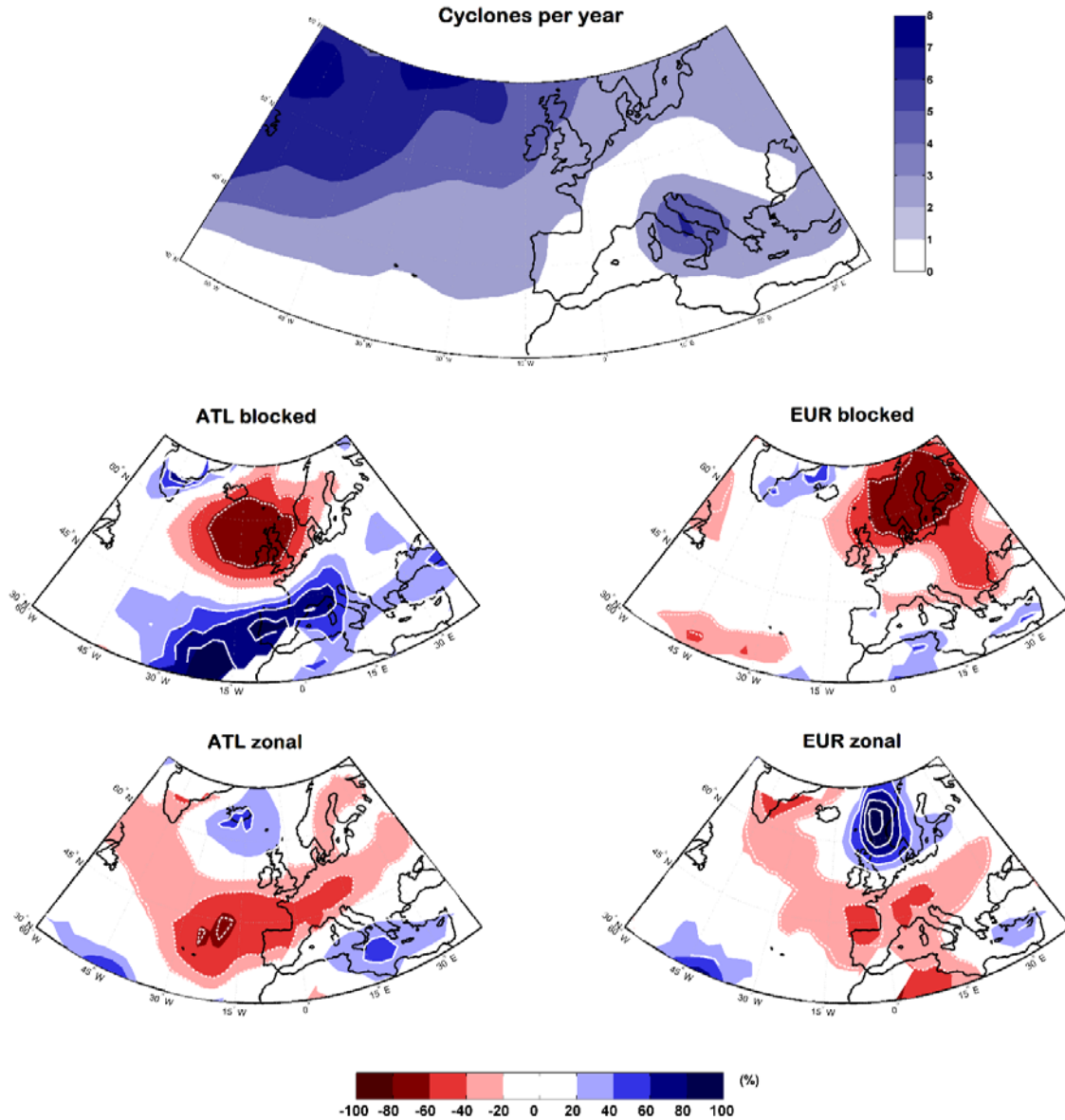


**Fig. 4.7** Top: annual mean frequency of non-stationary cyclone centers in the Atlantic-European sector (counted in  $2.5^\circ \times 2.5^\circ$  boxes). Middle row: annual mean changes (in %) in the cyclone frequency during blocking episodes in the Atlantic (middle left) and European (middle right) sectors; Bottom row: annual mean changes (in %) in the cyclone frequency during strong zonal flow episodes in the Atlantic (bottom left) and European (Bottom right) sectors; increases are shown with blue shading (solid white lines) and decreases with red shading (dotted white lines). Anomalies are only depicted in boxes where at least one cyclone per year was registered during the 1950–2007 climatology.

#### 4. Blocking impacts on Iberian precipitation and temperature

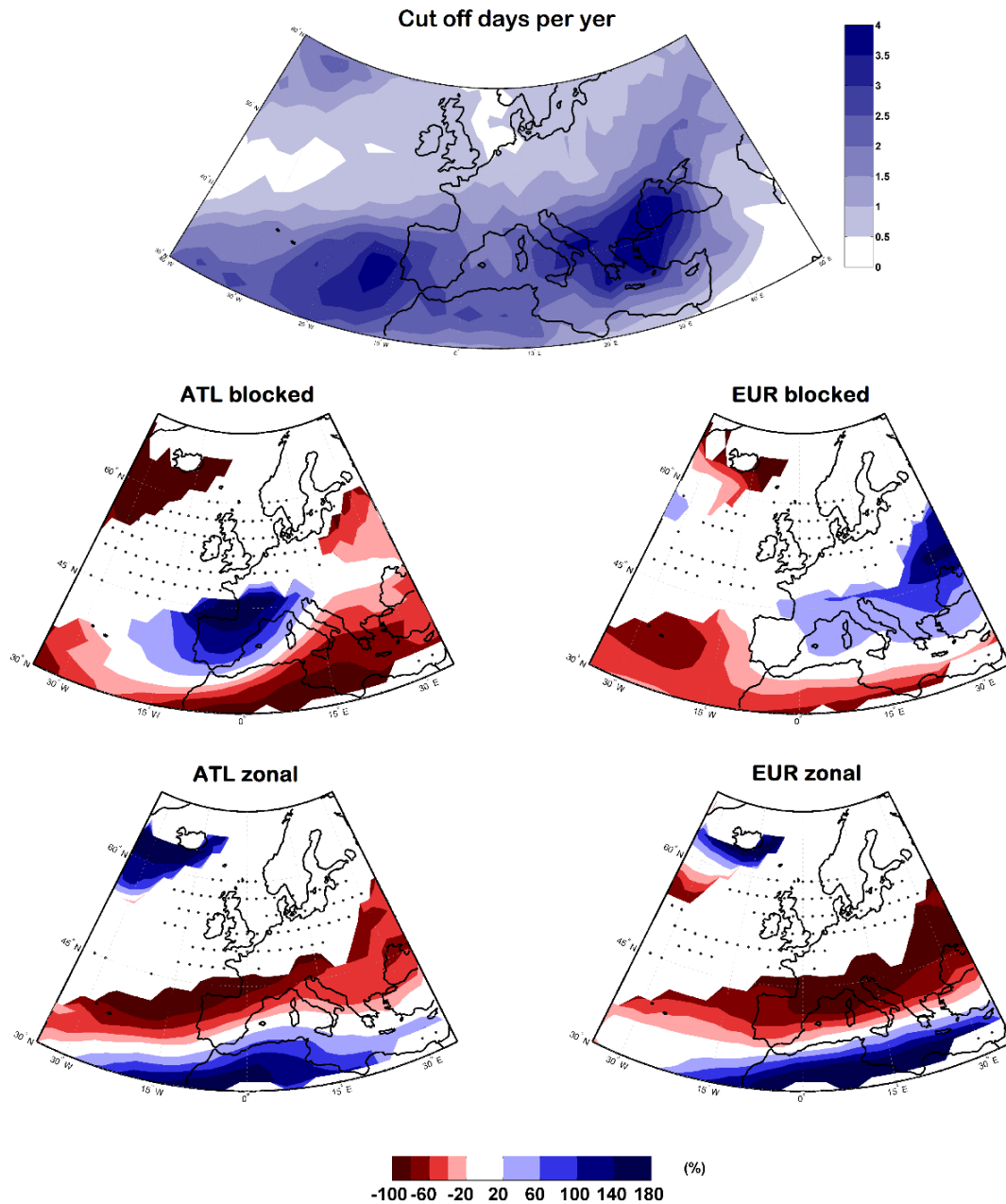


**Fig. 4.8** Top: annual mean frequency of cut off lows in the European- Mediterranean sector (counted in  $2.5^\circ \times 2.5^\circ$  boxes). Middle row: annual mean change (in %) in the frequency of cut-off lows during blocking episodes in the Atlantic (middle left) and European (middle right) sectors; Bottom row: annual mean change (in %) in the frequency of cut-off lows during strong zonal flow episodes in the Atlantic (bottom left) and European (bottom right) sectors; Areas of increase (decrease) are shown in blue (red). Anomalies are only depicted in boxes where at least one cut-off per year was registered during the 1950–2007 climatology. Black dots represent the areas with significant decreases that do not achieve that threshold.

Concerning changes in COLs activity, results show a significant increase around the Iberian Peninsula domain during ATL blocks (over 150 % in some areas) as presented in Fig. 4.8. There is also an increase during EUR blocks, but displaced towards Eastern Europe, although still appreciable in eastern IP (~50 %). The increase in COL and transient cyclones activity during ATL blocks is in fair agreement with the increase found in precipitation and atmospheric instability anomalies in southern IP. Regarding the responses found during EUR blocks, there is a slight decrease in cyclonic activity close to northeastern Iberia (Fig. 4.7), contrasting with a small increase of COL activity in the Mediterranean coast of the IP (Fig. 4.8). This fact suggests that the initial stages of COLs - corresponding to troughs located over the region which later develop and mature into COLs towards the east—may be the main cause for the significant increases in atmospheric instability and precipitation in the area.

Furthermore, the analysis of Fig. 4.7 (bottom panel) shows that in the IP region the responses in cyclone frequency to strong zonal flows are similar for the two sectors (both negative). This fact shows that the different precipitation responses to ATL and EUR zonal flows (see Fig. 4.4) are likely not related to changes in cyclone paths. On the contrary, the areas of higher reduction in COLs shift eastwards from ATL to EUR zonal flows (Fig. 4.8), apparently in better agreement with the respective regions of negative precipitation anomalies (Fig. 4.4). Still, we must bear in mind that both cyclones and COLs analyses were performed on coarser grids when compared to the high-resolution precipitation dataset, thus losing some information about the dependence of the precipitation responses on small changes in the location of these synoptic systems.

##### **4.1.5 Extreme value analysis**

As stated in the introduction, several areas of the IP are often affected by episodes of torrential precipitation, with significant contributions to seasonal totals, and important socio-economic impacts. This is particularly true for the eastern coasts of the IP, as the presence of warm Mediterranean waters (especially at the end of the summer and the beginning of autumn) fosters such precipitation regimes (e.g., García-Herrera et al., 2005a). We must bear in mind the results from Sect. 3, where it was evident that the significant increase in rainfall during blocking episodes over this region was not a result of an increase in the number of rainy days, thus suggesting a higher rate of heavy precipitation episodes during such atmospheric patterns. To check the efficiency of regional blocking patterns in promoting extreme rainfall events, we first computed the ratio between the frequency of blocking and strong zonal flow days with total precipitation above the local 90th percentile for the ATL and EUR sectors, as presented in Fig. 4.9.

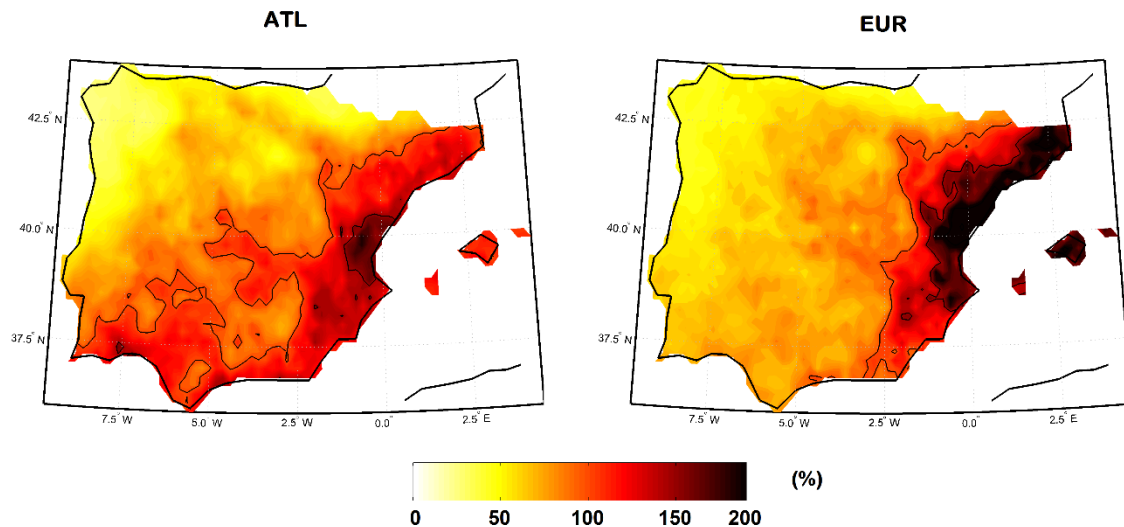


**Fig. 4.9** Extreme precipitation efficiency: quotient between the number of blocking days with daily precipitation above the 90th percentile and the number of zonal days with daily precipitation above the 90th percentile (in %) in the ATL (left panel) and EUR (right panel) sectors. Quotients above the 100 % isoline (thick black lines) are represented by darker reddish shading.

Easternmost regions of Spain (for ATL and EUR blocks) and southernmost regions of Spain and Portugal (for ATL blocks) have higher ratios of extreme days during blocking episodes, when compared to strong zonal flows. The opposite result is found for northwestern IP, where the rainiest days are more associated with strong zonal flow patterns. Scrutinizing in further detail these different extreme precipitation regimes, we performed an extreme value analysis on the high-resolution precipitation dataset in order to: (a) identify regions with homogeneous extreme precipitation regimes and find the model that better fits to their tailed distributions; (b) analyze the contribution of different weather regimes to extreme daily precipitation episodes in these distinct sectors.

Several authors have shown that the Generalized Pareto (GP) Distribution provides adequate fits for one-side tailed distributions as the one found for precipitation extremes. The use of this type of fit for precipitation extremes is useful to model parameters such as probability maps of specific threshold exceedances, or return levels and periods. For example, Vicente-Serrano et al. (2009) used this fit to model extreme precipitation events in areas of Spain during different phases of the NAO and the Mediterranean Oscillation, and Toreti et al. (2010) characterized extreme winter precipitation in Mediterranean coastal sites in association with anomalous atmospheric circulation patterns.

When performing an extreme value analysis, we must bear in mind that the sample sizes of extreme episodes need to be large enough to provide satisfying fits. This is not the case for all considered gridpoints of the dataset, as in some areas heavy precipitation events are particularly rare. Furthermore, adjusting such a large number of local models requires some caution, taking into account that the associated errors resulting from each particular fit may eventually lead to unreliable results. Hence, the spatial comparison and coherence of such a large number of fits must

#### 4. Blocking impacts on Iberian precipitation and temperature

be considered carefully. For this reason, we opted to first apply a spatial aggregation scheme, by considering four boxes of gridpoints. These boxes (Fig. 4.10) have been defined taking into account the different responses in precipitation regimes found in the previous sections, as well as areas where extreme events are spatially coherent and often lead to abundant precipitation and have more severe impacts. In addition, a fifth test box was defined in central areas of the IP, to check the fit in a region with a different regime of precipitation extremes. In order to perform this spatial aggregation of the data, it is necessary to check if these sub-domains defined heuristically actually represent homogeneous regions in terms of the extreme precipitation distribution. For this purpose, we used a methodology based on the L-Moments, where a statistic  $H1$  checks the degree of heterogeneity of a region in terms of precipitation extremes (for further details on the methodology see Hosking and Wallis, 1997). This test was applied separately to each box by considering the gridpoint sub-series containing only rainy days with precipitation above the local 90<sup>th</sup> percentile. For all boxes, the  $H1$  statistic presented values lower than 1, i.e., below the required threshold to consider regions as homogeneous (Hosking and Wallis, 1997). Since the defined regions are homogenous, for each specific day we considered the absolute maximum of all gridpoints inside the box, in order to obtain the precipitation extreme daily series of each box. Such a process significantly increases the number of extreme precipitation records, as compared to that obtained by considering fits for individual gridpoints.

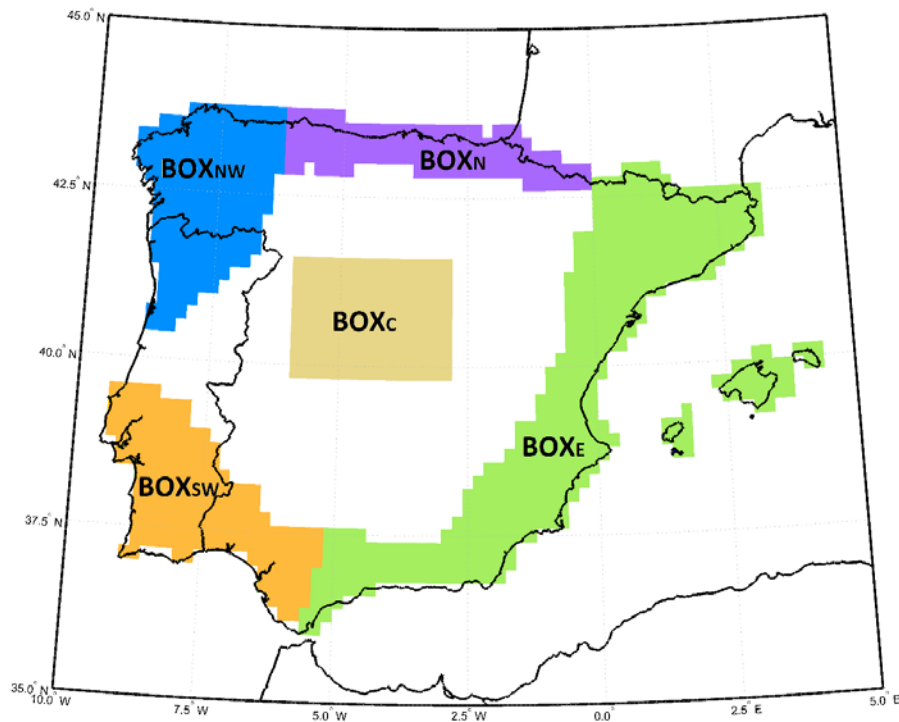


**Fig. 4.10** Boxes defined for the Generalized Pareto fit: northwest ( $BOX_{NW}$ ); north ( $BOX_N$ ), southwest ( $BOX_{SW}$ ); east ( $BOX_E$ ) and central ( $BOX_C$ ). These boxes were defined taking into account the precipitation anomaly patterns found in Section 3.1.3, and also the Iberian Peninsula geography and socioeconomic factors.

#### 4. Blocking impacts on Iberian precipitation and temperature

The above mentioned extreme daily series of each box were then used to assess whether the frequency of extreme precipitation events in each box and for different weather regimes is large enough to perform the extreme value analysis. Table 4.1 presents the number of rainy days with precipitation above the 90th percentile, and the frequency of such extremes occurring under blocked and zonal days. This exercise also allows analyzing the effectiveness of each considered weather pattern on promoting extreme precipitation days in the different areas of the IP.

**Table 4.1** Number of extreme rainy days (above 1 mm, with total precipitation above the 90th percentile) for each box, and the relative contribution of each considered weather pattern (in percentage with respect to the total number of extreme rainy days).

	Days	Block <sub>ATL</sub> (%)	Block <sub>EUR</sub> (%)	Block <sub>total</sub> (%)	Zonal <sub>ATL</sub> (%)	Zonal <sub>EUR</sub> (%)	Zonal <sub>total</sub> (%)	Other (%)
BOX <sub>NW</sub>	1901	5.4	8.8	14.2	25.9	6.0	31.9	53.9
BOX <sub>N</sub>	1842	8.8	8.1	16.9	19.3	3.9	23.2	59.8
BOX <sub>SW</sub>	1542	17.4	12.9	30.4	10.5	4.7	15.2	54.4
BOX <sub>E</sub>	1933	15.7	16.2	32.0	10.0	2.0	12.0	55.9
BOX <sub>C</sub>	1498	11.1	11.0	22.2	10.9	5.8	16.8	61.1

As it can be seen from Table 4.1, the sum of extreme days during blocked and zonal patterns corresponds to almost half of the total extreme days for any of the considered boxes. In the case of BOX<sub>NW</sub> and BOX<sub>N</sub>, the contribution of blocking to extreme precipitation days is near 15 %, while that of strong zonal flows is around 30 %. In BOX<sub>SW</sub> and BOX<sub>E</sub>, these results are reversed, in agreement with the overall pattern presented in Fig. 4.9, thus reinforcing the idea that blocking favors extreme events in these regions, while strong zonal flows (mainly those occurring over the ATL) are more decisive for extreme precipitation in the Atlantic areas of the IP. Regarding BOX<sub>C</sub>, there is a similar contribution of blocked and strong zonal flows, albeit with slightly higher percentages of extreme events during blocked patterns, particularly when they are located over the European sector. Therefore, the number of extreme precipitation events occurring under blocking and zonal flows is large enough to perform an extreme value analysis.

We next explored the theoretical model that better captures the distribution of the extremes daily series of each box. This was done by applying different models to the daily series of each considered box and constructing L-Moment Ratio diagrams to visually check the convenience of each fit (Fig. 4.11). These diagrams clearly point to the GP fit as the most suitable one for our extreme precipitation series in all boxes. Besides this visual inspection, we later checked the goodness-of-fit of models for each sub-region using the Anderson–Darling test (Wilks, 2011), as it will be detailed further ahead.

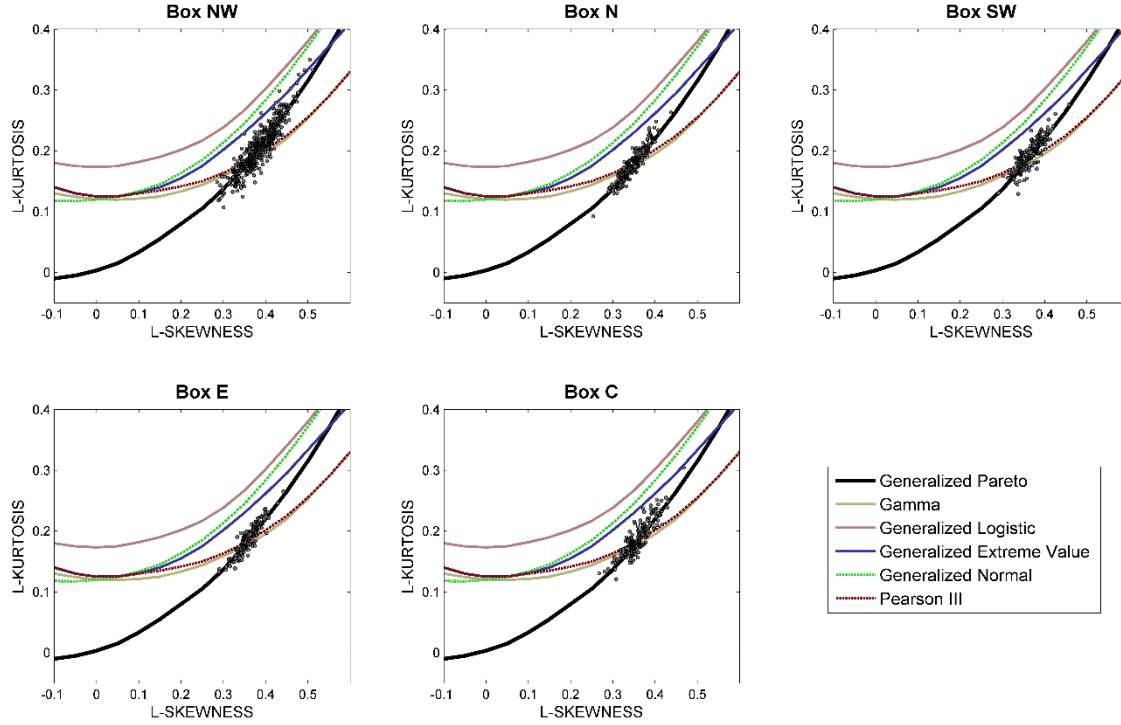


**Fig. 4.11** L-Moment Ratio diagrams for series of precipitation days above the 90th percentile in the five considered boxes inside the Iberian Peninsula. Different curves represent different types of Extreme Value distributions and grey dots correspond to the observed values in each box.

In order to perform the GP fit (Beirlant et al., 2004) for extreme precipitation events in each box, we have followed a scheme similar to the one presented by Vicente-Serrano et al. (2009). Thus, we defined discrete blocking and zonal events as sequences of at least 4 days under those particular synoptic conditions. While blocked events are more frequent over Europe, zonal patterns are more frequent in the ATL sector. The results of this classification indicate that zonal events tend to last longer than blocked events (~9 and ~7 days, respectively), and that for both types of events ATL patterns persist for slightly longer periods than EUR patterns. Then, once again using the extreme daily series of the individual boxes (previously obtained from the daily maxima inside each of these sub-regions), we obtained two different new time-series for each box, each one having a single precipitation value associated to each specific weather event. These two series are comprised by: (1) the maximum daily value of each event (PMAX); (2) the accumulated precipitation of each event (PTOT). This has been done in order to perform a temporal declustering over sequences of rainy days, and thus to avoid the presence of serial dependence or persistence.

Next, for each box, we followed a peak-over-threshold approach, by calculating the high percentiles of the series of rainy days, and then applying GP fits for the corresponding tails of the PTOT and PMAX time-series obtained for both weather patterns (blocked and strong zonal flow events). In order to decide the more appropriate percentile threshold, we relied on both graphical (probability–probability plots, see Supplementary Material, Fig. 4.14 and Fig. 4.15) and formal (Anderson–Darling test) selection techniques. Taking this into account we finally opted for the

#### 4. Blocking impacts on Iberian precipitation and temperature

90th percentile as a final threshold, and all presented GP fits were performed for the tail series based on this threshold. The confidence levels for the fits, as well as their corresponding tail and shape parameters are presented in Tables 4.2 and 4.3.

**Table 4.2** Confidence levels (**bold**) after the Anderson–Darling test, the tail parameter, and the scale parameter of each GP fit applied to the tailed distribution (above the 90th percentile) of the PMAX series of the five considered boxes of gridpoints, during blocking (left columns) and strong zonal events (right columns) in the ATL and EUR sectors.

$P_{MAX}$	Block <sub>ATL</sub>	Block <sub>EUR</sub>	Zonal <sub>ATL</sub>	Zonal <sub>EUR</sub>
BOX <sub>NW</sub>	<b>90</b> %/0.04/19.82	<b>85</b> %/−0.18/31.71	<b>89</b> %/−0.23/41.02	<b>92</b> %/−0.23/41.60
BOX <sub>N</sub>	<b>91</b> %/−0.10/25.90	<b>88</b> %/−0.19/29.42	<b>92</b> %/−0.23/29.83	<b>91</b> %/−0.20/27.08
BOX <sub>SW</sub>	<b>91</b> %/−0.18/34.06	<b>91</b> %/−0.09/23.70	<b>87</b> %/0.03/21.07	<b>87</b> %/−0.32/29.15
BOX <sub>E</sub>	<b>91</b> %/0.00/51.24	<b>86</b> %/−0.14/50.75	<b>95</b> %/0.02/47.73	<b>88</b> %/0.02/29.33
BOX <sub>C</sub>	<b>92</b> %/0.04/20.99	<b>94</b> %/0.05/23.52	<b>88</b> %/−0.20/29.68	<b>91</b> %/−0.13/34.98

**Table 4.3** Same as Table 4.2, but for the PTOT time series.

$P_{TOT}$	Block <sub>ATL</sub>	Block <sub>EUR</sub>	Zonal <sub>ATL</sub>	Zonal <sub>EUR</sub>
BOX <sub>NW</sub>	<b>91</b> %/0.05/90.80	<b>88</b> %/−0.10/122.36	<b>95</b> %/−0.10/236.02	<b>93</b> %/−0.10/236.02
BOX <sub>N</sub>	<b>88</b> %/−0.18/135.34	<b>93</b> %/−0.16/111.37	<b>93</b> %/−0.05/171.96	<b>91</b> %/−0.05/171.96
BOX <sub>SW</sub>	<b>91</b> %/0.04/121.87	<b>93</b> %/−0.23/132.36	<b>95</b> %/0.00/98.79	<b>94</b> %/0.00/98.79
BOX <sub>E</sub>	<b>94</b> %/−0.07/208.26	<b>94</b> %/−0.06/204.86	<b>95</b> %/−0.01/167.79	<b>94</b> %/−0.01/167.79
BOX <sub>C</sub>	<b>89</b> %/0.02/92.55	<b>95</b> %/−0.02/91.96	<b>93</b> %/−0.06/107.70	<b>91</b> %/−0.06/107.70

Overall, the confidence levels obtained after performing the Anderson–Darling test are high (above 90 %), thus giving us confidence on most of the performed fits, and once again reinforcing on the convenience of the GP fit to model precipitation tail distributions. The location parameter of the fits illustrates very well the different contribution of distinct weather regimes to extreme daily precipitation episodes at the regional scale. Higher values of this parameter are found for blocked patterns in southern and eastern areas (BOX<sub>E</sub> and BOX<sub>SW</sub>), contrarily to northern regions (BOX<sub>N</sub>, BOX<sub>NW</sub> and BOX<sub>C</sub>), where higher values are found for zonal flows. These regional differences become clearer when we analyze PTOT, for which the changes on the location parameter from blocked to zonal flows are higher, particularly for BOX<sub>NW</sub>. This is not surprising, since: (1) extreme precipitation days in Mediterranean (Atlantic) areas of the IP are strongly linked to blocked patterns (strong zonal flows); (2) large sequences of moderate to heavy rainfall are frequent in northwest Iberia during strong zonal synoptic conditions; (3) torrential episodes in the Mediterranean coasts occur essentially at shorter time scales. We must recall that the mean duration of strong zonal flow events is slightly larger than that of blocking events. This is obviously important when comparing the probabilities for PTOT, as different mean durations involve different expected accumulated values.

These results confirm the existence of different extreme precipitation regimes between northwestern and southeastern sectors of the IP, with the former being related to persistent

moderate precipitating events and the latter by short-lived intense episodes. They also demonstrate that these regional differences are to a large extent due to different triggering large-scale weather regimes (strong zonal flows and blocking patterns, respectively). These distinct atmospheric configurations play a very different contribution to the occurrence of extreme events in those regions, and although they are both related to anomalies of the zonal flow, they exhibit nearly opposite synoptic features and very different persistence signatures, thus shaping regional differences in the tailed distributions of precipitating events.

##### 4.1.6 Discussion

In this work, we made a reassessment of blocking impacts in precipitation regimes over the Iberian Peninsula, taking advantage of the recently developed high-resolution datasets for the two Iberian countries. The simple comparison between blocking composites obtained using a low-resolution dataset (NCEP) and the high-resolution dataset (IBERIA02) clearly shows that only the latter can represent adequately specific regional impacts. Furthermore, the difference between the impacts caused by blocking episodes in different sectors (Atlantic and Europe) is also perfectly clear using the high-resolution data. Overall, blocking occurrence induces a negative to positive marked dipole in precipitation from northwest to southeast Iberia, with a northeast shift of the largest positive anomalies from ATL blocks to EUR blocks. We must recall that the blocking structures tend to migrate eastwards in most cases, and hence the regional precipitation responses partially reflect blocking impacts at different stages of the blocking lifecycle.

Increases in precipitation rates above 50 % are found in some regions during blocked synoptic patterns. In particular, positive precipitation anomalies extend to most of the IP domain during ATL blocks, being larger in southern and southeastern areas of the IP, while during EUR blocks they tend to be more restricted to eastern Mediterranean regions. Nevertheless, the relevance of blocking on precipitation vanishes as we move towards the northwest. In these regions, the blocked patterns only contribute to less than 10 % of the total mean annual precipitation. Nearly opposite results are obtained for strong zonal flows. However, there are some important asymmetries in the precipitation signals between zonal and blocked patterns, suggesting some non-linear responses to changes in the westerly flow.

The synoptic configurations associated with blocking show negative Z500 anomalies to the south of the blocking centers. As a consequence, during blocking situations, storm-tracks tend to be deflected southwards, towards the IP domain, explaining part of the precipitation excess found over Iberia. Still, this shift is not completely compatible with the blocking-related precipitation deficits in northwest Iberia. In this case, changes in transport and moisture availability during blocking days (involving a reduced efficiency of Atlantic frontal systems located northwards of the IP) explain the reduction in rainfall amount. Other important dynamical factors seem to play a role in the precipitation responses to blocking over the Mediterranean region. In particular, the simultaneous increases in low pressure systems (particularly cut-off lows) affecting the area and atmospheric instability help to understand the blocking signatures in precipitation over the Mediterranean coast. This important rise in the frequency of cut-off lows in the IP area (particularly

during ATL blocks) is in agreement with Nieto et al. (2007), which noticed the increase of COL activity in the southern flank of Euro-Atlantic blocking systems. This sustains the importance of dynamical factors in shaping the precipitation regimes of the IP, especially in the Mediterranean areas. Furthermore, the high-resolution dataset reveals substantial differences on the precipitation responses to blocking over relatively small regions (mainly in the Mediterranean). This indicates a major importance of local processes (such as moisture convergence and deep convection) on the precipitation regimes of that part of Iberia and calls for further investigation, including the relevance and impact of Sea Surface Temperatures, and their connections and feedbacks with the particular synoptic patterns that arise from blocking situations.

On the other hand, we have found that, for most of the IP, the precipitation increases associated with blocking are due to changes in precipitation amount rather than changes in the number of precipitation days. In fact, despite the overall increase in precipitation under blocking action, there is either a concurrent decrease in the number of measurable rainfall days in most of the regions of Iberia (more pronounced in NW Iberia) or irrelevant changes in the number of rainy days. This fact indicates that rainfall regimes during blocking days are more extreme in southeastern Iberia, where the blocking contribution to annual totals is the greatest. The results are supported by the existence of a northwest-southeast dipole in the rate of days with extreme precipitation occurring under strong zonal flow and blocking.

Finally, we have performed an Extreme Value Analysis, fitting Generalized Pareto distributions to maximum daily precipitation and total accumulated precipitation series for distinct homogeneous sub-regions inside the IP during blocking and strong zonal episodes. This approach shows that extreme precipitation events during blocking conditions tend to be short-lived (i.e., isolated extremes at the daily scale), mainly in the Mediterranean, while zonal events are more relevant concerning the total episode accumulated precipitation in northwest Iberia.

**Acknowledgments** Pedro M. Sousa was supported by the Portuguese Science Foundation (FCT) through a doctoral GRANT (SFRH/BD/84395/2012). Alexandre M. Ramos was also supported by FCT in a postdoctoral GRANT (FCT/DFRH/SFRH/BPD/84328/2012). This work was partially supported by FEDER funds through the COMPETE (Programa Operacional Factores de Competitividade) Programme and by national funds through FCT (Fundação para a Ciência e a Tecnologia, Portugal) through project STORMEx FCOMP-01-0124-FEDER-019524 (PTDC/AAC-CLI/121339/2010).

### 4.1.7 Supplementary Material

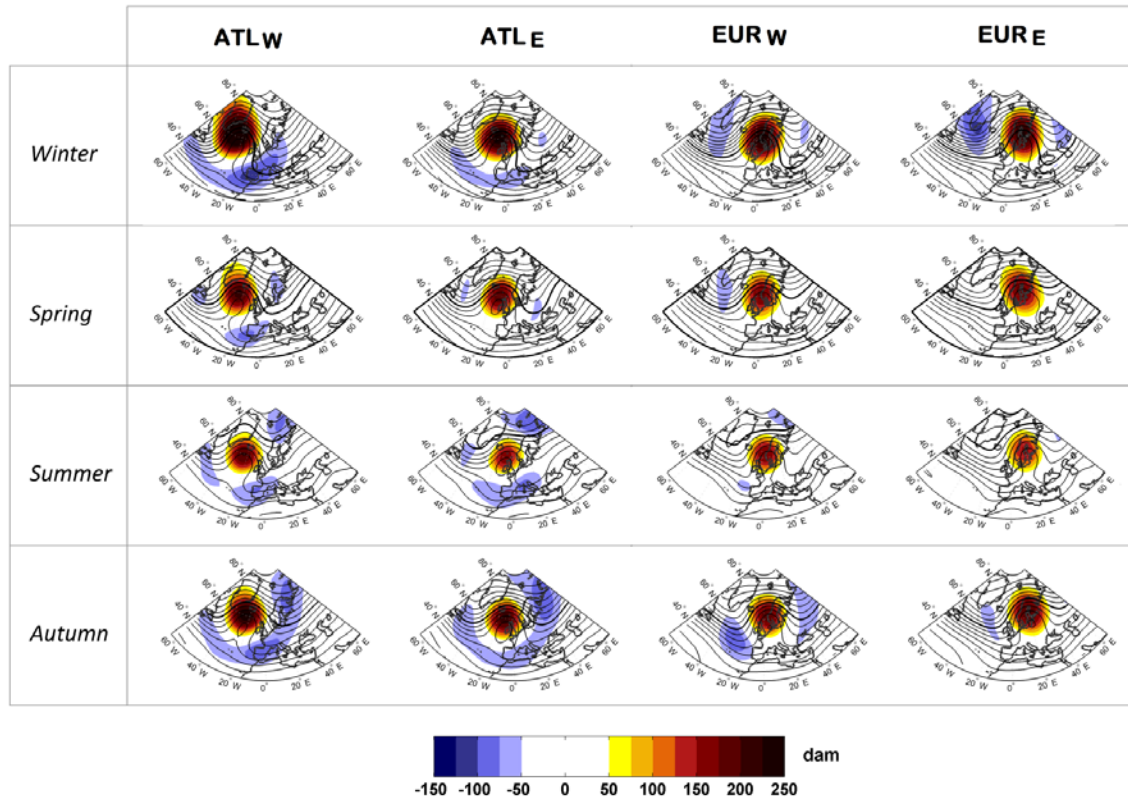


**Fig. 4.12** Composites of the daily anomalies (shaded areas) and absolute values (isolines) of 500 hPa geopotential height for blocking centers when considering sub-sectors 15° of longitude wide. All values are in decameters (dam) and the thick line represents the 550 dam isohypse.

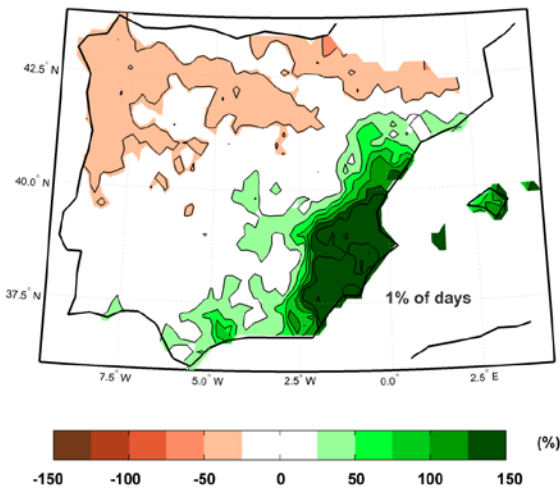


**Fig. 4.13** Annual composite of daily precipitation anomalies (%) in the Iberian Peninsula for Atlantic blocking days which occur exclusively in the a five day window prior to the occurrence of European blocking episodes. Only statistically significant anomalies at the 5% level are shown.

#### 4. Blocking impacts on Iberian precipitation and temperature

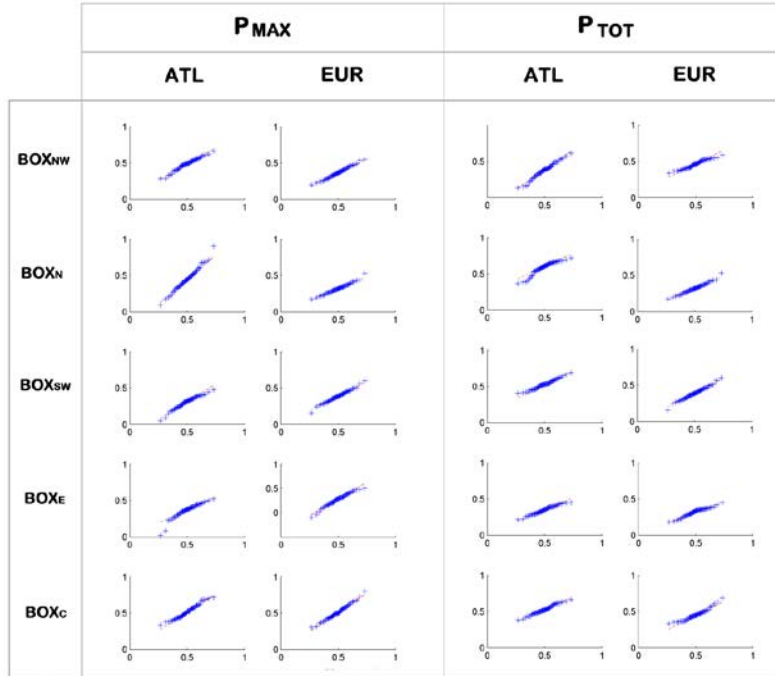


**Fig. 4.14** Probability-probability plots between the empirical distribution and the modeled Generalized Pareto distribution for maximum daily precipitation (P<sub>MAX</sub>) and total precipitation (P<sub>TOT</sub>) during blocking events in the Atlantic and European sectors in each of the considered boxes of gridpoints.

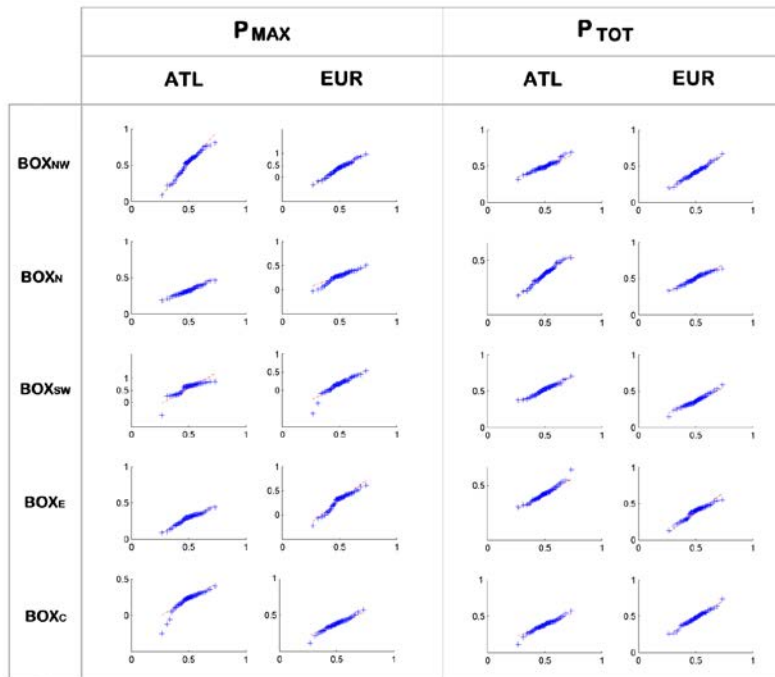


**Fig. 4.15** Same as Fig. 4.14, but for zonal events.

## 4.2 High-resolution Iberian rainfall deficits during ridge patterns

In this section we present additional results on the high-resolution precipitation responses to subtropical ridge episodes. Bearing in mind that some local signatures (particularly during summer ridges) are highly dependent on small shifts of the subtropical ridge location (see Section 2.1), here results are shown for subtropical ridges occurring within the four 15° longitudinal sectors that can impinge a significant impact in Iberia, namely: ATL<sub>W</sub> (30W-15W), ATL<sub>E</sub> (15W-0W), EUR<sub>W</sub> (0E-15E) and EUR<sub>E</sub> (15E-30E). Composites of relative anomalies in daily precipitation (in %) during winter and summer ridge days are presented in Fig. 4.16.

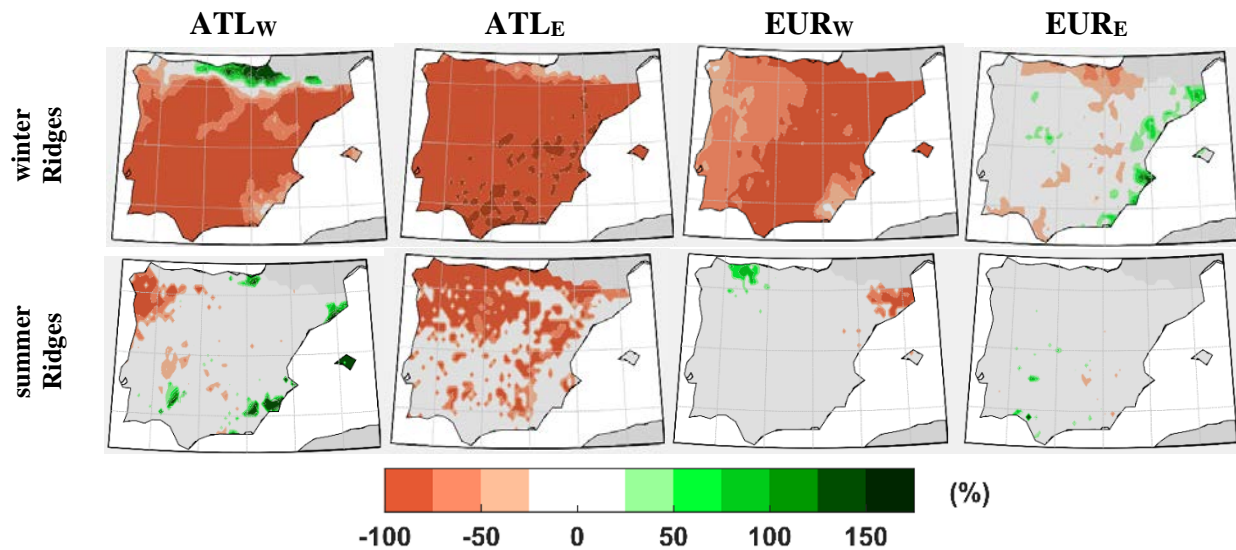


**Fig. 4.16** Composites of relative anomalies in daily precipitation (in %) for ridge days in the ATL<sub>W</sub>, ATL<sub>E</sub>, EUR<sub>W</sub> and EUR<sub>E</sub> sectors during winter (upper panels) and summer (lower panels). Only statistically significant anomalies at 5% significance level are depicted.

As it can be seen in the upper panels of Fig. 4.16, ridges in both ATL subsectors, as well as in EUR<sub>W</sub> result in dramatic decreases in daily precipitation rates. This is crucial for Iberian water availability, since most areas strongly depend on winter precipitation, which is the wettest season. These results are in good agreement with Santos et al. (2009), who stressed the key role played by eastern Atlantic ridges on Iberian drought episodes. Still, this high-resolution grid provides further details, which are masked in coarser datasets. For example, during ATL<sub>W</sub> ridges, the Cantabria region and the western Pyrenees have increased rainfall, contrarily to all other areas. This may be explained as follows: a ridge located far enough to the west of Iberia still enables northerly moist flows towards those mountainous areas, whereas the intense north-south Föhn effect will prevent positive precipitation anomalies south of the mountain ranges. For ridges located over Iberia (ATL<sub>E</sub>), decreases are striking over the entire peninsula, with some areas receiving no precipitation at all. On the other hand, ridges located eastwards (EUR<sub>E</sub>) are sufficiently distant to produce smaller impacts on precipitation.

During summer (Fig. 4.16, lower panels), the overall precipitation reductions are less significant and not so homogeneous, with larger spatial variability in the regional responses. It should be stressed that most areas are quite dry during this season (particularly central and southern sectors of the peninsula), and therefore these intense negative anomalies are relatively meaningless. Still, it is possible to find some significant localized precipitation increases during summer ATL<sub>w</sub> ridges, as well as in northwestern Iberia during EUR<sub>w</sub> ridges. Nevertheless, the relatively generalized negative impact on precipitation remains dominant in most areas for the majority of sub-regional ridge structures occurring in the ATL and EUR sectors, with the largest signal being associated to ATL<sub>E</sub> systems.

### 4.3 High-resolution Iberian temperature responses to blocks and ridges

Using the blocking and ridge catalogues, a finer scale analysis on high-resolution temperature responses over Iberia to those atmospheric patterns has also been performed. Similarly to the high-resolution Iberian precipitation dataset (IBERIA02), a maximum and minimum temperature dataset has been developed by Herrera et al. (2012), at the horizontal resolution of  $0.2^\circ \times 0.2^\circ$ . However, unlike the precipitation dataset, the temperature dataset is only currently available for Spanish meteorological stations. Thus, all results shown in this section do not include the Portuguese area of the Iberian Peninsula.

Composites of winter and summer maximum temperature anomalies during blocking and ridges are presented in Fig. 4.17 and Fig. 4.18, respectively. As in the previous section, here we show results for the weather systems occurring within the following  $15^\circ$  longitudinal sectors: ATL<sub>w</sub>, ATL<sub>E</sub>, EUR<sub>w</sub> and EUR<sub>E</sub>.

On the overall, the anomalies found over Iberia resemble those from the E-OBS dataset (Fig. 2.12 and Fig. 2.13), with cold temperatures being associated to blocks, and warm temperatures prevailing during ridges. Nevertheless, some regional particularities arise, which were not so well captured by the sparser E-OBS dataset. For example, there is a region with near normal maximum temperatures in the Ebro valley during winter EUR<sub>w</sub> ridges, contrasting with the overall warming Iberian response to this pattern. This difference is likely induced by prolonged foggy episodes that are frequent in this area, under stable anticyclonic conditions (Cuxart and Jimenez, 2010). On the other hand, the largest minimum temperature anomalies during winter ridges tend to occur in some mountainous areas, suggesting subsidence and thermal inversion patterns. It should be noted that the winter increases in maximum temperature during ridge episodes are larger than those observed for minimum temperature, due to reduced cloud cover under stable conditions and thus an increase of solar radiation during the day and also the loss of infrared radiation at night. In fact, some southwestern areas of Iberia experience slightly below average minimum temperatures during ATL ridges. Finally, the impact of the ridge patterns centered over the Iberian Peninsula (ATL<sub>w</sub> and EUR<sub>E</sub>) display a considerable stronger maximum temperature anomaly than the two other regional systems (Fig. 4.17).

#### 4. Blocking impacts on Iberian precipitation and temperature

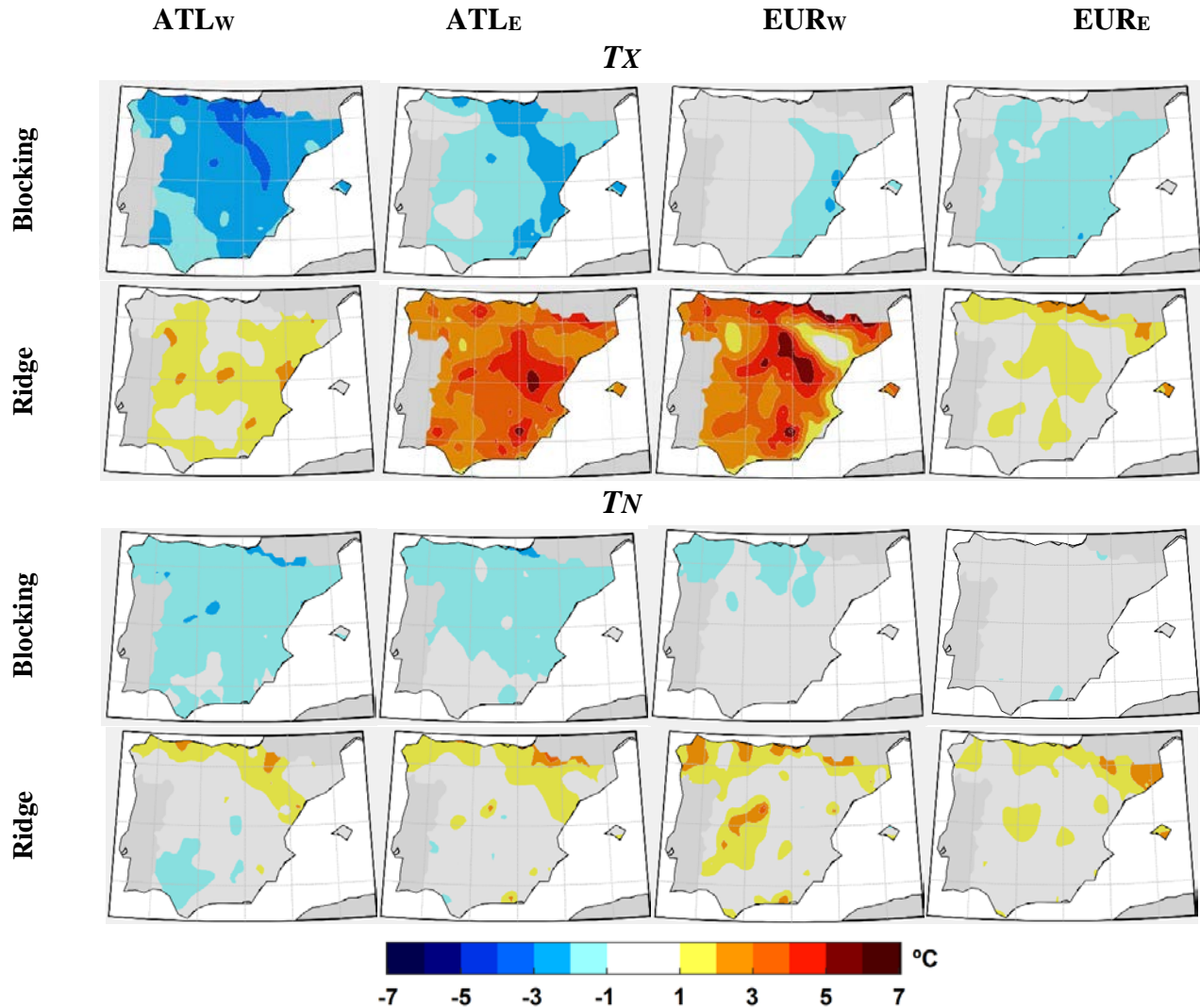


**Fig. 4.17** Composites of winter 2 m maximum (upper panels – TX) and minimum (lower panels – TN) temperature anomalies (in °C) for blocking and ridge days in the ATL<sub>W</sub>, ATL<sub>E</sub>, EUR<sub>W</sub> and EUR<sub>E</sub> sectors, based on the SPAIN02 high-resolution dataset. Only statistically significant anomalies at 5% significance level are depicted.

During winter blocking events, the associated decreases in maximum temperature are also larger than in minimum temperature, resulting in reduced daily amplitudes, particularly for ATL blocks (Fig 4.17). This is in agreement with the concurrent increase in cloud cover and precipitation, as shown in Sections 3.1 and 4.1, due to the blocking-induced southerly deviation of the storm-tracks. The temperature responses over Iberia during summer blocking (Fig. 4.18) are qualitatively similar to the ones found during winter, due to a combination of reduced insolation, and cold advection from higher latitudes in the eastern flank of the blocking systems (as previously discussed in Section 2.1).

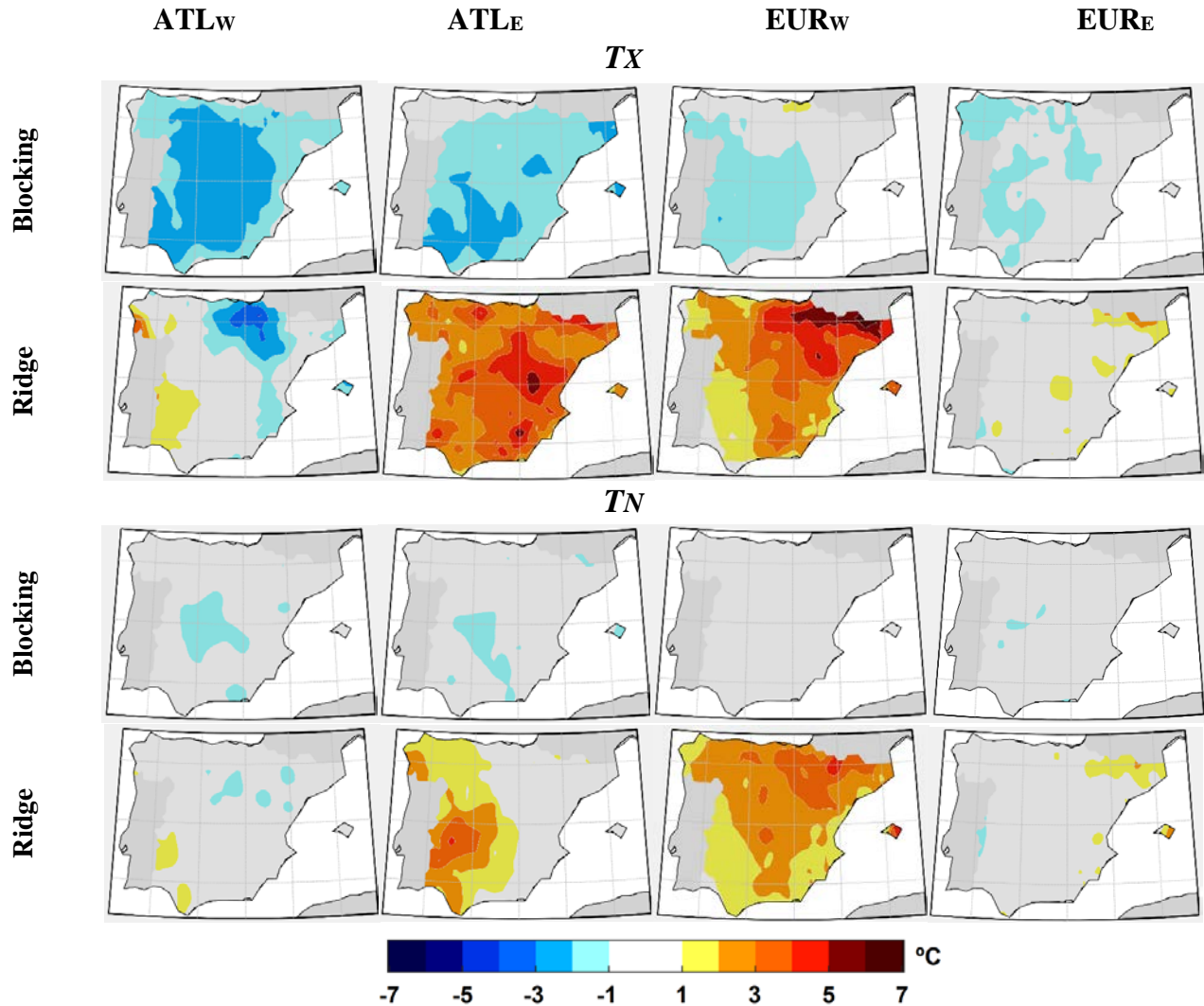


**Fig. 4.18** Same as Fig.4.17, but during summer.

As already mentioned in Section 2.1, ridge patterns are often associated with summer extreme temperature episodes in southern Europe, including the Iberian Peninsula (Fig. 4.18). Overall, the increases in minimum temperature associated to ridges are smaller, resulting in larger amplitudes of the daily temperature cycle, which can be explained by radiative heating (see Section 2.1.4). The composites of temperature anomalies during summer ridges are striking, being particularly generalized for ATL<sub>e</sub> and EUR<sub>w</sub> ridges, with most areas experiencing anomalies above +3°C. The temperature responses are particularly notorious in central Spain during ATL<sub>e</sub> ridges, or northeastern Spain during EUR<sub>w</sub> ridges (particularly the Pyrenees), which reach +7°C.

It is worth noting that anomalies are almost non-existent for ridges occurring in neighboring sectors to the Iberian peninsula, i.e. EUR<sub>e</sub> and ATL<sub>w</sub>, thus confirming that the exact location of the sub-tropical ridge axis is paramount to determine the areas that experience extremely warm conditions (Section 2.1). For example, for ATL<sub>w</sub> ridges, significant positive anomalies are found

#### ***4. Blocking impacts on Iberian precipitation and temperature***

---

in southern Galicia, but the region of Cantabria and Basque country experiences below average temperatures. Although data is unavailable for Portugal, the spatial pattern suggests the occurrence of relevant positive anomalies in westernmost Iberia under ATL<sub>W</sub> ridges.



## **Chapter 5**

### **Conclusions and open threads for Future work**

#### **Contents**

---

##### **5.1 Conclusions**

##### **5.2 Open threads for Future work**

*5.2.1 The feedbacks between blocking, droughts and wildfires*

*5.2.2 Future scenarios of blocking variability in the 21<sup>st</sup> century*

##### **5.3 Perspectives**

---

### Summary

#### Context and objectives

This chapter summarizes the main conclusions of the thesis and presents some preliminary results of ongoing work, thus providing perspectives for hopefully publishable material. Besides temperature and precipitation series, other climate-related phenomena, which are relevant from a socio-economic and environmental perspective (such as droughts and wildfires), are conditioned by the occurrence of blocking and sub-tropical ridge patterns. In Sections 5.2 and 5.3 additional examples of the impacts associated to blocking and ridge patterns are provided, which were considered outside the scope of the papers presented in Chapters 2-4. Particular attention is devoted to feedback processes between blocking/ridges and droughts, and their mediating role during the pre-fire season in the inter-annual variability of burnt areas in the Mediterranean basin. Furthermore, and taking into account the: 1) observed changes in Mediterranean droughts and drying trends in future projections; 2) previously discussed links between ridges and Mediterranean drought variability; 3) lack of studies addressing future changes in sub-tropical ridges (as opposed to the abundant literature about future blocking projections), a brief outlook and preliminary discussion of recent trends and future changes in sub-tropical ridges is provided by using models from the CMIP5 project.

#### Methods

The European Fire Database (EFD) is employed to characterize the southern European wildfires responses to blocking and ridges. The role played by preceding and immediate blocking/ridges in burnt areas is assessed separately by exploring both the pre-fire and the active (summer) fire seasons. Due to the pre-conditioning of soil moisture deficits in fire vulnerability, particular attention is paid to quantify the links between blocking/ridges and droughts by using the recently developed Standardized Precipitation Evapotranspiration Index (SPEI). The spatial correlation coefficients between droughts and atmospheric patterns (at different time scales) are also considered, in order to account for the feedbacks between winter-spring droughts and summer temperature extremes. Finally, an overview of recent (1950-2012) trends in ridge frequency over the Euro-Atlantic sector is performed, in order to explore potential difficulties in thresholds calibration for the ridge detection in CMIP5 GCMs.

#### Results

Blocking/ridge patterns exert an important effect on wildfire spatial extension at different time scales. During the pre-fire wet season, reduced blocking (increased ridge) frequency is associated with below average precipitation in southern Europe, thus promoting drought conditions and enhancing vegetation fire vulnerability in the following summer. Furthermore, during the fire season itself, these atmospheric patterns, and in particular summer ridges, impinge hot and dry conditions, which foster fire spread. The solely occurrence of anomalous blocking/ridge activity in either the pre-fire or the active fire season is not enough to explain the large inter-annual variability of burnt areas, and both conditions are required to account for the worst fire years in different southern European countries.

In the last decades, the frequency of sub-tropical ridges has increased in the Mediterranean areas. Future warming climate projections suggest additional increases along with the northward expansion of the sub-tropical high-pressure belt. However preliminary analyses reveal some limitations of the detection method used for ridges implying a clear need to develop new dynamical detection schemes, rather than methods purely based on anomaly fields, in order to increase confidence in future projections of ridge frequencies.

### 5.1 Conclusions

This thesis has addressed the seasonal impacts of atmospheric blocking in the Euro-Atlantic sector, with emphasis on regional and seasonal assessments that have often been overlooked in previous studies. Thus, a thorough characterization of blocking occurrence within different longitudinal sectors (Atlantic, European and Russian) was performed, prior to a comprehensive analysis of the associated climatic impacts of each blocking pattern over Europe, considering in particular the impacts on the precipitation and temperature distributions over distinct regional sectors.

The assessment of blocking impacts led to an important conclusion about the necessity to distinguish the climatology and impacts of high-latitude blocking from those of sub-tropical ridges. In this context, a novel ridge detection scheme was developed in Chapter 2, and a catalogue with their occurrence was computed, in order to compare it against the blocking catalogue. While ridges are frequent precursors of wave-breaking that may evolve into Omega-type blocks, or Rex-type blocks in a later stage, these lower latitude structures do not require a wave-breaking as blockings do. More importantly, their dynamical structure, and the fact they are located further south, impinge very contrasting (sometimes opposite) conditions over Europe, when compared to blocks.

Chapter 2 highlights the necessity to distinguish the latitudinal location of geopotential height maximum anomalies in order to assess their associated impacts in temperature (Sousa et al., 2017b). In fact, this allowed to clarify that most summer extreme heat episodes in southern Europe and Mediterranean areas should not be attributed to blocking, but rather to ridges, contrarily to what previous studies had imprecisely stated. For central and northern areas of the continent, both regimes are responsible for warm episodes, as radiative heating and subsidence are enhanced under anomalously high geopotential values. Contrarily, during winter, the temperature impacts of blocking and ridges are opposite. While blocks (particularly those located in the eastern Atlantic and western/central Europe) favor cold winter spells by reinforcing the cold advection through the northerly flows established in their eastern flank, winter ridge patterns are associated to above average temperatures and mild Atlantic air masses induced by stronger zonal flows.

A similar dichotomy was applied to the evaluation of the blocking impacts in European precipitation regimes in Chapter 3, by separating strong zonal flow and blocking regimes (Sousa et al., 2017a). Blocking patterns are associated with a clear north-south dipole consisting in negative (positive) precipitation anomalies in northern (southern) European areas. In the overall, these precipitation responses are explained by a blocking-induced split of the storm-track around its center location, which enhances cyclonic activity in southern Europe. However, increased atmospheric instability under such atmospheric configurations is additionally required to explain the reported increase in heavy precipitation over Mediterranean areas. During strong zonal flows, the precipitation anomaly pattern is essentially reversed, as compared to that of blocks. As ridges are associated with a stronger meridional pressure gradient north of their position (and a consequent enhancement of the zonal flow at higher latitudes), the precipitation signatures of sub-tropical ridges are similar to those obtained for strong zonal flow patterns. Thus, an increased

frequency of ridges leads to anomalously dry conditions in southern areas of the considered longitudinal sector of occurrence, particularly during winter. Finally, the results also suggest that the winter solid precipitation (snow covered soils) responses to blocking and ridges are better related to temperature than precipitation anomalies. Thus, while winter blocking occurrence leads to below average precipitation in large areas of central and northern Europe, the associated cold temperature patterns are in good agreement with the above-average observed responses in snow covered soil days over most European areas. On the opposite side, the mild winter conditions related to ridge occurrence inhibit snow cover in the European continent.

The specific responses over the Iberian Peninsula were explored in Chapter 4 by using higher-resolution datasets (Sousa et al., 2016). The results reveal regional signatures that are missed in coarser grids, particularly in what concerns the impact of topography in precipitation, hence confirming the need of high-resolution to address the regional and local responses to weather regimes. Thus, while blocking (strong zonal flow) is associated with increased (reduced) precipitation in most of Iberia, the northwestern tip of the Peninsula receives less (more) precipitation, in agreement with a reduced (increased) cyclonic frequency at higher latitudes and the resulting frontal activity that reaches this region. Blocking activity plays a crucial role on the precipitation regimes and the occurrence of heavy precipitation events in the southern half and the Mediterranean shores of Iberia. Regarding ridges, the results show that their impacts are more sensitive to the specific location of the sub-tropical ridge. In particular, ridges in the eastern Atlantic are strongly linked to the occurrence of dry and warm conditions over large parts of Iberia, thus leading to regional extreme summer temperature events. Furthermore, ridges located in the 15W-15E sector are responsible for generalized winter dry conditions in Iberia, diminishing considerably the total annual rainfall observed in the area.

## 5.2 Open threads for Future work

The characterization of the specific regional impacts of blocking patterns in primary climatological variables, such as temperature and precipitation, provides an appropriate background for framing the impacts in other variables and in other background conditions (i.e., future climate). Some of these questions correspond to ongoing work, whose preliminary results will be included in this section.

In particular, Section 5.2.1 is devoted to drought variability, which is strongly dependent on anomalous conditions in both temperature and precipitation. As such, the links between blocking/ridges and droughts can be framed taking into account the specific temperature (Chapter 2) and precipitation (Chapter 3) anomaly patterns associated to each regime. The decisive role of drought conditions in fire activity allows in turn an assessment of the possible impacts of blocking and ridges in wildfire inter-annual variability in southern European countries.

Droughts and wildfires are issues of special concern in the Mediterranean, which has been considered as a climate change hot-spot. Thus, finally, Section 5.2.2 provides an overview of recent studies on observed trends and future changes in blocking. To our knowledge, there are not

similar assessments for sub-tropical ridges, and hence, a substantial part of this section will focus on exploring recent trends in these systems. This will provide a first step to assess the projected changes in their occurrence and in the associated impacts, as a way to understand the contribution of changes in these weather regimes to the projected drying and warming of the Mediterranean, and the resulting threats to water availability (see the future perspectives in Section 5.3). The links between fires, drought occurrence, atmospheric circulation and climate change acquire special relevance in the Iberian Peninsula, which has been a central topic of this thesis. These questions were addressed in two papers developed during the PhD. within the scope of the European project FUME (Sousa et al., 2015; Trigo et al., 2013b). While they are considered outside the main scope of this thesis, their information is relevant for the ongoing work and the future perspectives, and hence, they have been included in the Annex.

### 5.2.1 The feedbacks between blocking, droughts and wildfires

Wildfire inter-annual and intra-annual variability in the Mediterranean area has been widely explored in recent decades (e.g. Pereira et al., 2005; Gudmundsson et al., 2014; Turco et al., 2017). It is well known that pre-conditioning (pre-fire season) may enhance vegetation stress, while the meteorological conditions during the peak of the fire season are the main trigger for fire ignitions (Pereira et al. 2013; Trigo et al., 2013b; Sousa et al., 2015; Gouveia et al., 2016; Amraoui et al., 2015). The links between climate and fire are often analyzed under the intermediate fire-productivity hypothesis (Pausas and Bradstock, 2006; Pausas and Paula, 2012), which suggests that fire risk oscillates between two minima, one dominated by high aridity conditions, under which fire spread is mostly limited by the fuel amount (Sousa et al., 2015a), and another characterized by low aridity, where fuels are abundant and fires are mainly limited by the soil moisture content (Ruffault et al., 2016; Turco et al., 2017). In fuel-limited ecosystems, antecedent wet conditions may regulate the fuel amount and its structure, while in relatively wet ecosystems, droughts and hot spells can influence dryness (Pausas and Paula, 2012).

On the overall, in Mediterranean climates, the vulnerability to very large wildfires is well related with drought occurrence (Gouveia et al., 2016). As water availability in most of these areas is highly reliant on the rainfall amount accumulated during winter and spring, below average precipitation in the wet season is often related with vegetation stress in the warmer months (Pellizzaro et al., 2007; Gouveia et al., 2012; Turco et al., 2017). However, wetter than average late spring conditions following dry winters can trigger a rapid biomass growth in certain Mediterranean areas, such as western Iberia, also enhancing forest vulnerability in the case of a following dry and hot summer (Pereira et al., 2013). As such, Mediterranean-type climates can be considered “intermediate” ecosystems, where both soil moisture and fuel amount can play a role in shaping fire regimes (Pausas and Paula, 2012; Gudmundsson et al., 2014; Turco et al., 2017).

In this context, we explore the links between blocking/ridge occurrence and wildfires in several southern European countries, using the European Fire Database (EFD – Camia et al., 2014), a database which assembles records for individual fire events from 21 countries of the European Union. The fire database covers slightly varying periods for each country spanning between the

## 5. Conclusions and open threads for Future work

early 1980s and early 2010s. These links should be considered for different time-lags and temporal scales, as these atmospheric patterns may play an important role in extreme summer temperature conditions (as shown in Chapter 2), as well as in soil moisture pre-conditioning (i.e., drought conditions).

To characterize drought conditions in Europe, the Standardized Precipitation Evaporation Index (SPEI) developed by Vicente-Serrano et al. (2010) was employed. This is a multiscalar drought index based on climatic data (precipitation and temperature), which can be used for determining the onset, duration and magnitude of drought with respect to normal conditions in a variety of natural and managed systems such as crops, ecosystems, rivers, water resources, etc. It is available on a monthly basis with a horizontal resolution of  $0.5^\circ \times 0.5^\circ$ , and for different time-scales, spanning between 1 and 24 months. Here, the 6-month time-scale was considered, thus the SPEI index for May, at the end of spring (representing the accumulated hydrological imbalance through the winter and spring) was compared against the anomalous occurrence of blocking and ridges in the previous months. Figure 5.1 shows the correlation between the May SPEI for each gridpoint and the anomalous frequency of blocks/ridges during January-May in the three  $30^\circ$  longitudinal sectors.

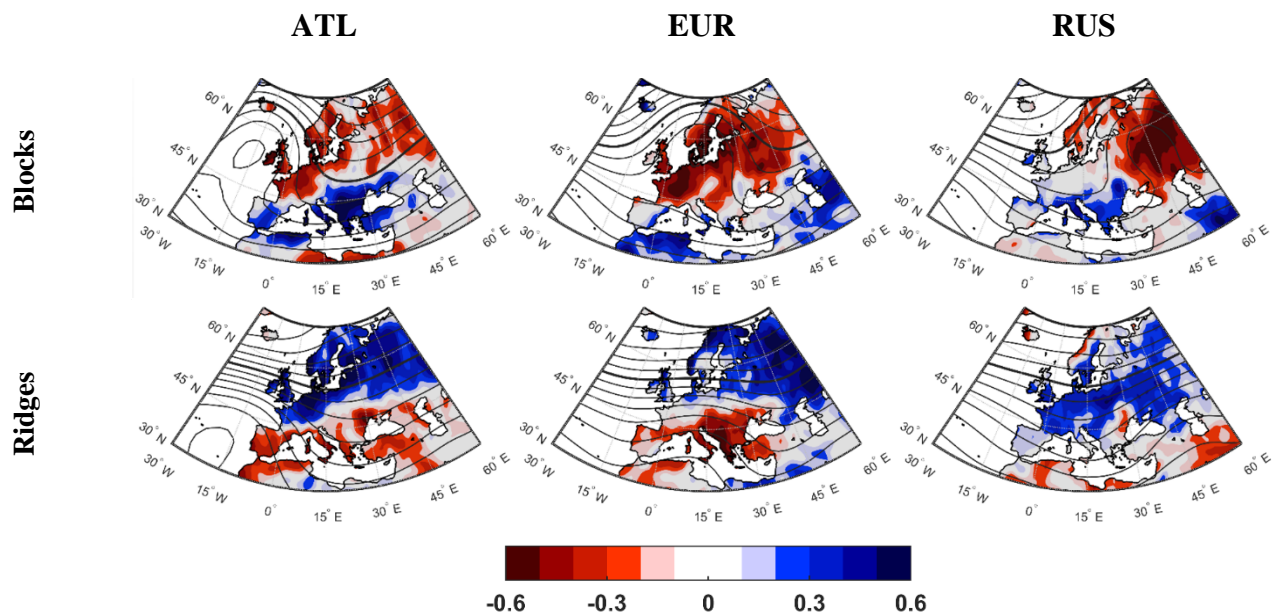


**Fig. 5.1** Pearson correlation coefficient between 6-month SPEI at the end of spring (May) and the previous month's anomaly (January-May) in the frequency of blocking (upper panel) and ridges (lower panel) occurring in the ATL (30W-0W), EUR (0E-30E) and RUS (30E-60E) sectors for the period 1950-2012.

The correlation coefficients are in relative good agreement with the previously discussed precipitation anomalies found for blocking (Section 3.1) and ridges (Section 3.3). The former impinge a dry fingerprint in central and northern areas of Europe, and wetter than average

## 5. Conclusions and open threads for Future work

conditions in southern Europe, while the latter shows a reversed meridional dipole in SPEI. Focusing on southern European areas, ridges are the main precursor of drought conditions (and of the subsequent incremented vegetation stress) in the pre-fire season (Fig. 5.1, lower panels). These links show the leading role of anomalous precipitation patterns during the colder and usually wetter months in modulating drought conditions towards late spring and early summer. This assessment only accounts for the pre-conditioning of the large-scale circulation in the fire season vulnerability (i.e., the potential for severe summer wildfires). However, the actual fire activity is also dependent on the occurrence of a following hot summer, which in turn can be also associated to concurrent anomalies in the frequency of blocking/ridges, as shown in Chapter 2.

To further check this dual role of precedent and current atmospheric patterns in the fire season itself, correlation coefficients were also computed between summer burnt areas in southern European countries (Portugal, Spain, Italy and Greece) and: 1) the anomalous frequency of blocking/ridge patterns between January and May (the pre-fire season); 2) anomalous frequency of blocking/ridge patterns between June and September (the fire season). These results are shown in Tables 5.1 and 5.2, respectively.

**Table 5.1** Pearson correlation coefficient between summer burnt area (June to September) and the anomalous frequency of blocks/ridges in each sector prior to the fire season (January to May). Bold values are statistically significant at the 5% level. Available fire records: Portugal (1980-2012); Spain (1985-2012); Italy (1985-2012); Greece (1983-2011).

	Atlantic	Europe	Russia
<b>Portugal</b>	0.17 / 0.14	0.04 / 0.14	-0.01 / -0.03
<b>Spain</b>	0.13 / 0.15	-0.06 / -0.08	-0.16 / -0.04
<b>Italy</b>	0.01 / 0.05	0.00 / <b>0.27</b>	-0.11 / -0.06
<b>Greece</b>	-0.12 / 0.06	0.01 / -0.03	-0.03 / -0.01

**Table 5.2** Same as Table 5.1 but considering the anomalous blocking and ridge frequency during the considered fire season (June to September).

	Atlantic	Europe	Russia
<b>Portugal</b>	-0.14 / <b>0.41</b>	-0.10 / -0.01	0.03 / -0.01
<b>Spain</b>	<b>-0.35</b> / <u>0.25</u>	<u>-0.26</u> / <u>0.21</u>	<b>-0.38</b> / 0.10
<b>Italy</b>	0.01 / 0.05	<b>-0.33</b> / <u>0.20</u>	0.06 / -0.19
<b>Greece</b>	<u>0.27</u> / <u>-0.24</u>	-0.13 / 0.02	0.10 / <u>-0.28</u>

Results show some statistically significant correlations (at the 5% significance level), particularly for anomalous patterns during the fire season. For example, a significant correlation is found between summer ATL ridges and fires in Portugal, as expected from the anomalous temperature responses during such episodes (Section 2.1). However, in the overall, previous and contemporary meteorological conditions alone do not explain a large fraction of the burnt area variability. In this sense, and besides non-meteorological factors (such as land-use, fire prevention and suppression measures), it is possible to hypothesize that the role of the atmospheric circulation

## 5. Conclusions and open threads for Future work

patterns in wildfires will maximize when both the anomalous frequencies of weather regimes during and before the fire season are considered simultaneously. This should help to explain a cumulative process which begins with winter and early spring atmospheric patterns promoting dry conditions, followed by summer synoptic conditions favoring regional warm temperatures, and thus fire ignitions. As a future work, this could be achieved by considering the conditional probability of fire activity subject to: 1) blocking/ridges in the previous season alone; 2) blocking/ridges in the fire season itself; 3) blocking/ridges in both seasons. Such analysis would also allow testing different combinations of weather regimes and seasons (e.g., less blocks in winter-spring and more ridges in summer).

In this context, it is worth noticing that several authors have described the feedback between winter-spring soil dryness in transitional climatic regions and the enhancement of European summer heat episodes (e.g., Fischer et al. 2007; Vautard et al. 2007, Seneviratne et al., 2010). In addition, Quesada et al. (2012) reported that winter-spring dryness precedes European heatwaves only if anticyclonic conditions occur in summer, thus stressing the key role of summer high-pressure systems. As a consequence, one should expect an enhanced summer fire risk if both conditions (preceding soil moisture deficits and summer high-pressure anomalies) are simultaneously met. To address this question, we computed the composites of late spring (May) SPEI and June-September Z500 anomalies for the most severe wildfire years (in terms of total burnt area) of each country (Fig. 5.2).

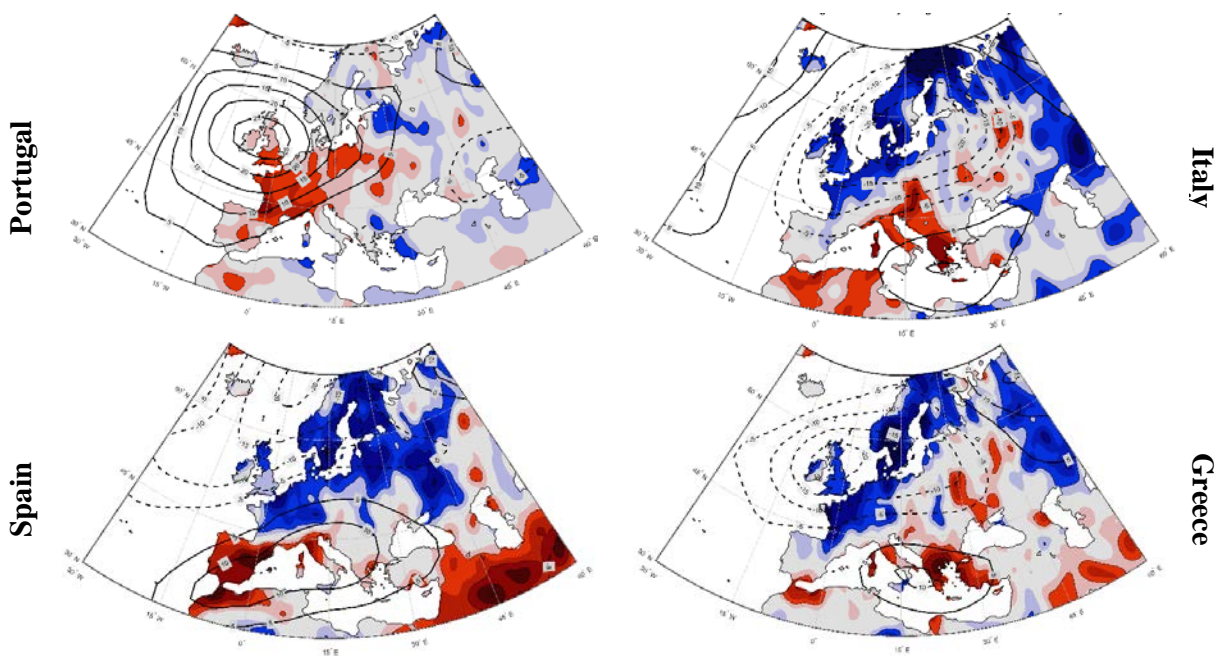


**Fig. 5.2** Composite of the 6-month SPEI at the end of spring (May, shading) and the following summer (June-September) 500 hPa geopotential height anomalies (black contours) for the 5 most severe years in terms of total burnt area. Period considered for each country as stated in Table 5.1.

## 5. Conclusions and open threads for Future work

As it can be seen, there is an overall spatial agreement between the affected countries (in terms of burnt area) and both late spring soil moisture deficits (SPEI) and positive summer Z500 anomalies, although with a number of regional nuances. Overall, it is reasonable to conclude that the worst fire seasons were accompanied by both preceding droughts and concurrent anticyclonic conditions in summer. However, it is important to acknowledge that these spatial patterns do not always occur over the considered country. For example, for the most severe fire years in Portugal, the summer high-pressure conditions and the preceding dryness occur over a large area of western and southwestern Europe. This may be explained by the findings of Vautard et al. (2007), who reported that winter soil moisture deficits in southern Europe tend to propagate towards central Europe throughout the following spring and summer. To check this hypothesis, we computed the composited monthly evolution of the SPEI index for the same set of severe years of each country (Fig. 5.3).

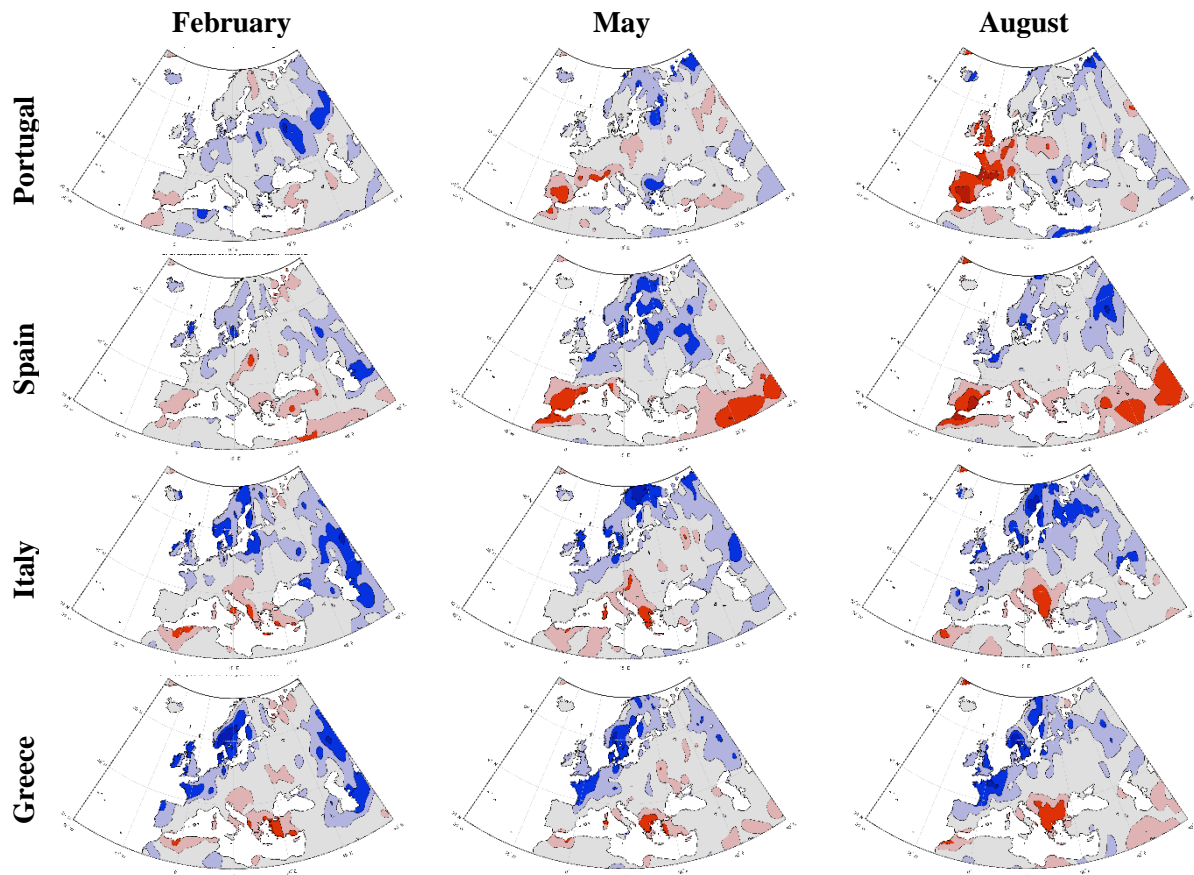


**Fig. 5.3** Composites of the intra-annual evolution of the 6-month SPEI for the 5 most severe years in terms of total burnt area in each considered country. Period considered for each country as stated in Table 5.1.

Portuguese wildfires (top panel, Figure 5.3) depict very well the previously described northward expansion of drought conditions along the western sectors of Europe from winter to summer. However, it should be stressed that the outstanding 2003 year (in terms of heatwaves and wildfire

occurrence) could induce biases in the composite due to its outlier nature. In the remaining cases, the pattern does not show such a northward expansion, but a localized aggravation of the drought conditions throughout late spring and summer. In all the cases, the SPEI anomalies are observed since spring, being collocated with the following summer Z500 anomalies shown in Fig. 5.2. These results suggest a possible feedback of the drought conditions on the atmospheric circulation (e.g., Fischer and Schär 2009), highlighting the need for further investigation of this soil-atmosphere coupling. In summary, while an anomalous occurrence of blocking/ridges before and during the fire season influences fire vulnerability in southern Europe, they are not necessarily a sufficient condition. In most cases, a winter-spring soil moisture deficit pre-conditioning (strongly linked with reduced blocking and/or enhanced ridges) and the occurrence of summer ridges are both required to trigger wildfires. While these results may provide some prospects on developing useful seasonal predictions of wildfire occurrence, particular caution must be taken concerning their representativeness due to the exploratory nature of this work.

### 5.2.2 Future scenarios of blocking variability in the 21<sup>st</sup> century

In recent decades, General Circulation Models (GCM) have improved their capacity to reproduce global and regional climate variability (Flato et al., 2013), as well as observed meteorological fields, with ever increasing skill scores under weather forecast mode (Magnussen and Källén. 2013). However, their relatively weak ability to reproduce the inception and duration of blocking patterns has been an undermining caveat through different generations of GCMs (D'Andrea et al., 1998; Scaife et al. 2010; Davini and D'Andrea, 2016). Taking into account the crucial impact of atmospheric blocking in the European climate, a good representation of its phenomenology in GCMs is required in order to increase confidence in future projections (Hoskins, 2013). The blocking underrepresentation in GCMs is particularly pronounced in the Euro-Atlantic sector, with different definitions and detection methods (e.g. anomalies versus flow reversal) being able to provide different quantitative results (e.g., Barriopedro et al. 2010b). In addition, Scaife et al. (2010) or Vial and Osborn (2012) attributed a large proportion of the diagnosed blocking errors to biases in the mean climate, particularly in the meridional gradient of the geopotential height fields. More recently, Davini and D'Andrea (2016) made a thorough inter-comparison between generations of models in the last 20 years. These authors show that, despite an overall improvement in GCMs, few advances have been made in blocking representation in the Euro-Atlantic sector. This latter work also corroborates findings from other authors (e.g. Berckmans et al. 2013, Matsueda et al., 2009; Anstey et al., 2013), which show that high-resolution models reduce the underestimation of blocking frequency, with the increase in the horizontal and vertical resolutions both playing an important role. Also recently, Pithan et al. (2016) suggested that the representation of large scale features such as jet-streams, blockings or storm-tracks can be improved by refining parameterizations of low-level drag.

Concerning future projections, and despite a number of discrepancies, there is some agreement on a decreasing trend of blocking frequency in the North Atlantic under increasing Greenhouse Gases Concentrations (e.g., Barnes et al. 2012; Dunn-Sigouin and Son, 2013), accompanied by a small increase in central/eastern Europe and western Russia, suggesting a northeastward migration

## 5. Conclusions and open threads for Future work

of blocking patterns (e.g. Sillman et al., 2009; de Vries et al., 2013). Other authors report an increase in prolonged blocks in the eastern Atlantic, particularly during winter (e.g. Mokhov et al. 2014). In agreement with these authors, Ruti et al. (2014) reported an association between longer blocking episodes and anthropogenic forcing.

Conversely, there have been no exhaustive studies regarding the projected changes in sub-tropical ridges, at least for the Euro-Atlantic sector. Kent et al. (2011) examined the representation of the Australian sub-tropical ridge in CMIP3 models, and projected an increase in its intensity in the 21<sup>st</sup> century, with an extension of its influence towards higher latitudes, thus aggravating drought episodes in the area. These results are in agreement with the overall positive projected trends in geopotential heights at such latitudes associated to the expansion of the Hadley cell (Lu et al., 2007).

Before exploring future changes, we analyze recent trends in the frequencies of sub-tropical ridges and high-latitude blocking over the Euro-Atlantic sector during the observational record. In Figs. 5.4 and 5.5, the time series of blocks and ridges frequencies occurring in each of the three considered longitudinal sectors (ATL, EUR and RUS) and the associated linear trends are depicted. This analysis was undertaken for the calibration period (1950-2012) and using the NCEP/NCAR reanalysis.

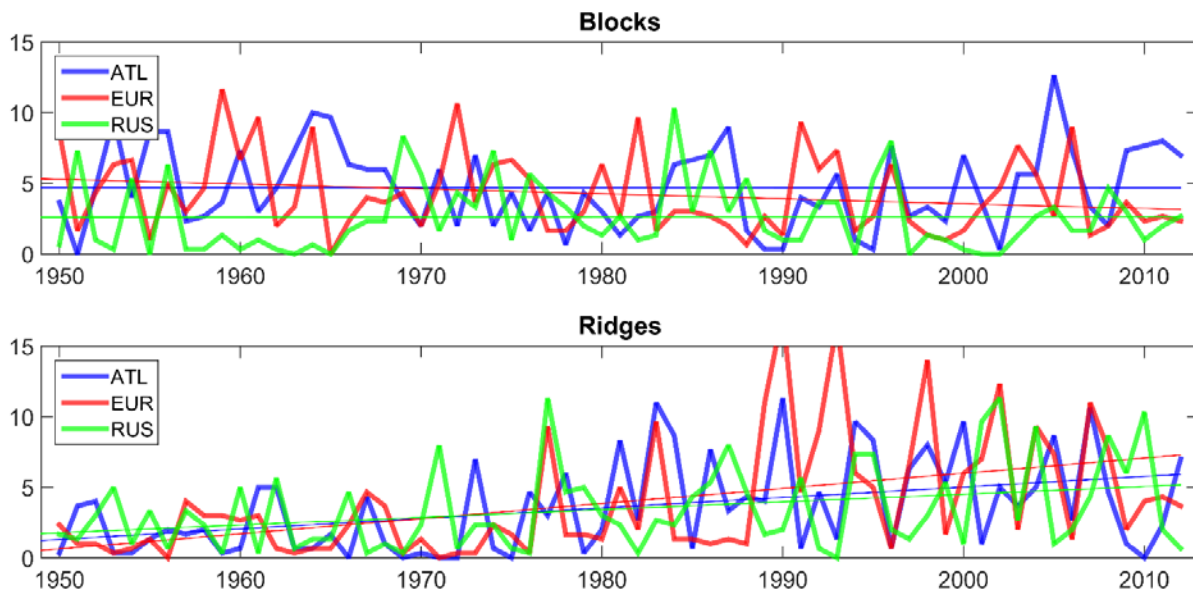


**Fig. 5.4** Winter time series of blocking (upper panel) and ridge (lower panel) frequencies of occurrence in the ATL (30W-0W), EUR (0E-30E) and RUS (30E-60E) sectors, for the period 1950-2012.

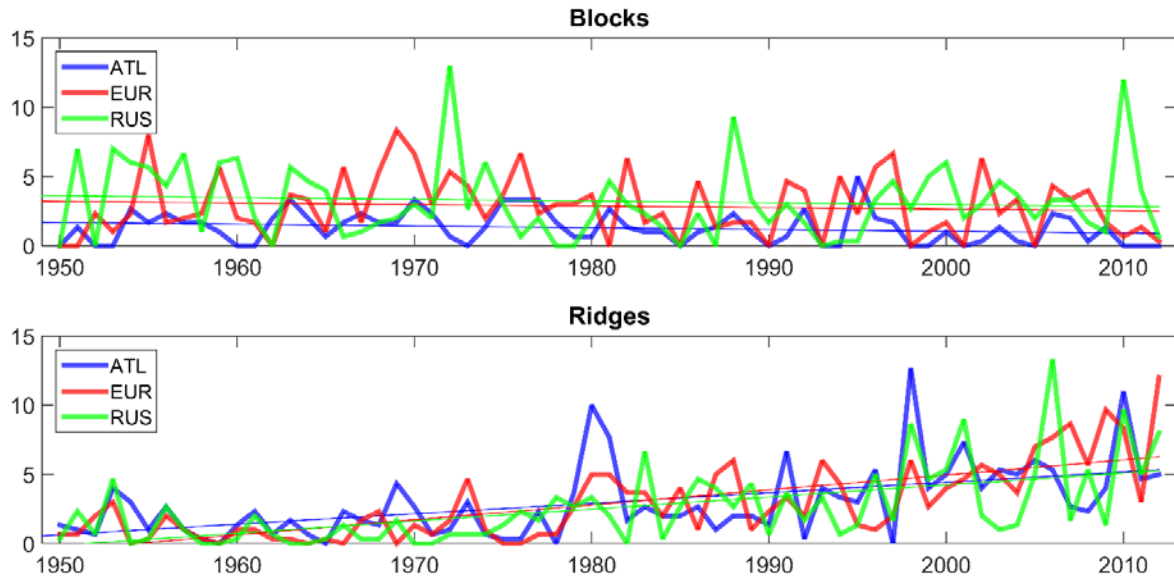


**Fig. 5.5** Same as Fig. 5.4, but for summer.

The analysis suggests a marked increase in the frequency of sub-tropical ridges in all sectors throughout the reference period (1950-2012). On the contrary, blocking frequencies have remained relatively stable, with only a slight decreasing frequency in winter EUR blocks (Fig. 5.4, upper panel, red line). This indicates more frequent and persistent northwards extensions of the sub-tropical high pressure belt, in good agreement with the aforementioned projections for the 21<sup>st</sup> century. Taking into account the temperature and precipitation impacts of ridges presented in Chapters 2 and 3, these results suggest a potential link between the warming and drying Mediterranean climate in the turning of the 20<sup>th</sup> century and the more frequent occurrence of ridge patterns.

In order to obtain a preliminary insight into future projections of sub-tropical ridges, a set of GCMs from the CMIP5 project (which are frequently referenced in recent literature) was used (BCC, CanESM2, EC-Earth, GFDL, IPSL, MPI, MRI and NorESM1), considering the RCP4.5 and RCP8.5 emission scenarios. As stated in Chapter 1, the analysis of future projections using anomaly-based detection methods is hampered by the definition of a baseline period and a threshold criterion, due to the presence of a constantly changing climatology (e.g., Barriopedro et al. 2010b). In order to quantify this potential effect, the 30-year running evolution of the Z500 median and the 80<sup>th</sup> percentile was computed in all boxes considered for the ridge detection (see Section 2.3). Figs. 5.6 and 5.7 show these changes between 1950 and 2100, for winter and summer, respectively.

## 5. Conclusions and open threads for Future work

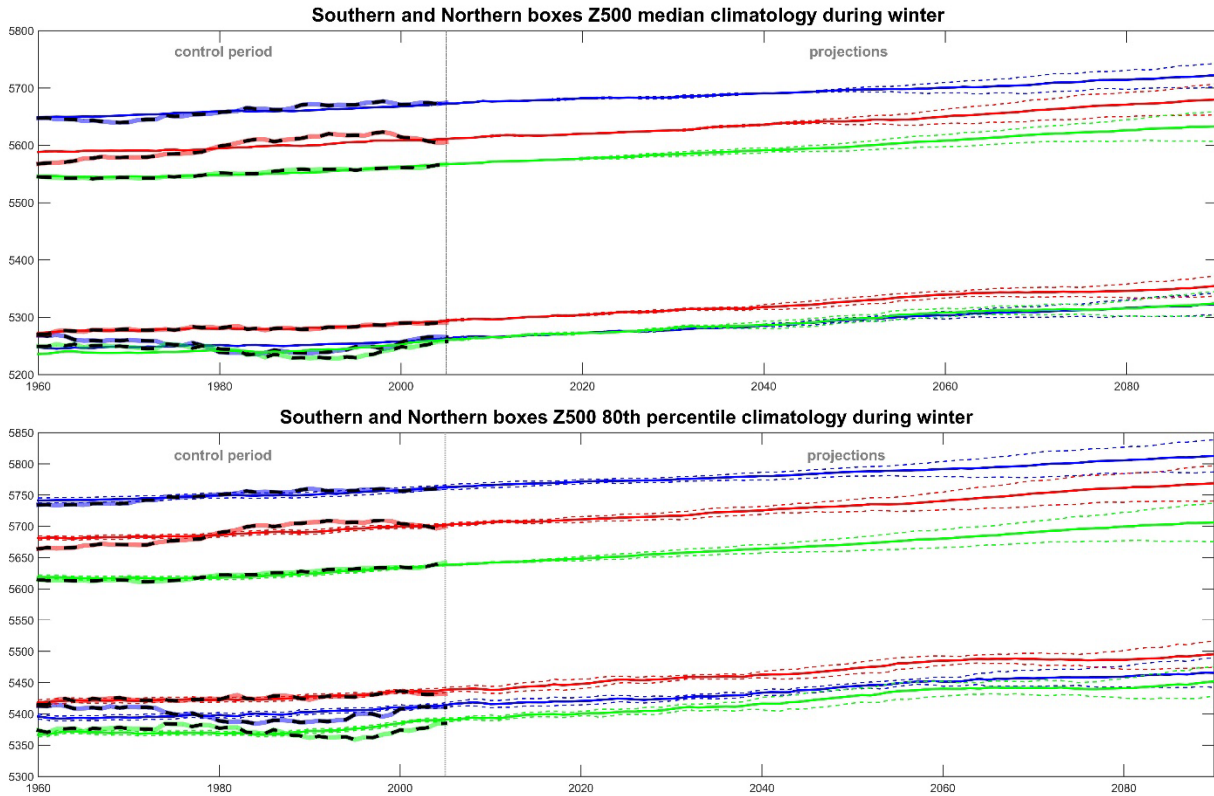


**Fig. 5.6** Z500 median (upper panel) and 80<sup>th</sup> percentile (lower panel) in the southern (upper lines) and northern (lower lines) boxes defined for ridge detection in the ATL (blue), EUR (red) and RUS (green) sectors. Thick lines represent the mean of all models and scenarios, while thin dashed lines represent the RCP8.5 (upper dashed lines) and RCP4.5 (lower dashed lines) separately. The thick dashed black lines left of the vertical line represent the values for the 1950-2012 period of the NCEP/NCAR reanalysis dataset.

The results indicate steady positive trends for both boxes throughout the entire period and for all scenarios. Summer increases (Fig. 5.7) in the median and 80<sup>th</sup> percentiles of Z500 are more marked, especially in the last decades of the 21<sup>st</sup> century and for the southern boxes, where ridges are detected. Winter changes (Fig. 5.6) are smaller, but once again larger for the 80<sup>th</sup> percentile than for the median. The Z500 increases at lower latitudes are in agreement with the northward expansion of the sub-tropical high pressure belt expected in a warming climate (Lu et al., 2007). In spite of this, from a dynamical perspective, the generalized Z500 increases do not necessarily involve a rise in the frequency of ridges or blocks. In fact, as mentioned before, blocking structures detected using a flow-reversal scheme actually show future declining trends. As far as ridges' detection is concerned, and considering that the approach based purely on anomalies does not require a wave-breaking, the projected changes in Z500 may relate to: 1) a generalized northward migration of the sub-tropical high pressure belt and/or; 2) an actual increase in the number of ridge structures.

## 5. Conclusions and open threads for Future work

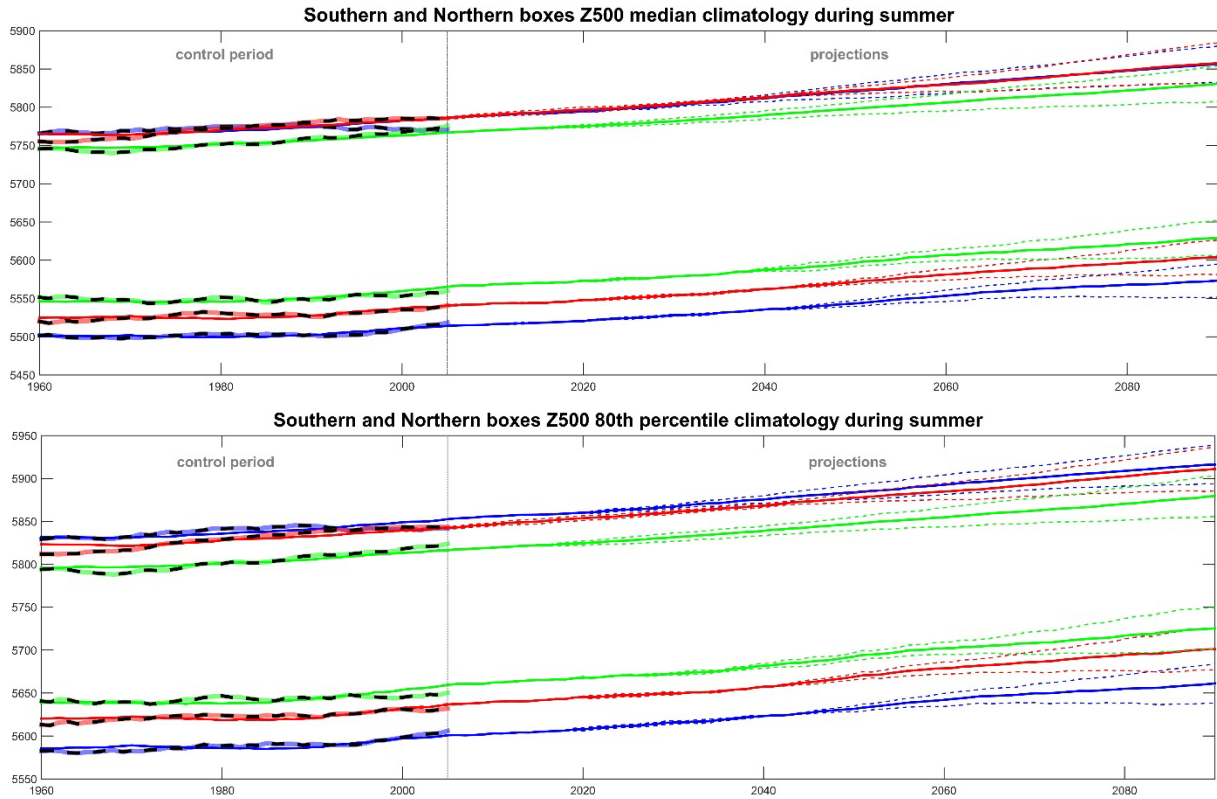


**Fig. 5.7** Same as Fig. 5.6 but for summer.

Taking into account the non-dynamical nature of our approach, this disentanglement cannot be achieved in such a framework. In order to deal with these Z500 trends, one may consider time-varying thresholds in the ridge detection scheme by using moving reference climatological periods (as shown in Figs. 5.6 and 5.7). However, the results of this approach do not reveal consistent trends in the frequencies/locations of ridges (not shown) among the considered models, neither between scenarios or different sectors. Furthermore, a similar approach, but considering a fixed threshold (1950-2012) for ridge detection, resulted in exaggerated increases by the late 21<sup>st</sup> century (above 70%). In this sense, we conclude that at least from an anomaly-based detection scheme, no further considerations about future projections of ridges may be made with confidence. Thus, there is a need for a dynamical approach in the ridge detection, such as latitudinal/longitudinal Z500 gradients (similar to those developed for blocking detection) in order to consider future projections with a higher level of reliability.

### 5.3 Perspectives

The estimation of uncertainties in decadal predictability and long-term future climate projections has been widely debated in the literature, particularly at the regional scale. Natural climate variability imposes inherent limitations to climate predictability and consequently to adaptation guidance (Deser et al., 2012). In this context, Shepherd (2014) stresses the distinct roles played by thermodynamic and dynamical changes in future climate projections. Whereas the confidence in changes controlled by thermodynamics is high, the same is not valid for circulation dynamics, which exert a strong control on regional climates. As a consequence, projections of meteorological fields that are strongly dependent on atmospheric circulation (e.g., precipitation) display large spread, as a consequence of different types of uncertainty (model, scenario, internal variability). Low-frequency internal variability and the sensitivity of the circulation response to model errors and climatic forcings are the main sources of uncertainty. The work by Horton et al. (2015) indicates that even though a significant portion of the observed changes in extreme temperatures results from regional and global-scale thermodynamic changes, changes in the frequency, persistence and duration of regional circulation patterns, including European blocking, acquire high relevance to explain recent changes at regional scales. Also, the rapid warming of the Arctic region (twice as fast as the global average) is happening at a pace greater than that simulated by climate models. The possible link between this Arctic amplification and an increase of extreme mid-latitude weather events (including both cold winters and summer heatwaves), as discussed by Cohen et al. (2014) and Comou et al. (2015), stresses the need to better understand the dynamical responses to changes in the external forcings.

In the context of the uncertainties associated with the large-scale dynamic component, a large effort was devoted in this work to disentangle blocking from ridge phenomena, as this will be increasingly necessary for modelling purposes. As a consequence, the analysis of future projections of both weather regimes, and the associated changes in their impacts, constitute one of the most immediate applications of the future work. Since the method developed for ridge detection is purely based on anomaly fields, it is necessary to acknowledge its limitation to interpret future changes from GCM projections. On the other hand, we are aware that blocking and ridge life cycles are not at all detached. In fact, and as described in Chapter 1, they often represent different stages of the life cycle of planetary wave-breaking occurrence. As such, the prospect of combining blocking and ridge detection schemes into a more unified algorithm capable of describing such life cycles constitutes a major line of future work, directly related with the achievements of this thesis.

In another context, and taking into account the substantial blocking impacts reported in this thesis, the exploration of the blocking responses to external forcings represents a very tangible topic of interest. Various authors have reported links between blocking and remote oceanic patterns (e.g., ENSO; [http://www.cpc.ncep.noaa.gov/products/precip/CWlink/blocking/enso/enso\\_stratification.shtml](http://www.cpc.ncep.noaa.gov/products/precip/CWlink/blocking/enso/enso_stratification.shtml)), decadal modes of oceanic variability (e.g., Atlantic Multidecadal Oscillation; Martinez, 2014) and other external forcings (e.g., solar forcing; Barriopedro et al. 2008). Thus, a deeper knowledge of such links could represent a huge step in terms of seasonal-to-decadal predictability in extratropical latitudes.



## References

- Altava/Ortiz V, Llasat M, Ferrari E, Atencia A, Sirangelo B (2010) Monthly rainfall changes in Central and Western Mediterranean basins, at the end of the 20th and beginning of the 21st centuries. *International Journal of Climatology* 31 (13): 1943-1958. doi: 10.1002/joc.2204
- Altenhoff AM, Martius O, Croci-Maspoli M, Schwiers C, Davies HC (2008) Linkage of atmospheric blocks and synoptic-scale Rossby waves: a climatological analysis. *Tellus Series A-Dynamic Meteorology and Oceanography* 60(5): 1053-1063. doi: 10.1111/j.1600-0870.2008.00354.x
- Amraoui M, Pereira MG, DaCamara CC, Calado TJ (2015) Atmospheric conditions associated with extreme fire activity in the Western Mediterranean region. *Science of the Total Environment*, 32–39. doi: 10.1016/j.scitotenv.2015.04.032
- Andrade C, Leite SM, Santos JA (2012) Temperature extremes in Europe: overview of their driving atmospheric patterns. *Nat. Hazards Earth Syst. Sci.* 12: 1671–1691. doi:10.5194/nhess-12-1671-2012
- Anstey JA, Davini P, Gray LJ, Woollings TJ, Butchar N, Cagnazzo C, Christiansen B, Hardiman SC, Osprey SM, Yang S (2013) Multi-model analysis of Northern Hemisphere winter blocking: Model biases and the role of resolution. *Journal of Geophysical Research: Atmospheres* 118: 3956–3971. doi:10.1002/jgrd.50231
- Arai M and Mukougawa H (2002) On the effectiveness of the eddy straining mechanism for the maintenance of blocking flows. *J. Meteorol. Soc. Jpn.* 80: 1089–1102.
- Baldwin MP and Dunkerton TJ (2001) Stratospheric harbingers of anomalous weather regimes. *Science* 294: 581–584. doi:10.1126/science.1063315
- Barnes EA, Slingo J, Woollings T (2012) A methodology for the comparison of blocking climatologies across indices, models and climate scenarios. *Climate Dynamics*, 38: 2467-2481, doi:10.1007/s00382-011-1243-6
- Barriopedro D, García-Herrera R, Lupo AR, Hernández E (2006) A climatology of northern hemisphere blocking. *J Clim* 19:1042–1063. doi:10.1175/JCLI3678.1
- Barriopedro D, García-Herrera R, Huth R (2008) Solar modulation of Northern Hemisphere winter blocking. *Journal of Geophysical Research* 113 (D14): D14118. doi: 10.1029/2008JD009789
- Barriopedro D, García-Herrera R, Trigo RM (2010a) Application of blocking diagnosis methods to General Circulation Models. Part I: A novel detection scheme. *Climate Dynamics* 35: 1373-1391. doi: 10.1007/s00382-010-0767-5
- Barriopedro D, García-Herrera R, González-Rouco JF, Trigo RM (2010b) Application of blocking diagnosis methods to General Circulation Models. Part II: model simulations. *Climate Dynamics*, 35 (7-8), 1393-1409. doi: 10.1007/s00382-010-0766-6
- Barriopedro D, Antón M, García JA (2010c) Atmospheric blocking signatures in total ozone and ozone mini-holes. *Journal of Climate* 23 (14): 3967-3983. doi: 10.1175/2010JCLI3508.1.

- Barriopedro D, Fischer EM, Luterbacher J, Trigo RM, García-Herrera R (2011) The Hot Summer of 2010: Redrawing the Temperature Record Map of Europe. *Science* 332: 220. doi: 10.1126/science.1201224
- Barriopedro D and Calvo N (2014) On the Relationship between ENSO, Stratospheric Sudden Warmings, and Blocking. *Journal of Climate* 27(12): 4704-4720. doi: 10.1175/JCLI-D-13-00770.1
- Barry RG and Carleton AM (2001) *Synoptic and dynamic climatology*. Routledge, London and New York. 2001. 620 pp. (hardback). ISBN 0 41503116 8
- Barry RG and Chorley RJ (2010) *Atmosphere, Weather, and Climate*. Taylor and Francis, 516pp.
- Bastos A, Gouveia CM, Trigo RM, Running SW (2014) Analysing the spatio-temporal impacts of the 2003 and 2010 extreme heatwaves on plant productivity in Europe. *Biogeosciences* 11(13): 3421-3435. doi: 10.5194/bg-11-3421-2014
- Belo-Pereira M, Dutra E, Viterbo P (2011) Evaluation of global precipitation data sets over the Iberian Peninsula. *J. Geophys. Res.* 116: D20101. doi:10.1029/2010JD015481
- Beirlant J, Goegebeur Y, Teugels J, Segers, J (2004) *Statistics of Extremes: Theory and Applications*. Wiley, USA.
- Beniston M (2012) Is snow in the Alps receding or disappearing? *WIREs Clim Change*. doi: 10.1002/wcc.179
- Berckmans J, Woollings T, Demory ME, Vidale PL, Roberts M (2013) Atmospheric blocking in a high resolution climate model: influences of mean state, orography and eddy forcing. *Atmospheric Science Letters* 14 (1): 34-40. doi: 10.1002/asl2.412
- Burt S (2013) The bitter winter of 1962/63. Imperial College, London, 16 March 2013.
- Bieli M, Pfahl S, Wernli H (2015) A Lagrangian investigation of hot and cold temperature extremes in Europe. *Q.J.R Meteorol. Soc.* 141: 98-108. doi 10.1002/qj.2339
- Bladé I, Liebmann B, Fortuny D, Oldenborgh GJ (2012) Observed and simulated impacts of the summer NAO in Europe: Implications for projected drying in the Mediterranean region. *Clim. Dyn.* 39: 709–727. doi:10.1007/s00382-011-1195-x.
- Black RX (1997) Deducing anomalous wave source regions during the life cycles of persistent flow anomalies. *J. Atmos. Sci.* 54: 895–907. doi: 10.1175/1520-0469(1997)054<0895:DAWSRD>2.0.CO;2
- Black E, Blackburn M, Harrison G, Hoskins B, Methven J (2004) Factors contributing to the summer 2003 European heatwave. *Weather* 59 (8): 217-223. doi: 10.1256/wea.74.04
- Boberg F, Berg P, Thejll P, Gutowski WJ, Christensen JH (2009) Improved confidence in climate change projections of precipitation evaluated using daily statistics from the PRUDENCE ensemble. *Climate Dynamics* 32(7–8): 1097–1106. doi:10.1007/s00382-008-0446-y
- Boberg F, Berg P, Thejll P, Gutowski WJ, Christensen JH (2010) Improved confidence in climate change projections of precipitation further evaluated using daily statistics from ENSEMBLES models. *Climate Dynamics* 35: 1509–1520. doi: 10.1007/s00382-009-0683-8

- Brönnimann S (2007) Impact of El Niño–Southern Oscillation on European climate. *Reviews of Geophysics* 45 (3): RG3003. doi: 10.1029/2006RG000199
- Brunner L, Hegerl GC, Steiner AK (2017) Connecting Atmospheric Blocking to European Temperature Extremes in Spring. *Journal of Climate* 30: 585-593. doi: <http://dx.doi.org/10.1175/JCLI-D-16-0518.1>
- Buehler T, Raible CC, Stocker TF (2011) The relationship of winter season North Atlantic blocking frequencies to extreme cold or dry spells in the ERA-40. *Tellus Ser. A* 63: 212–222. doi:10.1111/j.1600-0870.2010.00492.x
- Bulić IH, Branković Č, Kucharski F (2012) Winter ENSO teleconnections in a warmer climate. *Clim. Dyn.* 38 (7–8): 1593–1613. doi: 10.1007/s00382-010-0987-8
- Burgueno A, Martinez MD, Serra C, Lana X (2010) Statistical distributions of daily rainfall regime in Europe for the period 1951-2000. *Theoretical and Applied Climatology* 102: 213-226. doi: 10.1007/s00704-010-0251-5
- Camia A, Durrant T, San-Miguel-Ayanz J (2014) The European Fire Database – Technical specifications and data submission. European Commission – Executive Report.
- Casanueva A, Rodríguez-Puebla C, Frías MD, González-Reviriego N (2014) Variability of extreme precipitation over Europe and its relationships with teleconnection patterns. *Hidrology and Earth System Sciences* 18 (2): 709-725. doi: 10.5194/hess-18-709-2014
- Castro-Díez Y, Pozo-Vázquez D, Rodrigo FS, Esteban-Parra MJ (2002) NAO and winter temperature variability in southern Europe. *Geophysical Research Letters* 29 (8): 1160. doi: 10.1029/2001GL014042
- Cattiaux J, Vautard R, Cassou C, Yiou P, Masson-Delmotte V, Codron F (2010) Winter 2010 in Europe: A cold extreme in a warming climate. *Geophysical Research Letters* 37: L20704. doi:10.1029/2010GL044613
- Cattiaux J, Quesada B, Arakelian A, Codron F, Vautard R, Yiou P (2012) North-Atlantic dynamics and European temperature extremes in the IPSL model: sensitivity to atmospheric resolution. *Climate Dynamics* 40 (9-10): 2293-2310. doi: 10.1007/s00382-012-1529-3
- Chan SC and Nigam S (2009) Residual Diagnosis of Diabatic Heating from ERA-40 and NCEP Reanalyses: Intercomparisons with TRMM. *Journal of Climate* 22(2): 414-428. doi: 10.1175/2008JCLI2417.1
- Christensen, J.H., K. Krishna Kumar, E. Aldrian, S.-I. An, I.F.A. Cavalcanti, M. de Castro, W. Dong, P. Goswami, A. Hall, J.K. Kanyanga, A. Kitoh, J. Kossin, N.-C. Lau, J. Renwick, D.B. Stephenson, S.-P. Xie and T. Zhou, 2013: Climate Phenomena and their Relevance for Future Regional Climate Change. In: *Climate Change 2013: The Physical Science Basis. Contribution of Working Group I to the Fifth Assessment Report of the Intergovernmental Panel on Climate Change* [Stocker, T.F., D. Qin, G.-K. Plattner, M. Tignor, S.K. Allen, J. Boschung, A. Nauels, Y. Xia, V. Bex and P.M. Midgley (eds.)]. Cambridge University Press, Cambridge, United Kingdom and New York, NY, USA.
- Cohen J and Jones J (2011) A new index for more accurate winter predictions. *Geophysical Research Letters* 38: L21701. doi: 10.1029/2011GL049626

## References

---

- Cohen J, Screen JA, Furtado JS, Barlow M, Whittleston D, Coumou D, Francis J, Dethloff K, Entekhabi D, Overland J, Jones J (2014) Recent Arctic amplification and extreme mid-latitude weather. *Nature Geoscience* 7: 627-637. doi: 10.1038/ngeo2234
- Comou D, Lehmann J, Beckmann J (2015) The weakening summer circulation in the Northern Hemisphere mid-latitudes. *Science* 348 (6232): 324-327. doi: 10.1126/science.1261768
- Cook J, Nuccitelli D, Green SA, Richardson M, Winkler B, Painting R, Way R, Jacobs P, Skuce A (2013) Quantifying the consensus on anthropogenic global warming in the scientific literature. *Environmental Research Letters* 8 (2): 024024. doi: 10.1088/1748-9326/8/2/024024
- Cortesi N, Trigo RM, Gonzalez-Hidalgo JC, Ramos AM (2013) Modelling monthly precipitation with circulation weather types for a dense network of stations over Iberia. *Hidrology and Earth System Sciences* 17 (2): 665-678. doi: 10.5194/hess-17-665-2013
- Cortesi N, Gonzalez-Hidalgo JC, Trigo RM, Ramos AM (2014) Weather types and spatial variability of precipitation in the Iberian Peninsula. *Int. J. Climatol.* 34: 2661–2677. doi: 10.1002/joc.3866
- Croci-Maspoli M, Schwierz C, Davies HC (2007) Atmospheric blocking: space-time links to the NAO and PNA. *Clim Dyn* 29:713–725. doi:10.1007/s00382-007-0259-4
- Cuxart J and Jimenez MA (2010) Long-lasting Fog in the Ebro valley: a high-resolution mesoscale simulation. 5th International Conference on Fog, Fog Collection and Dew. Münster, Germany, 25–30 July 2010
- DaCamara CC, Kung EC, Baker WE, Lee BC, Corte-Real JAM (1991) Long-term analysis of planetary wave activities and blocking circulation in the Northern Hemisphere winter. *Beitr Phys Atmos* 64: 285–298.
- D’Andrea F, Tibaldi S, Blackburn M, Boer G, Deque M, Dix MR, Dugas B, Ferranit L, Iwasaki T, Kitoh A, Pope V, Randall D, Roeckner R, Straus D, Stern W, Van den Dool H, Williamson D (1998) Northern Hemisphere atmospheric blocking simulated by 15 atmospheric general circulation models in the period 1979-1988. *Clim Dyn.* 14 (6): 385-407. doi: 10.1007/s003820050230
- Davini P, Cagnazzo C, Gualdi S, Navarra A (2012a) Bidimensional Diagnostics, Variability, and Trends of Northern Hemisphere Blocking. *Journal of Climate* 25 (19): 6496-6509. doi: 10.1175/JCLI-D-12-00032.1
- Davini P, Cagnazzo C, Neale R, Tribbia J (2012b). Coupling between Greenland blocking and the North Atlantic Oscillation pattern. *Geophys. Res. Lett.* 39 (14): L14701. doi:10.1029/2012GL052315
- Davini P, Cagnazzo C, Anstey JA (2014) A blocking view of the stratosphere-troposphere coupling. *J. Geophys. Res. Atmos.* 119 (19): 11100-11115. doi: 10.1002/2014JD021703
- Davini P and D’Andrea F (2016) Northern Hemisphere Atmospheric Blocking Representation in Global Climate Models: Twenty Years of Improvements? *Journal of Climate* 29 (24): 8823-8840. doi: 10.1175/JCLI-D-16-0242.1

- Deser C, Phillips A, Bourdette V, Teng Haiyan (2012) Uncertainty in climate change projections: the role of internal variability. *Climate Dynamics* 38 (3): 527-546. doi: 10.1007/s00382-010-0977-x
- Dole RM and Gordon ND (1983) Persistent anomalies of the extratropical northern hemisphere wintertime circulation: geographical distribution and regional persistence characteristics. *Mon Weather Rev* 111:1567–1586. doi: 10.1175/1520-0493(1983)111<1567:PAOTEN>2.0.CO;2
- Dole RM (1986) The life cycles of persistent anomalies and blocking over the North Pacific. *Adv. Geophys* 29: 31-69.
- Dole RM (1989) Life cycles of persistent anomalies. Part I: Evolution of 500-mb height fields. *Monthly Weather Review* 117: 177-211.
- Dole RM, Hoerling M, Perlwitz J, Eischeid J, Pegion P, Zhang T, Quan X, Xu Taiyi, Murray D (2011) Was there a basis for anticipating the 2010 Russian heat wave? *Geophysical Research Letters* 38 (6): L06702 . doi: 10.1029/2010GL046582
- Dong B and Dai Aiguo (2015) The influence of the Interdecadal Pacific Oscillation on Temperature and Precipitation over the Globe. *Clim Dyn* 45 (9-10): 2667-2681. doi: 10.1007/s00382-015-2500-x
- Draxler RR and Rolph GD (2003) HYSPLIT (HYbrid Single-Particle Lagrangian Integrated Trajectory) Model access via NOAA ARL READY Website (<http://www.arl.noaa.gov/HYSPLIT.php>). NOAA Air Resources Laboratory, Silver Spring, MD.
- Dunn-Sigouin E and Son S (2013) Evaluation of Northern Hemisphere Blocking Climatology in the Global Environment Multiscale Model. *Monthly Weather Review* 141 (2): 707-727. doi: 10.1175/MWR-D-12-00134.1
- Égger J (1978) Dynamics of blocking highs. *J. Atmospheric Sci.* 35: 1788-1801.
- Fischer EM, Seneviratne SI, Vidale PL, Lüthi D, Schär D (2007) Soil Moisture-Atmosphere Interactions during the 2003 European Summer Heat Wave. *Journal of Climate* 20 (20): 5081-5099. doi: 10.1175/JCLI4288.1
- Fischer EM and Schär C (2009) Future changes in daily summer temperature variability: driving processes and role for temperature extremes. *Clim. Dyn.* 33: 917–935. doi: 10.1007/s00382-008-0473-8.
- Fischer EM and Knutti R (2015) Anthropogenic contribution to global occurrence of heavy-precipitation and high-temperature extremes. *Nature Climate Change* 5(6): 560-564. doi: 10.1038/nclimate2617
- Flato G, Marotzke J, Abiodun B, Braconnot P, Chou SC, Collins W, Cox P, Driouech F, Emori S, V Eyring, Forest C, Gleckler P, Guilyardi E, Jakob C, Kattsov V, Reason C, Rummukainen M (2013) Evaluation of Climate Models. In: *Climate Change 2013: The Physical Science Basis. Contribution of Working Group I to the Fifth Assessment Report of the Intergovernmental Panel on Climate Change* [Stocker, T.F., D. Qin, G.-K. Plattner, M. Tignor,

- S.K. Allen, J. Boschung, A. Nauels, Y. Xia, V. Bex and P.M. Midgley (eds.)). Cambridge University Press, Cambridge, United Kingdom and New York, NY, USA.
- Folland CK, Knight J, Linderholm HW, Fereday D, Ineson S, Hurrell JW (2009) The Summer North Atlantic Oscillation: Past, Present, and Future. *Journal of Climate* 22 (5): 1082-1103. doi: 10.1175/2008JCLI2459.1
- Fragoso M, Trigo RM, Zêzere JL, Valente MA (2010) The exceptional rainfall episode registered in Lisbon on 18 February 2008. *Weather* 65(2): 31-35. doi:10.1002/wea.513
- Gabriel A and Peters D (2008) A diagnostic study of different types of Rossby wave breaking events in the Northern Extratropics. *J. Meteorol. Soc. Japan* 86: 613–631. doi: 10.2151/jmsj.86.613
- Gámiz-Fortis SR, Esteban-Parra MJ, Pozo-Vázquez, Castro-Diéz Y (2011) Variability of the monthly European temperature and its association with the Atlantic sea-surface temperature from interannual to multidecadal scales. *International Journal of Climatology* 31: 2115-2140. doi: 10.1002/joc.2219
- García-Herrera R, Barriopedro D, Hernández E, Paredes D, Correoso JF, Prieto L (2005a) The 2001 Mesoscale Convective Systems over Iberia and the Balearic Islands. *Meteorol Atmos Phys* 90: 225–243. doi:10.1007/s00703-005-0114-2
- García-Herrera R, Díaz J, Trigo RM, Hernández E (2005b) Extreme summer temperatures in Iberia: health impacts and associated synoptic conditions. *Annales Geophysicae* 23: 239-251.
- García-Herrera R and Barriopedro D (2006) Northern Hemisphere snow cover and atmospheric blocking variability. *Journal of Geophysical Research-Atmospheres* 111(D21): D21104. doi: 10.1029/2005JD006975
- García-Herrera R, Paredes D, Trigo RM, Trigo IF, Hernández H, Barriopedro D, Mendes MT (2007) The outstanding 2004–2005 drought in the Iberian Peninsula: associated atmospheric circulation. *J. Hydrometeorol.* 8: 483–498, 2007. doi: <http://dx.doi.org/10.1175/JHM578.1>
- García-Herrera R, Dias J, Trigo RM, Luterbacher J, Fischer EM (2010). A Review of the European Summer Heat Wave of 2003. *Critical Reviews in Environmental Science and Technology* 40(4): 267-306. doi: 10.1080/10643380802238137
- García-Herrera and Barriopedro (2017, in review) Climate of the Mediterranean and North Africa. Oxford Research Encyclopedia of Climate Science. doi: 10.1093/acrefore/9780190228620.013.509
- Gimeno L, Nieto R, Trigo RM, Vicente S, Lopez-Moreno JI (2010) Where does the Iberian Peninsula moisture come from? An answer based on a Lagrangian approach. *Journal of Hydrometeorology*, doi: 10.1175/2009JHM1182.1 (Published)
- Gimeno L, Nieto R, Drumond A, Castillo R, Trigo RM (2013) Influence of the intensification of the major oceanic moisture sources on continental precipitation. *Geophysical Research Letters* 40: 1443-1450. doi:10.1002/grl.50338
- Gimeno L, Stohl A, Trigo RM, Domínguez F, Yoshimura K, Yu L, Drumond A, Durán-Quesada AM, Nieto R (2012) Oceanic and Terrestrial Sources of Continental Precipitation. *Reviews of Geophysics* 50: RG4003. doi:10.1029/2012RG000389

- Giorgi F and Lionello P (2008) Climate Change Projections for the Mediterranean Region. *Global and Planetary Change* 63: 90-104. doi: 10.1016/j.gloplacha.2007.09.005
- Gouveia CM, Bastos A, Trigo RM, DaCamara CC (2012) Drought impacts on vegetation in the pre- and post-fire events over Iberian Peninsula. *Natural Hazards Earth System Sciences* 12: 3123-3137. doi:10.5194/nhess-12-3123-2012
- Gouveia CM, Bistinas I, Liberato MLR, Bastos A, Koutsias N, Trigo RM (2016) The outstanding synergy between drought, heatwaves and fuel on the 2007 Southern Greece exceptional fire season. *Agricultural and Forest Meteorology* 218–219: 135–145. doi: 10.1016/j.agrformet.2015.11.023
- Grams CM, Wernli H, Bottcher M, Campa J, Corsmeier U, Jones SC, Keller JH, Lenz CJ, Wiegand L (2011) The key role of diabatic processes in modifying the upper-tropospheric wave guide: a North Atlantic case-study. *Quarterly Journal of the Royal Meteorological Society* 137 (661): 2174-2193 (B). doi: 10.1002/qj.891
- Green JSA (1977) The weather during July 1976: Some dynamical considerations of the drought. *Weather* 32: 120-128.
- Green HK, Andrews N, Armstrong B, Bickler G, Pebody R (2016) Mortality during the 2013 heatwave in England - How did it compare to previous heatwaves? A retrospective observational study. *Environmental Research* 147: 343-349. doi: 10.1016/j.envres.2016.02.028
- Gudmundsson L, Rego FC, Rocha M, Seneviratne SI (2014) Predicting above normal wildfire activity in southern Europe as a function of meteorological drought. *Enviro. Res. Lett.* 9 (2004): 084008. doi: 10.1088/1748-9326/9/8/084008
- Haines K and Holland AJ (1998) Vacillation cycles and blocking in a channel. *Quarterly Journal of the Royal Meteorological Society* 124: 873-895. doi: 10.1002/qj.49712454711
- Haylock MR, Hofstra N, Klein Tank AMJ, Klok EJ, Jones PD, New M (2008) A European daily high-resolution gridded dataset of surface temperature and precipitation. *J Geophys Res* 113:D20119. doi:10.1029/2008JD10201
- Herrera S, Gutierrez JM, Ancell R, Pons MR, Frias MD, Fernandez J (2012) Development and Analysis of a 50 year high-resolution daily gridded precipitation dataset over Spain (Spain02). *International Journal of Climatology* 32: 74-85. doi: 10.1002/joc.2256
- Hisdal H, Roald LA, Beldring S (2006) Past and future changes in flood and drought in the Nordic countries. *Climate Variability and Change - Hydrological Impacts*, IAHS publication 308: 502-507.
- Hoerling M, Eischeid J, Perlwitz J, Quan XW, Zhang T, Pegion P (2012) On the Increased Frequency of Mediterranean Drought. *Journal of Climate* 25 (6): 2146-2161. doi: 10.1175/JCLI-D-11-00296.1
- Hofstra N, Haylock M, New M, Jones PD (2009), Testing E-OBS European high-resolution gridded data set of daily precipitation and surface temperature. *Journal of Geophysical Research* 114: D21101. doi: 10.1029/2009JD011799

- Hofstra N, New M, McSweeney C (2010) The influence of interpolation and station network density on the distributions and trends of climate variables in gridded daily data. *Climate Dynamics* 35 (5): 841-858. doi: 10.1007/s00382-009-0698-1
- Homar V, Romero R, Ramis C, Alonso S (2002) Numerical study of the October 2000 torrential precipitation event over eastern Spain: analysis of the synoptic-scale stationarity. *Annales Geophysicae* 20 (12): 2047-2066.
- Horton DE, Johnson NC, Singh D, Swain DL, Rajaratnam B, Diffenbaugh NS (2015) Contribution of changes in atmospheric circulation patterns to extreme temperature trends. *Nature* 522(7557): 465-469. doi: 10.1038/nature14550
- Hosking JRM, Wallis JR (1997) *Regional Frequency Analysis, An Approach Based on L-Moments*. Cambridge University Press, Cambridge, UK.
- Hoskins B (2013) The potential for skill across the range of the seamless weather-climate prediction problem: a stimulus for our science. *Quarterly Journal of the Royal Meteorological Society* 139 (672): 573-584. doi: 10.1002/qj.1991
- Hoy A, Schucknecht A, Sepp M, Matschullat J (2014) Large-scale synoptic types and their impact on European precipitation. *Theoretical and Applied Climatology* 116 (1): 19-35. doi: 10.1007/s00704-013-0897-x
- Hughes M, Hall A, Fovell RG (2009) Blocking in Areas of Complex Topography, and Its Influence on Rainfall Distribution. *Journal of the Atmospheric Sciences* 66 (2): 508-518. doi: 10.1175/2008JAS2689.1
- Hurrell JW and Deser C (2009) North Atlantic climate variability: The role of the North Atlantic Oscillation. *J. Mar. Syst.* 78: 28–41. doi: 10.1016/j.jmarsys.2009.11.002
- Jacobbeit J, Wanner H, Luterbacher J, Beck C, Philipp A, Sturm K (2003) Atmospheric circulation variability in the North-Atlantic-European area since the mid-seventeenth century. *Clim. Dynam.* 20: 341–352. doi: 10.1007/s00382-002-0278-0
- Kalnay E, Kanamitsu M, Kistler R, Collins W, Deaven D, Gandin L, Iredell M, Saha S, White G, Woollen J, Zhu Y, Chelliah M, Ebisuzaki W, Higgins W, Janowiak J, Mo KC, Ropelewski C, Wang J, Leetmaa A, Reynolds R, Jenne R, Joseph D (1996) The NCEP/NCAR 40-year reanalysis project. *Bull Am Meteorol Soc* 77(3): 437–471. doi:10.1175/1520-0477(1996)077<0437:TNYRP>2.0.CO;2
- Kelley CP, Mohtadi S, Cane MA, Seager R, Kushnir Y (2015) Climate change in the Fertile Crescent and implications of the recent Syrian drought. *Proceedings of the National Academy of Sciences of the United States of America* 112 (11): 3241-3246. doi: 10.1073/pnas.1421533112
- Kent DM, Kirono DGC, Timbal B, Chiew FHS (2011) Representation of the Australian subtropical ridge in the CMIP3 models. *International Journal of Climatology* 33 (1): 48-57. doi: 10.1002/joc.3406
- Kington J (1999) The severe winter of 1697/98. *Weather* 54 (2): 43-49. doi: 10.1002/j.1477-8696.1999.tb06422.x

- Knox JL and Hay JE (1985) Blocking signatures in the northern hemisphere: Frequency distribution and interpretation. *Journal of Climatology* 5 (1): 1-16.
- Kottek M, Grieser J, Beck C, Rudolf B, Rubel F (2006) World Map of the Köppen-Geiger climate classification updated. *Meteorol. Z.* 15: 259-263. doi: 10.1127/0941-2948/2006/0130
- Kung EC, DaCamara CC, Baker WE, Susskind J, Park CK (1990) Simulations of winter blocking episodes using observed sea surface temperatures. *Quart. J. Roy. Meteor. Soc.* 116: 1053–1070. doi: 10.1002/qj.49711649503
- Kutiel H, Maheras P, Guika S (1996) Circulation and extreme rainfall conditions in the eastern Mediterranean during the last century. *International Journal of Climatology* 16: 73–92. doi: 10.1002/(SICI)1097-0088(199601)16:1<73::AID-JOC997>3.0.CO;2-G
- Kyselý J and Plavcová E (2010) A critical remark on the applicability of E-OBS European gridded temperature dataset for validating control climate simulations. *Journal of Geophysical Research* 115: D23118. doi:10.1029/2010JD014123
- Lavers AD and Villarini G (2013) The nexus between atmospheric rivers and extreme precipitation across Europe. *Geophysical Research Letters* 40 (12): 3259-3264. doi: 10.1002/grl.50636
- Lejenäs, H (1989) The severe winter in Europe 1941–1942: The large-scale circulation, cut-off lows, and blocking. *Bull. Am. Meteorol. Soc.* 70: 271–281.
- Li J, Sun C, Jin F (2013) NAO implicated as a predictor of Northern Hemisphere mean temperature multidecadal variability. *Geophysical Research Letters* 40 (20): 5497-5502. doi: 10.1002/2013GL057877
- Liberato MLR, Ramos AM, Trigo RM, Trigo IF, Durán-Quesada AM, Nieto R, Gimeno L (2012) Moisture Sources and Large-Scale Dynamics Associated With a Flash Flood Event, in *Lagrangian Modeling of the Atmosphere* (eds J. Lin, D. Brunner, C. Gerbig, A. Stohl, A. Luhar and P. Webley). *Geophys. Monogr. Ser.* 200: 111-126, American Geophysical Union, Washington, DC. doi: 10.1029/2012GM001244
- Liberato MLR, Pinto JG, Trigo RM, Ludwig P, Ordóñez P, Yuen D, Trigo IF (2013) Explosive development of winter storm Xynthia over the Subtropical North Atlantic Ocean. *Natural Hazards and Earth System Sciences* 13: 2239-2251. doi:10.5194/nhess-13-2239-2013
- Liu C, Tian B, Li K, Manney GL, Livesey NJ, Yung YL, Waliser DE (2014) Northern Hemisphere mid-winter vortex-displacement and vortex-split stratospheric sudden warmings: Influence of the Madden-Julian Oscillation and Quasi-Biennial Oscillation. *Journal of Geophysical Research: Atmospheres* 119(12): 12599-12620. doi: 10.1002/2014JD021876
- Ljungqvist FC, Krusic PJ, Brattstrom G, Sundqvist HS (2012) Northern Hemisphere temperature patterns in the last 12 centuries. *Climate of the past* 8 (1): 227-249. doi: 10.5194/cp-8-227-2012
- Lloyd-Hughes B and Saunders MA (2002) A drought climatology for Europe. *International Journal of Climatology* 22 (13): 1571-1592. doi: 10.1002/joc.846
- Lolis CJ, Bartzokas A, Katsoulis BD (2004) Relation between sensible and latent heat fluxes in the Mediterranean and precipitation in the Greek area during winter. *International Journal of Climatology* 24 (14): 1803-1816. doi: 10.1002/joc.1112

- Lowe R, Ballester J, Creswick J, Robine JM, Herrmann FR, Rodo X (2015) Evaluating the Performance of a Climate-Driven Mortality Model during Heat Waves and Cold Spells in Europe. *International Journal of Environmental Research and Public Health* 12(2): 1279-1294. doi: 10.3390/ijerph120201279
- Lu J, Vecchi GA, Reichler T (2007) Expansion of the Hadley cell under global warming. *Geophysical Research Letters* 34 (6): 8387-8393. doi: 10.1175/JCLI-D-12-00323.1
- Lupo AR and Smith PJ (1995) Planetary and synoptic-scale interactions during the life cycle of a mid-latitude blocking anticyclone over the North Atlantic. *Tellus* 47A: 575-596.
- Luterbacher J, Rickli R, Xoplaki E, Tinguely C, Beck C, Pfister C, Wanner H (2001) The Late Maunder Minimum (1675–1715) – a key period for studying decadal scale climatic change in Europe. *Clim. Change* 49: 441–462. doi: 10.1023/A:1010667524422
- Luterbacher J, Dietrich D, Xoplaki E, Grosjean M, Wanner H (2004) European seasonal and annual temperature variability, trends and extremes since 1500. *Science* 303: 1499–1503. doi: 10.1126/science.1093877
- Maeda S, Kobayashi C, Takano K, Tsuyuki T (2000) Relationship between singular modes of blocking flow and high-frequency eddies. *J. Meteorol. Soc. Jpn.* 78: 631–645.
- Magnunsson L and Källen E (2013) Factors Influencing Skill Improvements in the ECMWF Forecasting System. *Monthly Weather Review* 141 (9): 3142-3153. doi: 10.1175/MWR-D-12-00318.1
- Mann ME, Zhang ZH, Rutherford S, Bradley RS, Hughes MK, Shindell D, Ammann C, Faluvegi G, Ni FB (2009) Global signatures and dynamical origins of the Little Ice Age and Medieval climatic anomaly. *Science* 326: 1256–1260. doi: 10.1126/science.1177303
- Mann ME, Steinman BA, Miller SK (2014) On Forced Temperature Changes, Internal Variability and the AMO. *Geophysical Research Letters* 41 (9): 3211-3219. doi: 10.1002/2014GL059233
- Marcos R, Turco M, Bedia J, Llasat MC, Provenzale A (2015) Seasonal predictability of summer fires in a Mediterranean environment. *International Journal of Wildland Fire* 24(8): 1076-1084. doi: 10.1071/WF15079
- Mariotti A and Dell'Aquila A (2012) Decadal climate variability in the Mediterranean region: Roles of large-scale forcings and regional processes. *Clim. Dyn.* 38: 1129–1145. doi:10.1007/s00382-011-1056-7
- Martinez (2014) North Atlantic Amospheric Blocking and Atlantic Multidecadal Oscillation in CESM1 Large Ensemble Simulations. SOARS Manuscripts Summer 2014.
- Martius O, Schwierz C, Davies HC (2007) Breaking Waves at the Tropopause in the Wintertime Northern Hemisphere: Climatological Analyses of the Orientation and the Theoretical LC1/2 Classification. *Journal of the Atmospheric Sciences* 64 (7): 2576-2592 doi: 10.1175/JAS3977.1
- Martius O, Polvani M, Davies HC (2009) Blocking precursors to stratospheric sudden warming events. *Geophysical Research Letters* 36: L14806. doi: 10.1029/2009GL038776

- Masato G, Hoskins BJ, Woollings TJ (2011) Wave-breaking characteristics of mid-latitude blocking. *Q J R Meteorol Soc* 138:1285–1296. doi:10.1002/qj.990
- Masato G, Hoskins BJ, Woollings T (2013) Winter and Summer Northern Hemisphere Blocking in CMIP5 Models. *Journal of Climate* 26 (18): 7044-7059. doi: 10.1175/JCLI-D-12-00466.1
- Matsueda M, Mizuta R, Kusunoki S (2009) Future change in wintertime atmospheric blocking simulated using a 20-km-mesh atmospheric global circulation model. *J. Geophys. Res.*, 114: D12114, doi: 10.1029/2009JD011919
- Michel C, Riviere G, Terray L, Joly B (2012) The dynamical link between surface cyclones, upper-tropospheric Rossby wave breaking and the life cycle of the Scandinavian blocking. *Geophysical Research Letters* (39): L10806. doi: 10.1029/2012GL051682
- Miralles DG, Teuling AJ, van Heerwaarden CC, de Arellano JVG (2014) Mega-heatwave temperatures due to combined soil desiccation and atmospheric heat accumulation. *Nature Geoscience* 7 (5): 345-349. doi: 10.1038/NGEO2141
- Mokhov II, Timazhev AV, Lupo AR (2014) Changes in atmospheric blocking characteristics within Euro-Atlantic region and Northern Hemisphere as a whole in the 21st century from model simulations using RCP anthropogenic scenarios. *Global and Planetary Change* 122: 265-270. doi: 10.1016/j.gloplacha.2014.09.004
- Monteiro A, Carvalho V, Gois J, Sousa C (2013) Use of "Cold Spell" indices to quantify excess chronic obstructive pulmonary disease (COPD) morbidity during winter (November to March 2000-2007): case study in Porto. *International Journal of Biometeorology* 57(6): 857-870. doi: 10.1007/s00484-012-0613-z
- Muthers S, Matzarakis A, Koch E (2010) Summer climate and mortality in Vienna - a human-biometeorological approach of heat-related mortality during the heat waves in 2003. *Wiener Klinische Wochenschrift* 122(17-18): 525-531
- Nakamura H, Nakamura M, Anderson JL (1997) The role of high- and low-frequency dynamics in blocking formation. *Mon. Wea. Rev* 125: 2074–2093. doi: 10.1175/1520-0493(1997)125<2074:TROHAL>2.0.CO;2
- Neu U, Akperov MG, Bellenbaum N, Benestad R, Blender R, Caballero R, Cocozza A, Dacre HF, Feng Y, Fraedrich K, Grieger J, Gulev S, Hanley J, Hewson T, Inatsu M, Keay K, Kew SF, Kindem I, Leckebusch GC, Liberato MLR, Lionello P, Mokhov II, Pinto JG, Raible CC, Reale M, Rudeva I, Schuster M, Simmonds I, Sinclair M, Sprenger M, Tilinina ND, Trigo IF, Ulbrich S, Ulbrich U, Wang XL, Wernli H (2013) IMILAST - a community effort to intercompare extratropical cyclone detection and tracking algorithms. *Bulletin of the American Meteorological Society* 94 (4): 529–547. doi 10.1175/BAMS-D-11-00154.1
- Nieto R, Gimeno L, de la Torre L, Ribera P, Gallego D, García-Herrera R, García JA, Núñez M, Redaño A, Lorente J (2005) Climatological features of Cut-off low systems in the Northern Hemisphere. *Journal of Climate*, 18: 3085-3113. doi: <http://dx.doi.org/10.1175/JCLI3386.1>
- Nieto R, Gimeno L, de la Torre L, Ribera P, Barriopedro D, García-Herrera R (2007) Interannual variability of cut-off low systems over the European sector: the role of blocking and the northern hemisphere circulation modes. *Meteorology and Atmospheric Physics* 96: 85-101. doi: <http://dx.doi.org/10.1007/s00703-006-0222-7>

- Nishii K, Nakamura H, Orsolini YJ (2011) Geographical dependence observed in blocking high influence on the stratospheric variability through enhancement and suppression of upward planetary-wave propagation. *J. Clim.* 24 (24): 6408–6423. doi: 10.1175/JCLI-D-10-05021.1
- Pauling A, Luterbacher J, Casty C, Wanner H (2006) Five hundred years of gridded high-resolution precipitations over Europe and the connection to large-scale circulation. *Clim. Dynam.* 26: 387–405. doi: 10.1007/s00382-005-0090-8
- Pausas JG, Bradstock RS (2006) Fire persistence traits of plants along a productivity and disturbance gradient in mediterranean shrublands of south-east Australia. *Global Ecology and Biogeography* 16 (3): 330–340. doi: 10.1111/j.1466-8238.2006.00283.x
- Pausas JG and Paula S (2012) Fuel shapes the fire-climate relationship: evidence from Mediterranean ecosystems. *Global Ecol. & Biogeogr.* 21: 1074–1082. doi: 10.1111/j.1466-8238.2012.00769.x
- Pellizzaro G, Cesaraccio C, Duce P, Ventura A, Zara P (2007) Relationships between seasonal patterns of live fuel moisture and meteorological drought indices for Mediterranean shrubland species. *International Journal of Wildland Fire* 16, 232–241. doi: 10.1071/WF06081
- Peña-Ortiz C, Barriopedro D, García-Herrera R (2015) Multidecadal Variability of the Summer Length in Europe. *Journal of Climate* 28 (13): 5375–5388. doi: 10.1175/JCLI-D-14-00429.1
- Peñarrocha D, Estrela M, Millán M (2002) Classification of daily rainfall patterns in a Mediterranean area with extreme intensity levels: the Valencia region. *International Journal of Climatology* 22: 677–695. doi: 10.1002/joc.747
- Pereira MG, Trigo RM, DaCamara CC, Pereira JMC, Solange ML (2005) Synoptic patterns associated with large summer forest fires in Portugal. *Agric. For. Meteorol.* 129: 11–25. doi: 10.1016/j.agrformet.2004.12.007
- Pereira M, Calado T, DaCamara C, Calheiros T (2013) Effects of regional climate change on rural fires in Portugal. *Clim Res* 57:187–200. doi: 10.3354/cr01176
- Perkins SE, Pitman AJ, Holbrook NJ, McAneney J (2007) Evaluation of the AR4 climate models' simulated daily maximum temperature, minimum temperature, and precipitation over Australia using probability density functions. *Journal of Climate* 20: 4356–4376. doi: 10.1175/JCLI4253.1
- Pfahl S (2014) Characterising the relationship between weather extremes in Europe and synoptic circulation features. *Nat. Hazards Earth Syst. Sci.* 14: 1461–1475. doi: 10.5194/nhess-14-1461-2014
- Pfahl S, Schwierz C, Croci-Maspol M, Grams CM, Wernli H (2015) Importance of latent heat release in ascending air streams for atmospheric blocking. *Nature Geoscience* 8: 610–614. doi:10.1038/ngeo2487
- Pithan F, Shepherd TG, Zappa G, Sandu I (2016) Climate model biases in jet streams, blocking and storm tracks resulting from missing orographic drag. *Geophysical Research Letters* 43 (13): 7231–7240. doi: 10.1002/2016GL069551

- Poumadere M, Mays C, Le Mer S (2005) The 2003 heat wave in France: Dangerous climate change here and now. *Risk Anal.* 25 (6): 1483–1494. doi: 0.1111/j.1539-6925.2005.00694.x
- Pozo-Vázquez D, Gámiz-Fortis SR, Tovar-Pescador, Esteban-Parra MJ, Castro-Díez Y (2005) North Atlantic Winter SLP Anomalies Based on the Autumn ENSO State. *Journal of Climate* 18 (1): 97-103 doi: 10.1175/JCLI-3210.1
- Quesada B, Vautard R, Yiou P, Hirschi M, Seneviratne SI (2012). Asymmetric European summer heat predictability from wet and dry southern winters and springs. *Nat. Clim. Change* 2 (10): 736–741. doi: 10.1038/nclimate1536
- Quiroz RS (1984) The climate of 1983–84 winter. A season of strong blocking and severe cold in North America. *Mon Weather Rev* 112: 1894–1912. doi: DOI: 10.1175/1520-0493(1984)112<1894:TCOTWS>2.0.CO;2
- Ramos AM, Trigo RM, Liberato MLR. (2014) A ranking of high-resolution daily precipitation extreme events for the Iberian Peninsula. *Atmosph. Sci. Lett.* 15: 328–334. doi: 10.1002/asl2.507
- Ramos AM, Trigo RM, Liberato MLR, Tome R (2015) Daily precipitation extreme events in the Iberian Peninsula and its association with Atmospheric Rivers. *Journal of Hydrometeorology* (in press). doi: 10.1175/JHM-D-14-0103.1
- Rebetez M, Mayer H, Dupont O, Schindler D, Gartner K, Kropp J, Menzel A (2006) Heat and drought 2003 in Europe: a climate synthesis. *Ann For Sc* 63: 569–577. doi: 10.1051/forest:2006043
- Rex DF (1950a) Blocking action in the middle troposphere and its effect upon regional climate. Part I: an aerological study of blocking action. *Tellus* 2:196–211
- Rex DF (1950b) Blocking action in the middle troposphere and its effect upon regional climate. Part II: the climatology of blocking action. *Tellus* 2:275–301
- Rex DF (1951) The effect of Atlantic blocking action upon European climate. *Tellus* 3: 1–16.
- Ricard D, Ducrocq V, Auger L (2012) A Climatology of the Mesoscale Environment Associated with Heavily Precipitating Events over a Northwestern Mediterranean Area. *Journal of Applied Meteorology and Climatology* 51 (3): 468-488. doi: 10.1175/JAMC-D-11-017.1
- Robinson DA, Estilow TW, NOAA CDR Program (2012) NOAA Climate Data Record (CDR) of Northern Hemisphere (NH) Snow Cover Extent (SCE), Version 1. NOAA National Climatic Data Center. doi:10.7289/V5N014G9
- Rolph GD (2003) Real-time Environmental Applications and Display sYstem (READY) Website (<http://www.arl.noaa.gov/ready.php>). NOAA Air Resources Laboratory, Silver Spring, MD.
- Ruffault J, Moron V, Trigo RM, Curt T (2016) Objective identification of multiple large fire climatologies: an application to a Mediterranean ecosystem. *Environmental Research Letters* 11: 075006. doi: 10.1088/1748-9326/11/7/075006
- Ruti PM, Dell'Aquila A, Giorgi F (2014) Understanding and attributing the Euro-Russian summer blocking signatures. *Atmos. Sci. Lett.* 15(3): 204-210. doi: 10.1002/asl2.490

- Santos JA, Corte-Real J (2006) Temperature Extremes in Europe and Large-Scale Circulation: HadCM3 future scenarios. *Climate Research* 31: 3–18. doi: 10.3354/cr031003
- Santos JA, Andrade C, Corte-Real J (2008) North Atlantic transient eddies and winter precipitation in Portugal. *Geophysical Research Abstracts* 10: EGU2008-A-01820.
- Santos JA, Pinto JG, Ulbrich U (2009) On the development of strong ridge episodes over the eastern North Atlantic. *Geophysical Research Letters* 36: L17804. doi:10.1029/2009GL039086
- Santos JA, Wiillings T, Pinto JG (2013) Are the Winters 2010 and 2012 Archetypes Exhibiting Extreme Opposite Behavior of the North Atlantic Jet Stream? *Monthly Weather Review* 141(19): 3626–3640. doi: 10.1175/MWR-D-13-00024.1
- Santos JA, Pfahl S, Pinto JG, Wernli H (2015). Mechanisms underlying temperature extremes in Iberia: a Lagrangian perspective. *Tellus Series A-Dynamic Meteorology and Oceanography* 67: 26032. doi: 10.3402/tellusa.v67.26032
- Scaife AA, Woollings T, Knight J, Martin G, Hinton T (2010) Atmospheric Blocking and Mean Biases in Climate Models. *Journal of Climate* 23: 6132–6152. doi: 10.1175/2010JCLI3728.1
- Scherrer SC, Croci-Maspoli M, Schwierz C, Appenzeller C (2006) Two-dimensional indices of atmospheric blocking and their statistical relationship with winter climate patterns in the Euro-Atlantic region, *Int. J. Climatol.* 26, 233–249. doi: 10.1002/joc.1250
- van der Schrier G, van der Besselaar EJM, Klein Tank AMG, Verver G (2013) Monitoring European averaged temperature based on the E-OBS gridded dataset. *Journal of Geophysical Research: Atmospheres* 118(11): 5120–5135.
- Schwierz C, Croci-Maspoli M, Davies HC (2004) Perspicacious indicators of atmospheric blocking. *Geophys. Res. Lett.* 31: L06125. doi:10.1029/2003GL019341
- Seneviratne SI, Corti T, Davin E, Hirschi M, Jaeger EB, Lehner I, Orlowsky B, Teuling AJ (2010) Investigating soil moisture-climate interactions in a changing climate: A review. *Earth Sci. Rev.* 95: 125–161. doi: 10.1016/j.earscirev.2010.02.004
- Seneviratne SI, Donat MG, Mueller B, Alexander LV (2014) No pause in the increase of hot temperature extremes. *Nature Climate Change* 4(5): 161–163. doi: 10.1038/nclimate2145
- Seo K, Lee H, Frierson DMW (2016) Unraveling the Teleconnection Mechanisms that Induce Wintertime Temperature Anomalies over the Northern Hemisphere Continents in Response to the MJO. *J. Atmos. Sci.* 73 (9): 3557–3571. doi: 10.1175/JAS-D-16-0036.1
- Shepherd TG (2014) Atmospheric circulation as a source of uncertainty in climate change projections. *Nature Geoscience* 7: 703–708. doi: 10.1038/ngeo2253
- Shutts GJ (1983) The propagation of eddies in diffluent jetstreams: Eddy vorticity forcing of ‘blocking’ flow fields. *Quarterly Journal of the Royal Meteorological Society* 109: 737–761. doi: 10.1002/qj.49710946204
- Sillmann J and Croci-Maspoli M (2009) Present and future atmospheric blocking and its impact on European mean and extreme climate. *Geophysical Research Letters* 36: L10702. doi: 10.1029/2009GL038259

- Sillmann J, Croci-Maspoli M, Kallache M, Katz RW (2011) Extreme cold winter temperatures in Europe under the influence of north atlantic atmospheric blocking. *J. Clim.* 24(22): 5899–5913. doi:10.1175/2011JCLI4075.1
- Simolo C, Brunetti M, Maugeri M, Nanni T (2012) Extreme summer temperatures in Western Europe. *Adv. Sci. Res.* 8: 5– 9. doi: 10.5194/asr-8-5-2012
- Soares PMM, Cardoso RM, Ferreira JJ, Miranda PMA (2014) Climate change impact on Portuguese precipitation: ENSEMBLES regional climate model results. *Climate Dynamics* 117: D07114. doi: 10.1007/s00382-014-2432-x
- Sousa PM, Trigo RM, Aizpurua P, Nieto R, Gimeno L, Garcia-Herrera R (2011) Trends and extremes of drought indices throughout the 20th century in the Mediterranean. *Natural Hazards and Earth System Sciences* 11: 33-51. doi:10.5194/nhess-11-33-2011
- Sousa PM, Trigo RM, Pereira MG, Bedia J, Gutiérrez JM (2015) Different approaches to model future burnt area in the Iberian Peninsula. *Agricultural and Forest Meteorology* 202: 11-25. doi: 10.1016/j.agrformet.2014.11.018
- Sousa PM, Barriopedro D, Trigo RM, Ramos AM, Nieto R, Gimeno L, Turkman KF, Liberato MLR (2016) Impact of Euro-Atlantic blocking patterns in Iberia precipitation using a novel high resolution dataset. *Climate Dynamics*. doi: 10.1007/s00382-015-2718-7
- Sousa PM, Trigo RM, Barriopedro D, Soares PMM, Ramos AM, Liberato MLR (2017a) Responses of European precipitation distributions and regimes to different blocking locations. *Clim. Dyn.* doi: 10.1007/s00382-016-3132-5
- Sousa PM, Trigo RM, Barriopedro D, Soares PMM, Santos JA (2017b) European temperature responses to blocking and ridge regional patterns. *Cimate Dynamics*. doi: 10.1007/s00382-017-3620-2
- Spinoni J, Antofie T, Barbosa P, Bihari Z, Lakatos M, Szalai S, Szentimrey T, Vogt J (2013) An overview of drought events in the Carpathian Region in 1961–2010. *Adv. Sci. Res.* 10: 21–32. doi: 10.5194/asr-10-21-2013, 2013.
- Spinoni J, Naumann G, Vogt JV, Barbosa P (2015) The biggest drought events in Europe from 1950 to 2012. *Journal of Hydrology: Regional Studies* 3: 509-524. doi: 10.1016/j.ejrh.2015.01.001
- Su J, Zhang R, Wang H (2017) Consecutive record-breaking high temperatures marked the handover from hiatus to accelerated warming. *Scientific Reports* 7: 43735. doi: 10.1038/srep43735
- Tanaka HL (1998) Numerical Simulation of a Life-Cycle of Atmospheric Blocking and the Analysis of Potential Vorticity Using a Simple Barotropic Model. *Journal of the Meteorological Society of Japan* 76 (6): 983-1008.
- Tibaldi S and Molteni F (1990) On the operational predictability of blocking. *Tellus* 42A: 343–365, doi:10.1034/j.1600-0870.1990.t01-2-00003.x
- Tibaldi S, Tosi, Navarra A, Pedulli L (1994) Northern and Southern Hemisphere Seasonal Variability of Blocking Frequency and Predictability. *Monthly Weather Review* 122 (9): 1971-2003. doi: 10.1175/1520-0493(1994)122<1971:NASHSV>2.0.CO;2

- Toreti A, Xoplaki E, Maraun D, Kuglitsch FG, Wanner H, Luterbacher J (2010) Characterisation of extreme winter precipitation in Mediterranean coastal sites and associated anomalous atmospheric circulation patterns. *Nat. Hazards Earth Syst. Sci.* 10: 1037–1050. doi:10.5194/nhess-10-1037-2010
- Treidl RA, Birch EC, Sajecki P (1981) Blocking action in the northern hemisphere: a climatological study. *Atmos Ocean* 19:1–23. doi:10.1080/07055900.1981.9649096
- Trigo RM and DaCamara CC (2000) Circulation weather types and their impact on the precipitation regime in Portugal. *Int. J. Climatol.* 20: 1559 – 1581.
- Trigo RM, Trigo IF, DaCamara CC, Osborn TJ (2004) Winter blocking episodes in the European-Atlantic sector: climate impacts and associated physical mechanisms in the reanalysis. *Clim Dyn.* 23: 17–28. doi:10.1007/s00382-004-0410-4
- Trigo RM, García-Herrera R, Díaz J, Trigo IF, Valente MA (2005) How exceptional was the early August 2003 heatwave in France? *Geophysical Research Letters* 32: L10701, doi:10.1029/2005GL022410
- Trigo IF (2006a) Climatology and interannual variability of storm-tracks in the Euro-Atlantic sector: a comparison between ERA-40 and NCEP/NCAR reanalyses. *Climate Dynamics* 26 (2-3): 127-143. doi: 10.1007/s00382-005-0065-9
- Trigo RM, Pereira JMC, Pereira MG, Mota B, Calado MT, DaCamara CC, Santo FE (2006b) Atmospheric conditions associated with the exceptional fire season of 2003 in Portugal. *International Journal of Climatology* 26 (13): 1741-1757. doi: 10.1002/joc.1333
- Trigo RM, Valente MA, Trigo IF, Miranda M, Ramos AM, Paredes D, García-Herrera R (2008) The Impact of North Atlantic Wind and Cyclone Trends on European Precipitation and Significant Wave Height in the Atlantic. *Annals of the New York Academy of Sciences*, 1146: 212-234. doi: 10.1196/annals.1446.014
- Trigo RM, Ramos AM, Nogueira P, Santos FD, García-Herrera R, Gouveia C, Santo FE (2009) Evaluating the impact of extreme temperature based indices in the 2003 heatwave excessive mortality in Portugal. *Environmental Science & Policy* 12: 844-854. doi: 10.1016/j.envsci.2009.07.007
- Trigo RM, Gouveia C, Barriopedro D (2010) The intense 2007-2009 drought in the Fertile Crescent: Impacts and associated atmospheric circulation. *Agricultural and Forest Meteorology* 150: 1245-1257. doi: 10.1016/j.agrformet.2010.05.006
- Trigo RM, Añel J, Barriopedro D, García-Herrera R, Gimeno L, Nieto R, Castillo R, Allen MR, Massey N (2013a) The record Winter drought of 2011-12 in the Iberian Peninsula. In: Peterson TC, Hoerling MP, Stott PA, Herring S (eds) *Explaining Extreme Events of 2012 from a Climate Perspective*. *Bulletin of the American Meteorological Society* 94 (9): S41-S45.
- Trigo RM, Sousa PM, Pereira MG, Rasilla D, Gouveia CM (2013b) Modelling wildfire activity in Iberia with different Atmospheric Circulation Weather Types. *International Journal of Climatology* 36 (7): 2761-2778. doi: 10.1002/joc.3749

- Tsou C-H and Smith PJ (1990) The role of synoptic/planetary-scale interactions during the development of a blocking anti-cyclone. *Tellus* 42A: 174–193
- Tung KK and Lindzen RS (1979) Theory of stationary long waves. Part I. A simple theory of blocking. *Mon. Wea. Rev.* 107: 714–734. doi: 10.1175/1520-0493(1979)107<0714:ATOSLW>2.0.CO;2
- Turco M, von Hardenberg J, AghaKouchak A, Llasat MC, Provenzale A, Trigo RM (2017) On the key role of droughts in the dynamics of summer fires in Mediterranean Europe. *Nature Scientific Reports* 7:81. doi: 10.1038/s41598-017-00116-9
- Vautard R, Yiou P, D'Andrea F, de Noblet N, Viovy N, Cassou C, Polcher J, Ciais P, Kageyama M, Fan Y (2007) Summertime European heat and drought waves induced by wintertime Mediterranean rainfall deficit. *Geophys. Res. Lett.* 34: L07711. doi:10.1029/2006GL028001, 2007
- Vial J and Osborn TJ (2012) Assessment of atmosphere-ocean general circulation model simulations of winter Northern Hemisphere atmospheric blocking. *Climate Dynamics* 39: 95–112. doi: 10.1007/s00382-011-1177-z
- Vicente-Serrano and López-Moreno (2008) Differences in the non-stationary influence of the North Atlantic Oscillation on European precipitation under different scenarios of greenhouse gas concentrations. *Geophysical Research Letters* 35: L18710. doi: 10.1029/2008GL034832
- Vicente-Serrano SM, Beguería S, López-Moreno JI, El Kenawy AM, Angulo-Martinez M (2009) Daily atmospheric circulation events and extreme precipitation risk in northeast Spain: Role of the North Atlantic Oscillation, the Western Mediterranean Oscillation, and the Mediterranean. *Journal of Geophysical Research* 114: D08106. doi:10.1029/2008JD011492
- Vicente-Serrano SM, Beguería S, López-Moreno JI (2010) A Multiscalar Drought Index Sensitive to Global Warming: The Standardized Precipitation Evapotranspiration Index. *Journal of Climate* 23 (7): 1696–1718. doi: 10.1175/2009JCLI2909.1
- Vicente-Serrano SM, Trigo RM, López-Moreno JI, Liberato MLR, Lorenzo-Lacruz J, Beguería S, Morán-Tejeda E, El Kenawy A (2011) Extreme winter precipitation in the Iberian Peninsula in 2010: anomalies, driving mechanisms and future projections. *Climate Research* 46: 51–65. doi: 10.3354/cr00977
- Vicente-Serrano SM, López-Moreno J, Beguería S, Lorenzo-Lacruz J, Sanchez-Lorenzo A, García-Ruiz J, Azorin-Molina C, Morán-Tejeda E, Revuelto J, Trigo RM, Coelho F, Espejo F (2014) Evidence of increasing drought severity caused by temperature rise in southern Europe. *Environmental Research Letters* 9: L0044001. doi: 10.1088/1748-9326/9/4/044001
- de Vries H, Haarsma RJ, Hazeleger W (2012) Western European cold spells in current and future climate. *Geophysical Research Letters* 39: L04706. doi: 10.1029/2011GL050665
- de Vries H, Woolings TJ, Haarsma RJ, Hazeleger W (2013) Atmospheric blocking and its relation to jet changes in a future climate. *Climate Dynamics* 41 (9–10): 2643–2654. doi:10.1007/s00382-013-1699-7

## References

---

- Wallace JM and Gutzler DS (1981) Teleconnections in the Geopotential Height Field during the Northern Hemisphere Winter. *Monthly Weather Review* 109 (4): 784-812. doi: 10.1175/1520-0493(1981)109<0784:TITGHF>2.0.CO;2
- Walter K and Graf HF (2005) The North Atlantic variability structure, storm tracks, and precipitation depending on the polar vortex strength. *Atmospheric Chemistry and Physics* 5: 239-248.
- Wang L, Chen W, Zhou W, Chan JCL, Barriopedro D, Huang R (2010) Effect of the climate shift around mid 1970's on the relationship between wintertime Ural blocking circulation and East Asian climate. *International Journal of Climatology* 30 (1): 153-158. doi: 10.1002/joc.1876
- Wanner H, Pfister C, Brazdil R, Frich P, Frydendahl K, Jonsson T, Kington J, Lamb HH, Rosenhorn S, Wishman E (1995) Wintertime European circulation patterns during the Late Maunder Minimum cooling period (1675–1704). *Theor. Appl. Climatol.* 51: 167–175. doi: 10.1007/BF00867443
- White WB and Clark NE (1975) On the Development of Blocking Ridge Activity Over the Central North Pacific. *J. Atmos. Sci.* 32: 489-502.
- Wiedenmann JM, Lupo AR, Mokhov II, Tikhonova EA (2002) The climatology of blocking anticyclones for the Northern and Southern Hemispheres: block intensity as a diagnostic. *J. Clim.* 15 (23): 3459–3473. doi: 10.1175/1520-0442(2002)015<3459:TCOBAF>2.0.CO;2
- Wilks DS (2011) *Statistical Methods in the Atmospheric Sciences* (vol. 100). Academic Press, USA
- WMO (2012) Cold spell in Europe and Asia in late winter 2011/2012. [http://ane4bf-datap1.s3-eu-west-1.amazonaws.com/wmocms/s3fs-public/news/related\\_docs/dwd\\_2012\\_report.pdf](http://ane4bf-datap1.s3-eu-west-1.amazonaws.com/wmocms/s3fs-public/news/related_docs/dwd_2012_report.pdf)
- Woollings T, Hoskings B, Blackburn M, Berrisford P (2008) A New Rossby Wave–Breaking Interpretation of the North Atlantic Oscillation. *Journal of the Atmospheric Sciences* 65 (2): 609-626. doi: 10.1175/2007JAS2347.1
- Woollings T, Hannachi A, Hoskins B (2010a) Variability of the North Atlantic eddy-driven jet stream. *Quarterly Journal of the Royal Meteorological Society* 136 (649): 856-868. doi: 10.1002/qj.625
- Woollings T, Charlton-Perez A, Ineson S, Marshall AG, Masato G (2010b) Associations between stratospheric variability and tropospheric blocking. *J. Geophys. Res.* 115: D06108. doi:10.1029/2009JD012742
- Woollings T, Pinto JG, Santos JA (2011) Dynamical Evolution of North Atlantic Ridges and Poleward Jet Stream Displacements. *Journal of the Atmospheric Sciences* 68(5): 954-963. doi: 10.1175/2011JAS3661.1
- Woollings T, Franzke C, Hodson DLR, Dong B, Barnes EA, Raible CC, Pinto JG (2014). Contrasting interannual and multidecadal NAO variability. *Climate Dynamics* 45 (1-2): 539-556. doi: 10.1007/s00382-014-2237-y
- Wright JS and Fueglistaler S (2013) Large differences in reanalyses of diabatic heating in the tropical upper troposphere and lower stratosphere. *Atmos. Chem. Phys.* 13: 9565-9576. doi:10.5194/acp-13-9565-2013

## *References*

---

- Xoplaki E, Luterbacher J, Paeth H, Dietrich D, Steiner N, Grosjean M, Wanner H (2005) European spring and autumn temperature variability and change of extremes over the last half millennium, *Geophys. Res. Lett.* 32: L15713. doi:10.1029/2005GL023424
- Yamazaki A and Itoh H (2009) Selective absorption mechanism for the maintenance of blocking. *Geophys. Res. Lett.* 36: L05803- doi:10.1029/2008GL036770
- Yao Y and Luo DH (2014a) Relationship between zonal position of the North Atlantic Oscillation and Euro-Atlantic blocking events and its possible effect on the weather over Europe. *Science China-Earth Sciences* 57 (11): 2626-2638. doi: 10.1007/s11430-014-4949-6
- Yao Y and Luo DH (2014b) The Anomalous European Climates Linked to Different Euro-Atlantic Blocking. *Atmospheric and Oceanic Science Letters* 7 (4): 309-313. doi: 10.3878/j.issn.1674-2834.14.0001
- Yarnal B (1993) *Synoptic Climatology in Environmental Analysis*. Belhaven Press: London.
- Zampieri M, Toreti A, Schindler A, Scoccimarro E, Gualdi S (2016) Atlantic multi-decadal oscillation influence on weather regimes over Europe and the Mediterranean in spring and summer. *Global and Planetary Change*. doi: 10.1016/j.gloplacha.2016.08.014



## **Annex**

### **A. Different approaches to model future burnt area in the Iberian Peninsula**

*Pedro M. Sousa, Ricardo M. Trigo, Mário G. Pereira, Joaquín Bedia, Jose M. Gutiérrez*

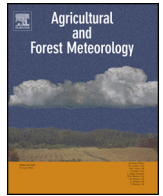
*Paper published in Agricultural and Forest Meteorology (Sousa et al., 2015)*

### **B. Modelling wildfire activity in Iberia with different atmospheric circulation weather types**

*Ricardo M. Trigo, Pedro M. Sousa, Mário G. Pereira, Domingo Rasilla, Célia M. Gouveia*

*Paper published in International Journal of Climatology (Trigo et al., 2013b)*





# Different approaches to model future burnt area in the Iberian Peninsula



Pedro M. Sousa<sup>a,\*</sup>, Ricardo M. Trigo<sup>a</sup>, Mário G. Pereira<sup>b,a</sup>,  
Joaquín Bedia<sup>c</sup>, Jose M. Gutiérrez<sup>c</sup>

<sup>a</sup> Instituto Dom Luiz, University of Lisbon, Lisbon, Portugal

<sup>b</sup> Centre for the Research and Technology of Agro-Environmental and Biological Sciences, CITAB, University of Trás-os-Montes and Alto Douro, UTAD, Quinta de Prados, 5000-801 Vila Real, Portugal

<sup>c</sup> Meteorology Group, Institute of Physics of Cantabria (IFCA), CSIC – University of Cantabria, 39005 Santander, Spain

## ARTICLE INFO

### Article history:

Received 11 August 2014

Received in revised form

12 November 2014

Accepted 22 November 2014

### Keywords:

Wildfires

Iberian Peninsula

Regional climate models

Regression models

Future projections

Pyro-regions

## ABSTRACT

In this work we developed projections for future fire regimes in the Iberian Peninsula using outputs from Regional Climate Model (RCM) from the ENSEMBLES project. Wildfires are the cause of major ecological and economic impacts in this region, and the increasing evidence of climate change consequences in this region raises concerns on the future impacts of fires in the Iberian forests ecosystems. Our results confirm that the inter-annual variability of total burnt area is mainly controlled by meteorological conditions, in spite of the current efforts for fire control and suppression. We also show that this meteorology dominance over fire activity is not only true during the fire season itself, but also that certain specific meteorological backgrounds (such as prolonged droughts) may enhance the risk for severe wildfire episodes in some areas. Based on a previous classification of the Iberian Peninsula into four distinct pyro-regions, we developed statistical models which reproduce about two thirds of the inter-annual variability of the burnt area, using meteorological variables as predictors (calibrated with data from the ERA-Interim reanalysis). Specific models were developed for each sub-domain, testing their robustness for extrapolation under climate-change conditions. Using an ensemble of state-of-the-art RCM future climate scenarios, we present future BA projections considering two alternative techniques of statistical correction of model data often used in climate change impact studies: (1) unbiasing method; (2) delta change method. Our results clearly project large increases in mean burnt areas for all the considered pyro-regions, despite some fluctuations regarding each considered technique. By 2075, mean burnt areas could be about two to three times larger than in the present, taking into account current climate projections for the next century, and non-significant changes in other external factors, such as human activity, fire suppression or land use.

© 2014 Elsevier B.V. All rights reserved.

## 1. Introduction

Wildfires are not a recent hazard in the Iberian Peninsula; nevertheless, it is unquestionable that some of the most dramatic episodes have occurred since the turning of the century, particularly in western Iberia. The years of 2003 and 2005 correspond to landmark fire seasons in the fire history of Portugal, being responsible for the highest values of burnt area (hereafter, BA) since 1980 (Trigo et al., 2006; Pereira et al., 2011). Likewise, in the

contiguous northwestern Spanish province of Galicia, the year of 2006 was characterized by a very high number of fires and large burned area (San-Miguel-Ayanz et al., 2013). It is well known the important human role on the shaping of fuel availability, which has a great impact in fire activity in Mediterranean ecosystems (de la Cueva et al., 2006; Costa et al., 2010; Pausas and Fernández-Muñoz, 2012). Some Iberian fire prone areas, such as the eastern coast of Spain (e.g. Valencia, Murcia, Catalonia) have witnessed a significant decrease of summer wildfire since the mid-90s, partly attributable to significant improvements in fire prevention and suppression schemes (Turco et al., 2013), taken after some of the worst fire occurrences in the region.

Nonetheless, apart from the anthropogenic influence and in spite of the fire suppression efforts in the Euro-Mediterranean areas, meteorological drivers play a key role in modulating the

\* Corresponding author at: Instituto Dom Luiz, Faculdade de Ciências, Universidade de Lisboa Campo Grande, Ed C8, Piso 6, 1749-016 Lisboa, Portugal.

Tel.: +351 217500855; fax: +351 217 500 807.

E-mail address: [ppsousa@fc.ul.pt](mailto:ppsousa@fc.ul.pt) (P.M. Sousa).

inter-annual variability of *BA* (Bedia et al., 2014), which is strongly controlled by summer meteorological conditions (Pereira et al., 2005; Trigo et al., 2006, 2013), specially during drought episodes (Pausas and Fernández-Muñoz, 2012; Gouveia et al., 2012), and to a lesser extent by previous precipitation, as antecedent conditions affect primary productivity (and hence fuel availability, Koutsias et al., 2013). In this regard, the recent work by Trigo et al. (2013) shows that this variability can be fairly well reproduced by statistical models based solely on meteorological variables. Despite significant and costly efforts in prevention and suppression made in recent years by national authorities, the recent rise in the frequency of extreme hot events (Ramos et al., 2011) and drought episodes in the Iberian area (García-Herrera et al., 2007; Sousa et al., 2011), has made its toll in scarring Iberian forests, as for instance, during episodes such as the mega-heatwave that affected western Europe in 2003 (Trigo et al., 2006; García-Herrera et al., 2010), most often related with the occurrence of large atmospheric blocking episodes (Trigo et al., 2005; Barriopedro et al., 2011). Such episodes lead to extremely dry atmospheric conditions that favor fire ignitions over a vegetation under hydric/hydrological stress and very low fuel moisture content.

The strong meteorological forcing over fire regimes raises serious concerns on the future of the Mediterranean basin forests, as most Global and Regional Climate Models (hereafter GCMs and RCMs) project an important warming in these areas (Brands et al., 2011; Ramos et al., 2011; Frias et al., 2012) leading to an increased fire danger potential (Bedia et al., 2013, 2014). Significant changes in precipitation regimes should also be expected, mainly in monthly mean precipitation and intra-annual variability, characterized by less precipitation outside the winter season, as well as a tendency toward more extreme events (Giorgi and Lionello, 2008; Argüeso et al., 2012). To address this issue, several authors have attempted to explicitly model future *BA* series based on different climate change scenarios (Carvalho et al., 2007; Pereira et al., 2013; Amatulli et al., 2013). Regardless of the method used and the inherent model uncertainties, all approaches consistently point to a much higher future *BA*.

It is widely recognized that RCM outputs cannot be directly applied in impact studies due to the biases inherited from the driving GCM (see e.g. Turco et al., 2013b), as well as those introduced by the regional climate model (RCM) as a result of different model errors and parameterizations (c.f., Christensen et al., 2008; Herrera et al., 2010). Thus, a validation/calibration process is needed before using this data in impact applications. This process requires the availability of historical data (or high-resolution reanalysis) to calibrate the model outputs in a particular region of interest. Besides, climate models present some difficulties in realistically representing intrinsic variability, a fact which may hamper future projections, especially for those variables in which daily scale processes are dominant. Different bias correction methods have been proposed and tested in the literature to adjust model biases and/or daily variability using observations, being the unbiasing and delta methods (Déqué, 2007) the most simple and popular ones. On the one hand, the unbiasing method (hereafter BC) operates by just modifying the mean magnitude of the future simulation by subtracting the difference of the control simulation and the corresponding control observations (generally on a monthly basis), thus not affecting the distributional properties of the simulated series. On the other hand, the delta change method (henceforth DCM) uses the control (daily) observations of the target variables as the future daily baseline, adapting their mean state and variance according to the projected (monthly) model changes, thus preserving the daily variability associated to the observed meteorological variables. This technique has been previously applied in the context of wildfire research (Flannigan et al., 2013) although comparative studies of both approaches in the framework of wildfire research are lacking

to date. In this study, we investigate both types of model correction techniques for the estimation of future *BA* in the Iberian Peninsula.

The aim of this study is the generation of plausible future *BA* scenarios for the Iberian Peninsula in order to ascertain the potential impacts of climate change on wildfires. To this aim, the following steps are addressed:

- (1) We analyze the relationships between inter-annual variability of observed *BA* and meteorological conditions, in particular the meteorological patterns associated with intense wildfire seasons;
- (2) We develop statistical regression models capable to reproduce the inter-annual variability of *BA* series during the 1981–2005 control period, testing them with control simulation data from a set of state-of-the-art RCMs from the EU-funded project ENSEMBLES (van der Linden and Mitchell, 2009).
- (3) We assess the uncertainty of the future projections derived from the bias correction technique by comparing the projected *BA* results after using either BC or DCM methods.

The manuscript is structured as follows:

The datasets and methodologies used are presented in Section 2 while an outlook at the control period fire climatology of Iberia and of each sub-domain is performed in Section 3. The links with meteorology, the development of the statistical model using observed data, the performance of RCMs simulations for the control period and the projected future scenarios are presented in Section 4. Finally, the discussion of the obtained results and used methods are found in Section 5.

## 2. Data and methods

### 2.1. Fire data

Portuguese fire data was obtained from the *Autoridade Florestal Nacional* (Pereira et al., 2011), while Spanish data was obtained from the *Dirección General de Biodiversidad* (Mérida et al., 2007). Building on both databases, we used the recent joint Iberian wildfire database (Trigo et al., 2013), encompassing their common period 1981–2005. Monthly *BA* time series are spatially disaggregated by (66) Continental administrative regions (hereafter AR), that correspond to (18) *Distritos* in Portugal, and (48) *Provincias* in Spain - (excluding the Atlantic archipelagos). We also computed the monthly Normalized Burnt Area (*NBA*) for each AR, defined as the quotient between the amount of *BA* in each AR and the corresponding area of the AR (Fig. 1).

Despite the important inter-annual variability, the northwestern sector of Iberia presents the highest rates of *NBA* in most years. Years 1981, 1985, 1989, 1995 and specially 2005 stand out as particularly severe in this sector, with annual *NBA* above 25‰ for a large number of AR. On the other hand, the years of 1991, 1995, 2003 and 2004 were particularly harsh in southwestern regions of the Peninsula. The Mediterranean area is also prone to some dramatic wildfire summers, namely before 1995. In contrast with other regions where summer fires explain most of the annual *NBA*, a well defined late winter or early spring fire season is found in the northernmost areas of Iberia (with similar magnitude compared to summer months), as shown in Fig. 2. In fact, this earlier peak is also found in northwest Iberia, but in this case, much smaller in magnitude when compared to the mean summer *NBA*. These different fire regimes have also been addressed in a preceding work (Trigo et al., 2013), where a cluster analysis allowed the identification of four spatially homogeneous pyro-regions (Fig. 2): northwest (NW-CLU), southwest (SW-CLU), north (N-CLU) and east (E-CLU).

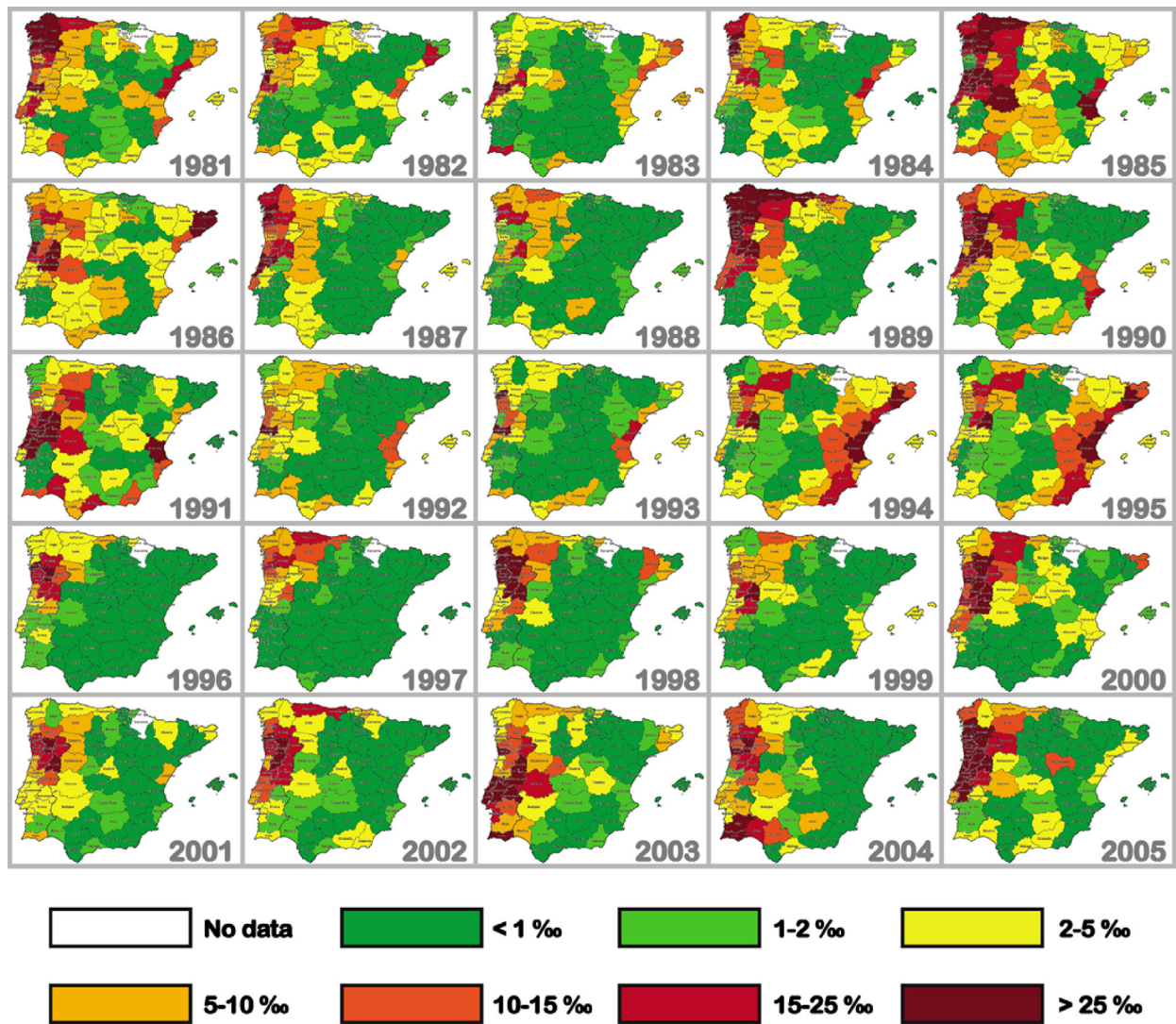


**Fig. 1.** Inter-annual variability of the Normalized Burnt Area (NBA) in each Administrative Region (AR) of the Iberian Peninsula for the 1981–2005 period. The NBA is defined as the quotient between the amount of Burnt Area in each of the AR and the area of the AR (both in hectares) and depicted presented in per mil (‰).

## 2.2. Current climate data

We used the ERA-Interim reanalysis (Dee, 2011) as the reference climatology for the control period. A number of recent works

(Mooney et al., 2011; Kishore et al., 2011; Bedia et al., 2012) give a positive feedback about this dataset, when compared to other reanalysis products. Furthermore, the large number of meteorological variables available (at several height levels, and at the sub-daily

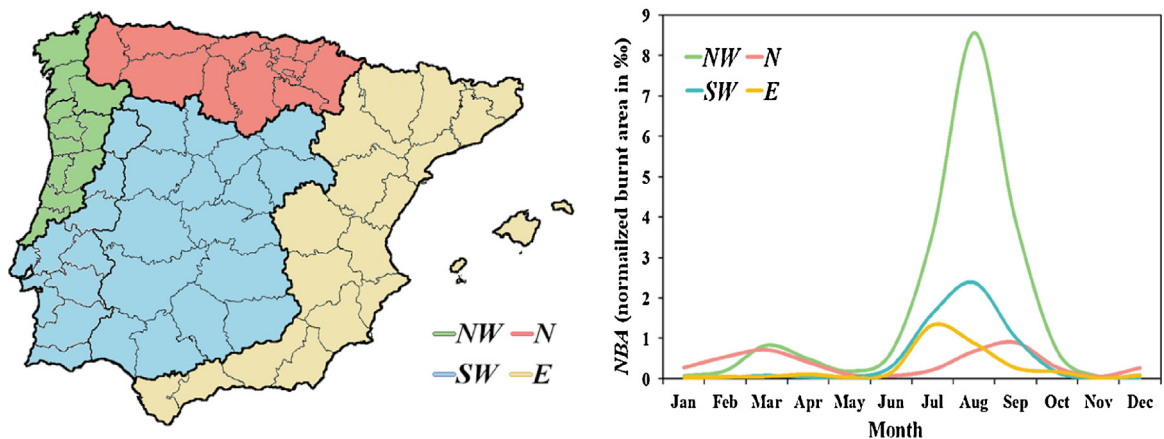


**Fig. 2.** Spatial extension (left panel) and mean monthly series (1981–2005) of Normalized Burnt Area (right panel) of the 4 clusters considered inside the Iberian Peninsula. These clusters correspond to relatively homogeneous fire regimes for the 66 Administrative Regions (AR) of Iberia, adapted from the work by Trigo et al. (2013).

scale) allows a better characterization of the specific daily weather conditions in each of the four Iberian sub-regions. Given the high number of variables and time resolution (6-hourly) of the reanalysis data, we applied a pre-selection procedure based on correlation analysis between time series of BA and meteorological variables, identifying 12UTC 2m air temperature (hereafter,  $T$ ), 12UTC 500 hPa geopotential height (hereafter,  $Z$ ) and daily precipitation (hereafter,  $P$ ) as the preferred candidate predictors. Mean sea level pressure (hereafter,  $MSLP$ ) series were also considered, but only for drawing synoptic charts.

### 2.3. Future climate projections

We used the RCM simulations of the ENSEMBLES project (van der Linden and Mitchell, 2009). From all available models, we selected a subset of four RCMs (Table 1) which presented satisfying results in the objective evaluation procedure of the RCM performance over Portugal and Spain (Soares et al., 2012; Herrera et al., 2010). The RCM simulations cover for a control period (1981–2001) and the future scenario simulations extend until 2100 in most cases, with a horizontal spatial resolution of about 25 km (Christensen et al., 2010). Since the ERA-Interim training period spans from 1981 to 2005, and in order to obtain verification series with the same length for each RCM, forcing data from the A1B scenarios was used during the last four years, completing the small gap for 2002–2005. These simulations for the control period were used firstly to compare the performance of RCMs against ERA-Interim in modeling past BA series, and secondly to calibrate the statistical models before using them to project future scenarios of BA. In this study, we have considered the future time slices 2001–2025, 2026–2050 and 2051–2075.

### 2.4. Forward stepwise regression models

From the pre-selected pool of potential predictors (see Section 2.2), a forward stepwise regression analysis was performed in order to reproduce BA values for each cluster. This method tests all possible predictors, maintaining those that explain more variance of the predictand (BA) time series, following a standard procedure in atmospheric sciences (Wilks, 2011). During this process, the algorithm tests all combinations of predictors in order to exclude the redundant ones, thus avoiding the problem of multicollinearity (Alin, 2010; Garg and Tai, 2012; Kraha et al., 2012), which may hamper model interpretability.

The robustness of the statistical models was tested by performing a 5-fold cross-validation scheme to each cluster's model (c.f., Supplementary Material – S1). This validation is crucial as non-robust models can be highly biased by outliers and, therefore, an overestimation on the performance metrics would exist. An additional precautionary step was taken forcing all models to retain 4 predictors at most (the most correlated with BA amongst the predictors chosen by the forward stepwise regression). These two precautions were taken since the time series are only 25 years long (1981–2005), and short training series carry the danger of overfitting when too many predictors are considered in the model (Hurvich and Tsai, 1989; Hawkins, 2004).

In addition, BA series in E-CLU are not homogeneous, presenting higher values prior to the early 1990s with a peak-point in the year 1994, and decreasing significantly afterwards (Fig. 3. See also Turco et al., 2013), thus requiring the application of a correction factor taking into account the two periods separately (discussed in Section 3.2).

In order to check model performance, we used four measures of goodness of fit (Wilks, 2011), namely the mean absolute error (MAE), the Spearman rank correlation coefficient ( $\rho_{sp}$ ), the adjusted

explained variance ( $\bar{r}^2$ ), and the skill score against the climatology (SS), being the latter two metrics given by Eqs. (1) and (2):

$$\bar{r}^2 = 1 - \frac{n-1}{n-(k+1)}(1-r^2) \quad (1)$$

$$SS = \frac{RMSE - RMSE_{ref}}{RMSE_{perf} - RMSE_{ref}} \times 100 \quad (2)$$

where  $n$  is the sample size,  $k$  is the number of predictors and  $r$  is the Pearson correlation coefficient.  $RMSE_{ref}$  is the root mean square error of the climatology series – a perfect model would have  $RMSE_{perf}$  equal to 0.

Finally, the robustness assessment undertaken also seeks to ascertain if the linear models developed can be confidently applied for extrapolation, at least under “moderate” climate change (warming) conditions. The approach is described in detail in Gutiérrez et al. (2012), and it is essentially based on working with anomalous warm historical periods as proxies of future climate change conditions in order to test the ability of the models to reproduce warmer periods outside the learning space of the model. More specifically, the warm period is taken out from the training data and used to test the resulting model (c.f., Supplementary Material S1).

### 2.5. RCM data biases and distributions

It is widely recognized nowadays that, despite the improved confidence in regional climate model simulations (Herrera et al., 2010; Maule et al., 2013; Ehret et al., 2012; Teutschbein and Seibert, 2012), RCMs still reveal some limitations when attempting to represent present climate (e.g. biases and unreliable variances). In order to understand the ability of each chosen RCM to reproduce the present climate in the Iberian domain, a series of procedures were applied and some statistical metrics were computed, for each pyro-region of the Iberian Peninsula, and for different model output correction methods. In particular, two different simple bias correction techniques have been considered (the unbiasing and delta change methods, BC and DCM, respectively; Déqué, 2007) as detailed in the following sections.

#### 2.5.1. The unbiasing method

The simplest bias correction procedures consist in removing the difference between the means and the ratio of the variability between observed and simulated time series obtained for the reference period (Huntingford et al., 2006; Ines and Hansen, 2006). However, this approach has several caveats: (1) corrections in the variability will only work well for variables with Gaussian distributions (e.g. temperature, geopotential height) and not for heavily tailed distributions (e.g. precipitation); (2) the intrinsic daily variability of each RCM will be kept, meaning that although means and standard deviations can be controlled, poor reproductions of the observed daily variability will subsist using this method.

Nevertheless, because this is the most widely used approach adopted by modelers we decided to maintain this simple bias correction as a benchmark correction procedure. Taking into account these factors, the following BC was applied to the pre-selected variables (as referred in Section 2.1) to obtain future series of temperature (3), geopotential height (4) and precipitation (5):

$$T_{unbiased(t,m)} = T_{RCMfut(t,m)} + (\overline{T_{ERAcl(m)}} - \overline{T_{RCMctl(m)}}) \quad (3)$$

$$Z_{unbiased(t,m)} = Z_{RCMfut(t,m)} + (\overline{Z_{ERAcl(m)}} - \overline{Z_{RCMctl(m)}}) \quad (4)$$

$$P_{unbiased(t,m)} = P_{RCMfut(t,m)} + (\overline{P_{ERAcl(m)}} / \overline{P_{RCMctl(m)}}) \quad (5)$$

The subscripts RCM and ERA correspond to Regional Climate Model and ERA-Interim reanalysis, respectively; the subscripts *ctl* and *fut* refer to the control (1981–2005) and any considered future

**Table 1**

Regional Climate Models (RCMs) considered in this study, including the model acronym, developing institute and main reference.

Model	Institute	Reference
HadRM3Q0	Hadley Center – UK Met Office (HADLEY)	Collins et al. [2006]
RACMO2	Koninklijk Nederlands Meteorologisch Instituut (KNMI)	van Meijgaard et al. [2008]
REGCM3	Abdus Salam International Centre for Theoretical Physics (ICTP)	Pal et al. [2007]
REMO	Max Planck Institute for Meteorology (MPI)	Jacob et al. [2001]

period, respectively; the bars denote the temporal average; finally, the  $t$  and  $m$  indexes correspond to each particular day and month of simulation.

### 2.5.2. The delta change method

In our statistical models the most important predictors are sampled at daily scale, and therefore the poor representation of daily variability using the traditional bias correction may hamper the resulting BA models. To overcome this drawback, the DCM has been used in recent years to simulate future meteorological time series based on RCM outputs when the daily variability is of crucial importance (e.g. Hawkins et al., 2013; Ruiter, 2012). The main distinction in this approach consists in correcting observed time series in order to adjust them to expected forthcoming changes, rather than correcting raw RCM output series. This process enables the construction of future time series which preserve observed daily variability. Naturally, this approach does not address significant changes in the nature of the daily variability regimes, but still, both mean and variability can be adjusted to obtain the future series.

Once again, changes in the mean are easy to obtain while changes in the standard deviations are only simple to perform with near Gaussian distributions. The future time series of temperature and geopotential height using the DCM are obtained using the following expressions:

$$T_{\text{delta}(t,m)} = \overline{T_{\text{RCMfut}(m)}} + \frac{\sigma_{T_{\text{RCMfut}}(m)}}{\sigma_{T_{\text{RCMctl}}(m)}} (T_{\text{ERActl}(t,m)} - \overline{T_{\text{RCMctl}(m)}}) \quad (6)$$

$$Z_{\text{delta}(t,m)} = \overline{Z_{\text{RCMfut}(m)}} + \frac{\sigma_{Z_{\text{RCMfut}}(m)}}{\sigma_{Z_{\text{RCMctl}}(m)}} (Z_{\text{ERActl}(t,m)} - \overline{Z_{\text{RCMctl}(m)}}) \quad (7)$$

where the nomenclature of Eqs. (3)–(5) was adopted and the symbol  $\sigma$  corresponds to the standard deviations for each particular period.

As stated before, in the case of precipitation, transforming the standard deviation of the series is not a simple and particularly effective task, as the precipitation series distribution is heavily one side tailed. To obtain future series of daily precipitation using the delta change method we had to perform several steps. The first was

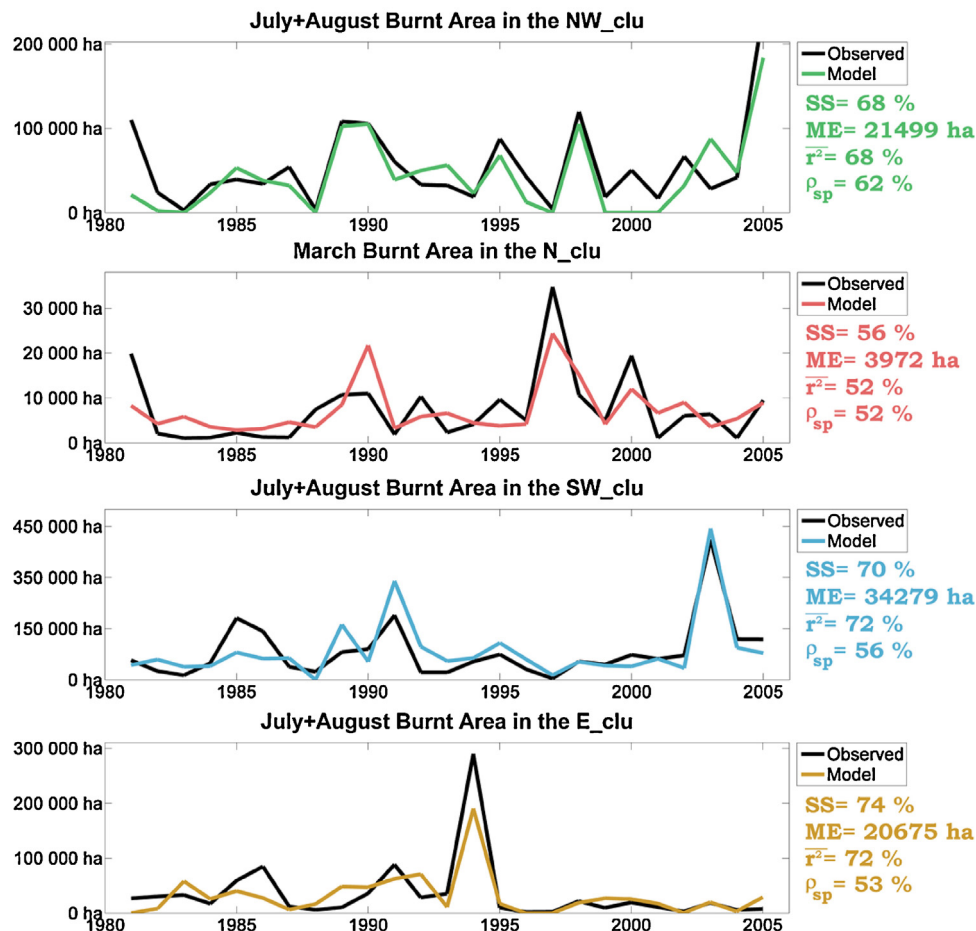


**Fig. 3.** Observed (black lines) and modeled (colored lines) time series for the July plus August (March in the N cluster) Burnt Area in each cluster of the Iberian Peninsula. Modeled series result from a forward stepwise regression which uses as predictors meteorological variables from the ERA-Interim re-analysis dataset (air temperature, precipitation and geopotential height time series).

to make a delta change correction to the daily precipitation series of ERA-Interim, but only rectifying the mean:

$$P_{\text{delta}(t,m)} = P_{\text{ERActl}(t,m)} + (P_{\text{RCMfut}(m)} - P_{\text{RCMctl}(m)}) \quad (8)$$

This process enables changes in the mean precipitation, but at this point it totally discards changes in the intra-monthly variability of the series. To address this issue, rather than trying to correct the standard deviations of such a non-Gaussian distribution we opted to correct the number of dry days. For that purpose, we first calculated the ratio of future change of dry days for each month in each RCM, and corrected the expected number of future dry days in each specific month:

$$\text{DRY}_{\text{delta}(m)} = \text{DRY}_{\text{ERActl}(m)} \times (\text{DRY}_{\text{RCMfut}(m)} / \text{DRY}_{\text{RCMctl}(m)}) \quad (9)$$

Once more, all subscripts meaning is the same as in the previous equations. The difference between the expected and observed number of dry days in each particular month ( $D$ ) corresponds to the number of lowest precipitation days in each month that is forced to have zero precipitation, in order to obtain the expected number of dry days estimate in each month from (9). Naturally this forcing will change the total precipitation of the month, resulting in this value being slightly above (below) the expected in the case of removing (adding) dry days to the original series. This excess (lack) of precipitation is then equally distributed (removed) from the remaining rainy days of the month. The resulting series will permit to have monthly climatologies that present the mean and number of dry days, as expected from (8) and (9).

### 2.5.3. The observed-simulated distributions comparison

Model biases for each meteorological variable, month and spatial sub-domain were verified and removed from the series for the control period (1981–2005). Then, distributions of  $BA$  simulated using ERA-Interim data and RCM outputs were compared with the distribution of observed  $BA$  series for the control period, in order to identify which RCM models simulate better the present fire climatology and may provide greater confidence when simulating  $BA$  for future scenarios.

To compare the similarity between time series of meteorological variables or  $BA$  from two different models or sources, we check the agreement between their probability distributions, to account for differences in the mean and in higher order moments. Two skill scores were used for this purpose: the two-sample Kolmogorov–Smirnov test ( $KS_{\text{statistic}}$ ) and the  $PDF_{\text{score}}$  (Brands et al., 2012).

The  $KS_{\text{statistic}}$  is a non-parametric test used to check the null hypothesis that two separate samples come from the same theoretical distribution. The  $KS_{\text{statistic}}$  is defined as follows:

$$KS_{\text{stat}} = \max_{i=1}^{2n} |F(z_i) - G(z_i)| \quad (10)$$

where  $n$  is the length of the time-series,  $F$  and  $G$  are the empirical cumulative frequencies of each time-series, and  $z_i$  denotes the  $i$ th data value of the sorted joined sample. The  $KS_{\text{statistic}}$  is bounded between 0 and 1, and high distributional similarity is indicated by low values. Serial autocorrelation must be addressed when computing the  $KS_{\text{statistic}}$ , leading to an effective smaller sample size  $n^*$ , obtained using the following expression:

$$n^* = n \frac{1 - p_1}{1 + p_1} \quad (11)$$

where  $p_1$  is the lag-1 autocorrelation coefficient.

The  $PDF_{\text{score}}$  is a measure of agreement between two distributions, where the common overlapping of the two probability density functions (PDFs) is calculated. The PDFs are estimated using

a number ( $N$ ) of equally spaced bins, here defined as by Shimazaki and Shinomoto (2007). The two normalized PDFs are then compared as follows to obtain the  $PDF_{\text{score}}$ :

$$PDF_{\text{score}} = \sum_{i=1}^N \min \{f(m_i), (g(m_i))\} \quad (12)$$

where  $f$  and  $g$  are the relative frequencies of each PDF, and  $m_i$  is the corresponding bin index. The  $PDF_{\text{score}}$  also spans between 0 and 1, but contrary to the  $KS_{\text{statistic}}$ , a high degree of similarity between the two distributions corresponds to a score near 1. In order to avoid the opposite scale direction of the two considered scores, the value of 1 minus the  $KS_{\text{statistic}}$  (hereafter  $1 - KS_{\text{statistic}}$ ) will be presented instead. Thus, in both cases the degree of match between distributions will always grow from 0 to 1.

## 3. Understanding the inter-annual variability of burnt areas

The main drivers of inter-annual variability of burnt areas in Iberia in the four considered clusters were identified by discriminating the influence of pre-conditioning climatic conditions – i.e., the accumulated stress on vegetation, and the consequent susceptibility during the fire season – and the meteorological conditions that foster fire ignition and spread during the fire season (Trigo et al., 2013). As stated in Section 2.1, there is a very similar peak near March in the NW-CLU and N-CLU, although quite different in its relative importance on the annual totals. This fact led us to focus only on the more representative season in terms of  $BA$  activity in each region, for the sake of readability. The main links between the inter-annual  $BA$  variability in each cluster and meteorological forcing are next analyzed, in order to retain the most relevant variables that correlate with  $BA$  series. This procedure will enable to test and select the sub-set of meteorological indices which will be used to develop statistical regression models.

### 3.1. Links with meteorological indices

The influence of selected meteorological fields ( $T$ ,  $Z$  and  $P$ ) over  $BA$  series was tested using correlation analysis – performed at monthly (considering inter-annual anomalies) and daily scales (considering annual absolute values). For some meteorological variables monthly anomalies are well correlated with Iberian  $BA$  series (e.g. Pereira et al., 2005), still in some particular cases they can mask some important daily-scale extreme weather episodes which trigger large fires, but do not affect significantly the monthly anomaly (Trigo et al., 2013). To account for these situations, we computed monthly percentiles for each variable. Then, we calculated monthly time series of the relative frequency of days exceeding those percentiles. In the case of  $T$  and  $Z$  – to take into account the occurrence of extremely hot days – we considered the 90th, 95th and 98th percentiles. In the case of  $P$  – with the attention focused on the sequences of dry days – the application of the same principle lead to the computation of monthly frequencies of days where the mean precipitation in the whole cluster area was below 0.5 mm, 1 mm and 2 mm.

We computed the correlations (Pearson's  $r$ ) between  $BA$  and monthly time series of anomalies or frequencies of extreme days for each variable during the fire season months, and also from previous months (up to 7 months before). The results are shown in Tables 2 and 3.

Table 2 is restricted to the links between  $BA$  and meteorological conditions during the fire season, revealing favorable conditions to trigger fire ignition and spread, regardless of the meteorological background. As expected, results are dominated by monthly

**Table 2**

Highest four values of the Pearson product-moment correlation coefficient (Pearson's  $r$ ) obtained between monthly burnt area and monthly statistics (anomaly and number of days, NDays) of meteorological variables (12UTC 2m air temperature:  $T$ ; geopotential height at the 500 hPa level:  $Z$ ; daily precipitation:  $P$ ) during the fire season for each cluster. Values of the Pearson's  $r$  presented here are significant at the 5% level.

	Pearson's $r$	Month	Variable	
NW.CLU	+0.53	August	$T$	Monthly anomaly
	+0.45	July	$T$	NDays > 95th percentile
	−0.42	August	$P$	Monthly anomaly
SW.CLU	+0.40	August	$T$	NDays > 95th percentile
	+0.84	August	$T$	NDays > 98th percentile
	+0.77	August	$T$	NDays > 95th percentile
	+0.63	August	$T$	NDays > 90th percentile
	+0.56	August	$Z$	NDays > 95th percentile
N.CLU	+0.68	March	$Z$	NDays > 98th percentile
	+0.68	March	$P$	NDays < 0.5 mm
	+0.64	March	$T$	NDays > 90th percentile
	+0.64	March	$Z$	NDays > 95th percentile
E.CLU	+0.44	July	$T$	NDays > 98th percentile
	+0.42	August	$P$	NDays < 1 mm
	+0.40	August	$Z$	NDays > 90th percentile
	+0.38	July	$T$	Monthly anomaly

**Table 3**

Same as Table 2 but considering lagged Pearson's  $r$  obtained between monthly burnt area and monthly statistics of meteorological variables in the months preceding the fire season.

	Pearson's $r$	Month	Variable	
NW.CLU	+0.45	June	$T$	Monthly anomaly
	+0.40	June	$T$	NDays > 90th percentile
	−0.34	January	$P$	Monthly anomaly
	−0.33	June	$P$	Monthly anomaly
SW.CLU	+0.48	February	$P$	Monthly anomaly
	+0.45	June	$T$	Monthly anomaly
	+0.45	June	$T$	NDays > 95th percentile
	+0.38	May	$P$	Monthly anomaly
	+0.59	February	$Z$	NDays > 90th percentile
N.CLU	+0.58	February	$Z$	NDays > 95th percentile
	+0.54	February	$Z$	Monthly anomaly
	+0.49	February	$P$	NDays < 0.5 mm
	−0.34	April	$T$	Monthly anomaly
E.CLU	+0.34	May	$P$	NDays < 0.5 mm
	+0.33	May	$P$	NDays < 1 mm

frequencies of high percentile exceedances of  $T$ , although frequencies of dry days also grant important correlations in the E.CLU and N.CLU. In the N.CLU (where the focus is in early spring) the frequency of days with extremely high values of  $Z$  is also positively correlated with  $BA$ , meteorologically related with anomalous stable, clear sky and dry conditions in March.

Concerning the months prior to the fire season (i.e. meteorological background), rather different forcing is found for each cluster (Table 3). In the case of the NW.CLU, the summer  $BA$  is significantly associated with above-average temperature in late spring and below-average precipitation in January and June, suggesting that drier-than-average winters and springs in this wet region enhance vegetation vulnerability due to hydric stress, making it more susceptible to burn in the following summer (Chuvieco et al., 1999).

In the SW.CLU, dry and warm conditions in late spring or early summer are also related with high values of  $BA$ . But unlike NW.CLU, a positive correlation between winter precipitation and summer  $BA$  series is found. This shows that for this drier region of Iberia, above-average winter precipitation favors vegetation growth enhancing fuel availability in summer (Pereira et al., 2005; Trigo et al., 2013). In the N.CLU, the most important meteorological background influence is concentrated in the immediately preceding month (February), when the meteorological variables highly

correlated with March  $BA$  are quite similar to the ones found in Table 2, reinforcing the idea that high values of  $BA$  in the northernmost sector of Iberia tend to be related with anomalous persisting high-pressure systems (blocking episodes) over the region.

For the easternmost region (E.CLU), we find three statistically significant links, two of them referring to below-average precipitation in spring, which suggests that in this region the persistence of dry conditions may also enhance vegetation vulnerability during the fire season. Nevertheless, the lack of significant links reduces the prospects of using this type of background meteorological variables as good proxies for  $BA$  predictability in the E.CLU. These results unveil the crucial role of meteorological drivers on  $BA$  in the Iberian Peninsula. This is particularly true for western sectors (NW.CLU and SW.CLU), where one-predictor truncated models (not shown), using only the monthly frequencies of days above the 95th and 98th percentiles of  $T$ , respectively, explain about 50% of the inter-annual  $BA$  variability in the months of July and August.

### 3.2. Statistical hindcast models

Following the stepwise predictor selection procedure and the additional restrictions presented in Section 2.2, the best performing models obtained for each of the pyro-regions are described by the following set of equations.

For the NW.CLU:

$$BA_{Jul+Aug} = +581000 Tpct95_{Jul+Aug} - 35000 Panom_{Jul+Aug} + (53300) - 0.15 BA_{prev}$$

For the SW.CLU:

$$BA_{Jul+Aug} = +1920000 Tpct98_{Jul+Aug} + 11600 Panom_{Feb+May} + (52000)$$

For the N.CLU:

$$BA_{Mar} = +133000 (Tpct90_{Mar} \times Zpct90_{Feb}) + 20500P < 0.5 \text{ mm}_{Feb+Mar}$$

For the E.CLU:

$$BA_{Jul+Aug} = +1600 Tanom_{Jul+Aug}^{\Delta\#} + 2900 P < 1 \text{ mm}_{Jul+Aug}^{\Delta\#}$$

where indices  $pct90$ ,  $pct95$  and  $pct98$  correspond to monthly frequencies of exceedances for the corresponding percentiles (Section 3.1), while indices  $<0.5 \text{ mm}$  and  $<1 \text{ mm}$  correspond to monthly frequencies of days with precipitation smaller than 0.5 mm and 1 mm, respectively;  $anom$  indices refer to the monthly anomaly; the symbol  $\Delta$  corresponds to an aggravating factor based on the number of months with a deficit in rainfall;  $BA_{prev}$  refers to a weighting of the area burnt in the previous 3 years; the symbol  $\#$  denotes a correction factor due to the existence of a break-point in the series (as previously discussed in Section 2.4). The aggravation factor based on the conditions of “accumulation of dry months” was introduced to take into account the hydric deficit inherited from antecedent meteorological conditions.

In Figure 3, the resulting hindcast  $BA$  time series (using the ERA-Interim reanalysis) are compared with the observed  $BA$  series for each of cluster for the control period, including the model performance metrics.

All cross-validated models attained SS values above +50%, i.e. significantly better than the simpler persistence approach (Fig. 3). Furthermore, all models explain more than 50% of the regional  $BA$  reduced variance. This is particularly notable for the NW.CLU and

SW\_CLU, where the models are able to adequately reproduce exceptional years in terms of BA (2005 and 2003), attaining around a 70% of explained variance. Similar performance was attained in the E\_CLU, but in this case the high performance of the models may be partially inflated by the nature of the series after 1994 – these were all years with very small BA totals, as indicated by the large divergence between  $r^2$  and  $\rho_{sp}$  (being the latter metric insensitive to the confronted variable magnitudes). Finally, the lowest scores are found in the N\_CLU (focused in March). Yet, some of the most severe years (in terms of observed BA in this region) were reproduced by the model (e.g., 1990, 1997 and 2000). Furthermore, despite the relatively low scores attained they still represent more than half of the reduced variance. We must stress that the values of BA series in this region are about one order of magnitude below the ones found in the remaining clusters.

### 3.3. Synoptic forcing during severe wildfire episodes

Taking into account the strong meteorological forcing of BA described in Section 3.2, and in order to distinguish the different meteorological configurations that favor the occurrence of these conditions, we computed composites of meteorological fields during these extreme days. Composites were computed on the ( $T$ ,  $Z$  and  $MSLP$ ) meteorological fields (Fig. 4), providing an overview of the typical synoptic patterns related with large fires in each pyro-region. Despite some differences, all four composites present a common sharp positive  $T$  anomaly over most of southwestern Europe, with their maxima (regarding the IP) centered at the corresponding pyro-region.

In the case of March fires in the N\_CLU, the composite (near 100 days) presents well above average  $T$  in all of Europe, associated to a very large positive anomaly of  $Z$  over France, also expressed at the surface level. This particular continental blocking configuration promotes subsidence over the region, and in the particular case of northern Spain, brings a marked southerly flow, with exceptionally dry and warm conditions down slope of the Cantabrian Range (Foehn winds). Spatial patterns of the composites for the remaining clusters reveal anomalous conditions more restricted to southwestern Europe, but with similar magnitude in  $T$  anomalies in the target areas, also intimately related with large positive anomalies of  $Z$  and  $MSLP$ . The position of the positive anomaly of  $Z$  fields during July and August and associated with fires in the E\_CLU is quite similar to the previously referred case, but smaller in magnitude, promoting the advection of warmer African air over Iberia. Trigo et al. (2013) stated that extremely hot days in the Mediterranean façade require a surface flow from west or northwest in order to cease mild Mediterranean breezes. Nevertheless, as seen in Section 3.2, the model for this cluster suggests a stronger dependence on the lack of precipitation days during July and August as convective precipitation in late summer is relatively frequent in the area. The obtained composite is highly compatible with the occurrence of prolonged dry spells in the E\_CLU. NW\_CLU and SW\_CLU exhibit quite similar synoptic configurations. In both regions, large BA is driven by extreme dry and hot days, directly related with the location of high pressure systems in the Atlantic region between Iberia and the British Isles. The main differences between the two composites are the tilting of the ridge and the surface pressure configuration. The positive anomaly of  $Z$  is tilted westwards (eastwards) in the case of the NW\_CLU (SW\_CLU). The spatial location of the highest anomaly in  $T$  depends on the surface pressure configuration, portrayed by the position of the thermally induced low. In both cases, easterly synoptic flows that attenuate Atlantic breezes are required.

The  $Z$  anomalies in the composites suggest the existence of Atlantic (continental) blocking in the cases of NW\_CLU and SW\_CLU

(N\_CLU and E\_CLU). It is rather difficult to classify the type of blocking pattern associated (i.e. Omega, Diffluent, etc.) since these maps do not correspond to a few isolated days, but to composites ranging between 50 and 100 days, depending on the case. This type of approach naturally smooths meteorological fields as it can capture different types of blocking events and configurations centered in similar locations.

## 4. Future scenarios of burned area

### 4.1. RCM performance in the control period

The ability of each RCM to reproduce the observed distribution during the control period (1981–2005) was based on two metrics: the  $PDF_{score}$  and the  $KS_{statistic}$ . The validation results for each individual meteorological variable analysis are presented as Supplementary Material (S2). Considering the hindcast models calibrated with ERA-Interim as the benchmark, the performance of the considered RCMs modeling BA series for the control period was generally lower, most likely due to their poor representation of daily variability (as highlighted in Section 2.3). The SW\_CLU is the only region where the ERA-Interim performance on modeling BA series is slightly overridden by the RCM models. On the contrary, the lowest RCM performance occurred in the E\_CLU. The summary of all BA models performance is summarized in Fig. S5 of the Supplementary Material.

### 4.2. Future climate scenarios in Iberia

Before projecting future BA, we assessed the predicted future climatologies for the three future 25-year periods in each domain (Tables 4–7), focusing on the meteorological variables used as predictors.

Obtained results reveal that in the northwestern sector of Iberia all models project a rise of 2–3 °C in  $T$  during the months of July and August, while the standard deviation does not undergo significant changes (Table 4). These projections imply a larger frequency of extremely hot days in the future, thus favoring larger BA. It was shown that in this pyro-region summer rainfall is also closely related to BA (Section 3.2) and all RCMs projections suggest a decrease in summer  $P$  (in most models near to 50%) during the 21st century, particularly after 2050. Likewise, the projected number of rainy days in the July–August period is projected to decrease nearly a quarter by most models except for the REGCM3, where changes in rainfall regimes are not so significant.

A similar sharp continuous increase in 12UTC July and August  $T$  is projected for the SW\_CLU (about 4 °C for the 2051–2075 period according to the HADRM3Q0 and REMO models, Table 5). Values of the standard deviation for the future  $T$  time series remain very similar to the ones found for the control period. All models except HADRM3Q0 suggest very few changes in the accumulated  $P$  during February and May (related to the available biomass in the following summer) but show a decrease in the number of rainy days, unveiling a drastic change of the precipitation regime, most accentuated in the case of the HADRM3Q0 model projections (to about one third in these months).

Concerning the N\_CLU (Table 6) and focusing on changes in late winter or early spring climatology, an increase of the mean March  $T$ , especially in the later period (2051–2075) is projected. However, for the mid-21st century most models present mean values slightly below the control period and a small increase in the standard deviation, related to an increase in the variability of meteorological conditions in this region. The exception is the HADRM3Q0 model, which projects a continuous rise in  $T$  (of about 3 °C during the whole period) and a decrease in the mean February plus March  $P$ , as well

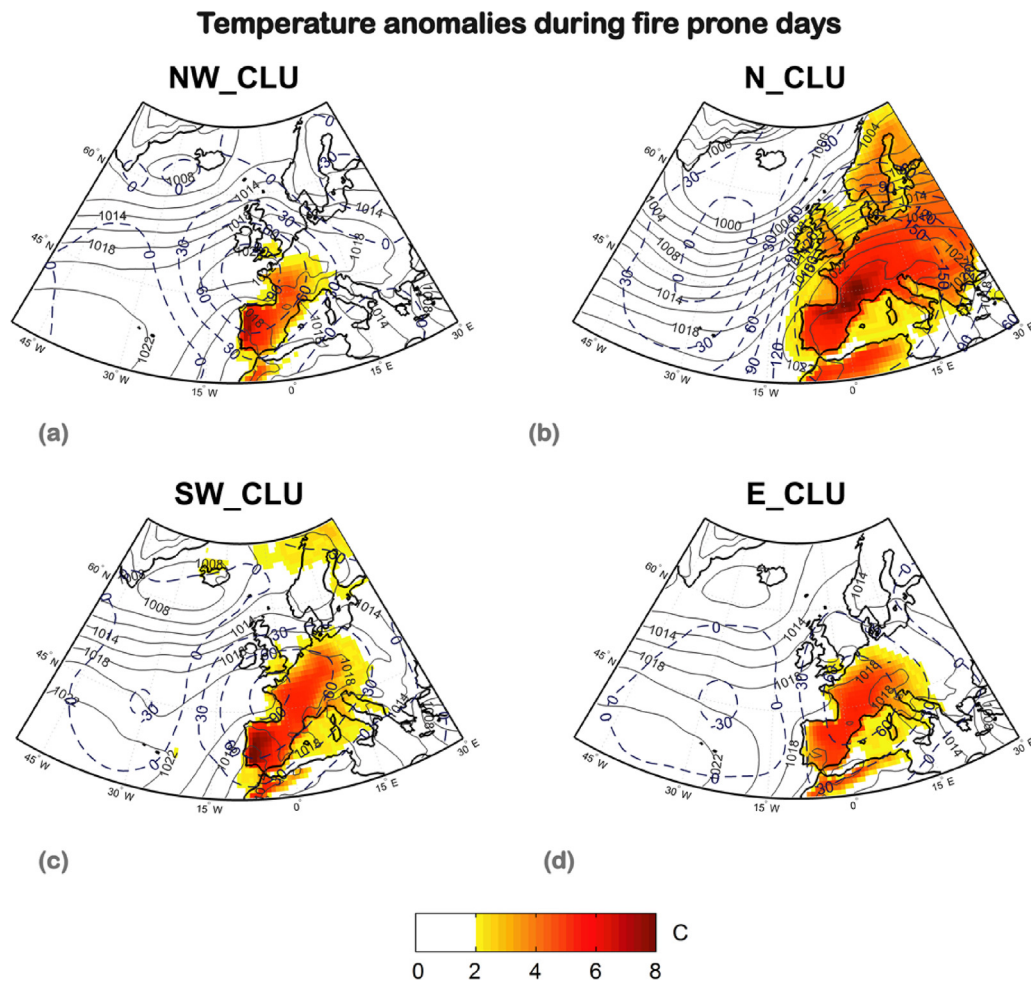


**Fig. 4.** Composites for the 12UTC 2 meter temperature anomaly (shaded), mean sea level pressure (solid lines) and geopotential height at the 500 hPa anomaly (dashed lines) for July and August days (except in the N.CLU, for February and March) where: (a) temperature exceeds the 95th percentile in the NW.CLU; (b) temperature exceeds the 90th percentile in the N.CLU; (c) temperature exceeds the 98th percentile in the SW.CLU; (d) temperature exceeds the 90th percentile in the E.CLU. Temperature anomalies are only depicted if above 2 degrees.

**Table 4**

Mean 12UTC 2m air temperature (standard deviation), and mean precipitation (number of rainy days) during July and August in the NW.CLU. First column corresponds to ERA-Interim climatology in the control period; second column shows RCMs biases during the control period; the remaining columns show corrected climatologies for future simulations in three different temporal windows, for each RCM.

NW.CLU	1981–2005 (control)	1981–2005 model bias	2001–2025	2026–2050	2051–2075	RCM
July & August mean 12UTC T2m	24.9 C (3.2)	+3.2 C (+0.9) +2.1 C (+1.8) +1.3 C (+2.1) +2.0 C (+1.4)	25.6 C (3.6) 24.6 C (3.3) 24.4 C (3.3) 24.8 C (3.4)	26.3 C (3.4) 25.0 C (3.0) 24.9 C (3.1) 25.2 C (3.0)	27.9 C (3.3) 27.3 C (3.0) 27.0 C (3.0) 27.7 C (3.2)	HADRM3Q0 RACMO2 REGCM3 REMO
July + August Precipitation	56 mm (34)	–32 mm (+2) –19 mm (–7) +8 mm (+4) +5 mm (+1)	66 mm (33) 52 mm (30) 55 mm (31) 50 mm (31)	48 mm (28) 42 mm (28) 47 mm (29) 41 mm (28)	32 mm (26) 31 mm (26) 46 mm (30) 30 mm (26)	HADRM3Q0 RACMO2 REGCM3 REMO

**Table 5**

Same as Table 4 but for the SW.CLU.

SW.CLU	1981–2005 (control)	1981–2005 model bias	2001–2025	2026–2050	2051–2075	RCM
July & August mean 12UTC T2m	28.4 C (3.2)	+5.6 C (0.0) +2.0 C (+0.4) +2.5 C (+0.4) +3.2 C (+0.2)	29.8 C (3.3) 29.3 C (3.4) 29.1 C (3.4) 29.5 C (3.4)	31.0 C (3.6) 30.3 C (3.0) 30.3 C (3.1) 30.5 C (3.1)	32.5 C (3.3) 32.3 C (3.1) 32.0 C (3.2) 32.6 C (3.2)	HADRM3Q0 RACMO2 REGCM3 REMO
February + May Precipitation	86 mm (39)	+21 mm (+3) +36 mm (+3) +45 mm (+7) +46 mm (+3)	70 mm (34) 82 mm (34) 85 mm (34) 85 mm (34)	67 mm (33) 78 mm (34) 76 mm (32) 80 mm (35)	59 mm (31) 84 mm (33) 81 mm (33) 82 mm (34)	HADRM3Q0 RACMO2 REGCM3 REMO

**Table 6**

Same as Table 4 but for the N.CLU and during the month of March.

N.CLU	1981–2005 (control)	1981–2005 model bias	2001–2025	2026–2050	2051–2075	RCM
March mean 12UTC T2m	11.5 C (3.5)	–0.9 C (+0.5) –1.9 C (–0.1) –1.9 C (3.8) –0.5 C (3.7)	11.8 C (3.4) 11.8 C (3.8) 11.9 C (3.8) 12.1 C (3.8)	13.1 C (3.4) 11.4 C (3.8) 11.3 C (3.7) 11.4 C (3.7)	14.3 C (3.5) 13.2 C (4.2) 12.9 C (3.9) 13.2 C (3.9)	HADRM3Q0 RACMO2 REGCM3 REMO
February + March Precipitation	113 mm (41)	+89 mm (+7) +134 mm (+12) +151 mm (+11) +125 mm (+9)	114 mm (39) 114 mm (37) 116 mm (37) 115 mm (36)	107 mm (38) 120 mm (39) 121 mm (40) 125 mm (38)	99 mm (37) 121 mm (38) 123 mm (38) 126 mm (37)	HADRM3Q0 RACMO2 REGCM3 REMO

as on the number of rainy days. On the contrary, the HADRM3Q0 model is the only to predict a decrease in  $P$  along with the steep rise in  $T$  in this region of Iberia.

Finally, for the E.CLU (Table 7), all RCMs project a continuous rise in  $T$ . The HADRM3Q0 model shows an increase larger than  $4^{\circ}\text{C}$ , projecting the most accentuated warming trend in Iberia among all models analyzed. As in the other cases, no significant changes are expected for  $T$  standard deviation. The number of rainy days is expected to decrease according to all model simulations. HADRM3Q0's projections of mean  $P$  are almost 50% lower than for the control period, with an also remarkable decrease in the number of rainy days (from 37 to 26). The REGCM3 is the only model that presents a small increase (2 mm) in mean  $P$ , but once again, with precipitation regimes being less regular, as the number of rainy days also decreases (8–14%).

#### 4.3. Modeling future fire regimes

Both BC and DCM correction methods were applied to each RCM and pyro-region in order to construct future  $BA$  series. One further experiment was performed to increase the number of tested future scenarios, consisting in two different methods of estimating the future predictors: (1) they all are calculated against the fixed 1981–2005 means and percentiles; (2) they are calculated against each correspondent previous 25-year period means and percentiles. Naturally, the first method (hereafter, FIX.CLIM) will result in more drastic trends in future  $BA$  series, while the second method (hereafter, MOV.CLIM) will tend to ease those trends. This second approach was considered just as a simplistic way to emulate a certain level of gradual adaptation to climatic changes, rather than assuming that all other non-meteorological variables related with fires (vegetation dynamics, human factors, etc.) will remain unchanged, as a result of the FIX.CLIM approach.

The relative changes in the mean  $BA$  estimated for each cluster after BC (Fig. 5) or the DCM (Fig. 6) are represented by circular areas, where inner and outer radius correspond to the two predictor estimation methods (MOV.CLIM and FIX.CLIM, respectively). These changes in future  $BA$  series are framed over axes that represent  $T$  and  $P$  changes during the simulation period, in order to facilitate their interpretation. The discussion of the obtained results will be focused mainly on the models which presented better scores in reproducing  $BA$  series distribution in the control period.

**Table 7**

Same as Table 4 but for the E.CLU.

E.CLU	1981–2005 (control)	1981–2005 model bias	2001–2025	2026–2050	2051–2075	RCM
July & August mean 12UTC T2m	27.6 C (2.5)	+4.1 C (+0.8) +0.2 C (+0.6) –0.7 C (+0.7) +1.5 C (+0.4)	29.0 C (2.6) 28.4 C (2.7) 28.3 C (2.6) 28.6 C (2.7)	30.4 C (2.9) 29.4 C (2.5) 29.2 C (2.5) 29.4 C (2.5)	32.0 C (2.6) 31.2 C (2.5) 30.7 C (2.5) 31.4 C (2.4)	HADRM3Q0 RACMO2 REGCM3 REMO
July + August Precipitation	37 mm (37)	+6 mm (+15) +0 mm (+1) +56 mm (+20) +24 mm (+9)	32 mm (31) 38 mm (33) 38 mm (34) 35 mm (32)	30 mm (26) 31 mm (31) 34 mm (32) 28 mm (30)	23 mm (26) 29 mm (30) 39 mm (32) 24 mm (29)	HADRM3Q0 RACMO2 REGCM3 REMO

All models and methods reveal positive trends in future  $BA$  in all regions, but the dispersion amongst projections is quite significant. As expected, results obtained with the FIX.CLIM and MOV.CLIM methods have important differences, with the latter presenting lower changes in future mean  $BA$ . We must recall that the projections in Fig. 5 reflect the intrinsic daily variability of the RCM, reducing the confidence of model behavior for future scenarios.

In fact, in the NW.CLU the projected negative change in  $P$  and positive change  $T$  during summer results in a significant increase in mean  $BA$  series. For example, considering the HADRM3Q0 and REMO models and the FIX.CLIM simulations, estimated relative changes are above 500% (which corresponds to a trend of about  $3800\text{ ha year}^{-1}$ ) and  $400\%$  (about  $2800\text{ ha year}^{-1}$ ), respectively. The trends in the MOV.CLIM simulations for these same models are reduced to less than half, but still more than doubling the present mean annual  $BA$ . For the N.CLU the rises in  $T$  drive important positive changes in  $BA$ , albeit the slight increase in  $P$  projected by most models. The RCM which performed better for this region in the control period (REGCM3) still projects four times more  $BA$  at the end of the considered future period ( $300\text{ ha year}^{-1}$  trend) using the BC. In the SW.CLU, where RCM models performed slightly better than ERA-Interim during the control period, relatively similar trends in future  $BA$  were found. Using FIX.CLIM simulations the relative changes range between  $400\%$  and  $600\%$  ( $3500\text{--}4500\text{ ha year}^{-1}$ ), while using the MOV.CLIM simulations these trends decrease drastically to one third. Finally, in the E.CLU, we found comparable trends amongst all models except the HADRM3Q0, which yielded wildly large results ( $500\%$  and  $1000\%$ ), which seem unreliable in the light of the results presented in Section 4.1. The  $BA$  relative changes projected by the RACMO2 range between  $250\%$  and  $350\%$  (ca.  $850\text{ ha year}^{-1}$  and  $1300\text{ ha year}^{-1}$ ).

Projected  $BA$  changes obtained with the DCM correction method using FIX.CLIM and MOV.CLIM experiments are more moderate than in the case of BC. In the NW.CLU, the HADRM3Q0 model projects  $BA$  changes ranging between  $300\%$  and  $400\%$  ( $1500\text{--}2500\text{ ha year}^{-1}$  trends), while the REMO projects slightly higher changes. In the N.CLU, projections of  $BA$  using HADRM3Q0 model simulations are very high and quite different from all other models which present relative changes smaller than  $250\%$  (around  $140\text{ ha year}^{-1}$ ). We must recall that the HADRM3Q0 model stands alone by projecting a decrease in the mean February and March  $P$  in this region, associated to a more significant rise in late winter  $T$

## BA projections using the unbiasing method

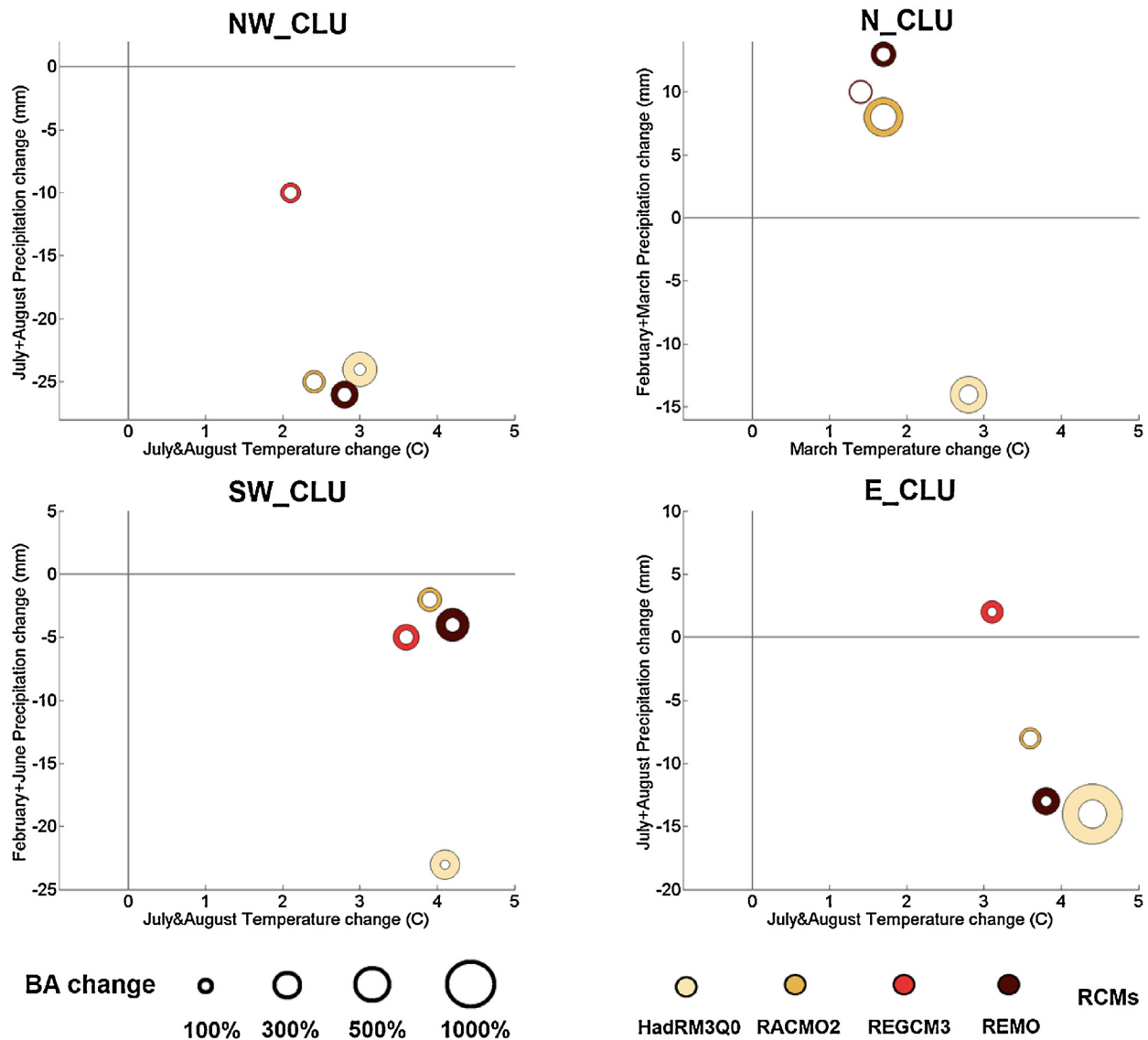


**Fig. 5.** Mean Burnt Area (BA) relative change throughout 1981–2075 in the four considered Iberian clusters using the unbiasing method, and their dependence on the temperature (x-axis) and precipitation (y-axis) changes, during the same period. Different colors represent simulations from different RCMs, and the radius of the circles represents the BA trend magnitudes – outer circle corresponds to FIX.CLIM simulations (1981–2005 fixed benchmark climatology) and inner circle corresponds to MOV.CLIM simulations (time-moving benchmark climatology).

than the other RCMs. In the SW.CLU, quite stable trends of about 400% and 500% were found when using the FIX.CLIM simulations, with a smaller decrease being found for the MOV.CLIM simulations (about half of the relative change projected with FIX.CLIM). In the E.CLU, the significant rise in summer *T* associated with an important decrease in summer *P* and number of rainy days (see Section 5.2) may explain the dramatic rate of change projected for *BA*, even using the MOV.CLIM simulations. For example, *BA* projections with RACMO2 outputs range between 500% and 800%, while with REMO are between 700% and 900%. A change of 900% would correspond to a trend of around  $3600 \text{ ha year}^{-1}$ . These discrepancies found in different scenarios, along with the inherent difficulty of constructing a statistical model due to the presence of a significant break-point in the control period *BA* series raises major doubts on the its robustness, so the results for this pyro-region should be looked cautiously.

Having such a large range of projected future scenarios, we decided to construct ensemble series for each cluster. This enables

us not only to summarize the expected trends in each region, but also to quantify the dispersion amongst projections. A total of eight projected members for each cluster were considered as a result of using four RCMs and two bias correction procedures. The FIX.CLIM and MOV.CLIM simulations were considered separately by the two different shadings in each panel of Fig. 7, having each one of these simulations 8 members, as stated before.

The clearest outcome from these ensembles is the obvious tendency of increment in mean annual *BA* in all Iberian regions, regardless of the used methodology. As referred before, a more sharp increase is found when future climatology is compared directly against the control period (1981–2005). Comparing future climatologies with moving reference states (lighter shades) naturally brings a certain degree of relieve on the projected *BA* scenarios. The Atlantic sector clusters (NW.CLU and SW.CLU) clearly present a smaller dispersion amongst projections, a detail which is not particularly surprising. In fact, since the first stages of the construction

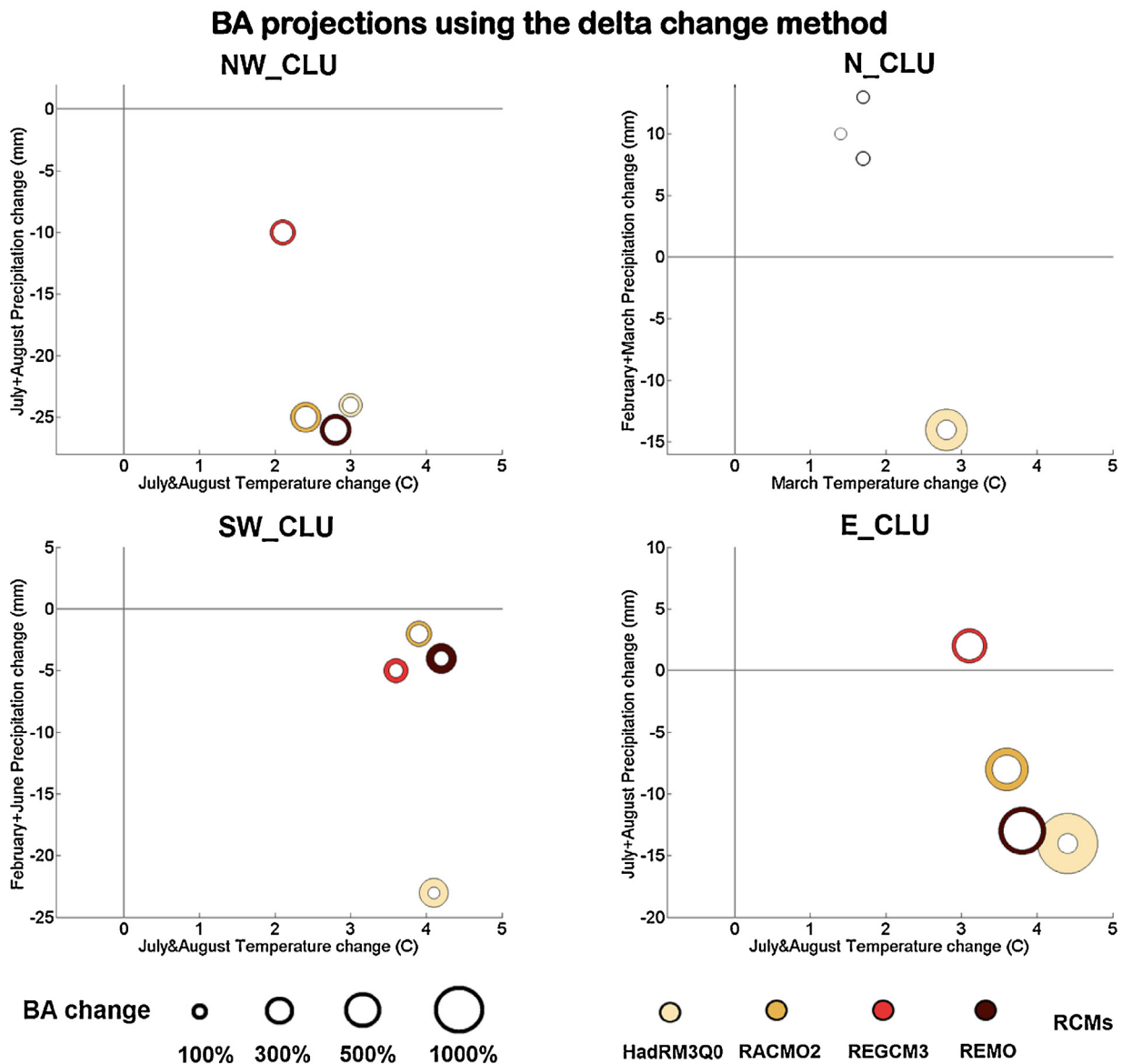


Fig. 6. Same as Fig. 5, but using the delta change method for future trends estimation.

of these statistical models, it was evident that meteorology alone explained a larger part of the BA variability in these western clusters. Consequently, the higher level of uncertainty found for future BA projections in the N\_CLU and E\_CLU is also not unforeseen. The large dispersion found in the upper part of the E\_CLU and N\_CLU is driven by the HADRM3Q0 model, which presents the highest rises in mean  $T$  in almost all areas, and also is the only model which predicts a decrease in February and March  $P$  in northernmost areas.

Even though it is clear that different approaches result in a relatively wide range of severity scenarios, the overall ensemble means point to about 2 or 3 three times more BA in most Iberian regions, except for the northern façade where the mean projections change fall slightly above a doubling factor.

## 5. Concluding remarks

Our work has shown that statistical models which use monthly frequencies of exceedances of high percentiles of noon temperature (from the ERA-Interim dataset) as the key predictor can be quite effective in representing the inter-annual variability of burnt area (explaining more than two thirds of the variance in most areas).

This is a concise method to represent the most propitious conditions for fire ignition and spread – sequences of abnormally hot and dry days. Furthermore, these models recall the need to rely on daily scale data in order to account for these short temporal scale features, although larger time-scales prove to be sufficient regarding the meteorological background. These results are particularly compelling for western areas of Iberia, where meteorology alone is more crucial on wildfire activity (Trigo et al., 2013), while in other areas external factors have a larger weight (Bedia et al., 2014).

The role of atmospheric blocking on wildfire variability (Trigo et al., 2006) was scrutinized in each pyro-region, and our composites show that the specific locations of high pressure anomaly centers establish the direction of surface flows, thus distinguishing the synoptics that originate inland dry and warm air advection in each domain. In addition, the occurrence of a meteorological background marked by prolonged blocking events is directly related with a higher vegetation stress that arises from prolonged dry spells (Flannigan et al., 2000; Gedalof et al., 2005; Soja et al., 2007).

Future fire regime projections based on GCM or RCM outputs must be carefully considered, as besides the inherent model

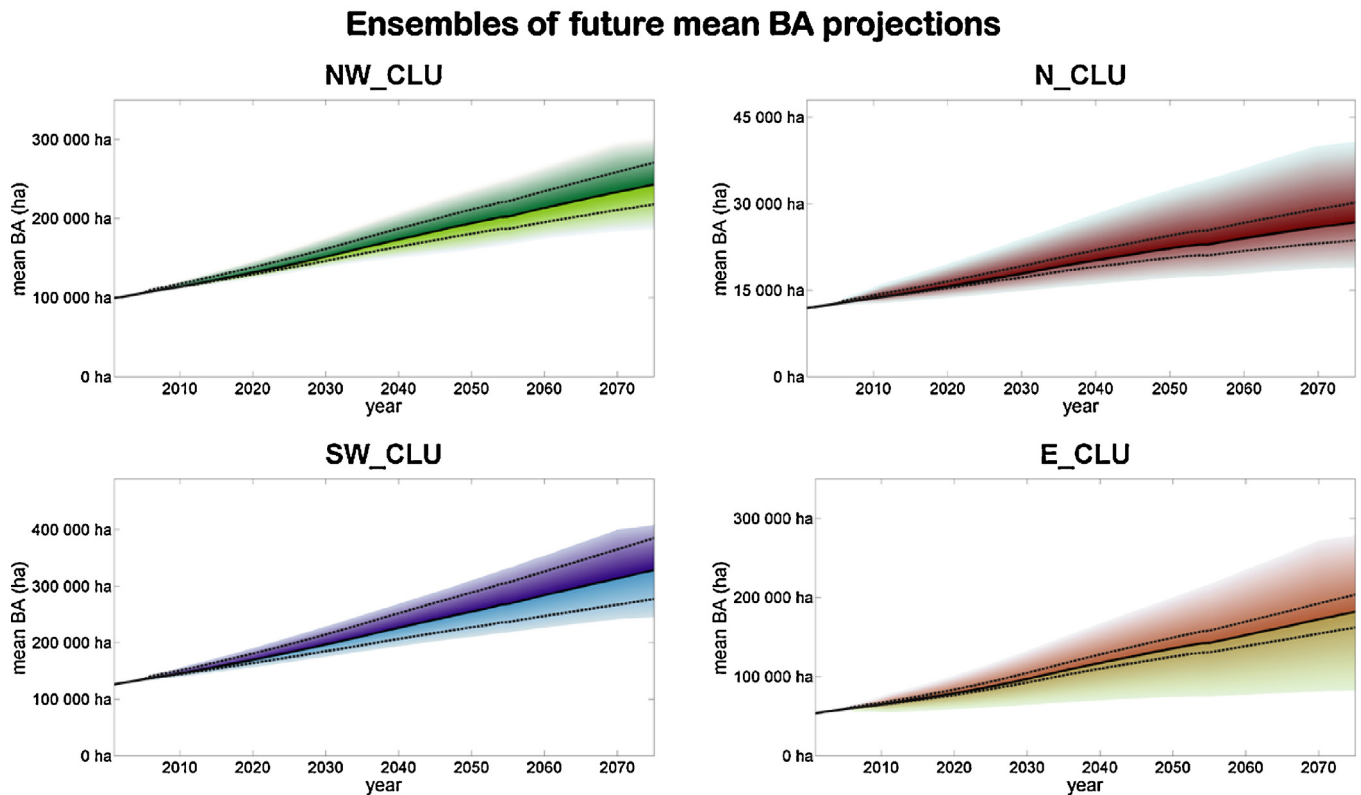


**Fig. 7.** Ensembles of projected mean Burnt Area (BA) until 2075 in the four Iberian clusters. The solid line represents the mean of all 16 considered members of the simulations presented in Figs. 5 and 6. The above dashed line represents the mean of the 8 FIX.CLIM simulations, while the below shaded line represents the mean of the 8 MOV.CLIM simulations. Darker (lighter) shades represent ensemble uncertainties of FIX.CLIM (MOV.CLIM) simulations, and where obtained using the inter-quartiles of each group of simulations. A 25-year moving average was applied to all series.

uncertainties and projections spread, other confounding factors exist (mainly anthropogenic, see e.g. King et al., 2013), and also climate-vegetation feedbacks affecting burned area should be considered (e.g. Krawchuk and Moritz, 2010; Pausas and Paula, 2012). Furthermore, the extent of the feedback on the concentration of aerosols, particulates and black carbon induced by an increased spatial and temporal frequency of wildfires is a quite significant issue, particularly on the perturbations which should be considered on climate models (Lavoué et al., 2000; Gillett et al., 2004; Randerson et al., 2006; Hodzic et al., 2007; Sommers et al., 2014). Nevertheless, the RCMs performance during our control period gave us enough confidence to extrapolate them to a warmer period, such as expected in the upcoming decades. All our future projections point toward a significant rise in mean annual BA in all pyro-regions - ensembles future means between 200% and 300% by 2075. Carvalho et al. (2007) predicted a much larger increase (near 500%) in BA for mainland Portugal by the end of the 21st century. Such differences highlight the crucial importance of how the intrinsic daily variability in RCMs is managed when constructing future scenarios. We feel confident that the delta change method results as a good and simple alternative to the more conventional unbiased method in order to circumvent the inaccurate representation of current climate in RCMs, namely at the daily scale. However, since the nature of daily variability will also change in the future, no correction method can completely avoid this problem.

It is evident that as further away from the present climate we try to extrapolate, the more weight external factors will have. Surely at some point prior to 2075 the influence of these external factors will overtake the validity of present time models purely based on meteorology. In particular, we stress that the incorporation of land-use change models in this type of simulations may be a determinant factor for extending the validity and confidence of extrapolations

based on model projections, as already discussed by Moss et al. (2010) and Brovkin et al. (2013). In conclusion, as any other projections based on RCM data, these trends should be envisaged carefully, and seen as a tendency based on the current state of fire prevention, forest management, and projected climate scenarios. In fact, the main lesson to take from such alarming projections is the urge for preparing and mitigating changes that seem inevitable in terms of climate and environment, as current state-of-the-art modeling insists in warming and drying trends in the Mediterranean, and particularly on the Iberian Peninsula (MARN, 2006; AEMET-IM, 2011; Ramos et al., 2011; Gouveia et al., 2011).

### Conflicts of interests

The authors have no conflict of interest to declare.

### Acknowledgements

Pedro M. Sousa was supported by *Fundação para a Ciência e a Tecnologia* (FCT) through a doctoral grant (SFRH/BD/84395/2012). We would like to acknowledge the FIRE-MODSAT project (EXPL/AGR-FOR/0488/2013) for providing background information on the context of the Portuguese wildfires. Mario Gonzalez Pereira was supported by national funds by FCT - Portuguese Foundation for Science and Technology, under the project PEst-OE/AGR/UI4033/2014.

### Appendix A. Supplementary data

Supplementary data associated with this article can be found, in the online version, at <http://dx.doi.org/10.1016/j.agrformet.2014.11.018>.

## References

- Agencia Estatal de Meteorología (AEMET-IM), 2011. Atlas climático de España y Portugal, <http://www.aemet.es/serviciosclimaticos/datosclimaticos/atlas.climatico>
- Alin, A., 2010. Multicollinearity. *Wiley Interdiscip. Rev. Comput. Stat.* 2 (3), 370–374, <http://dx.doi.org/10.1002/wics.84>.
- Amatulli, G., Camia, A., San-Miguel-Ayaz, J., 2013. Estimating future burned areas under changing climate in the EU-Mediterranean countries. *Sci. Total Environ.* 450–451, 209–222, <http://dx.doi.org/10.1016/j.scitotenv.2013.02.014>.
- Argüeso, D., Hidalgo-Muñoz, J.M., Gámiz-Fortis, S.R., 2012. High-resolution projections of mean and extreme precipitation over Spain using the WRF model (2070–2099 versus 1970–1999). *J. Geophys. Res. D: Atmos.* 117, D12108, <http://dx.doi.org/10.1029/2011JD017399>.
- Barriopedro, D., Fisher, E., Luterbacher, J., Trigo, R.M., García-Herrera, R., 2011. The hot summer of 2010: redrawing the temperature record map of Europe. *Science* 322, 220, <http://dx.doi.org/10.1126/science.1201224>.
- Bedia, J., Herrera, S., Gutiérrez, J.M., Zavala, G., Urbieto, I.R., Moreno, J.M., 2012. Sensitivity of fire weather index to different reanalysis products in the Iberian Peninsula. *Nat. Hazards Earth Syst. Sci.* 12, 699–708, doi:10.5194/nhess-12-699-2012.
- Bedia, J., Herrera, S., Martín, D.S., Koutsias, N., Gutiérrez, J.M., 2013. Robust projections of Fire Weather Index in the Mediterranean using statistical downscaling. *Clim. Change* 120, 229–247, <http://dx.doi.org/10.1007/s10584-013-0787-3>.
- Bedia, J., Herrera, S., Camia, A., Moreno, J.M., Gutierrez, J.M., 2014. Forest fire danger projections in the Mediterranean using ENSEMBLES regional climate change scenarios. *Clim. Change* 122, 185–199, <http://dx.doi.org/10.1007/s10584-013-1005-z>.
- Brands, S., Taboada, J.J., Cofiño, A.S., Sauter, T., Schneider, C., 2011. Statistical downscaling of daily temperatures in the NW Iberian Peninsula from global climate models: validation and future scenarios. *Clim. Res.* 48, 163–176, <http://dx.doi.org/10.3354/cr00906>.
- Brands, S., Gutiérrez, J.M., Herrera, S., Cofiño, A.S., 2012. On the use of reanalysis data for downscaling. *J. Clim.* 25 (7), 2517–2526.
- Brovkin, V., Boysen, L., Arora, V.K., Boisier, J.P., Cadule, P., Chini, L., Claussen, C., Friedlingstein, P., Gayler, V., van den Hurk, B.J.J.M., Hurrett, G.C., Jones, C.D., Kato, E., Noblet-Ducoudré, N., Pacifico, F., Pongratz, J., Weiss, M., 2013. Effect of anthropogenic land-use and land-cover changes on climate and land carbon storage in CMIP5 projections for the twenty-first century. *J. Clim.* 26 (18), 6859–6881.
- Carvalho, A., Flannigan, M.D., Logan, K., Gowman, L.M., Miranda, A.I., Borrego, C., 2007. The impact of spatial resolution on area burned and fire occurrence projections in Portugal under climate change. *Clim. Change* 98, 177–197, <http://dx.doi.org/10.1007/s10584-009-9667-2>.
- Christensen, J., Boberg, F., Christensen, O., Lucas-Picher, P., 2008. On the need for bias correction of regional climate change projections of temperature and precipitation. *Geophys. Res. Lett.* 35, L20709, <http://dx.doi.org/10.1029/2008GL035694>.
- Chuvieco, E., Deshayes, M., Stach, N., Cocero, D., Riaño, D., 1999. Short-term fire risk: foliage moisture content estimation from satellite data. In: Chuvieco, E. (Ed.), *Remote Sensing of Large Wildfires in the European Mediterranean Basin*. Springer (University of Alcalá, Spain), Berlin, p. 228.
- Costa, L., Thonicke, K., Poulter, B., Badek, F.W., 2010. Sensitivity of Portuguese forest fires to climatic, human, and landscape variables: subnational differences between fire drivers in extreme fire years and decadal averages. *Reg. Environ. Change* 11 (3), 543–551, <http://dx.doi.org/10.1007/s10113-010-0169-6>.
- Dee, D., National Center for Atmospheric Research Staff, 2011. The Climate Data Guide: ERA-Interim, Available at: <https://climatedataguide.ucar.edu/reanalysis/era-interim>
- Déqué, M., 2007. Frequency of precipitation and temperature extremes over France in an anthropogenic scenario: model results and statistical correction according to observed values. *Glob. Plan. Change* 57, 16–26, <http://dx.doi.org/10.1016/j.gloplacha.2006.11.030>.
- de la Cueva, A.V., del Barrio, J.M.G., Quero, M.O., Palomares, O.S., 2006. Recent fire regime in peninsular Spain in relation to forest potential productivity and population density. *Int. J. Wildland Fire* 15, 397–405, <http://dx.doi.org/10.1071/WF05071>.
- Ehret, U., Zehe, E., Wulfmeyer, V., Warrach-Sagi, K., Liebert, J., 2012. HESS opinions should we apply bias correction to global and regional climate model data? *Hydrol. Earth Syst. Sci. Discuss.* 9 (4), 5355–5387, <http://dx.doi.org/10.5194/hess-16-3391-2012>.
- Flannigan, M.D., Stocks, B.J., Wotton, B.M., 2000. Climate change and forest fires. *Sci. Total Environ.* 262 (3), 221–229, [http://dx.doi.org/10.1016/S0048-9697\(00\)00524-6](http://dx.doi.org/10.1016/S0048-9697(00)00524-6).
- Flannigan, M., Cantin, A.S., de Groot, W.J., Wotton, M., Newbery, A., Gowman, L.M., 2013. Global wildland fire season severity in the 21st century. *For. Ecol. Manag.* 294, 54–61, <http://dx.doi.org/10.1016/j.foreco.2012.10.022>.
- Friás, M.D., Miguez, R., Gutierrez, J.M., Mendez, F.J., 2012. Future regional projections of extreme temperatures in Europe: a nonstationary seasonal approach. *Clim. Change* 113, 371–392, <http://dx.doi.org/10.1007/s10584-011-0351-y>.
- García-Herrera, R., Paredes, D., Trigo, R.M., Trigo, I.F., Hernández, H., Barriopedro, D., Mendes, M.T., 2007. The outstanding 2004–2005 drought in the Iberian Peninsula: associated atmospheric circulation. *J. Hydrometeorol.* 8, 483–498, <http://dx.doi.org/10.1175/JHM578.1>.
- García-Herrera, R., Díaz, J., Trigo, R.M., Luterbacher, J., Fisher, E., 2010. A review of the European summer heat wave of 2003. *Crit. Rev. Environ. Sci. Technol.* 40, 267–306, <http://dx.doi.org/10.1080/1064338080238137>.
- Garg, A., Tai, K., 2012. Comparison of regression analysis, Artificial Neural Network and genetic programming in Handling the multicollinearity problem. In: *Proceedings of International Conference on Modelling, Identification & Control (ICMIC)*. IEEE, pp. 353–358.
- Gedalof, Z.E., Peterson, D.L., Mantua, N.J., 2005. Atmospheric, climatic, and ecological controls on extreme wildfire years in the northwestern United States. *Ecol. Appl.* 15 (1), 154–174, <http://dx.doi.org/10.1890/03-5116>.
- Gillett, N.P., Weaver, A.J., Zwiers, F.W., Flannigan, M.D., 2004. Detecting the effect of climate change on Canadian forest fires. *Geophys. Res. Lett.* 31, 18.
- Giorgi, F., Lionello, P., 2008. Climate change projections for the Mediterranean region. *Glob. Planet. Change* 63, 90–104.
- Gouveia, C., Liberato, M.L.R., DaCamara, C.C., Trigo, R.M., 2011. Modelling past and future wine production in the Portuguese Douro Valley. *Clim. Res.* 48, 349–362, <http://dx.doi.org/10.3354/cr01006>.
- Gouveia, C.M., Bastos, A., Trigo, R.M., DaCamara, 2012. Drought impacts on vegetation in the pre- and post-fire events over Iberian Peninsula. *Nat. Hazards Earth Syst. Sci.* 12, 3123–3137, <http://dx.doi.org/10.5194/nhess-12-3123-2012>.
- Gutiérrez, J.M., San-Martin, D., Brands, S., Manzanar, R., Herrera, S., 2012. Reassessing statistical downscaling techniques for their robust application under climate change conditions. *J. Clim.* 26 (1), 171–188, <http://dx.doi.org/10.1175/JCLI-D-11-00687.1>.
- Herrera, S., Fita, L., Fernández, J., Gutiérrez, J.M., 2010. Evaluation of the mean and extreme precipitation regimes from the ENSEMBLES regional climate multi-model simulations over Spain. *J. Geophys. Res.* 115, D21, <http://dx.doi.org/10.1029/2010JD013936>.
- Hawkins, D.M., 2004. The problem of overfitting. *J. Chem. Inf. Comput. Sci.* 44 (1), 1–12, <http://dx.doi.org/10.1021/ci0342472>.
- Hawkins, E.D., Osborne, T.M., Ho, C.K., Challinor, A.J., 2013. Calibration and bias correction of climate projections for crop modelling: an idealised case study over Europe. *Agric. For. Meteorol.* 170, 19, <http://dx.doi.org/10.1016/j.agrformet.2012.04.007>.
- Hodžić, A., Madronich, S., Bohn, B., Massie, S., Menut, L., Wiedinmyer, C., 2007. Wildfire particulate matter in Europe during summer 2003: meso-scale modeling of smoke emissions, transport and radiative effects. *Atmos. Chem. Phys.* 7 (15), 4043–4064.
- Huntingford, C., Stott, P.A., Allen, M.R., Lambert, F.H., 2006. Incorporating model uncertainty into attribution of observed temperature change. *Geophys. Res. Lett.* 33 (5), L05710, <http://dx.doi.org/10.1029/2005GL024831>.
- Hurvich, C.M., Tsai, C.L., 1989. Regression and time series model selection in small samples. *Biometrika* 76 (2), 297–307, <http://dx.doi.org/10.1093/biomet/76.2.297>.
- Ines, A.V.M., Hansen, J.W., 2006. Bias correction of daily GCM rainfall for crop simulation studies. *Agric. For. Meteorol.* 138, 44–53, <http://dx.doi.org/10.1016/j.agrformet.2006.03.009>.
- King, K.J., Cary, G.J., Bradstock, R.A., Marsden-Smedley, J.B., 2013. Contrasting fire responses to climate and management: insights from two Australian ecosystems. *Glob. Change Biol.* 19 (4), 1223–1235, <http://dx.doi.org/10.1111/gcb.12115>.
- Koutsias, N., Xanthopoulos, G., Founda, D., Xystrakis, F., Nioti, F., Pleniou, M., Mallinis, G., Arianoutsou, M., 2013. On the relationships between forest fires and weather conditions in Greece from long-term national observations (1894–2010). *Int. J. Wildland Fire* 22, 493–507.
- Krawchuk, M.A., Moritz, M.A., 2010. Constraints on global fire activity vary across a resource gradient. *Ecology* 92, 121–132, <http://dx.doi.org/10.1890/09-1843.1>.
- Kraha, A., Turner, H., Nimon, K., Zientek, L.R., Henson, R.K., 2012. Tools to support interpreting multiple regression in the face of multicollinearity. *Front. Psychol.* 3 (44), <http://dx.doi.org/10.3389/fpsyg.2012.00044>.
- Kishore, P., Ratnam, M.V., Namboothiri, S.P., Velicogna, I., Basha, G., Jiang, J.H., Igarashi, K., Rao, S.V.B., Sivakumar, V., 2011. Global (50°S–50°N) distribution of water vapor observed by COSMIC GPS RO: Comparison with GPS radiosonde, NCEP, ERA-Interim, and JRA-25 reanalysis data sets. *J. Atmos. Solar Terr. Phys.* 73 (13), 1849–1860, <http://dx.doi.org/10.1016/j.jastp.2011.04.017>, ISSN 1364-6826.
- Lavoué, D., Lioussé, C., Cachier, H., Stocks, B.J., Goldammer, J.G., 2000. Modeling of carbonaceous particles emitted by boreal and temperate wildfires at northern latitudes. *J. Geophys. Res.: Atmos.* (1984–2012) 105 (D22), 26871–26890.
- Maule, C.F., Thejll, P., Christensen, J.H., Svendsen, S.H., Hannafor, J., 2013. Improved confidence in regional climate model simulations of precipitation evaluated using drought statistics from the ENSEMBLES models. *Clim. Dyn.* 40 (1–2), 155–173, <http://dx.doi.org/10.1007/s00382-012-1355-7>.
- Ministerio de Medio Ambiente, Marino y Rural (MARN), 2006. Los incendios forestales en España decenio 1996–2005 (<http://www.marm.es/biodiversidad/temas/defensa-contra-incendios-forestales/decenio.1996>).
- Mérida, J.C., Primo, E., Eleazar, J., Parra, J., 2007. Las Bases de Datos de Incendios Forestales como herramienta de planificación: utilización en España por el Ministerio de Medio Ambiente. Organismo Autónomo de Parques Nacionales, M. de M.A. (Ed.). In: *Proceedings of the 4th International Wildland Fire Conference*, Sevilla, Spain, 13–18 May [In Spanish]. <http://www.fire.uni-freiburg.de/sevilla-2007/contributions/doc/cd/SESIONES.TEMATICAS/ST4/Merida.et.al.SPAIN.DGB.pdf>
- Mooney, P.A., Mulligan, F.J., Fealy, R., 2011. Comparison of ERA-40, ERA-Interim and NCEP/NCAR reanalysis data with observed surface air temperatures over Ireland. *Int. J. Clim.* 31 (4), 545–557, <http://dx.doi.org/10.1002/joc.2098>.

- Moss, R.H., Edmonds, J.A., Hibbard, K.A., Manning, M.R., Rose, S.K., Van Vuuren, D.P., Carter, T.R., Emori, S., Kainuma, M., Kram, T., Meehl, G.A., Mitchell, J.F.B., Nakicenovic, N., Riahi, K., Smith, S.J., Stouffer, R.J., Thomson, A.M., Weyant, J.P., Wilbanks, T.J., 2010. *The next generation of scenarios for climate change research and assessment*. *Nature* 463 (7282), 747–756.
- Pausas, J.G., Fernández-Muñoz, S., 2012. Fire regime changes in the Western Mediterranean Basin: from fuel-limited to drought-driven fire regime. *Clim. Change* 110 (1–2), 215–226, <http://dx.doi.org/10.1007/s10584-011-0060-6>.
- Pausas, J.G., Paula, S., 2012. Fuel shapes the fire–climate relationship: evidence from Mediterranean ecosystems. *Glob. Ecol. Biogeogr.* 21, 1074–1082, <http://dx.doi.org/10.1111/j.1466-8238.2012.00769.x>.
- Pereira, M.G., Trigo, R.M., DaCamara, C.C., Pereira, J.M.C., Solange, M.L., 2005. Synoptic patterns associated with large summer forest fires in Portugal. *Agric. For. Meteorol.* 129, 11–25, <http://dx.doi.org/10.1016/j.agrformet.2004.12.007>.
- Pereira, M.G., Malamude, B.D., Trigo, R.M., Alves, P.I., 2011. The history and characteristics of the 1980–2005 Portuguese Rural Fire Database. *Nat. Hazards Earth Syst. Sci.* 11, 1–16, <http://dx.doi.org/10.5194/nhess-11-1-2011>.
- Pereira, M.G., Calado, T.J., DaCamara, C.C., Calheiros, T., 2013. Effects of regional climate change on rural fires in Portugal. *Clim. Res.* 57, 187–200, <http://dx.doi.org/10.3354/cr01176>.
- Randerson, J.T., Liu, H., Flanner, M.G., Chambers, S.D., Jin, Y., Hess, P.G., Pfister, G., Mack, M.C., Treseder, K.K., Welp, L.R., Chapin, F.S., Harden, J.W., Goulden, M.L., Lyons, E., Neff, J.C., Schuur, E.A.G., Zender, C.S., 2006. *The impact of boreal forest fire on climate warming*. *Science* 314 (5802), 1130–1132.
- Ramos, A., Trigo, R.M., Santo, F.E., 2011. Evolution of extreme temperatures in Portugal: reporting on recent changes and future scenarios. *Clim. Res.* 48, 177–192, <http://dx.doi.org/10.3354/cr00934>.
- Ruiter, A., 2012. Delta-change Approach for CMIP5 GCMs. Royal Netherlands Meteorological Institute – Ministry of Infrastructure and the Environment: Trainee Report, <http://www.knmi.nl/bibliotheek/stageverslagen/trainee-report-Ruiter.pdf>.
- San-Miguel-Ayanz, J., Moreno, J.M., Camia, A., 2013. Analysis of large fires in European Mediterranean landscapes: lessons learned and perspectives. *For. Ecol. Manag.* 294, 11–22, <http://dx.doi.org/10.1016/j.foreco.2012.10.050>.
- Shimazaki, H., Shinomoto, S., 2007. A method for selecting the bin size of a time histogram. *Neural Comput.* 19, 1503–1527, <http://dx.doi.org/10.1162/neco.2007.19.6.1503>.
- Soares, P.M., Cardoso, M.R., Miranda, P.M., Viterbo, P., Belo-Pereira, M., 2012. Assessment of the ENSEMBLES regional climate models in the representation of precipitation variability and extremes over Portugal. *J. Geophys. Res. D: Atmos.* 117, D07114, <http://dx.doi.org/10.1029/2011JD016768>.
- Soja, A.J., Tchekakova, N.M., French, N.H., Flannigan, M.D., Shugart, H.H., Stocks, B.J., Sukhinin, A.I., Parfenova, E.I., Chapin, F.S., Stackhouse, P.W., 2007. Climate-induced boreal forest change: predictions versus current observations. *Glob. Planet. Change* 56 (3), 274–296, <http://dx.doi.org/10.1016/j.gloplacha.2006.07.028>.
- Sommers, W.T., Loehman, R.A., Hardy, C.C., 2014. *Wildland fire emissions, carbon, and climate: science overview and knowledge needs*. *For. Ecol. Manag.* 317, 1–8.
- Sousa, P.M., Trigo, R.M., Aizpurua, P., Nieto, R., Gimeno, L., Garcia-Herrera, R., 2011. Trends and extremes of drought indices throughout the 20th century in the Mediterranean. *Nat. Hazards Earth Syst. Sci.* 11 (1), 33–51, <http://dx.doi.org/10.5194/nhess-11-33-2011>.
- Trigo, R.M., García-Herrera, R., Díaz, J., Trigo, I.F., Valente, M.A., 2005. How exceptional was the early August 2003 heatwave in France? *Geophys. Res. Lett.* 32, L10701, <http://dx.doi.org/10.1029/2005GL022410>.
- Trigo, R.M., Pereira, J.M.C., Pereira, M.G., Mota, B., Calado, M.T., DaCamara, C.C., Santo, F.E., 2006. Atmospheric conditions associated with the exceptional fire season of 2003 in Portugal. *Int. J. Clim.* 26 (13), 1741–1757, <http://dx.doi.org/10.1002/joc.1333>.
- Trigo, R.M., Sousa, P., Pereira, M.G., Rasilla, D., Gouveia, C.M., 2013. Modeling wildfire activity in Iberia with different atmospheric circulation weather types. *Int. J. Clim.*, <http://dx.doi.org/10.1002/joc.3749>.
- Turco, M., Llasat, M.C., Tudela, A., Castro, X., Provenzale, A., 2013. Decreasing fires in a Mediterranean region (1970–2010, NE Spain). *Nat. Hazards Earth Syst. Sci.* 13, 649–652, <http://dx.doi.org/10.5194/nhess-13-649-2013>.
- Turco, M., Sanna, A., Herrera, S., Llasat, M.C., Gutiérrez, J.M., 2013b. *Large biases and inconsistent climate change signals in ENSEMBLES regional projections*. *Clim. Change* 120 (4), 859–869.
- Teutschbein, C., Seibert, J., 2012. Bias correction of regional climate model simulations for hydrological climate-change impact studies: review and evaluation of different methods. *J. Hydrol.* 456, 12–29, <http://dx.doi.org/10.1016/j.jhydrol.2012.05.052>.
- van der Linden, P., Mitchell, J., 2009. *ENSEMBLES: Climate change and its impacts: Summary of research and results from the ENSEMBLES project*, report. Met Off. Hadley Cent., 160, Exeter, 1012 UK.
- Wilks, D.S., 2011. *Statistical Methods in the Atmospheric Sciences*, vol. 100. Academic Press, USA.



# Modelling wildfire activity in Iberia with different atmospheric circulation weather types

Ricardo M. Trigo,<sup>a,b\*</sup> Pedro M. Sousa,<sup>a</sup> Mário G. Pereira,<sup>c,a</sup> Domingo Rasilla<sup>d</sup> and Célia M. Gouveia<sup>a</sup>

<sup>a</sup> IDL, University of Lisbon, Lisbon, Portugal

<sup>b</sup> Departamento de Engenharias, Universidade Lusófona, Lisboa, Portugal

<sup>c</sup> Centro de Investigação e de Tecnologias Agro-Ambientais e Biológicas (CITAB), Universidade de Trás-os-Montes e Alto Douro, Vila Real, Portugal

<sup>d</sup> GIMENA, Departamento de Geografía, Urbanismo y OT, Universidad de Cantabria, Santander, Spain

**ABSTRACT:** This work focuses on the spatial and temporal variability of burnt area (BA) in the entire Iberian Peninsula (IP) and on the construction of statistical models to reproduce the inter-annual variability. A novel common dataset was assembled for the whole IP by merging the registered BA from 66 administrative regions of both Portugal and Spain. We applied a cluster analysis to identify larger regions with similar fire regimes and results point to the existence of four clusters (Northwestern, Northern, Southwestern and Eastern) whose spatial patterns and seasonal fire regimes are shown to be related with constraining factors such as topography, vegetation cover and climate conditions. The relationship between BA at monthly time scale with both long-term climatic pre-conditions and short-term synoptic forcing was assessed using correlation and regression analysis based on: (1) temperature and precipitation from 2 to 7 months in advance to fire peak season, (2) synoptic weather patterns derived from 11 distinct Weather Types Classifications (WTC). Different relations were obtained for each IP region with a relevant link being identified between BA and short-term synoptic forcing for all clusters, while the relation with long-term climatic preconditioning was relevant for all but one cluster. Stepwise regression models based on the best climatic and synoptic circulation predictors were developed with cross-validation to avoid over fitting. The performance of the models varies within IP regions, though models exclusively based on WTC tend to better reproduce the annual BA time series than those merely based on pre-conditioning climatic information. Nevertheless, the use of both synoptic and climatic predictors provides the best results, particularly for the two western clusters, with Pearson correlation coefficient values higher than 0.7. Finally, it is shown that typical synoptic configurations that favour high values of BA correspond to dry and warm wind flows associated with anti-cyclonic regimes.

**KEY WORDS** wildfires; Iberian Peninsula; weather types; cluster analysis; regression models

Received 14 November 2011; Revised 29 April 2013; Accepted 3 May 2013

## 1. Introduction

It is widely known that, as a consequence of the Mediterranean type of climate, the southern European countries (Portugal, Spain, France, Italy and Greece) are particularly affected by summer fires (Barbosa *et al.*, 2007; JRC, 2010). The frequent warm and dry meteorological conditions found in summer play an obvious role in the triggering and spreading of these fires. Moreover, recent and future trends towards a dryer (Mariotti *et al.*, 2008; Mariotti, 2010; Sousa *et al.*, 2011) and warmer (Giorgi, 2006; Fischer and Schär, 2010) Mediterranean climate will tend to exacerbate the problem. However, while the prevailing weather conditions play an important role it must be acknowledged that human contribution is also significant either in Spain (Valbuena-Carabaña *et al.*,

2010) or in Portugal (Costa *et al.*, 2010). For example, the widespread abandonment and depopulation of rural areas in Iberia in the last decades has contributed to an increase in fuel availability for the ignition and spreading of fires (Pausas and Vallejo, 1999; Lloret *et al.*, 2002). This pattern of events is in line with the rest of the Mediterranean basin, where areas of scarcely relevance for agriculture were either converted to forest plantations or abandoned to the natural process of ecological succession, often converted to shrublands and woodlands (Moreno *et al.*, 1998; Pausas and Vallejo, 1999). In fact, it should be noticed that the use of fire as a tool to modify the landscape has been used on much longer temporal scales throughout the Holocene in both southern Iberian Peninsula (IP) (Gil-Romera *et al.*, 2010) as well as in northern Iberia (Rubiales *et al.*, 2008).

Among all northern Mediterranean regions, it must be stressed that wildfires constitute a major and recurrent hazard in the IP. Their occurrence is responsible for a very large amount of burnt area (BA) every year, as well as for significant human and socio-economical impacts.

\* Correspondence to: R. M. Trigo, Centro de Geofísica da Universidade de Lisboa, Faculdade de Ciências, Univ. de Lisboa, Campo Grande, Ed C8, Piso 6, 1749-016 LISBOA, Portugal. E-mail: rmtrigo@fc.ul.pt

For example, during the period 1980–2009, the average annual BA by wildfires in Portugal (Spain) was about 109 000 ha (177 000 ha) (Pereira *et al.*, 2011a). However, if we compute the ratio of total BA by the country total land area, Portugal leads the rank of European countries most affected by fires, with a ratio up to three times higher than Italy, the second most fire-affected country (Pereira *et al.*, 2011a). Nevertheless spatial distribution patterns of fire occurrences and BA are not homogeneous within southern Europe, neither within each country (JRC, 2010). On the basis of data compiled between 1985 and 1997 (European Commission, 1998), northwestern Iberia (Portugal and the Spanish Provinces of Galicia) is the European region with the largest percentage of fire occurrences (roughly 50% of total number of fires), followed by southern Italy (10%) and the triangle Provence-Tuscany-Corsica (7%) (EC, 1998; Pereira *et al.*, 2005). However, one should be careful because these annual average values hide a remarkable level of inter-annual variability. For example, focusing on the burned surface in Portugal between 2003 and 2007, the exceptional summers of 2003 (450 000 ha) and 2005 (380 000 ha), present the highest values of BA since robust statistics started to be compiled in 1980 (Trigo *et al.*, 2006; Pereira *et al.*, 2011a), contrast with average-summers like 2004 or 2006 (120 000 and 80 000 ha of BA, respectively), or even 2007, which represents the second lowest record with just 30 000 ha of BA (Pereira *et al.*, 2011a).

The number of fires and their extent in mid-latitude regions are controlled primarily by natural factors (e.g. topography, weather conditions and vegetation cover), by land management practices responsible for anthropogenic ignitions, and also by fire prevention, management and suppression efforts. Changes in the frequency of occurrence of specific atmospheric conditions, which are favourable to the outbreak and consequent spreading of large wildfires, can help explaining the magnitude of this inter-annual variability (Viegas and Viegas, 1994; Pyne *et al.*, 1996; Kunkel, 2001). In the context of large fire occurrences in the IP, a number of works has focused objectively on the role played by meteorological factors, namely in Portugal (Trigo *et al.*, 2006; Hoinka *et al.*, 2009; Carvalho *et al.*, 2008) and in Spain (Vázquez and Moreno, 1993; Piñol *et al.*, 1998; Pausas, 2004; Padilla and Vega-García, 2009; Rasilla *et al.*, 2010; Pausas and Fernández-Muñoz, 2011). Moreover, several works have proved that Iberian fires are also associated with the occurrence of anomalous climate in the preceding seasons (Viegas and Viegas, 1994; Pereira *et al.*, 2005). However, a growing number of studies focused on the anthropogenic contribution towards the spatial distribution of Iberian fires (Vélez, 1993; Badía *et al.*, 2002; Lloret *et al.*, 2002; Vázquez *et al.*, 2002; Cueva *et al.*, 2006; Costa *et al.*, 2010). Among these, one of the most comprehensive approaches corresponds to the recent work of Costa *et al.* (2010), where the authors focus on the sensitivity of Portuguese forest fires to climatic, human activity and landscape. Similarly, in Cueva *et al.* (2006),

the authors showed the dependence of regional patterns of forest fires in Spain on numerous human, landscape and climatic factors that change frequently in time and space.

Despite the amount of studies, there are still issues to be further addressed in relation to the interactions between meteorological conditions, vegetation dynamics and fires. In the Mediterranean region, drought periods can have strong impacts in vegetation activity (Gouveia *et al.*, 2009), with significant losses of crop yields (Austin *et al.*, 1998), decreasing of terrestrial net primary production (Zhao and Running, 2010) and forest growing (Martínez-Villalta *et al.*, 2008) and increasing the risk of forest fires (Pausas, 2004). It is now widely accepted that changes in large-scale atmospheric circulation is partially responsible for decreasing precipitation trends and higher frequency of drought episodes over Iberia (Paredes *et al.*, 2006; García-Herrera *et al.*, 2007). Moreover, such a trend towards a drier Mediterranean climate is in very good agreement with state-of-the-art climate change projections for different future scenarios (Giorgi, 2006). Finally, other studies have proved that the occurrence of major droughts in southern Europe during the preceding winter and spring seasons can enhance the amplitude of heat waves on the following summer (Seneviratne *et al.*, 2006; Fischer *et al.*, 2007), implying that these two phenomena (droughts and heat waves) are closely related.

A number of studies have used remote sensing imagery-derived datasets over the Mediterranean region to analyse changes in vegetation activity (Vicente-Serrano and Heredia-Lacaustra, 2004; Gouveia *et al.*, 2008), have determined the impact of droughts (Vicente-Serrano, 2007; Gouveia *et al.*, 2009) and have monitored plant recovery after fire (Viedma *et al.*, 2006; Gouveia *et al.*, 2010). Several vegetation indices can be used to assess vegetation dynamics; however, the Normalized Difference Vegetation Index (NDVI) is the most widely employed (Myneni *et al.*, 1995; Gouveia *et al.*, 2008).

Pereira *et al.* (2005) found that the daily synoptic variability in Portugal is the most important driver of favourable local fire-prone weather conditions. Bearing this in mind, atmospheric circulation classifications become an important potential tool to study the role of weather in wildfire occurrence in the IP. Furthermore, impacts on fire activity of large scale circulation patterns in the atmosphere and in the ocean have been used with the aim of developing short- and long-range forecast models for wildfire occurrences by several authors. In this respect, Flannigan *et al.* (2001) explored the relationship between Pacific sea surface temperature (SST) and BA in Canada to build a forecasting model of monthly and seasonal fire activity. Here, we intend to apply a similar approach on the specific context of the IP, and to introduce Weather Types Classification (WTC) on a deeper assessment of fire-season predictability for this region. In this work, we will be mostly focused on the relationship between meteorological and BA inter-annual variability, through the use of summer synoptic circulation and previous climatological conditions in the entire IP.

WTCs are a recurrent and fairly simple method to describe atmospheric circulation variability at daily and sub-daily scale, as they provide discrete characterizations of the atmospheric conditions. They have been widely used in several contexts and, as a consequence, a large variety of classification methods (automated or not) have been developed with multiple purposes. Here we are considering the WTCs developed within the framework of the COST Action 733—Harmonization and applications of WTC for European Regions (COST733) catalogue.

The COST733 catalogue comprehends the largest set of classifications ever assembled for different regions of Europe. These are based on numerous methods and meteorological variables and have been applied to several spatial domains centred on different European sub-regions. We intend to make the best use of this catalogue and perform an objective comparison on the ability of each classification to explain wildfire variability in the IP domain. Numerous objective comparisons for the catalogue have been performed on several areas of study, such as heavy precipitation occurrence (Lupikasza, 2010; Twardosz, 2010), extreme values of air temperature (Ustrnul *et al.*, 2010), lightning activity (Pineda *et al.*, 2010), air pollution (Lésniok *et al.*, 2010). Preliminary works relating WTC with wildfire occurrences have been developed for Iberia (Rasilla *et al.*, 2010) and Greece (Kassomenos, 2010). However, Rasilla *et al.* (2010) did not use WTC from the COST733 catalogue, but rather his own classifications, based on Principal Components and Cluster analyses.

Therefore, the main objectives of this work are the following:

- (1) To obtain a novel comprehensive wildfire dataset for the entire IP and to distinguish fairly independent regions in terms of BA characteristics and fire regime for each region;
- (2) To provide an interpretation on the spatial distribution of BA in terms of the topography, climate and vegetation dynamics in the IP;
- (3) To analyse the relationships and dependence of BA inter-annual variability with previous seasonal climatological conditions, namely precipitation and air temperature;
- (4) To examine the performance of the different WTC available from COST733 catalogue as indicators for the BA inter-annual variability;
- (5) To test the ability of simple statistical regression models to reproduce the inter-annual variability of BA, using climatological data and WTC as predictors.

The rest of this manuscript has the following structure: the datasets used in this study and the climate of IP are described in Section 2, while the identification of the most important spatial regions with identical fire behaviour was obtained with cluster analysis in Section 3. The links between BA for each cluster and previous meteorological fields and/or the frequency of each weather type (WT)

are evaluated in Section 4, while Section 5 provides a description of the most important WT patterns associated with fire occurrences at each cluster previously identified. Finally, section 6 is devoted to the discussion of obtained results and to present the conclusions of this study.

## 2. Datasets and main characteristics of the study area

This work relies on three types of data series, namely: (1) WT catalogues and meteorological variables; (2) BA in both Iberian countries (Portugal and Spain) and (3) vegetation index.

### 2.1. WT catalogues

WTC data was obtained from the COST733 project (Philipp *et al.*, 2010) and although available since 1958 it ends in 2001, which constrains its use to the 22-year long period (1980–2001) to be coincident with fire data. We only considered classifications with nine categories (in a total of 11 classifications), and exclusively worked in the domain D09 that is centred over the IP. This domain (amongst all available for the catalogue) is represented in Figure 1, together with all the remaining regional and pan-European domains. The acronym of the considered 11 classifications is presented in Table I, together with the climatic elements and main methodological methods used in their construction.

### 2.2. A climate characterization of the IP

The climate of the study area is characterized by using the mean monthly precipitation and temperature series obtained from long Climatic Research Unit (CRU) gridded dataset—version TS3.0 at the resolution of  $0.5^\circ \times 0.5^\circ$  latitude (Mitchell and Jones, 2005). To assess the IP climatology within the appropriate context, we must acknowledge the main physical attributes of the region, namely the topography and mountain ranges. These geographical characteristics and the political borders of the Iberian countries are depicted in Figure 2.

Maps of annual averages of surface temperature and precipitation in the IP computed for the 1980–2005 period using the CRU gridded dataset are shown in Figure 3. The overall patterns are quite similar to higher resolution Iberian climate atlas maps of annual average mean air temperature and precipitation computed for the 1971–2000 period (AEMET-IM, 2011) obtained with observed data from a large number of meteorological and udometric stations. The annual precipitation in the IP (Figure 3, top panel) presents a SE–NW gradient, with higher values in the coastal regions extending from Lisbon, in central Portugal to Galicia (northwestern Spain) and also to the northern mountainous regions (including the Cantabria and Pyrenees) and the lowest values found in the southern-eastern corner of the IP. Annual mean air temperature (Figure 3, bottom panel)

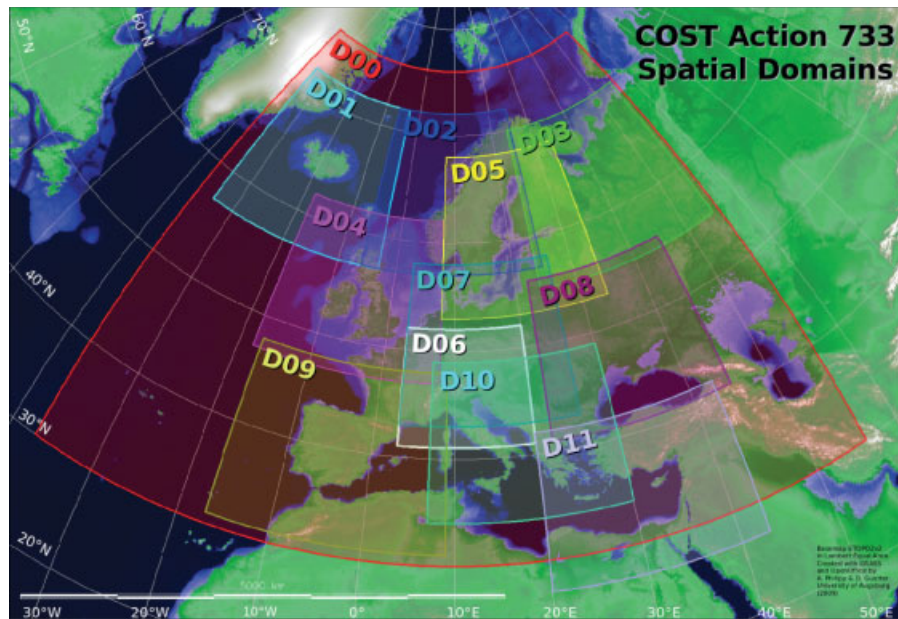


Figure 1. European Spatial domains defined by COST Action 733—Harmonization and Applications of Weather Type Classifications for European regions (COST733Wiki, 2011). Catalogues/classifications used in this work were produced for domain D09 (Iberian Peninsula, Western Mediterranean), 31°N—48°N (18 points), 17°W—9°E (27 points).

Table I. Summary of the 11 Weather Type Classifications (WTC) characteristics used in this study obtained from COST733 (COST733Wiki, 2011), namely the acronym of the WTC, main methodology and meteorological variables used for the weather typing classification.

WTC	Method	Meteorological variables
CKMEANSC09	k-means	SLP
ESPLC09	spatial similarity index of daily maps	SLP
KHC09	spatial correlation of daily maps	SLP
LITADVE	direction of advection, cyclonicity	SLP
LUNDC09	correlation-based	SLP
NNWC09	artificial neural networks	SLP
PCACAC09	S-mode PCA, k-means	SLP
PETISCOC09	correlation-based	SLP
SANDRAC09	simulated annealing	SLP
SANDRASC09	simulated annealing of sequences	SLP
WLKC09	direction of advection, cyclonicity	U700,V700, Z925 and Z500

seems to be dominated by the latitudinal change and the topography with values ranging between about 20 °C in southern Spain to about 2.5 °C in the high regions in the north of Spain and Pyrenees.

### 2.3. A fire database for the IP (1980–2005)

We have considered BA data from fire occurrences over Portugal and Spain in order to produce a joint database for Iberia (and Balears islands) as these European countries

have long and homogeneous time series of fire data since 1980 (Barbosa *et al.*, 2007; JRC, 2010). Portuguese fire data was obtained from the Autoridade Florestal Nacional (AFN, 2011), while Spanish data was obtained from the Dirección General de Biodiversidad. Pereira *et al.* (2011a) provides a comprehensive description of the history and characteristics of the Portuguese fire database for the 1980–2005 period. It was found that during the 1980s the minimum amount of BA was 0.1 ha (i.e. all fires smaller than 0.1 ha were not considered) and this threshold has been reduced subsequently, being currently in the order of 0.0001 ha. These changes are important as they introduce artificial trends on the number of fires time series and, consequently, on the average BA per fire. However, the contribution of all these very small fires does not change significantly the annual (or summer) BA (Pereira *et al.*, 2011a). The Spanish database has also been analysed in the recent past (Moreno *et al.*, 1998) and has been shown to be increasingly reliable (Carracedo Martín *et al.*, 2009). Although available since 1976, two northern Spanish regions present significant amounts of missing data: Álava (1980–1984) and Navarra (1980–1984 and 1994–2002). These missing values were replaced by the long-term monthly mean BA in each of these regions, a procedure with very limited impact as these regions present mean annual BA values below 0.5 and 0.1% of their total areas, respectively.

This new Iberian database refers to the common period of 1980–2005 for both countries BA time series. Monthly BA time series are spatially disaggregated on similar size administrative regions (AR): in the case of Portugal by *Distritos*, and in the case of Spain by *Provincias* (Figure 4). For both countries, we have

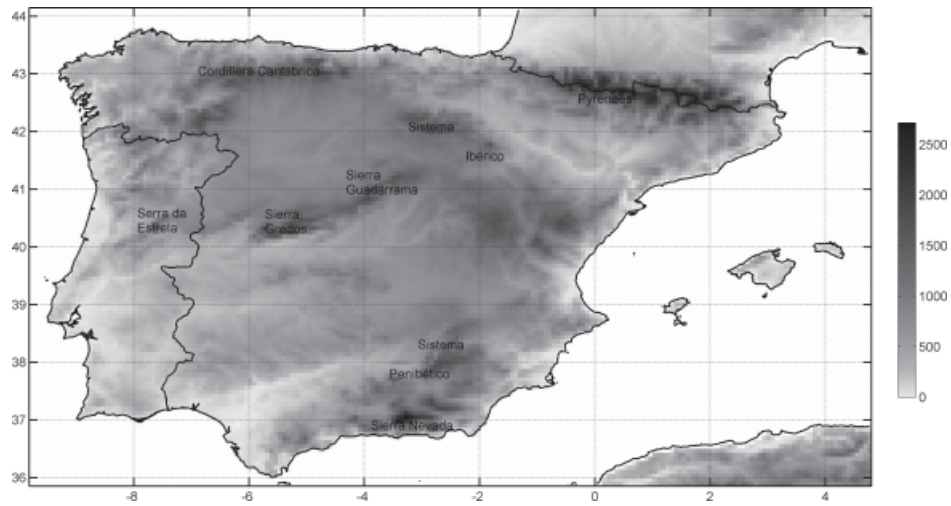


Figure 2. Main topographical features of Iberian Peninsula, including mountain ranges and the political borders of both Iberian countries.

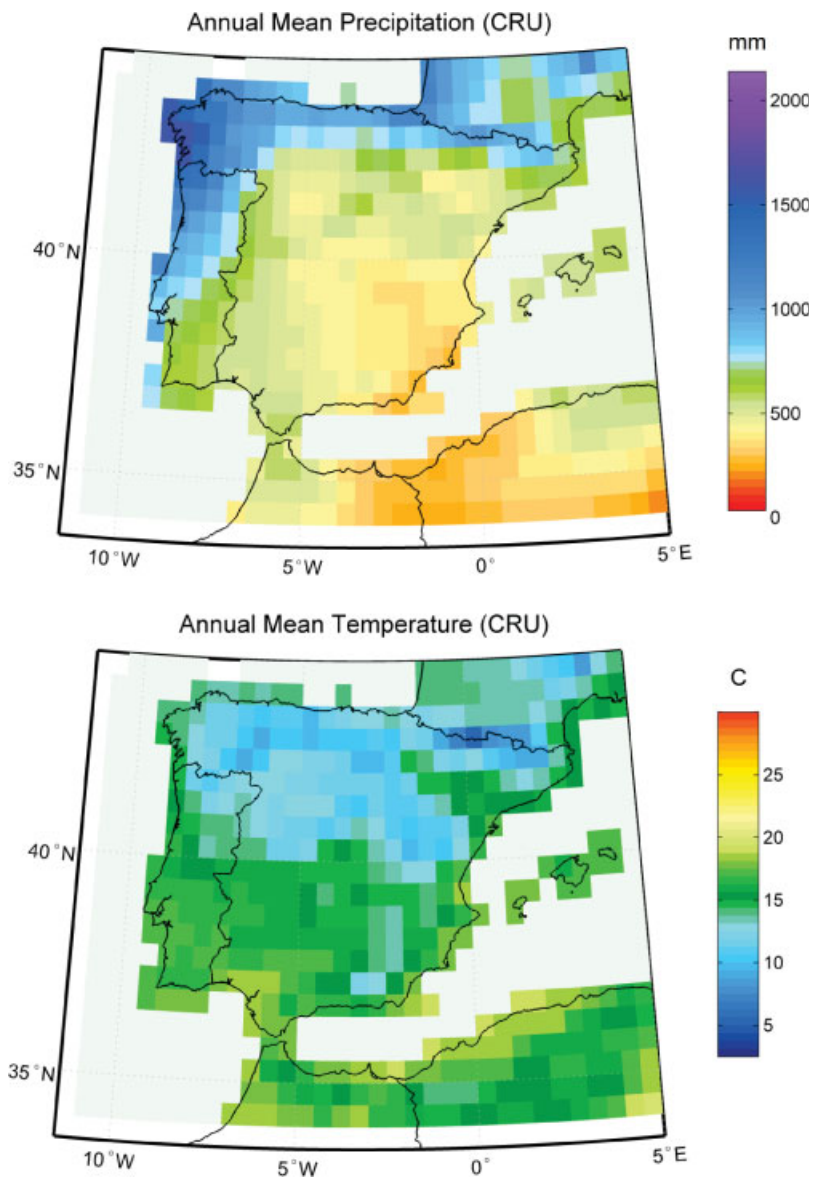


Figure 3. Annual mean precipitation (top panel) and temperature (bottom panel) over Iberia for the 1980–2005 period, based on the high resolution dataset from the Climatic Research Unit (CRU) gridded dataset version TS3.0 (Mitchell and Jones, 2005).



Figure 4. Annual mean normalized burnt area (NBA) in the Iberian Peninsula for the 1980–2005 period (in permillage) on a regional basis, composed by the Portuguese (*Distritos*) and Spanish (*Provincias*) administrative regions (AR). The NBA is defined as the quotient between the amount of burned area (BA) in each of the AR and the area of that AR.

not used the BA observed in the Portuguese (Azores and Madeira for Portugal) and Spanish (Canary Islands) Atlantic archipelagos and, in the end, the database spatial domain covers a total of 66 AR: 18 in Portugal and 48 in Spain. As these AR have considerably different surface areas, it is not appropriate (for some purposes) to compare BA directly among them. To circumvent this problem, besides the absolute amount of BA per region we have also computed the monthly Normalized Burnt Area (NBA) for each AR, defined as the quotient between the amount of BA in each of the AR and the area of the corresponding AR. Since both these quantities have the same units, NBA will be presented in permillage. After this normalization procedure, the monthly and annual averages for the NBA dataset for each of the 66 AR were computed. Annual mean NBA values for all the 66 Iberian AR (Figure 4) reveal that the northwestern sector of Iberia, which includes central and northern Portugal and northwestern Spain (mostly Galicia and Asturias), is the most affected by wildfires, presenting averaged values higher than 20‰. The eastern and northeastern coastal areas of Spain (Catalunya and Valencia) are also moderately prone to wildfires (with NBA values between 10 and 20‰ of their total area). Most central and southern regions of Iberia (except the Algarve region) do not present significant amounts of annual NBA (below 5‰). However, it must be acknowledged that this analysis based on NBA values still presents a caveat, since the normalization with the total districts/province's surface area can induce a bias in the final results. In fact, ARs have different percentage of vegetated area and some ARs (e.g. Zaragoza in Spain or Algarve in Portugal) have a relatively small fraction of forestry surface, albeit highly concentrated in smaller mountainous sub-domains.

#### 2.4. Vegetation dynamics in IP

NDVI monthly anomalies, with 8 km of spatial resolution, were obtained from the Global Inventory Modelling

and Mapping Studies (GIMMS) dataset and correspond to the most complete and longest remote sensing dataset, covering the entire Mediterranean region, for the period 1982–2006 (Tucker *et al.*, 2005).

Vegetation over the Mediterranean basin and specifically over the IP presents high diversity, resulting from climate, landscape, topography and other factors. To identify the main types of vegetation cover over Iberia, a cluster analysis of the monthly means of NDVI for the entire period was performed, using four clusters depicted in Figure 5 (top panel). These four clusters correspond approximately to the four main vegetation types over Iberia. The cluster represented in blue coincides almost exactly with the extension of the Eurosiberian phytoclimatic region across the IP (Rivas Martínez, 1987), characterized by low temperature and abundant and regular water supply. The spatial domain of this cluster broadly corresponds to regions included within the 800 mm isohyets, a threshold traditionally used to delimitate the 'green' (Csa, Csb and Cfb on Köppen Classification) Iberia from the drier Mediterranean regions. Its natural vegetation is alpine or deciduous forest, currently composed by pastures and secondary forest plantations (eucalyptus, pinus) that presents high activity throughout the entire year, with a maximum in spring (Figure 5, bottom panel), but deeply dependent on water resources. The cluster represented in yellow groups two different landscapes: (1) an ecotone transition (semideciduous forest) through the southern piedmont of the mountains of northern Spain (Cordillera Cantábrica and Pyrenees) and (2) the typical Mediterranean sclerophyllous forests (sometimes grazed—*dehesas*) across most of the mountains and plateaus of central and southern IP. This cluster comprehends large areas of annual (mainly not irrigated) crops characterized by the overall highest NDVI values during the entire seasonal cycle and with a maximum in summer (Figure 5, bottom panel). The cluster represented in green corresponds to the central areas of both Mesetas

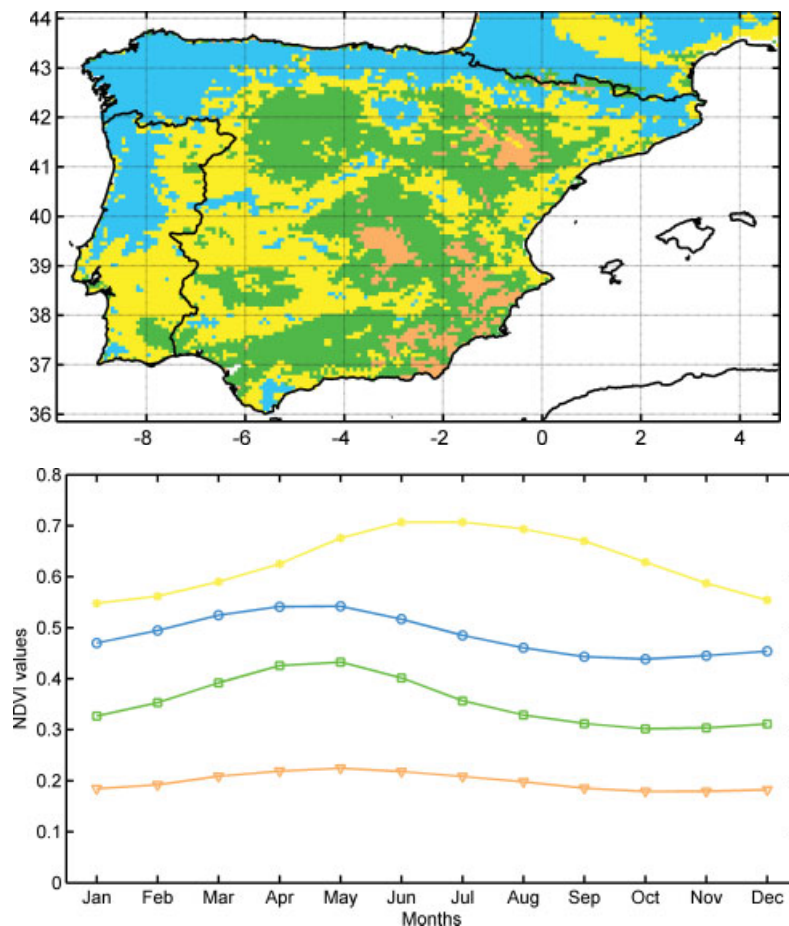


Figure 5. Spatial distribution of the four clusters of NDVI obtained with GIMMS dataset for the period 1982–2006 (top panel) and the annual cycles of monthly NDVI that characterize the centroids of the four identified clusters (bottom panel).

and the Ebro and Guadalquivir basins, besides some spots along the Mediterranean coast of the IP. These regions seem to share in common a dominant (in some cases irrigated) agricultural activity. This cluster presents lower vegetation activity (lower NDVI values) than the previous two, with a maximum during spring, due to the availability of water during this season—a feature usually associated to scrublands. The last cluster, plotted in orange presents very low values of NDVI over the entire year (Figure 5, bottom panel), corresponding to the typical regions characterized with very sparse vegetation or even bare soil. It resembles the most arid environments of the IP, (Ebro valley, La Mancha, SE Spain), characterized by a stepped-like vegetation (when/where there is vegetation) as consequence of high summer temperatures and scarce annual precipitation (below 400 mm).

### 3. Regionalizing fire regimes in the IP

In the previous section, BA datasets from both Iberian countries were merged and a preliminary analysis was performed to obtain the spatially NBA dataset. These procedures were required before applying the methodology that aims to objectively identify the most important fire regimes within the IP. For this

purpose, we performed a Cluster Analysis, using the K-means algorithm, on the NBA in the 66 considered AR disposed in a T-mode matrix. We decided to retain four statistically significant clusters (Figure 6), since the obtained pattern presents regions with higher spatial homogeneity in comparison with spatial configurations attained with a higher number of clusters, as it will be shown later. Furthermore, this result is concordant with the defined regionalization defined by Rasilla *et al.* (2010), also with four sub-regions, and presents a strong resemblance with the operative regionalization used by the Spanish authorities (MARN, 2011).

We must stress that the configuration presented in Figure 6 does not correspond exactly to the cluster analysis output. A small number (six) of neighbouring Spanish AR were swapped in order to define a more spatially homogeneous set of four clusters. These AR are identified with a small circle in Figure 6 and these changes were considered valid to perform, as they refer to ARs with low mean annual values of NBA (usually below 5‰, as shown in Figure 2). Taking into account the geographical location of the resulting four clusters, these were named respectively: northwest (NW\_CLU); southwest (SW\_CLU); north (N\_CLU) and east (E\_CLU).



Figure 6. Spatial extension of the four clusters obtained for the normalized burnt area in the 66 administrative regions (AR) of Iberia. Black dots identify the AR that originally belonged to different clusters but were reassembled to increase spatial coherence. Legend: blue—northwest cluster (NW\_CLU); yellow—southwest cluster (SW\_CLU); green—east cluster (E\_CLU); and, magenta—north cluster (N\_CLU).

The NW\_CLU aggregates the northern half of Portugal and the extreme northwest of Spain, including most of the ARs with higher values of mean annual BA. The SW\_CLU represents the southern and interior areas of Portugal (including Guarda, the AR with the highest mean annual BA), as well as many ARs of central and southwestern of Spain. The coastal and pre-coastal ARs east of Gibraltar correspond to the E\_CLU (including the Balears islands). Finally, the N\_CLU corresponds to the regions located in the mountainous sectors of northern Spain (including Asturias, Cantabria and the Basque Country).

The main purpose of applying this Cluster Analysis was to identify the Iberian regions with similar temporal variability. In fact, all four regions shown in Figure 6 have a clear annual cycle of the mean monthly NBA, with the main differences being found in the amplitude and timing of the maximum values (Figure 7, top panel). The NW\_CLU clearly represents the AR more affected by wildfires, with nearly 10% of the total area being burned, on average, every August. The mean peaks of the other clusters are all below 3% of their area. Interestingly, two of the identified clusters present two maxima, with the NW\_CLU revealing a much larger peak in August and a smaller one in March. The northernmost areas of Iberia are concentrated in the N\_CLU that presents two peaks, both comparable in magnitude (relatively small although), in spring (March) and late summer (September). Finally, the two remaining clusters are characterized by a single summer maximum in July and in August in the case of E\_CLU and SW\_CLU cluster, respectively.

The boxplots of monthly NBA (Figure 7, bottom panel) also help to characterize the intra-annual evolution of location (median), dispersion (IQR), range (maximum minus minimum) and asymmetry characteristics of the NBA distribution in each cluster. In general, the annual evolution of location, range and dispersion statistics present a similar annual cycle of the mean monthly NBA, with similar ratios between the amplitude and timing of the maximum values. Only a few number of discrepancies of that annual cycle are worth to mention, namely: (1) the median in July is similar than the one in August for the SW\_CLU; (2) secondary maximum values of the median (the first peak, in late winter and beginning of spring) occurs in February, and not in March as for the mean monthly NBA, and is about 75% higher for N\_CLU than for the NW\_CLU. The temporal evolution of the quartile skewness reveals that monthly NBA distribution is essentially positive skewed, (with a few exceptions), presenting high intra-annual variability and smaller values for the western clusters (NW\_CLU and SW\_CLU) during summer/fire season and the opposite behaviour for the other two cluster (except for N\_CLU in June and July).

The spatial patterns of the four NBA clusters and the correspondent fire regimes are also in good agreement with topography (Figure 2), climate conditions (Figure 3) and vegetation dynamics (Figure 5). Actually, the NW\_CLU corresponds to the relatively low land coastal areas in the north western Atlantic coast of the IP while the SW\_CLU includes the lowlands in the SW region of the IP and the large Meseta Central (Figure 2). This central

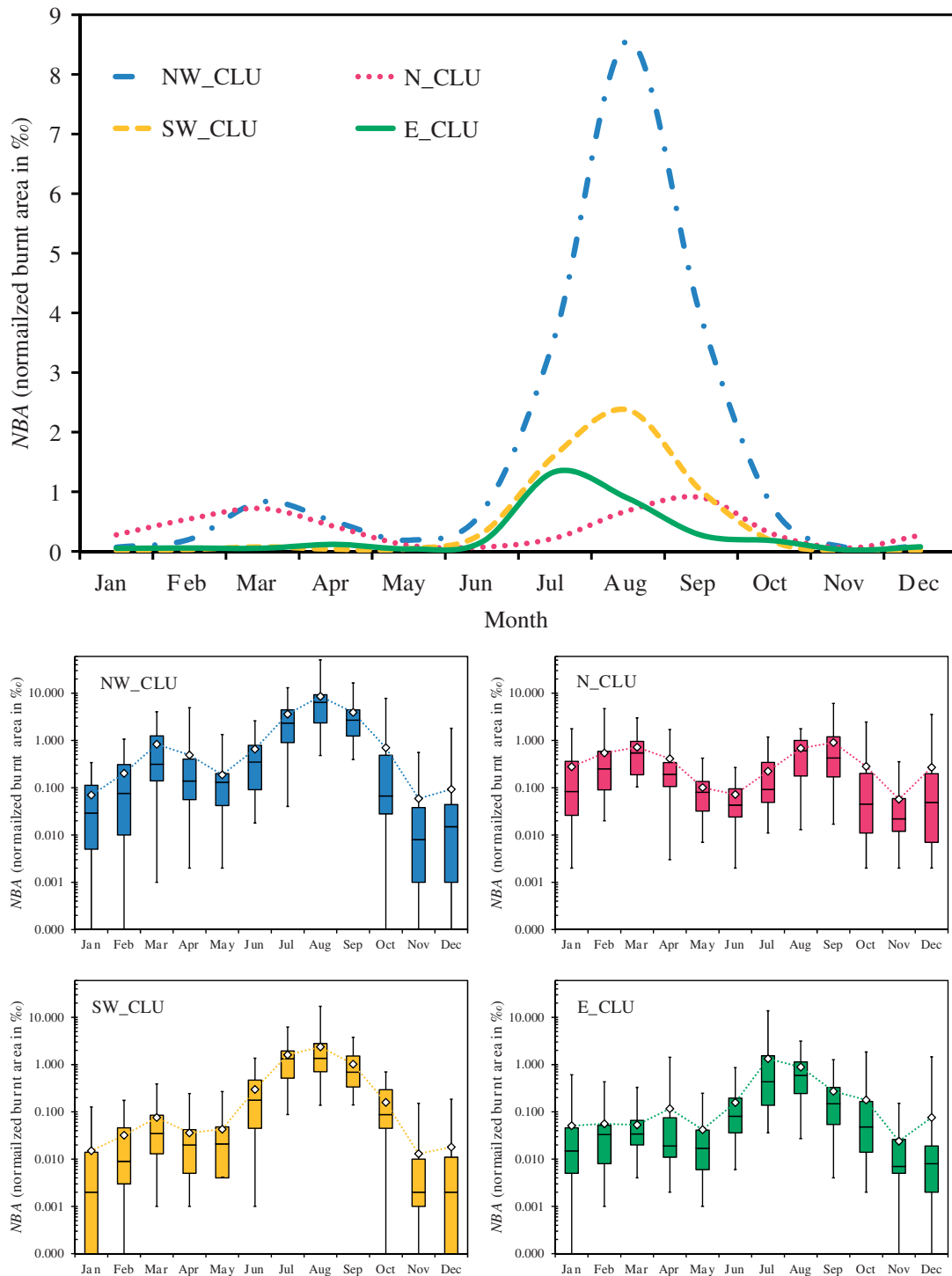


Figure 7. Mean monthly time series (above) and boxplots (below) of normalized burned area (NBA—defined as the quotient between the amount of BA in each of the AR and the area of the AR, both in hectares), in the 1980–2005 period for the four NBA clusters shown in Figure 6 and using the same colour palette as in Figure 6.

and high plateau is surrounded by the Cantabrian Mountains (Cordillera Cantábrica) region that corresponds to the N\_CLU and by the Ibérico and Penibético systems which delimits the E\_CLU along with the Mediterranean coasts of Iberia (Figure 2). The climate of these four regions is also very different and helps to put into perspective some characteristics of their vegetation cover (Figure 5) and fire regime (Figures 6 and 7), namely the

yearly amount of BA, the fire season duration and peak timing. Besides mean annual precipitation and temperature spatial patterns (Figure 3), the climate characterization of IP requires some knowledge on the intra-annual temporal and spatial variability, e.g. the typical conditions during the cold (winter) and warm (summer) seasons. According to the Iberian Climate Atlas (AEMET-IM, 2011), the winter and summer mean precipitation and

temperature conditions in these four regions are as follows. The N\_CLU and NW\_CLU are clearly the wettest clusters (Figure 3) and that implies a compatible vegetation cover (blue colour in Figure 5). However, these two fire regime clusters diverge in terms of their annual temperature. Thus the N\_CLU is characterized by wet and cold winters and by humid and fresh summers (AEMET-IM, 2011) which supports the fact that this is one of the regions less affected by wildfires (Figure 7). On the contrary, the climate (and associated vegetation cover) of the NW\_CLU is the most appropriate for the occurrence and development of fires during the dry and hot summer season because these conditions follow the humid and mild winters (AEMET-IM, 2011). Figure 4 confirms (through the NBA spatial pattern) that these are the most favourable conditions for the occurrence of wildfires, allowing the existence and development of live fuels during the wet and mild season (winter and early spring) and the vegetation stress conditions during hot and dry seasons (late spring and summer). The two remaining clusters are associated with drier climates and mostly non-forested vegetation cover (Figure 5). Climate in the E\_CLU is characterized by dry winters (with small exceptions in the Pyrenees) and by even dryer and hot summers (AEMET-IM, 2011). The existence of meteorological favourable dry and hot conditions that promote the occurrence of wildfires during the summer season is not supported by the existence of appropriate vegetation cover, because this arid environment seriously limits the fuels availability (Pausas and Fernández-Muñoz, 2011). In fact, the cluster represented in light green in Figure 5 corresponds to areas with extremely low NDVI values (Figure 5 bottom panel), which is a typical of bare soil or very sparse vegetation. In this situation, and even with meteorological conditions that favour fire ignition, there is a very low probability of having large fire events/activity. The SW\_CLU region is characterized by extremely hot and dry summers but has a less homogeneous climate conditions during the mild and humid winter, with a gradient of both temperature and precipitation in the NE–SW direction. Vegetation cover in this area is dominated by sparse vegetation, with a maximum of vegetation activity in spring (green in Figure 5) and rain feed crops that mature in late spring and early summer (yellow in Figure 5).

#### 4. Modelling the inter-annual variability of BA

##### 4.1. The influence of previous climatic conditions

Although fire ignition is most of the times dependent on human activities (either by accident, negligence or intentionally) the probability of a fire ignition to grow into a large and severe event is highly dependent on the existence of the appropriate meteorological conditions (Pyne *et al.*, 1996). Nevertheless, besides the meteorological conditions at the time of the fire ignition, previous climatic conditions play a very important role, as they are directly related to soil dryness and vegetation

hydric stress during the fire season. Some relations have been identified in specific regions, such as over Portugal (Pereira *et al.*, 2005; Trigo *et al.*, 2006; Hoinka *et al.*, 2009), where besides the usual link between summer fires and previous months dryness and warmth, wet months in mid-spring also reveal to be related to more BA in the fire season, as they promote the growth of vegetation which may act as fuel when fires are triggered. However, the exact nature of these relations between appropriate previous climatic conditions and BA varies from area to area and from season to season.

Taking into account the similar fire regime within each of the four clusters defined in Section 3, and in order to assess the role of previous climatic conditions on the inter-annual variability of BA, values of the Pearson correlation coefficient ( $R$ ) between BA time series (not NBA) in each cluster and relevant antecedent climatic variables (precipitation and temperature) over the region were computed as a procedure to reduce the dimensionality and pre select predictors with greater potential. It should be noted that BA and NBA present similar seasonal cycles, but the need of using NBA in the previous section was related with the necessity of performing the cluster analysis using a more appropriate fire statistic that facilitates the comparison among clusters (Figure 6) and the corresponding seasonal evolution (Figure 7). The CRU-TS3.0 mean monthly precipitation and temperature dataset were used to compute mean spatial average series for each cluster domain, i.e. selecting all grid-points coincident with the area of the spatial configuration associated to each cluster depicted in Figure 6. Instead of using absolute values of climate variables to test their usefulness as predictors, the developed models will rely on monthly anomalies time series, computed by removing the long-term mean from the spatially averaged monthly time series in each cluster. This procedure does not change the Pearson correlation coefficient but effectively removes the annual cycle in order to retain time series of temperature and precipitation anomalies in each of the four Iberian fire cluster regions. As it was seen in Section 2.3, each cluster presents a peak of BA at different timings of the year, or even two peaks during different seasons. Bearing this in mind, eventual links between BA in those peak months and the time series of anomalous meteorological fields were checked from 2 to 7 months in advance. For example, in order to study potential previous climatic influences for the August BA observed in the NW\_CLU, we tested the existence and statistical significance of Pearson correlation coefficients between this variable and the meteorological monthly time series from January to June. The highest values of  $R$  between each variable and each BA cluster for the considered months are presented in Table II. No results are presented for N\_CLU, as none of the tested  $R$  values were statistically significant at the 5% level.

These previous climatological variables can integrate the pool of potential predictors and be used as predictors in statistical hindcast models of BA (hereafter CLI\_models). The purpose of such relative crude models is not to

Table II. Summary of the highest correlation coefficients obtained between observed BA series for NW\_CLU, SW\_CLU and E\_CLU clusters, in July and August (the months of highest values of BA, for these clusters) and the monthly mean temperature (T) and precipitation (P) time series in the seven previous months.

Month	Cluster		
	NW_CLU	SW_CLU	E_CLU
July	May T (+0.55)	May T (+0.41)	May T (+0.44)
	May P (−0.48)	May P (−0.49)	
August	May T (+0.45)	May T (+0.36)	Jan T (−0.51)
	May P (−0.47)	Jun P (−0.58)	

Correlations presented here are statistically significant at the 5% level.

develop quasi-operational summer BA models for each region but simply to assess the contribution potential to BA predictability based on pre-disposing climatic conditions. For this purpose, a forward stepwise regression was applied to the temperature and precipitation monthly anomaly time series, in order to reproduce BA monthly time series for each cluster. This method tests all possible predictors and selects the one that explain more variance of the predictand (BA), and then looks for the most relevant remaining predictors that surpass a pre-defined level of statistical significance (here defined as the 5% level). For the three clusters that present the main peaks of BA during summer months (e.g. NW\_CLU, SW\_CLU and E\_CLU), three models were developed and tested to simulate the BA in (1) July, (2) August and (3) July + August. In the case of the N\_CLU, which presents two BA peaks (in March and September) models for those two specific periods were tested. Eventual problems related to over fitting were mitigated by employing the always stringent cross-validation scheme, usually known as the leave-one-out scheme (Wilks, 2006). In this approach, a single observation from the original sample is retained for validation, and the remaining observations are used as training data. Besides, all models were forced to retain four predictors at most. All these precautionary steps were taken because the time series are only 22 years long (1980–2001, since WTC data was only available until 2001), and this implies that using a large number of predictors could be misleading.

Values of the Pearson correlation coefficient between observed and modelled (with CLI\_models) BA time series in each cluster for all these cases are summarized in Figure 8. These results reveal that the role played by previous climatic conditions diverges for the different clusters (Figure 8). Winter and spring climatic conditions play an important role for the very active NW areas. Although we find modest  $R$  values between observed and modelled BA time series for both July and August BA,  $R$  increases (to about 0.5) and surpasses the statistical significance level for the July + August BA. Results obtained for the SW\_CLU and E\_CLU show that pre-conditioning climatic predictors appear to be useful for estimating the BA in August, but not as clearly as

for July. For the N\_CLU (not presented in Figure 8) we did not obtain statistical models for any of the considered months, as none of the possible previous climatic predictors were retained by selection method. This result means that BA in March and September are not clearly associated to remote previous anomalous climatic conditions in this cluster.

#### 4.2. Links with WT frequencies

The objective of this section (and the main motivation of this work) is to assess the performance of the WTC from the COST733 catalogue over the Iberia region in what respects to their capacity of discriminating weather conditions that favour the occurrence of large values of BA. The focus will be on the conditions in the months of occurrence of fires, or at the most, the previous one.

Every single day in the study period (1980–2001) was classified in one of the nine specific categories of each WTC. To make this information operational, monthly frequencies of each category were computed for all WTC used in this study. Then, following the same approach used for the CLI\_models, correlation analysis was used as a pre-selection procedure to identify the WTC most related with BA time series in each cluster.

The highest values of the Pearson correlation coefficients between time series of BA in each cluster and monthly frequencies of each WT are presented in Table III. Taking into account that several classifications present few significant values of  $R$  with BA time series, the remaining of the analysis was restricted to the five most promising WTC, namely: LUNDC09, NNWC09, PCACAC09, PETISCOC09 and WLKC09. This restriction is objective as it is solely based on the magnitude of the statistical relationships observed between the BA in each cluster and the WT frequencies for certain classifications.

The BA statistical models based on time series of monthly frequencies of each WT (WTC\_models) for each of the four clusters were developed following the same approach used to develop the CLI\_models (i.e. a forward stepwise predictor selection procedure, limited to retain at most four predictors and using cross-validation). This approach will enable us to distinguish which of the considered five classifications tend to better reproduce the appropriate classes of weather conditions that are related to months with high values of BA in Iberia. At this stage, the climatic information from previous seasons was neglected and we are only focused on the WTC predictors. Aiming to develop the best BA models and to assess the possible added value of incorporating both types of information (rather than using only WTC or only previous meteorological data alone) a third type of hindcast models (TOT\_models) was developed. In this case, both classes of variables are integrated in the potential pool of predictors used to construct the models and the remaining exact same procedures as in the previous models are carried out.

Despite the simplifications assumed previously (number of clusters retained, months to analyse and WTC kept

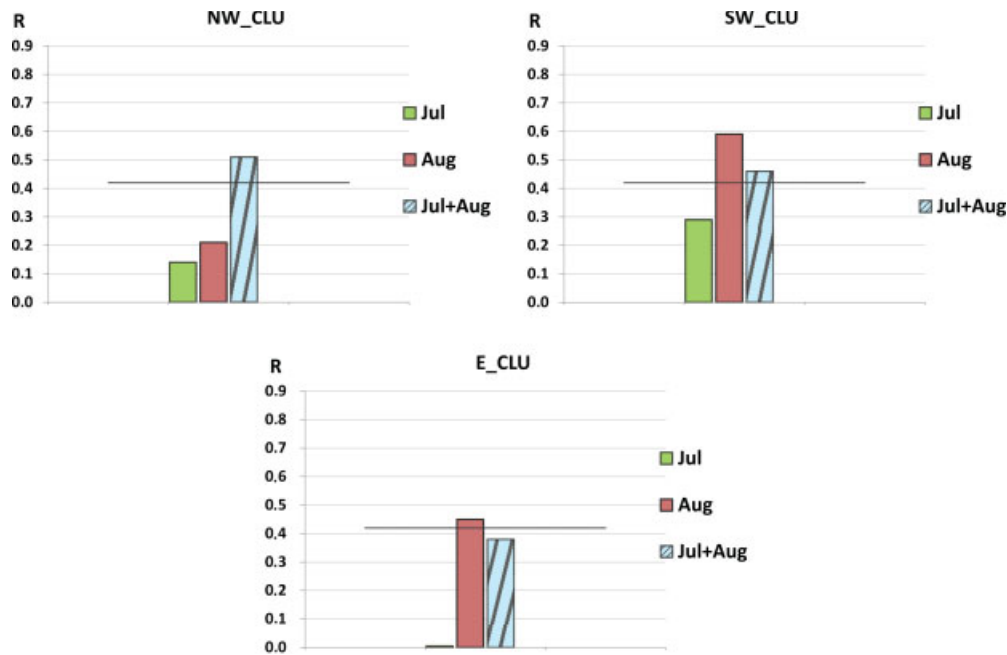


Figure 8. Values of the Pearson correlation coefficient ( $R$ ) between observed and modelled time series of monthly burnt areas in the northwest (NW\_CLU), southwest (SW\_CLU) and east (E\_CLU) clusters of normalized burned area (NBA). The models use climatic variables as predictors (CLI\_models) in hindcast mode and the grey line represents statistical significance at the 5% level.

Table III. As Table II, but for the best correlation coefficients between observed BA series (for each of the four clusters) in the considered months and the COST733 catalogue WTCs.

Month	Cluster			
	NW_CLU	SW_CLU	E_CLU	N_CLU
March	–	–	–	Feb WLKC09-5 (+0.64) Mar CKMEANS09-5 (+0.58) Mar SANDRASC09-6 (+0.56)
July	Jul PCACAC09-8 (+0.66) Jul PETISCOC09-5 (+0.61) Jun NNWC09-4 (–0.58)	Jun SANDRAC09-4 (–0.55) Jul KHC09-2 (+0.54) Jun PETISCOC09-3 (–0.53)	Jul WLKC09-4 (+0.94) Jul PETISCOC09-7 (+0.64) Jun LUNDC09-2 +0.57	–
August	Aug LUNDC09-4 (+0.70) Jul NNWC09-3 (+0.65) Aug PETISCOC09-2 (+0.68)	Aug PCACAC09-4 (+0.72) Aug PETISCOC09-8 (+0.59) Aug LUNDC09-2 (+0.56)	Aug PCACAC09-4 (+0.62) Jul LUNDC09-6 (+0.56) Jul WLKC09-4 (+0.53)	–
September	–	–	–	Sep KHC09-4 (+0.62) Sep SANDRASC09-1 (–0.52) Sep LUNDC09-2 (+0.51)

Only WTCs catalogues whose weather types frequencies show significant correlation (at the 5% level) with Burned Area series are displayed. WTCs names and characteristics are described in Table I.

in the analysis) a large number of models were developed as a result of retaining five different WTC, four clusters and at least 2 months to predict. Thus, for the sake of simplicity, we have summarized results in a simpler display (Figure 9) of the Pearson correlation coefficient value between the observed and simulated BA time series for all the tested models. For each cluster, classification and month, the plot includes two bars, the lighter one (at front) representing the result achieved with the WTC\_models and the darker one (at back) representing the TOT\_models, that incorporates both WTC and previous climatic conditions as possible predictors. For this reason, the darker bar is only visible in the cases where TOT\_models produce better models than WTC\_models. This representation simplifies the comparison between

the performances of all models, the assessment of the ability of each WTC to describe the BA variability, and the understanding to what extent (and for each cluster) previous climatic data improves the results obtained from WTC predictors-based models. Several major results emerge from the analysis of Figure 9, namely:

- (1) Higher values of  $R$  were obtained for both western sectors of Iberia (NW\_CLU and SW\_CLU), fact which suggest that it will be more susceptible to reconstruct BA series using this type of statistical models and predictors in these regions;
- (2) In general, TOT\_models present higher performance than the corresponding WTC\_models and CLI\_models, which means that the use of both WTC

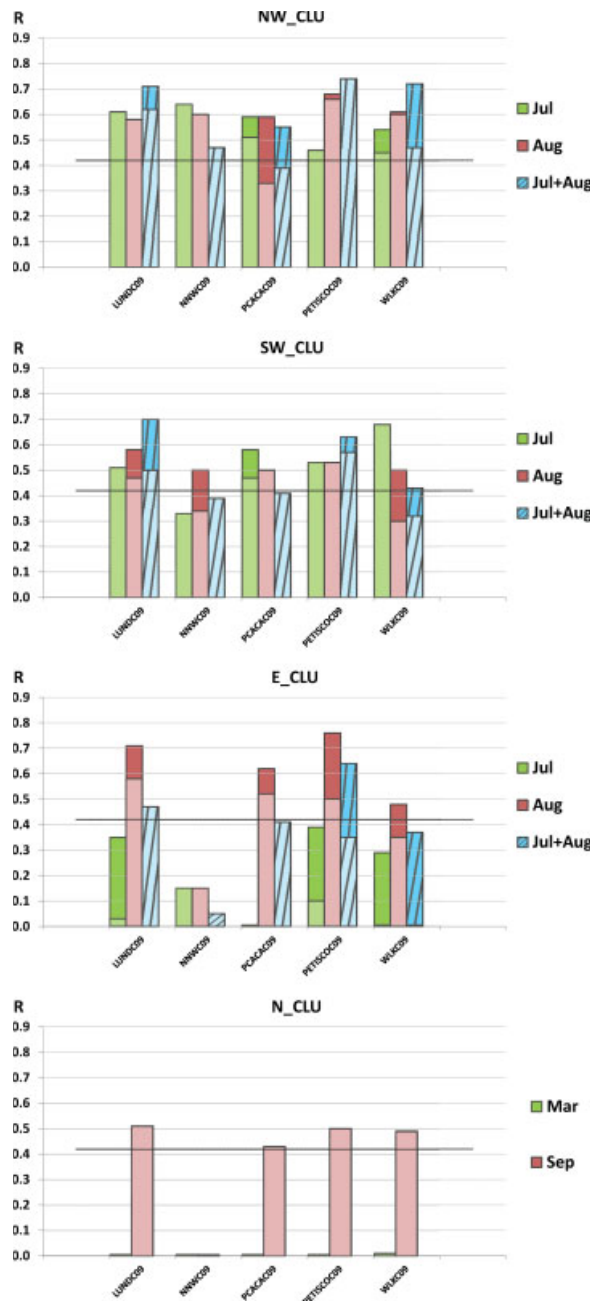


Figure 9. Values of the Pearson correlation coefficient ( $R$ ) between observed and modelled time series of monthly burnt areas in the northwest (NW\_CLU), southwest (SW\_CLU), east (E\_CLU) and north (N\_CLU) clusters of normalized burned area (NBA), using as predictors in light shaded bars just the WTC (WTC\_models) and in dark shaded bars using both WTC and climatic variables (TOT\_models). Dark shaded bars are only visible whenever TOT\_models present better performance than WTC\_models.

and previous meteorological conditions as predictors provides an added value in the vast majority of cases.

For example, in the NW\_CLU the value of the Pearson correlation coefficient for most of the models surpasses the 5% significance line. In this region, good results are found for both July and August BA time series. Nevertheless, the July + August models present the best

performance in NW\_CLU (in three of the five tested WTC). In the SW\_CLU, the month which models are more able to reproduce BA variance varies according to the considered classifications. TOT\_models present better results than CLI\_models but, the main feature is that the use of WTC as predictors improves substantially the reconstruction of BA series in July, which was quite modest when using climatological information only. Results for August are slightly better but not statistically significant, showing that the wildfire climatology in SW\_CLU and this month is essentially related to years with propitious conditions cumulated in previous months. In the E\_CLU August BA models tend to present better results (in four of the five classifications), while July models fall below the 5% level of statistical significance. As no satisfying CLI\_models were obtained for the N\_CLU, we find the best TOT\_models for this region to be equivalent to the best WTC\_models. In this cluster, statistically significant BA models were only obtained for September.

The procedure for statistical validation of the models is not based solely on the Pearson correlation coefficient. The Mean Absolute Error (MAE) has also been computed for all models presented here. We found a good agreement between the results obtained with the two measures of goodness of fit, for example, the higher the correlation coefficients, the lower the MAE between observed and modelled series (not shown).

Finally, it is not an easy task to rank the best WTC classifications for any cluster as it depends on the target month. However, PETISCOC09, WLKC09 and LUNDC09 can be considered the most satisfying for NW\_CLU. It is also rather difficult to select the best performing classifications in the SW\_CLU, but LUNDC09, PCACAC09 and PETISCOC09 may be considered to be those that provide the best results on the overall. The PETISCOC09, LUNDC09 and PCACAC09 classifications present the best results for the E\_CLU. For the N\_CLU, the region with the poorest model performance, statistically significant models were only found for September and with the WLKC09, LUNDC09 and PETISCOC09 WTC.

## 5. Synoptic analysis

It was shown in the previous section that the statistical models (TOT\_models) which combine prior climatic information (temperature and precipitation anomalies) and non-lagged WTC series usually present better performance, when reconstructing the inter-annual variability of BA series of Iberia, particularly in the most affected western sectors. To have a further understanding on the role that the latter predictors have on these models, the mean sea level pressure anomaly composite fields of the retained classes for each model in each cluster were analysed in more detail. Once again, taking into account the considerably large number of models and predictors, we opted to summarize results in a concise way (Figure

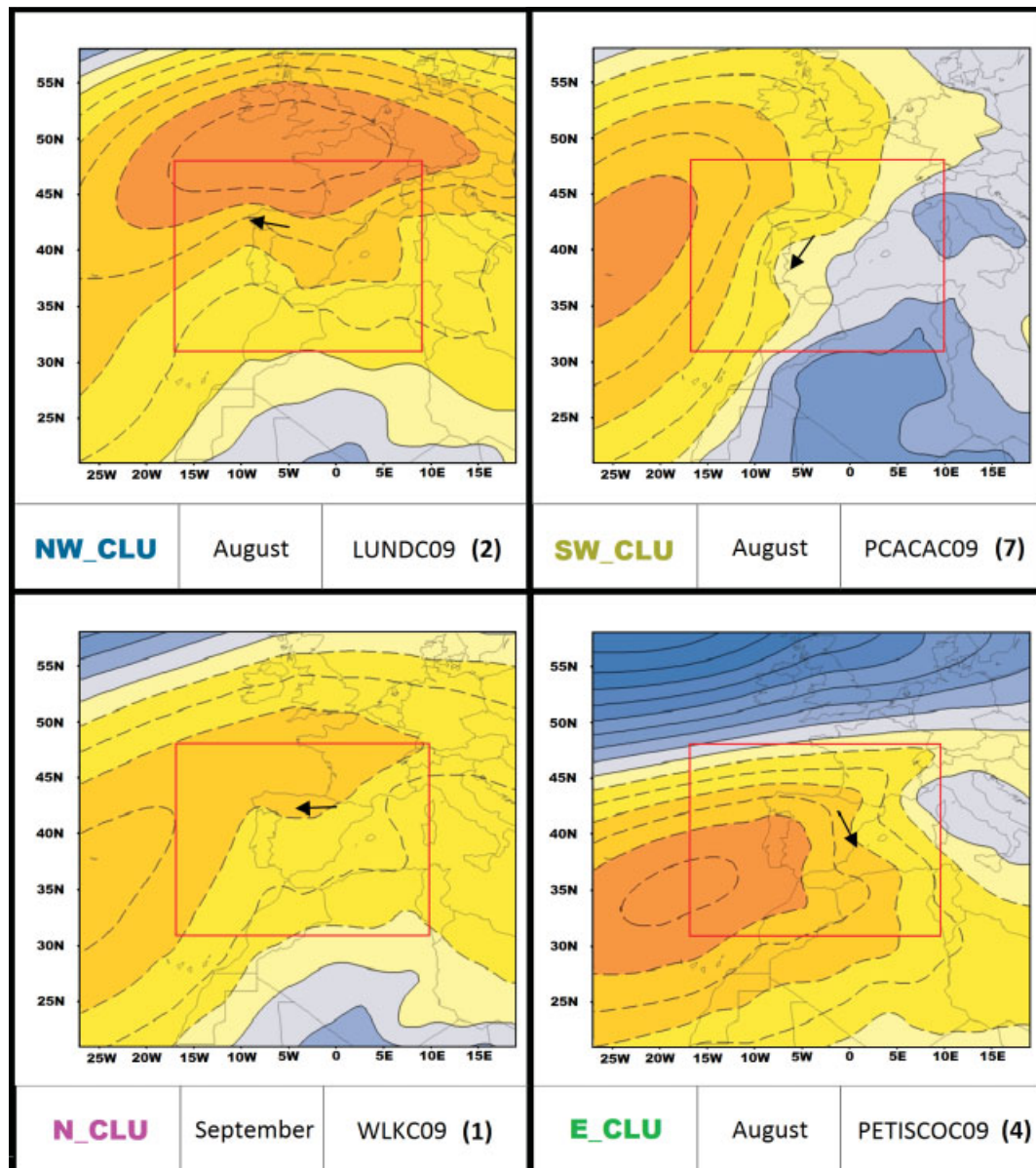


Figure 10. Composites of surface pressure anomaly (2 hPa interval isolines, with dashed lines corresponding to positive anomalies) in months (lower central box) with higher values of BA in each cluster (lower left box) and for specific weather type classifications (lower right box) that are highly correlated with BA series. Black arrows represent the anomalous wind direction in the respective cluster, revealing the origin and characteristics of the advected air masses.

10). The shown composites characterize the typical synoptic configurations driving the main surface wind flow and heat advection that predominate during months with very high values of BA in each cluster.

The majority of the retained classes correspond to very similar synoptic configurations, independently of the WTC. In all cases, and as expected, the composites reveal atmospheric anti-cyclonic circulation patterns usually associated with stable and dry conditions. The obtained spatial configurations foster prevailing warm and dry winds from inland, rather than moist and cool air advection from the sea, either from the Atlantic Ocean or the Mediterranean. The main difference between the results for each cluster can be found in the location of the high-pressure region, which induces different directions

of the surface wind flow. This type of circulation is clearly evident in the composites identified when analysing the most coastal confined clusters (NW, N and E). In the NW\_CLU of Iberia, we find that hazardous fire seasons are related to WTs with prevailing winds from the east or southeast components. The composite of surface pressure anomaly obtained for the NW\_CLU (Figure 10) is very similar to the spatial pattern obtained for the sea level air pressure composite for the 10% highest BA days in Portugal and the corresponding 10% anomaly for the 1980–2000 period (Pereira *et al.*, 2005). The Mediterranean areas that compose the E\_CLU present important fire episodes when the circulation is essentially from the northwest (Figure 10). Regions from the N\_CLU have fire incidence with dominating southeast

or east winds. In this latter case, and in particular for coastal areas, it is also quite evident that besides being an inland wind, it is also a downslope wind from the Cantabria mountainous region towards the coast, promoting additional drying and warming of air masses (Föhn effect). This is also the process that helps to understand the obtained results for the SW\_CLU, where the anomalous composites point to prevailing winds from the north or northwest components. It should be reminded that in this cluster the highest values of the NBA are found for some ARs of Portugal (namely Guarda, Castelo Branco and Santarém), which are located downstream of the main orographic barriers in that domain. It should also be kept in mind that this cluster covers a much wider area of the peninsula (Figure 6), comprehending not only the referred Portuguese AR but also a large part of central and southern Spain, where NBA values are generally low. The wide structure of this cluster may partially explain the absence of a clearly inland originated wind patterns in the presented composite.

## 6. Discussion and conclusions

In this work, a comprehensive and novel wildfire database for the entire IP was established by merging information from both Iberian countries which is essential for studying spatial and temporal patterns of fire occurrences and BAs in Iberia. Moreover, such a database can be useful for further developments on a wider European context. Using this Iberian dataset, we were able to perform a cluster analysis to distinguish between different sub-regions with similar monthly fire regimes within the IP. This analysis proved to be efficient in discriminating four independent regions, as they differ both on the timing and intensity of the seasonal peaks of NBA. The analysis of the mean annual cycle of NBA clearly highlights the western half of Iberia as more prone to large wildfire activity, particularly in central and northern areas of Portugal and northwestern areas of Spain. Paradoxically, being neither the driest nor the most irregular region in terms of rainfall in the Iberian context, the exceptional high frequency of forest fires in NW\_CLU denotes the relevant role of a combination of weather-climate, vegetation, geographical and human factors upon fire dynamics. Some northeastern areas of Spain also present relevant mean annual values of NBA, but generally at a smaller magnitude than the previous. This fact leads us to pay particular attention to the results and statistical models of westernmost clusters. In fact the relatively low values of NBA found in the other clusters reduce the possibility of a deeper analysis, and increase the danger of misinterpretation of the results and of the efficiency of the tested statistical models. As expected, the highest mean monthly values of NBA area were found in summer months, as higher temperatures and lower humidity foster appropriate conditions for fire ignitions. Westernmost regions tend to present higher mean values of NBA

in the month of August, while areas along the Mediterranean basin present a peak in July. Northern areas (both N\_CLU and NW\_CLU) have two annual peaks, one in summer and one in late winter or early spring. While in the NW\_CLU this cold season peak is almost insignificant when compared to the summer peak, in the regions around Cantabria and Asturias both peaks are comparable, although of relatively small amplitude.

The purpose of this study was to undertake an objective comparison between the ability of different WTC available from the COST733 project, in terms of discriminating the synoptic conditions that favour large wildfire activity in Iberia. This was done for classifications with nine classes, and the procedure includes: (1) correlation analysis between monthly BA and the monthly frequencies of each WT, used as a predictor pre-selection tool; followed by a (2) regression analysis to derive statistical hindcast models of monthly BA (WTC\_models) for all the clusters, and testing their ability to reproduce the inter-annual variability of the observed series. Similar approaches were adopted in previous studies in many different areas (Pereira *et al.*, 2011b). To avoid multicollinearity, in ecological modelling studies it is common to adopt two criteria: (i) pairwise correlation using Spearman's or Pearson's  $R$  correlation coefficient between predictors lower than given thresholds, e.g. 0.7 (Elith *et al.*, 2006; Wisz and Guisan, 2009); and (ii) Generalized Variance Inflation Factor (GVIF) lower than 5 (Neter *et al.*, 1996). In this study,  $R$  between every pair of predictors was less or equal 0.5, while GVIF computed with SAM (Rangel *et al.*, 2010) was always less than 2.

To contextualize this modelling approach, models based solely on climatic information from the pre-fire season (CLI\_models) were initially developed in order to compare the results obtained with both models. This procedure enabled us to distinguish between regions of the IP where pre-fire season temperature and precipitation play an important role on the magnitude of the fire season, and areas where this information has relatively low predictability value. Summer large wildfire activity is highly related to previous climatic conditions in the northwestern sector of Iberia. This result is in agreement with the previous work by Pereira *et al.* (2005), which states that spring conditions are determinant on the propensity for large values of BA during the warmest months, mainly by (1) the level of dryness imposed by previous climatic conditions and (2) the rate of vegetation growth in spring, which leads to an additional fuel accumulation during summer extreme warm episodes. We have attempted to use other variables related with the pre-fire season climate, such as the Palmer Drought Standardized Index (PDSI), however, this has not improved the quality of the models, being rejected during the stepwise regression procedure.

A third set of statistical models was computed using both referred types of information as potential predictors (TOT\_models). This was done in order to see the added value of merging WTC and previous climatic conditions information. It should be stressed that all models were cross-validated to avoid over fitting. As

expected, in almost all cases, best results were obtained for the TOT\_models. The larger improvements were found for months and clusters where CLI\_models results were poorer. In northwestern areas, previous climatic conditions information was already sufficient to produce quite robust hindcast models. The difference in the predictability of BA amid different areas is quite evident in the correlation coefficient and MAE between hindcast and observed time series. Overall, we found the most robust statistical hindcast models for the NW\_CLU (the one with the highest mean annual values of NBA), and the worst performing models in the N\_CLU (the one with the lowest mean annual values of NBA and with two similar sized peaks in March and September).

There is no clear or consensual result pointing to one particular WTC that performs better on the purpose of modelling BA time series in all Iberian regions. Depending on the considered region and month, the best performing classification change. However, some of the tested classifications tend to present the best results more frequently: PETISCOC09, WLKC09 and LUNDC09. Each of these WTC presents some of the most satisfying results in at least two clusters, while other classifications do not present good performances in none of the considered regions and months that were analysed and were therefore discarded from the remaining of the analysis. In the western sectors of Iberia (NW\_CLU and SW\_CLU), several WTC used alone are sufficient to developed statistical significance models at the 5% level. In these clusters, the variance of July BA time series is less explained by previous climatic conditions alone than in August or July + August BA time series, but there was a significant gain by introducing current WTC information. This difference between July and August models might result from the fact that the ignition of a fire in the middle of August does not always require an extreme ‘synoptic forcing’, due to the accumulation of previous hot and dry spells, while earlier in July a large fire might require a more intense ‘synoptic forcing’ to be initiated. In the Mediterranean coastal areas, BA in July was also difficult to model based purely on previous climatological conditions, and in this particular case, the WTC information does not improve significantly the models—only the BA in August and in July + August time series can be well reproduced by these statistical models. A study by Millán *et al.* (1998) suggests that in this region, early summer fire activity is highly related to the penetration of sea breezes inland, during well established warm and dry conditions in the interior, while in late summer westerly dry and warm inland flows (*Poniente*) play a more important role. This fact may provide some context for the poor results obtained with the models of BA in July, as sea breezes occur frequently at the mesoscale (i.e. at a finer resolution than the considered datasets in this work), while the *Poniente* conditions can be well represented at the synoptic scale. Models for the northernmost regions present the worst results even when both types of information are used as predictors, although some

few WTC can present interesting results. Three possible facts might help to explain such regional discrepancies: (1) the low performance of the N\_CLU and E\_CLU models might result from an insufficient level of spatial aggregation to solve the climatological and topographical complexity of both regions; (2) the reliability of the seasonal models is reduced, as the BA in the NW\_CLU reveals to be a consequence of a large number of ‘small’ fires, while when we move to the southeast most of the BA rests on a few large forest fires; (3) as a response of such level of complexity, atmospheric mechanisms might combine themselves in a nonlinear way, sometimes reinforcing the total forcing, sometimes weakening it. In any case, the analysis of those facts is beyond the scope of this paper.

It was also important to assure that WT predictors which were retained by the selection method corresponded to synoptic patterns associated with large wild-fire activity episodes. The composites for the majority of WTs that were retained as predictors for each cluster correspond to stable conditions, where the specific region is influenced by warm and dry air masses. The atmospheric processes that could enhance the susceptibility for large BA are associated to either the advection of hot and dry inland air to coastal regions, or diabatic heating and drying on the downslope side of the mountainous systems.

On the overall, and despite being almost impossible to identify the WTC more suitable to discriminate BA in Iberia, it is quite clear that their information is very useful and valuable enough to develop statistical models that can explain the variability of BA in this region. In fact, instead of picking and focusing on one or two particular classifications *a priori*, we find a more efficient type of approach to take them all initially into account, and use objective criteria and automatic methods to select the classifications with better performance in each particular case.

Regionalized scenarios of climate change for Spain (MARN, 2005; AEMET-IM, 2011) and Portugal show a sustained warming (Ramos *et al.*, 2011) and a reduction of the precipitation (Gouveia *et al.*, 2011), more remarkable during spring, outcome of the reduction of Atlantic storm systems (Lorenzo *et al.*, 2011). Consequently, the overall increase of the fire risk associated to a warmer world should be enhanced in western Iberia due to the long-term reduction of the springtime precipitation. The good performance of models in this region offers a promising tool to simulate the BA amount from the outputs of the regional climate models. Finally, we must acknowledge the fact that some of the Iberian regions characterized in this work might be affected by the existence of asymmetric trends in BA annual values. In particular, it has been shown that Spain reveals a negative trend of BA in the last three decades while Portugal has not revealed such pattern, being more appropriately characterized by an increasing tendency between the 1980s and 2000s (Pereira *et al.*, 2011a).

## Acknowledgements

This work was supported by European Union Funds (FEDER/COMPETE—Operational Competitiveness Programme) and by national funds (FCT—Portuguese Foundation for Science and Technology) under the project FCOMP-01-0124-FEDER-022692, the project FLAIR (PTDC/AAC-AMB/104702/2008) and the EU 7th Framework Program through FUME (contract number 243888). We are also in debt to the Autoridade Florestal Nacional, the Portuguese Forest service for providing the Portuguese fire data and to Cátia Teixeira for the final text revision of the manuscript.

## References

- Agencia Estatal de Meteorología (AEMET-IM). 2011. Atlas climático de España y Portugal [http://www.aemet.es/es/serviciosclimaticos/datosclimatologicos/atlas\\_climatico](http://www.aemet.es/es/serviciosclimaticos/datosclimatologicos/atlas_climatico)
- AFN (Autoridade Florestal Nacional). 2011. Statistics: Wildfire Data [Online] Available at: <http://www.afn.min-agricultura.pt/portal/dudd/estatisticas/estatistica-2013-dados-sobre-incendios-florestais> [Accessed 1 March 2011].
- Austín RB, Cantero-Martínez C, Arrúe JL, Playán E, Cano-Marcellán P. 1998. Yield–rainfall relationships in cereal cropping systems in the Ebro river valley of Spain. *European Journal of Agronomy* **8**: 239–248.
- Badía A, Saurí D, Cerdan R, Llurdes JC. 2002. Causality and management of forest fires in Mediterranean environments: an example from Catalonia. *Environmental Hazards* **4**: 23–32.
- Barbosa P, Amatulli G, Boca R, Camia A, Kucera J, Libertà G, San-Miguel Ayanz J, Schmuck G, Schulte E, Dierks HH. 2007. Forest Fires in Europe 2006, EUR 22931 EN—Joint Research Centre—Institute for Environment and Sustainability, Luxembourg: Office for Official Publications of the European Communities, EUR—Scientific and Technical Research series: ISSN 1018–5593.
- Carvalho A, Flannigan MD, Logan K, Miranda AI, Borrego C. 2008. Fire activity in Portugal and its relationship to weather and the Canadian Fire Weather Index System. *International Journal of Wildland Fire* **17**(3): 328–338.
- Carracedo Martín V, Diego Liaño C, García Codrón JC, Rasilla Álvarez D. 2009. *Incendios forestales*. Davinci Continental, S.L.
- COST 733 Wiki. 2011. Harmonisation and Applications of Weather Type Classifications for European regions or COST733 spatial domains for Europe. Available at: [http://geo21.geo.uni-augsburg.de/cost733/wiki/Cost733\\_Wiki\\_Main](http://geo21.geo.uni-augsburg.de/cost733/wiki/Cost733_Wiki_Main) [Accessed 30 May 2013].
- Costa L, Thonicke K, Poulter B, Badek FW. 2010. Sensitivity of Portuguese forest fires to climatic, human, and landscape variables: subnational differences between fire drivers in extreme fire years and decadal averages. *Regional Environmental Change* **11**(3): 543–551. DOI: 10.1007/s10113-010-0169-6
- Cueva AV, Barrio JMG, Quero MO, Palomares OS. 2006. Recent fire regime in peninsular Spain in relation to forest potential productivity and population density. *International Journal of Wildland Fire* **15**(3): 397–405. DOI: 10.1071/WF05071
- Elith J, Graham CH, Anderson RP, Ferrier M, Dudík S, Guisan A, Hijmans RJ, Huettmann F, Leathwick JR, Lehmann A, Li J, Lohmann LG, Loiselle BA, Manion G, Moritz C, Nakamura M, Nakazawa Y, McC Overtton J, Peterson AT, Phillips SJ, Richardson K, Scachetti-Pereira R, Schapire RE, Soberón J, Williams S, Wisz MS, Zimmermann NE. 2006. Novel methods improve prediction of species' distributions from occurrence data. *Ecography* **29**: 129–151.
- European Commission. 1998. Common Information System on Forest Fires, 1985–1997 study. *European Commission, Directorate-General Agriculture*: DG VI FII-2.
- Fischer EM, Schär C. 2010. Consistent geographical patterns of changes in high-impact European heatwaves. *Nature Geoscience* **3**: 398–403. DOI: 10.1038/NGEO866
- Fischer EM, Seneviratne SI, Lüthi D, Schär C. 2007. Contribution of land-atmosphere coupling to recent European heatwaves. *Geophysical Research Letters* **34**: L06707.
- Flannigan MD, Wotton B. 2001. Climate, weather and area burnt. In *Forest Fires—Behavior and Ecological Effects*, Johnson EA, Miyanishi K (eds). Academic Press: San Diego; 351–373.
- García-Herrera R, Paredes D, Trigo RM, Trigo IF, Hernández H, Barriopedro D, Mendes MT. 2007. The outstanding 2004/05 drought in the Iberian Peninsula: associated atmospheric circulation. *Journal of Hydrometeorology* **8**: 483–498.
- Gil-Romera G, Carrión JS, Pausas JG, Fernández S, Burjachs F. 2010. Holocene fire activity and vegetation response in South-Eastern Iberia. *Quaternary Science Reviews* **29**: 1082–1092.
- Giorgi F. 2006. Climate change hot-spots. *Geophysical Research Letters* **33**: L08707.
- Gouveia C, Trigo RM, DaCamara CC, Libonati R, Pereira JMC. 2008. The North Atlantic Oscillation and European Vegetation Dynamics. *International Journal of Climatology* **28**: 1835–1847.
- Gouveia C, Trigo RM, DaCamara CC. 2009. Drought and vegetation stress monitoring in Portugal using Satellite Data. *Natural Hazards and Earth System Sciences* **9**: 185–195.
- Gouveia C, DaCamara CC, Trigo RM. 2010. Post fire vegetation recovery in Portugal based on SPOT-VEGETATION data. *Natural Hazards and Earth System Sciences* **10**: 673–684.
- Gouveia C, Liberato MLR, DaCamara CC, Trigo RM. 2011. Modelling past and future wine production in the Portuguese Douro Valley. *Climate Research* **48**: 349–362. DOI: 10.3354/cr01006
- Hoinka KP, Carvalho A, Miranda AI. 2009. Regional-scale weather patterns and wildland fires in central Portugal. *International Journal of Wildland Fire* **18**(1): 36–49.
- JRC: Forest Fires in Europe 2009. Report EUR 24502 EN. 2010. JRC-IES/Land Management & Natural Hazards Unit. ISSN 1018–5593. [Online] Available at: <http://effis.jrc.europa.eu/reports/fire-reports/> [Accessed 1 April 2011].
- Kassomenos P. 2010. Synoptic circulation control on wild fire occurrence. *Physics and Chemistry of the Earth* **35**: 544–552. DOI: 10.1016/j.pce.2009.11.008
- Kunkel KK. 2001. Surface energy budget and fuel moisture. In *Forest Fires—Behaviour and Ecological Effects*, Johnson EA, Miyanishi K (eds). Academic Press: San Diego; 303–350.
- Leśniok M, Małarzewski L, Niedźwiedz T. 2010. Classification of circulation types for Southern Poland with an application to air pollution concentration in Upper Silesia. *Physics and Chemistry of the Earth, Parts A/B/C* **35**(9–12): 516–522.
- Lloret F, Calvo E, Pons X, Díaz-Delgado R. 2002. Wildfires and landscape patterns in the Eastern Iberian Peninsula. *Landscape Ecology* **17**: 745–759.
- Lorenzo MN, Ramos AM, Taboada JJ, Gimeno L. 2011. Changes in Present and Future Circulation Types Frequency in Northwest Iberian Peninsula. *PLoS One* **6**(9–12): e16201. DOI: 10.1371/journal.pone.0016201
- Lupikasza E. 2010. Relationships between occurrence of high precipitation and atmospheric circulation in Poland using different classifications of circulation types. *Physics and Chemistry of the Earth, Parts A/B/C* **35**(9–12): 448–455.
- Mariotti A. 2010. Recent changes in Mediterranean water cycle: a pathway toward long-term regional hydroclimatic change? *Journal of Climate* **23**: 1513–1525.
- Mariotti A, Zeng N, Yoon J, Artale V, Navarra A, Alpert P, Li LZ. 2008. Mediterranean water cycle changes: transition to drier 21st century conditions in observations and CMIP3 simulations. *Environmental Research Letters* **3**: 044001. DOI: 10.1088/1748-9326/3/4/044001
- Ministerio de Medio Ambiente, Marino y Rural (MARN). 2011. Los incendios forestales en España decenio 1996–2005 ([http://www.marm.es/es/biodiversidad/temas/defensa-contra-incendios-forestales/decenio\\_1996\\_2005\\_tcm7-19437.pdf](http://www.marm.es/es/biodiversidad/temas/defensa-contra-incendios-forestales/decenio_1996_2005_tcm7-19437.pdf)) [Accessed 21 September 2011].
- Martínez-Villalta J, López BC, Adel N, Badiella L, Ninyerola M. 2008. Twentieth century increase of Scots pine radial growth in NE Spain shows strong climate interactions. *Global Change Biology* **14**: 2868–2881.
- Millán M, Estrela MJ, Badenas C. 1998. Meteorological Processes Relevant to Forest Fire Dynamics on the Spanish Mediterranean Coast. *Journal of Applied Meteorology* **37**: 83–100. DOI: 10.1175/1520-0450(1998)037<0083:MPRTFF>2.0.CO;2
- Ministerio de Medio Ambiente, Marino y Rural (MARN). 2005. Evaluación preliminar de los impactos en España del cambio climático (<http://www.marm.es/es/cambio-climatico/temas/impactos-vulnerabilidad-y-adaptacion/iniciativas-en-el-ambito-nacional/evaluacion-preliminar-de-los-impactos-en-espana-del-cambio-climatico/>) [Accessed 29 October 2011].

- Myneni RB, Hall FG, Sellers PJ, Marshak AL. 1995. The interpretation of spectral vegetation indexes. *IEEE Transactions on Geoscience and Remote Sensing* **33**: 481–496.
- Mitchell TD, Jones PD. 2005. An improved 258 method of constructing a database of monthly climate observations and associated high-resolution grids. *International Journal of Climatology* **25**: 693–712.
- Moreno JM, Vázquez A, Vélez R. 1998. Recent history of forest fires in Spain. In *Large Forest Fires*, Moreno JM (ed). Backhuys: Leiden; 159–186.
- Neter J, Kutner M, Nachtshe C, Wasserman W. 1996. *Applied Linear Regression Models*, 3 edn. Boston: McGraw-Hill.
- Padilla M, Vega-García C. 2009. On the comparative importance of fire danger rating indices and their integration with spatial and temporal variables for predicting daily human-caused fire occurrences in Spain. *International Journal of Wildland Fire* **20**(1): 46–58. DOI: 10.1071/WF09139
- Paredes J, Trigo RM, García-Herrera R, Trigo IF. 2006. Understanding precipitation changes in Iberia in early spring: weather typing and storm-tracking approaches. *Journal of Hydrometeorology* **7**: 101–113.
- Pausas JG. 2004. Changes in fire and climate in the Eastern Iberian Peninsula (Mediterranean Basin). *Climatic Change* **63**: 337–350.
- Pausas JG, Vallejo R. 1999. The role of fire in European Mediterranean ecosystems. In *Remote Sensing of Large Wildfires in the European Mediterranean Basin*, Chuvieco E (ed). Springer-Verlag: Berlin; 3–16.
- Pausas JG, Fernández-Muñoz S. 2011. Fire regime changes in the Western Mediterranean Basin: from fuel-limited to drought-driven fire regime. *Climatic Change* **110**(1–2): 215–226. DOI: 10.1007/s10584-011-0060-6
- Pereira MG, Trigo RM, DaCamara CC, Pereira JMC, Solange ML. 2005. Synoptic patterns associated with large summer forest fires in Portugal. *Agricultural and Forest Meteorology* **129**: 11–25. DOI: 10.1016/j.agrformet.2004.12.007
- Pereira MG, Malamud BD, Trigo RM, Alves PI. 2011a. The History and Characteristics of the 1980–2005 Portuguese Rural Fire Database. *Natural Hazards and Earth System Sciences* **11**: 1–16. DOI: 10.5194/nhess-11-1-2011
- Pereira MG, Caramelo L, Gouveia C, Gomes-Laranjo J, Magalhães M. 2011b. Assessment of weather-related risk on chestnut productivity. *Natural Hazards and Earth System Sciences* **11**: 1–12. DOI: 10.5194/nhess-11-12-011
- Philipp A, Bartholy J, Beck C, Erpicum M, Magalhães M, Esteban P, Huth R, James P, Jourdain S, Krennert T, Lykoudis S, Michalides S, Pianko K, Post P, Rassilla Álvarez D, Schiemann R, Spekat A, Tymvios FS. 2010. COST733CAT – a database of weather and circulation type classifications. *Physics and Chemistry of the Earth* **35**: 360–373.
- Pineda N, Esteban P, Trapero L, Soler X, Beck C. 2010. Circulation types related to lightning activity over Catalonia and the Principality of Andorra. *Physics and Chemistry of the Earth, Parts A/B/C* **35**(9–12): 469–476.
- Piñol J, Terradas J, Lloret F. 1998. Climate warming, wildfire hazard and wildfire occurrence in coastal Eastern Spain. *Climatic Change* **38**: 345–357.
- Pyne SJ, Andrews PL, Laven RD. 1996. *Introduction to Wildland Fire*, 2 edn. New York: John Wiley & Sons.
- Ramos A, Trigo RM, Santo FE. 2011. Evolution of extreme temperatures in Portugal: reporting on recent changes and future scenarios. *Climate Research* **48**: 177–192. DOI: 10.3354/cr00934
- Rangel TFLVB, Diniz-Filho JAF, Bini LM. 2010. SAM: a comprehensive application for Spatial Analysis in Macroecology. *Ecography* **33**: 46–50.
- Rasilla DF, García-Codron JC, Carracedo V, Diego C. 2010. Circulation patterns, wildfire risk and wildfire occurrence at continental Spain. *Physics and Chemistry of the Earth* **35**: 553–560. DOI: 10.1016/j.pce.2009.09.003
- Rivas Martínez S. 1987. Memoria del mapa de series de vegetación de España 1: 400.000. ICONA. Ministerio de Agricultura, Pesca y Alimentación, Madrid. ISBN 84-85496-25-6.
- Rubiales JM, García Amorena I, García Álvarez S, Gómez Manzanque F. 2008. The Late Holocene extinction of *Pinus sylvestris* in the West of the Cantabrian Range. *Journal of Biogeography* **35**(10): 1840–1850. DOI: 10.1111/j.1365-2699.2008.01925.x
- Seneviratne SI, Lüthi D, Litschi M, Schär C. 2006. Land-atmosphere coupling and climate change in Europe. *Nature* **443**: 205–209. DOI: 10.1038/nature05095
- Sousa P, Trigo RM, Aizpurua P, Nieto R, Gimeno L, García-Herrera R. 2011. Trends and extremes of drought indices throughout the 20th century in the Mediterranean. *Natural Hazards and Earth System Sciences* **11**: 33–51.
- Trigo RM, Pereira JMC, Pereira MG, Mota B, Calado MT, DaCamara CC, Santo FE. 2006. Atmospheric conditions associated with the exceptional fire season of 2003 in Portugal. *International Journal of Climatology* **26**(13): 1741–1757.
- Tucker CJ, Pinzon JE, Brown ME, Slayback D, Pak EW, Mahoney R, Vermote E, El Saleous N. 2005. An extended AVHRR 8-km NDVI data set compatible with MODIS and SPOT vegetation NDVI data. *International Journal of Remote Sensing* **26**: 4485–4498.
- Twadowsz R. 2010. An analysis of diurnal variations of heavy hourly precipitation in Kraków using a classification of circulation types over southern Poland. *Physics and Chemistry of the Earth, Parts A/B/C* **35**(9–12): 456–461.
- Ustrnul Z, Czekierda D, Wypych A. 2010. Extreme values of air temperature in Poland according to different atmospheric circulation classification. *Physics and Chemistry of the Earth, Parts A/B/C* **35**(9–12): 429–436.
- Valbuena-Carabaña M, López de Heredia U, Fuentes-Utrilla P, González-Doncel I, Gil L. 2010. Historical and recent changes in the Spanish forests: A socio-economic process. *Review of Palaeobotany and Palynology* **162**(3): 492–506.
- Vázquez A, Moreno MJ. 1993. Sensitivity of fire occurrence to meteorological variables in Mediterranean and Atlantic areas of Spain. *Landscape and Urban Planning* **24**: 129–142.
- Vázquez A, Pérez B, Fernández-González F, Moreno JM. 2002. Recent fire regime characteristics and potential natural vegetation relationships in Spain. *Journal of Vegetation Science* **13**: 663–676.
- Vélez R. 1993. High intensity forest fires in the Mediterranean Basin: natural and socioeconomic causes. *Disaster Manage* **5**: 16–20.
- Vicente-Serrano SM. 2007. Evaluating the Impact of drought using Remote Sensing in a Mediterranean, semi-arid region. *Natural Hazards* **40**: 173–208.
- Vicente-Serrano SM, Heredia-Laclaustra A. 2004. NAO influence on NDVI trends in the Iberian Peninsula (1982–2000). *International Journal of Remote Sensing* **25**: 2871–2879.
- Viedma O, Moreno JM, Rieiro I. 2006. Interactions between land use/land cover change, forest fires and landscape structure in Sierra de Gredos (central Spain). *Environmental Conservation* **33**: 212–222.
- Viegas DX, Viegas MT. 1994. A relationship between rainfall and burned area for Portugal. *International Journal of Wildland Fire* **4**(1): 11–16.
- Wilks DS. 2006. *Statistical Methods in the Atmospheric Sciences*, 2 edn. Amsterdam: Academic Press.
- Wisz MS, Guisan A. 2009. Do pseudo-absence selection strategies influence species distribution models and their predictions? An information-theoretic approach based on simulated data. *BMC Ecology* **9**: 8.
- Zhao M, Running SW. 2010. Drought-Induced Reduction in Global Terrestrial Net Primary Production from 2000 through 2009. *Science* **30**: 940–943.



